LIÈGE université
Gembloux
Agro-Bio Tech

CHINESE ACADEMY OF AGRICULTURAL SCIENCES

Optimization of Antibiotic Leucinostatin Bioactivity and Production in Bio-control Fungus *Purpureocillium lilacinum*

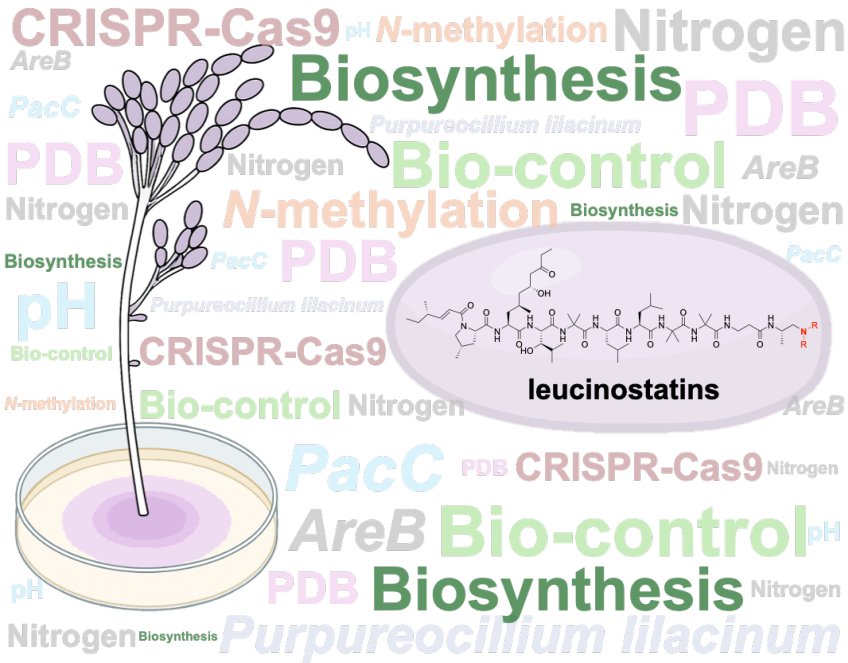

Zixin Li

Promoters : **Prof. Philippe Jacques**

Prof. Yan Li

2025

COMMUNAUTÉ FRANÇAISE DE BELGIQUE
UNIVERSITÉ DE LIÈGE – GEMBLOUX AGRO-BIO TECH

Optimization of Antibiotic Leucinostatin Bioactivity and Production in Bio-control Fungus *Purpureocillium lilacinum*

Zixin Li

Dissertation originale présentée (ou essai présenté) en vue de l'obtention du grade de doctorat en sciences agronomiques et ingénierie biologique

Promoteur(s) : Prof. Philippe Jacques
Prof. Yan Li
Année civile (= année du dépôt) : 2025

Abstract

Purpureocillium lilacinum (formerly *Paecilomyces lilacinus*) is a filamentous fungus widely recognized for its potential in biological control. In addition to parasitizing nematode eggs and enzymatically degrading cell membranes, *P. lilacinum* produces leucinostatins—antibiotic lipopeptides with broad-spectrum bioactivity. Previous studies have identified the leucinostatin biosynthetic gene cluster in *P. lilacinum* PLBJ-1. However, the influence of tailoring enzymes within the cluster on the structure and bioactivity of leucinostatins remains unclear. Moreover, strategies to enhance their production through optimization of cultivation conditions have yet to be established. These gaps hinder the effective application of leucinostatins. To address this, we investigated both the genetic basis of leucinostatin bioactivity and strategies to improve their production. Enhancing leucinostatin bioactivity or yield is crucial for fully realizing their therapeutic and agricultural potential.

Structure–activity relationship (SAR) studies on leucinostatins and their derivatives have highlighted the importance of the C-terminus in modulating bioactivity. Consistent with this, the leucinostatins produced by *P. lilacinum* PLBJ-1 display varying degrees of methylation at their C-terminal ends. Since *N*-methylation is known to significantly influence the bioactivity of natural products, we focused our investigation on the putative methyltransferase LcsG. Disruption of the *lcsG* gene led to a near-complete loss of leucinostatins with methylated termini. After recombinant LcsG was obtained, in vitro enzymatic assays and structural analysis of the resulting reaction products confirmed that LcsG catalyzes iterative *N*-methylation at the terminal free amine of leucinostatins. Structure-function relationship studies further elucidated the likely catalytic mechanism of LcsG. Meanwhile, novel methylated leucinostatins generated through LcsG-catalyzed reactions exhibited activity against the human pathogen *Cryptococcus neoformans* and the plant pathogen *Phytophthora infestans*. Notably, the methylated products showed enhanced activity against *C. neoformans* compared to their parent molecules. To our knowledge, LcsG is the first reported free-standing *N*-methyltransferase capable of catalyzing the terminal modification of nonribosomal peptide (NRP)-class compounds. These findings deepen the understanding of *N*-methylation mechanisms in peptides and open new avenues for engineering methylated molecules with enhanced antibiotic properties.

To improve leucinostatin yield, we also investigated the influence of culture conditions. Significant differences in fungal growth and leucinostatin production were observed when *P. lilacinum* PLBJ-1 was cultured in hand-made potato dextrose broth (PDB-M), as compared to commercial formulations (PDB-C). Compared to PDB-C, PDB-M was associated with a higher increase in pH and a lower nitrogen content—two environmental factors known to affect fungal metabolism. We identified the pH regulator PlPacC and nitrogen regulator PlAreB as critical factors influencing fungal growth and leucinostatin production. CRISPR-Cas9-mediated gene disruption revealed that PlPacC functions as a positive regulator of both environmental pH alkalinization and leucinostatin production, whereas PlAreB acts as a negative regulator of leucinostatin biosynthesis. Additionally, deletion of these genes impacted

fungal growth and sporulation, suggesting their broader role in developmental and metabolic processes. These insights provide a foundation for optimizing fungal culture conditions and enhancing the production of bioactive compounds, with promising applications in improving bio-control efficacy.

In conclusion, this study advances our understanding of leucinostatin biosynthesis in *P. lilacinum* and offers valuable strategies for improving its bioactivity and production. These findings pave the way for future research and potential applications in antimicrobial drug development and biological control.

Keywords: *Purpureocillium lilacinum,* leucinostatins, N-methyltransferase, PacC, AreB

Résumé

Purpureocillium lilacinum (anciennement *Paecilomyces lilacinus*) est un champignon filamenteux largement reconnu pour son potentiel en lutte biologique. En plus de parasiter les œufs de nématodes et de dégrader enzymatiquement les membranes cellulaires, *P. lilacinum* produit des leucinostatines — des lipopeptides antibiotiques présentant une large gamme d'activités bioactives. Des études antérieures ont identifié le cluster de gènes biosynthétiques des leucinostatines chez *P. lilacinum* PLBJ-1. Cependant, l'influence des enzymes de modification post-synthétique présentes dans ce cluster sur la structure et la bioactivité des leucinostatines reste mal comprise. De plus, les stratégies visant à améliorer leur production par l'optimisation des conditions de culture n'ont pas encore été établies, ce qui freine leur application efficace.

Pour remédier à ces lacunes, nous avons étudié à la fois les bases génétiques de la bioactivité des leucinostatines et des approches pour en améliorer la production. L'amélioration de leur bioactivité ou de leur rendement est cruciale pour exploiter pleinement leur potentiel thérapeutique et agricole.

Des études de relation structure-activité (SAR) sur les leucinostatines et leurs dérivés ont souligné l'importance de l'extrémité C-terminale dans la modulation de leur activité biologique. De manière cohérente, les leucinostatines produites par P. lilacinum PLBJ-1 présentent différents degrés de méthylation en position terminale. Étant donné que la N-méthylation influence fortement la bioactivité des produits naturels, nous avons concentré notre étude sur la méthyltransférase putative LcsG. L'invalidation du gène *lcsG* a entraîné une disparition quasi totale des leucinostatines méthylées. La protéine LcsG recombinante a ensuite été purifiée, et des essais enzymatiques in vitro et des analyses structurales des produits de réaction ont confirmé que LcsG catalyse la *N*-méthylation itérative de l'amine terminale des leucinostatines. Des études de relation structure-fonction ont permis d'élucider le mécanisme catalytique probable de LcsG. Par ailleurs, les nouvelles leucinostatines méthylées générées via les réactions catalysées par LcsG ont montré une activité antifongique accrue contre le pathogène humain *Cryptococcus neoformans* et le pathogène végétal *Phytophthora infestans*. À notre connaissance, LcsG constitue la première *N*-méthyltransférase indépendante identifiée comme capable de modifier l'extrémité terminale de composés de type peptides non ribosomiques (NRP). Ces résultats approfondissent notre compréhension des mécanismes de *N*-méthylation dans les peptides et ouvrent la voie à l'ingénierie de molécules méthylées dotées de propriétés antibiotiques améliorées.

Dans le but d'optimiser le rendement en leucinostatines, nous avons également étudié l'influence des conditions de culture. Des différences significatives de croissance fongique et de production de leucinostatines ont été observées lorsque *P. lilacinum* PLBJ-1 était cultivé dans un milieu PDB maison (PDB-M) par rapport aux formulations commerciales (PDB-C). Comparé au PDB-C, le PDB-M présentait une augmentation plus marquée du pH et une teneur en azote plus faible — deux facteurs environnementaux connus pour affecter le métabolisme fongique. Nous avons

identifié le régulateur de pH PlPacC et le régulateur de l'azote PlAreB comme des facteurs clés influençant la croissance et la production de leucinostatines. La disruption génique médiée par CRISPR-Cas9 a révélé que PlPacC agit comme un régulateur positif de l'alcalinisation du pH environnemental ainsi que de la production de leucinostatines, tandis que PlAreB joue le rôle de régulateur négatif de la biosynthèse des leucinostatines. De plus, la suppression de ces gènes a impacté la croissance fongique et la sporulation, suggérant leur implication plus large dans les processus métaboliques et développementaux. Ces résultats constituent une base pour l'optimisation des conditions de culture et l'amélioration de la production de composés bioactifs, avec des applications prometteuses en lutte biologique.

En conclusion, cette étude fait progresser notre compréhension de la biosynthèse des leucinostatines chez *P. lilacinum* et propose des stratégies efficaces pour améliorer leur bioactivité et leur production. Ces résultats ouvrent la voie à de futures recherches et à des applications potentielles dans le développement de médicaments antimicrobiens et de solutions de lutte biologique.

Mots-clés *: Purpureocillium lilacinum, leucinostatines, N-méthyltransférase, PacC, AreB*

Acknowledgments

After a long journey, I finally made it to the finish line with my doctoral thesis. When I look back on this time, I realize just how special and important it has been for me. I'm incredibly thankful for everyone who walked this road with me.

First and foremost, I want to thank my two excellent advisors, Professor Philippe Jacques and Professor Yan Li. You both were like beacons of light for me in the academic world. Every time I hit a roadblock in my studies, you were there, ready to share your knowledge and help me find my way. You didn't just support me when I faced academic challenges, you also made sure I felt supported and understood in my personal life. Your kindness and patience meant the world to me.

I'm also super grateful to my jury members. You took the time to read my work and gave me some valuable feedback. Your suggestions helped me see things from a different angle and made my thesis way better than it would have been otherwise. I really appreciate their time and effort.

I can't forget my colleagues and friends. You guys were my rock. When I was feeling down or stressed, you were there to lift me up. We laughed together, we worked together, and we even struggled together. It was amazing to have such a supportive group around me. I feel so lucky to have met all of you, and I'll always cherish the memories we made.

A big shout-out to the China Scholarship Council (CSC) for their financial support. That really took a load off my mind and let me focus on my research.

And last but not least, I want to thank my family. My husband Hao Chen, my parents, and my son Mingli. You guys are my superheroes. This journey wasn't always easy, and there were moments when I felt overwhelmed. But you were always there, giving me love, understanding, and endless encouragement. Mingli, my little angel, your innocent and pure love always had a way of making everything feel better. You all wrapped me in a blanket of love and support that kept me going even when things got tough.

I'll never forget this journey or the people who made it possible. Your support and love have been my strength, and I'm so grateful for every moment we've shared.

Zixin Li

2025 in Gembloux, Belgium

Table of contents

List of figures

List of tables

List of acronyms

6-APA: 6-aminopenicillanic Acid
7-ACA: 7-aminocephalosporanic Acid
7-ADCA: 7-amino-desacetoxycephalosporanic Acid
A domain: Adenylation Domain
ACP: Carrier Protein
AHMOD: 2-amino-6-hydroxy-4-methyl-8-oxodecanoic Acid
AI: Artificial Intelligence
Aib: Aminoisobutyric Acid
AT: Acyltransferase
BCA: Biological Control Agent
BGC: Biosynthtic Gene Cluster
C domain: Condensation Domain
CDS: Coding Sequence
CLP: Cyclic Lipopeptide
CRISPR-Cas9: Clustered Regularly Interspaced Short Palindromic Repeats Associated Protein 9
CyA: Cyclosporin A
CYC: Cyclase
DB: Destruxin B
DH: Dehydratase
DMF: Dimethylformamide
DMPD: N1,n1-dimethylpropane-1,2-diamine
DMSO: Dimethyl Sulfoxide
Dtxs: Destruxins
E domain: Epimerase Domain
EDTA: Ethylenediaminetetraacetic Acid
ER: Enoyl Reductase
ES+: Electrospray Ionization In Positive Mode
ESCRT: Endosomal Sorting Complex Required For Transcript
ESI: Electrospray Ionization
FPP: Farnesyl Pyrophosphate
FPPS: Catalyzed By Farnesyl Pyrophosphate Synthase
GFP: Green Fluorescent Protein
GFPP: Geranylfarnesyl Pyrophosphate
GFPPS: Catalyzed By Geranylfarnesyl Pyrophosphate Synthase
GGPP: Geranylgeranyl Pyrophosphate
GGPPS: Catalyzed By Geranylgeranyl Pyrophosphate Synthase
GPP: Geranyl Pyrophosphate
GPPS: Catalyzed By Geranyl Pyrophosphate Synthase

GT: Glycosyltransferase
HDV: Liver Hepatic Delta Virus
HEPES: 4-(2-hydroxyethyl)-1-piperazineethanesulfonic Acid
HexPP: Hexaprenyl Pyrophosphate
HexPPS: Catalyzed By Hexaprenyl Pyrophosphate Synthase
HH: Hammerhead
HPLC: High-performance Liquid Chromatography
HRESI-MS-MS: High-resolution Electrospray Ionization Tandem Mass Spectrometry
HyLeu: Hydroxyleucine
IPTG: Isopropyl B-d-1-thiogalactopyranoside
ISR: Induced Systemic Resistance
KR: Ketoreductase
KS: Ketoacyl Synthase
LC–MS: Liquid Chromatography-mass Spectrometry
Leu: Leucine
LeuA: Leucinostatin A
LeuA0: Leucinostatin A0
LeuB: Leucinostatin B
LeuC: Leucinostatin C
LeuD: Leucinostatin D
LeuH: Leucinostatin H
LeuK: Leucinostatin K
LeuK0: Leucinostatin K0
LeuK1: Leucinostatin K1
LeuK2: Leucinostatin K2
LeuK3: Leucinostatin K3
MAFFT: Multiple Alignment Using Fast Fourier Transform
MD: Molecular Dynamics
MeHA: Methylhex-2-enoic Acid
MePro: 4-methyl-proline
MES: 2-(n-morpholino)ethanesulfonic Acid
MIC: Minimal Inhibitory Concentration
MOPS: 3-(n-morpholino)propanesulfonic Acid
MPD: N-methylpropane-1,2-diamine
MT: Methyltransferase
NAD(P)H/NAD(P)+: Nicotinamide Adenine Dinucleotide (phosphate), Reduced Form/ Nicotinamide Adenine Dinucleotide (phosphate), Oxidized Form
NCCLS: Clinical Laboratory Standards
NHS: N-hydroxysuccinimide
NMR: Nuclear Magnetic Resonance

NMT: N-methyltransferases
NRP: Nonribosomal Peptide
NRPS: Non-ribosomal Peptide Synthetase
OMT: O-methyltransferase
OSMAC: One Strain-many Compounds)
PCP: Peptidyl Carrier Protein Domain
PD: Propane-1,2-diamine
PDA: Potato Dextrose Agar
PDB-C: Commercial Potato Dextrose Broth
PDB-M: Hand-made Potato Dextrose Broth
PEG: Polyethylene Glycol
PGA: Penicillin G Acylase
PKS: Polyketide Synthase
PPT: Post-translational Phosphopantetheinylation
Q-TOF: Quadrupole Time-of-flight Mass Spectrometry
QM/MM: Quantum Mechanics / Molecular Mechanics
RMSD values: Root-mean-square Deviation Values
RSM: Response Surface Methodology
SAH: S-adenosyl-l-homocysteine
SAM: S-adenosyl-l-methionine
SAR: Structure-activity Relationship
SD: Standard Deviation
SD/-Trp-Ura dropout medium: Synthetic Defined Medium Lacking Tryptophan And Uracil
SDS–PAGE: Sodium Dodecyl Sulfate-polyacrylamide Gel Electrophoresis
SLF: Submerged Liquid Fermentation
SSF: Solid-state Fermentation
SSN: Sequence Similarity Network
TE: Thioesterase
TFA: Trifluoroacetic Acid
THF: Tetrahydrofuran
TMD: 7-transmembrane Domain
Tukey's HSD: Tukey’s Honestly Significant Difference Test
UPLC: Ultra Performance Liquid Chromatography
WT: Wild-type
βAla: B-alanine

Chapter 1

General introduction

1. Context of this thesis

Purpureocillium lilacinum was initially classified as *Penicillium lilacinum* by Thom in 1901, and then it was revised as *Paecilomyces lilacinus* by Samson in 1974. It is recognized for its significant role in biological control and the production of bioactive compounds. Two strains of *P. lilacinum* (PL11 and 251) have been approved as microbial pesticides in the European Union. The European Food Safety Authority (EFSA) evaluated the nematicidal efficacy and risk profiles of both strains against *Meloidogyne* spp. under field and permanent greenhouse conditions. Strain 251 demonstrated sufficient efficacy and was considered to pose a low risk to human health and the environment in both settings, while strain PL11 exhibited confirmed efficacy and acceptable safety under greenhouse conditions (Anastassiadou et al., 2022; Anastassiadou et al., 2020).

This fungus exhibits potent bio-control activity against a variety of plant pathogens. There are several cases of its antagonistic action against fungal pathogens. The strain *P. lilacinum* QLP12 and its fermentation broth showed a high inhibition activity on fungal mycelium growth of the eggplant pathogen *Verticillium dahliae* both in the greenhouse and the field (Lan et al., 2017). *P. lilacinum* and its culture filtrate can suppress the growth and secondary metabolism of the orange postharvest pathogen *Penicillium digitatum* (Elsherbiny et al., 2021).

Additionally, this fungus exhibits bio-control activity against pests. Virulence tests have shown that *P. lilacinum* PL-1 can inhibit *Myzus persicae* (green peach aphids) and *Spodoptera frugiperda* (Liu et al., 2022). Inoculations with 1×10^6 conidia ml^{-1} of *P. lilacinum* resulted in the death of 85.6% (80.6–89.7) of the *Acromyrmex lundii* (leaf-cutting ants) (Goffre & Folgarait, 2015). The endophytic colonization of tomato by *P. lilacinum* increased the mortality of *Bemisia tabaci* (whiteflies) and reduced the emergence of adults 35 days post-exposure compared to control plants (Sani et al., 2023). *P. lilacinum* TBRC 10638 demonstrated high efficacy against *Scirtothrips dorsalis* (Chili Thrips) in both greenhouse and field trials, achieving up to 80% control when applied at a concentration of 10^8 spores/mL (Panyasiri et al., 2022).

Its nematocidal properties are well-documented, demonstrating efficacy against a wide range of plant-parasitic nematodes in various economically significant crops. The inhibitory effects of *P. lilacinum* AUMC on *Meloidogyne incognita* were evaluated: the highest second-stage juvenile (J2) mortality rate of 97.6% and inhibited egg hatching by 79.8% after 72 hours of exposure (Isaac et al., 2021). Besides, *P. lilacinum* strain 251, a key formulation of many commercial bionematicides, has been found to infect *Globodera pallida* (potato cyst nematodes) (Mhatre et al., 2022). Furthermore, inoculation with *P. lilacinum* strain ESALQ2593 in greenhouse trials on *Phaseolus vulgaris* L. (common bean) seeds decreased the population of *Heterodera glycines* (Silva et al., 2022).

The mechanism underlying its nematode control involves the parasitization of nematode eggs (Xu et al., 2021). Microscopic observation revealed that *P. lilacinum* directly penetrated the eggs of *M. incognita*, making contact with the juveniles inside (Figure 1-1) (Khan & Tanaka, 2023).

Additionally, this fungus can damage cell membranes to suppress pathogen. The increase in relative conductivity in *P. digitatum* mycelia after exposure to the culture of *P. lilacinum* suggests that the integrity of the cell membrane of *P. digitatum* was compromised (Elsherbiny et al., 2021). The degradation of pathogens can be attributed to the production of enzymes that hydrolyze proteins and chitin (Fang et al., 2009). *P. lilacinum* was reported to produce both protease and chitinase (Barra et al., 2015; Girardi et al., 2022). In the previously mentioned case of antagonism against green peach aphids and fall armyworms, the chitinase-related genes were upregulated during the *P. lilacinum* PL-1 infection.

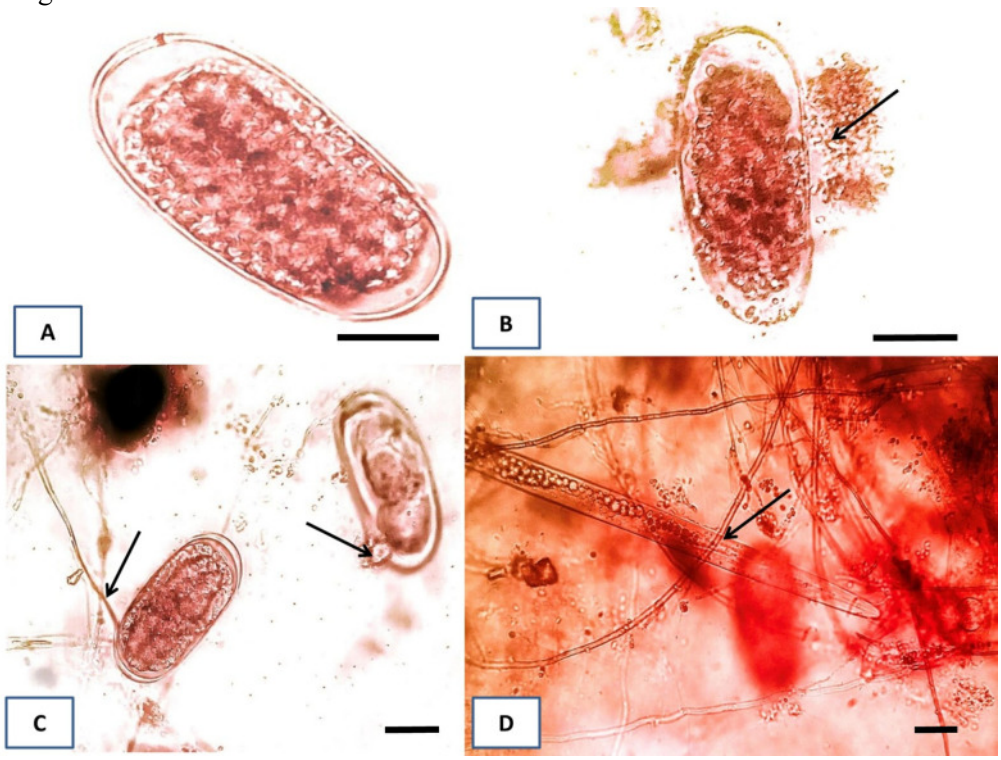

Figure 1-1: Direct effects of *P. lilacinum* on *M. incognita* eggs and juveniles. Microscopic observation was performed during the incubation of *P. lilacinum* with *M. incognita* eggs (B and C) and juveniles (D) on PDA agar plates. An intact egg was shown in (A). Arrows indicate penetration and aggregation of fungal conidia and mycelia in eggs (B and C) and attaching to a J2 juvenile (D). Scale bars = 50 µm (Khan & Tanaka, 2023).

The production of secondary metabolites known as leucinostatins is also recognized as a key bio-control mechanism (Figure1-2, Table 1-1) (Wang et al., 2016). These nanopeptides, assembled by nonribosomal peptide synthetases (NRPSs), exhibit broad-spectrum biological activities. Leucinostatin A (LeuA), leucinostatin B (LeuB), leucinostatin D (LeuD), leucinostatin H (LeuH), and leucinostatin K (LeuK) have been reported to be active against various fungi and Gram-positive bacteria (Fukushima et al., 1983; Radics et al., 1987; Rossi et al., 1987). These leucinostatins,

along with other members of the leucinostatin family, have also shown activity against gray mold *Botrytis cinerea* (Liu et al., 2020), plant pathogen *Phytophthora infestans* and *P. capsici* (Wang et al., 2016). Research has described the leucinostatins as nematicides and indicated that leucinostatins in *P. lilacinum* are indicators of nematicidal activity (Park et al., 2004). Beyond their agricultural applications, leucinostatins have also shown potential in inhibiting cancer cells and protozoa (Brand et al., 2021; Kawada et al., 2010; Kil et al., 2020).

The mode of action of leucinostatins primarily involves disrupting mitochondrial function, including the inhibition of ATP synthase and the destabilization of the inner mitochondrial membrane's permeability (Kawada et al., 2010; Niu et al., 2024).

Current structure–activity relationship (SAR) studies, based on chemical synthesis and structural modifications, have highlighted that the α-helical conformation, the hydrophobicity of the side chains, the hydroxyleucine at position 7, and the C-terminal amine are critical determinants of the biological activity of this class of compounds (Figure 1-2) (Brand et al., 2021; L. Rimle et al., 2025). Regarding the C-terminal amine, one study demonstrated that introducing a carboxylic acid at the C-terminus reduced the preferential cytotoxicity against cancer cells under glucose-deprived conditions by approximately tenfold (Momose et al., 2019). Another study showed a positive correlation between the basicity of the terminal amine and the biological activity of leucinostatins (Brand et al., 2021). Additional research found that modifications affecting the hydrophobicity of the C-terminal group also significantly influenced biological activity (Niu et al., 2024). These findings highlight the potential of C-terminal amine modification to enhance the biological activity of the compounds.

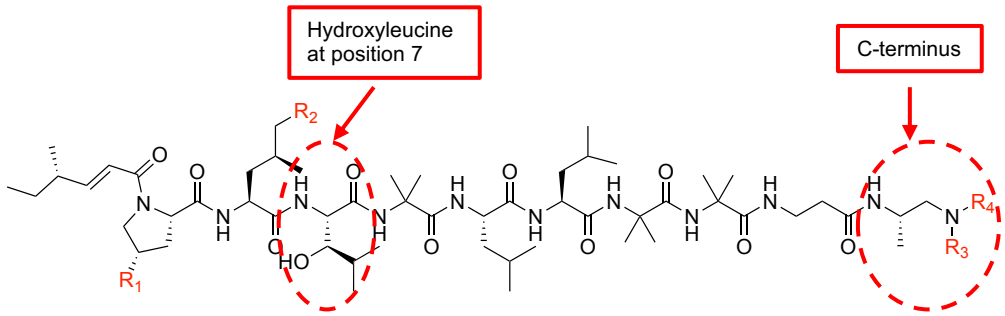

Figure 1-2: The molecular structure of leucinostatins. The hydroxyleucine residue at position 7 and the C-terminal part are indicated.

Table 1-1 : Structures and molecular weights of leucinostatins

Leucinosatain	**R1**	**R2**	**N (R3,R4)**	**$[M+H]^+$**
A	Me	$CH_3CH_2COCH_2(OH)CH$-	NMe_2	1218
B	Me	$CH_3CH_2COCH_2(OH)CH$-	NHMe	1204
C	Me	$CH_3CH_2COCH_2(OH)CH$-	NH_2	1190
D	Me	H	NMe_2	1118

F	Me	H	NHMe	1104
H	Me	H	$N(O)Me_2$	1134
K	Me	$CH_3CH_2COCH_2(OH)CH$-	$N(O)Me_2$	1234
A2	Me	$CH_3CH_2COCH{=}CH$-	NMe_2	1200
B2	Me	$CH_3CH_2COCH{=}CH$-	NHMe	1186
L	H	$CH_3CH_2COCH_2(OH)CH$-	NHMe	1190
M	Me	?	?	1220
N	Me	-OH	NHMe	1120
O	Me	$(C_{11}H_{17}O_3)$-	NMe_2	1314
P	Me	?	NMe_2	1214
Q	Me	$(C_{11}H_{17}O_3)$-	NHMe	1300
R	Me	$CH_3CH_2COCH_2CH_2$-	NMe_2	1202
S	Me	$CH_3CH_2CH(OH)CH_2CH_2$-	NMe_2	1204
T	H	H	NHMe	1090
U	Me	$CH_3CH_2COCH_2(OH)CH$-	NHMe	1218
V	H	$CH_3CH_2COCH_2(OH)CH$-	NMe_2	1204
W	Me	$(C_{10}H_{15}O_3)$-	NHMe	1286
X	H	?	?	1086
Z	Me	$CH_3CH_2COCH_2(OCH_3)CH$-	NMe_2	1232
I	H	Me	NMe_2	1104
II	H	H	NHMe	1120
III	H	$CH_3CH_2CH(OH)CH_2CH_2$-	NMe_2	1190
IV	Me	$CH_3CH_2CH(OH)CH_2CH_2$-	NHMe	1190
V	H	$CH_3CH_2COCH_2(OH)CH$-	NMe_2	1204

The biosynthetic gene cluster responsible for leucinostatin production has been identified in *P. lilacinum* PLBJ-1 (Figure 1-3, Table 1-2). Within this cluster, the NRPS gene lcsA and two transcription factors, *lcsL* and *lcsF*, have been functionally characterized (Jiao et al., 2019; Wang et al., 2016). In addition, genes encoding a putative polyketide synthase (*lcsC*), a putative ligase (*lcsD*), and a putative thioesterase (*lcsE*) have also been shown to be essential for leucinostatin biosynthesis. Based on gene knockout results and bioinformatic analyses, a putative biosynthetic pathway of leucinostatins in *P. lilacinum* PLBJ-1 was proposed. The process is initiated by the reducing polyketide synthase gene *lcsC*, which synthesizes the fatty acid side chain 4-methylhex-2-enoic acid. This intermediate is subsequently activated by the acyl-CoA ligase *lcsD* and transferred to the nonribosomal peptide synthetase *lcsA* via the thioesterase *lcsE*. The NRPS then assembles a linear peptide chain through sequential incorporation of amino acids. Finally, the peptide undergoes a series of tailoring modifications, resulting in the formation of mature leucinostatin compounds. Functionally, they demonstrated that the antagonistic activity of *P. lilacinum* PLBJ-1 against the oomycete plant pathogens Phytophthora infestans and *P. capsici* is dependent on leucinostatins (Wang et al., 2016). However, the roles of other genes within the cluster, as well as global regulatory factors in the fungus that may influence leucinostatin biosynthesis, remain largely unexplored.

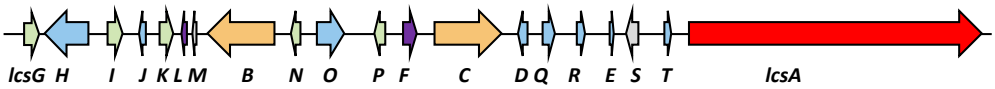

Figure 1-3: Schematic representation of the leucinostatin biosynthetic gene cluster in *P. lilacinum* PLBJ_1.

Table 1-1: Description of the genes in the leucinostatin biosynthetic cluster.

Gene ID	Name	Conserved domain	Predicted function	Functional Validation
VFPBJ_02521	*lcsG*	Methyltransf_2	O-methyltransferase	N-methyltrasnferase (This study)
VFPBJ_02522	*lcsH*	ABC_tran	ABC transporter	
VFPBJ_02523	*lcsI*	p450	Cytochrome P450	
VFPBJ_02524	*lcsJ*	4HBT_2	Thioesterase-like	
VFPBJ_02525	*lcsK*	p450	Cytochrome P450	
VFPBJ_11780	*lcsL*	bZIP	Transcriptional regulator	Transcriptional regulator (Jiao et al., 2019)
VFPBJ_02526	*lcsM*		Hypothetical protein	
VFPBJ_02527	*lcsB*	KS-AT-DH-MET-ER-KR	PKS	
VFPBJ_02528	*lcsN*	p450	Cytochrome P450	
VFPBJ_02529	*lcsO*	ABC1	ABC transporter	
VFPBJ_02530	*lcsP*	Aminotran_4	Aminotransferase	
VFPBJ_02531	*lcsF*		Transcriptional regulator	Transcriptional regulator (Wang et al., 2016)
VFPBJ_02532	*lcsC*	KS-AT-DH-MET-ER-KR-ACP	PKS	Deletion abolishes leucinostatin production (Wang et al., 2016)
VFPBJ_02533	*lcsD*	AMP-binding domain	Acyl-CoA ligase	Deletion abolishes leucinostatin

				production (Wang et al., 2016)
VFPBJ_11781	*lcsQ*	tRNA-synt_2c	tRNA synthetases	
VFPBJ_02534	*lcsR*	Lactamase_B	Zn-dependent hydrolases	
VFPBJ_02535	*lcsE*	Thioesterase	Thioesterase	Deletion abolishes leucinostatin production (Wang et al., 2016)
VFPBJ_02536	*lcsS*		Hypothetical protein	
VFPBJ_02538	*lcsT*	CC3_like_SDR_a	Epimerase	
VFPBJ_02539	*lcsA*	PCP-(C-A-PCP)*10-NAD	NRPS	Transcriptional regulator (Wang et al., 2016)
VFPBJ_02540	*lcsH*	ABC2_membrane	ABC transporter	

Leucinostatins are a class of nonribosomal peptides consisting of nine amino acid residues, including seven nonstandard and structurally unusual α-amino acids. Among these, the AHMOD residue (2-amino-6-hydroxy-4-methyl-8-oxodecanoic acid) poses a significant synthetic challenge due to its complex structure. The total synthesis of Leucinostatin D (LeuD), which lacks the AHMOD unit, was accomplished in 1992. In contrast, the total synthesis of Leucinostatin A (LeuA), which contains the AHMOD residue, was not achieved until 2017. This synthetic route involved multiple catalytic asymmetric transformations, making the large-scale synthesis of leucinostatin analogs technically demanding (Abe et al., 2017; Kuwata et al., 1992; Watanabe et al., 2021). Consequently, most studies on the biological activity of leucinostatins continue to rely on compounds isolated and purified from fungal fermentation broths or obtained from commercial sources (Brand et al., 2021; Niu et al., 2021; Niu et al., 2024; Lukas Rimle et al., 2025). Therefore, enhancing leucinostatin production through optimization of fermentation conditions or manipulation of fungal regulatory elements remains a critical strategy for enabling further pharmacological research and potential industrial applications. Regarding fermentation optimization, multiple studies have explored strategies to enhance *P. lilacinum* productivity. For instance, optimizing a basic mineral medium has been reported to maximize the production of keratinolytic protease (Cavello & Cavalitto, 2013). The use of wheat bran as a substrate in solid-state fermentation (SSF) has been shown to enhance the biomass production (Mousumi Das et al., 2020). Additionally, studies utilizing a combination of media formulations (Mascarin et al., 2015) have optimized the conditions for submerged liquid fermentation (SLF) to promote the microsclerotia formation (Silva et al., 2022). Furthermore, the spent mushroom

substrate has been used as a basal medium to formulate *P. lilacinum* granules, which were evaluated for their efficacy in controlling soybean cyst nematodes (Gao et al., 2023). Another study compared four different solid substrates—rice, rice seeds, corn, and wheat bran—to determine optimal SSF conditions for conidial production. However, to date, no research has focused on optimizing the fermentation conditions for leucinostatins production, and the key culture medium components required for their biosynthesis remain unknown.

Given the importance of leucinostatins in agriculture and other fields, this study aims to optimize both their bioactivity and yield. In **Chapter 3**, we investigate the function of the cluster-associated tailoring enzyme, the *N*-methyltransferase LcsG, and its role in modulating leucinostatin activity. In **Chapter 4**, we explore how environmental factors such as ambient pH and nitrogen content affect leucinostatin production. Furthermore, we identify two transcriptional regulators in *P. lilacinum* PLBJ-1—PlPacC, a pH-responsive regulator, and PlAreB, a nitrogen regulator—and characterize their influence on leucinostatin biosynthesis.

The detailed outline of the thesis is presented below：

Chapter 1: General introduction

Chapter 2: Thesis Objectives, hypothesis, and experimental design

Chapter 3 (Article 1): Characterization of a methyltransferase for iterative N-methylation at the leucinostatin termini in *Purpureocillium lilacinum* (This chapter demonstrates that a fungal NMT LcsG for the iterative terminal *N*-methylation of a family of NRPs, leucinostatins. Gene deletion results suggest that LcsG is essential for leucinostatins methylation. Results from in vitro assays and HRESI-MS-MS analysis reveal the methylation sites as NH_2, $NHCH_3$ and $N(CH_3)_2$ in the *C*-terminus of various leucinostatins. LcsG catalysis yields new lipopeptides, some of which demonstrate effective antibiotic properties against the human pathogen *Cryptococcus neoformans* and the plant pathogen *Phytophthora infestans*. Multiple sequence alignments and site-directed mutagenesis of LcsG indicate the presence of a highly conserved SAM-binding pocket, along with two possible active site residues (D368 and D395). Molecular dynamics simulations show that the targeted *N* can dock between these two residues. Thus, this study suggests a method for increasing the variety of natural bioactivity of NPRs and a possible catalytic mechanism underlying the *N*-methylation of NRPs.）

Li Z, Jiao Y, Ling J, Zhao J, Yang Y, Mao Z, Zhou K, Wang W, Xie B, Li Y. Commun Biol. 2024 Jun 22;7(1):757.

Chapter 4 (Article 2): The bio-control fungus *Purpureocillium lilacinum* PLBJ-1 produces leucinostatins, a class of nonribosomal peptides (NRPSs) with broad-spectrum antimicrobial activities. However, the molecular mechanisms underlying the optimization of culture conditions for leucinostatin production remain unexplored. Previous research showed that PLBJ-1 synthesizes leucinostatins more effectively in hand-made Potato Dextrose Broth (PDB-M) than in commercially available PDB (PDB-C). Elementary analysis of these two media indicated that difference in leucinostatin yield was correlated with variations in pH dynamics and nitrogen content.

Subsequent experiments under different initial pH and nitrogen levels confirmed that an alkaline environment and reduced nitrogen availability could enhance leucinostatin production. To investigate the regulators involved, CRISPR-Cas9-mediated gene disruptions were performed on the pH-responsive transcription factor PlPacC and the nitrogen regulator PlAreB. The disruption of either *PlPacC* or *PlAreB* resulted in a marked reduction in biomass and sporulation in *P. lilacinum* PLBJ-1. Specifically, *PlPacC* disruption impaired environmental pH regulation and significantly decreased leucinostatin production. In contrast, *PlAreB* disruption led to an increased leucinostatin yield. Overall, these findings demonstrate that environmental pH and nitrogen availability are the critical factors governing leucinostatin biosynthesis, acting through two key transcriptional regulators, PlPacC and PlAreB. This study lays a molecular foundation for future large-scale optimization of leucinostatin fermentation.

Chapter 5: General discussion

Chapter 6: Conclusion and perspective.

2. Literature Review

2.1. Biological control agents

Plant diseases are consistently harmful to the yield and quality ofglobal agricultural productivity, leading to an approximate annual yield loss ranging between 20% and 30% in five main crops (Savary et al., 2019). One of the most widely adopted strategies to control them is the use of chemical pesticides. The over-reliance on chemical pesticides poses significant environmental and health risks, including the contamination of water sources, soil degradation, and adverse effects on non-target species, leading to biodiversity loss (Pimentel et al., 1992). For sustainable development, greener alternatives or complements to chemical pesticides for controlling plant diseases are urgently needed. Biological control or bio-control is the use of living organisms to suppress the population density or impact of a specific pest organism, making it less abundant or less damaging than it would otherwise be (Alabouvette & Steinberg, 2006). Biological control agents (BCAs) offer a promising strategy to control plant diseases due to their potential to avoid the environmental and health risks associated with chemical residues.

2.1.1. Bacterial biological control agents

Numerous bacterial genera have been reported to have the capability to protect plants from fungal and bacterial pathogens, such as *Agrobacterium* spp., *Alcaligenes* spp., *Arthrobacter* spp., *Bacillus* spp., *Enterobacter* spp., *Erwinia* spp., *Pseudomonas* spp., *Rhizobium* spp., *Serratia* spp., *Stenotrophomonas* spp., *Streptomyces* spp., and *Xanthomonas* spp. (Bonaterra et al., 2022). Among these, *Bacillus* spp., *Pseudomonas* spp., and *Streptomyces* spp. are most extensively researched. To date, 21 bacterial-derived BCAs have been approved as biopesticides in the European Union, with 16 belonging to *Bacillus* spp., 2 to *Pseudomonas* spp., and 2 to *Streptomyces* spp (Table 1-3) (https://food.ec.europa.eu/plants/pesticides/eu-pesticides-database_en, accessed on 1 May 2025).

Table 1-2: Bacterial-Derived Bio-control Agents (BCAs) Approved as Biopesticides in the European Union (EU Pesticides Database, accessed 1 May 2025).

Genera	Strain	Target Pathogen	Host Plamt	Mode of action	Active Substance ID
Bacillus spp.	*B. amyloliquefaciens (*formerly *subtilis*) str. QST 713	*Fusarium* spp., *Pythium* spp., *Rhizoctonia* spp.	Potatoes, top fruit, stone fruit, soft fruit, herbs & ornamentals	B, I	1018
	B. amyloliquefaciens AH2	*Botrytis cinerea*	Grapes	C, B, I	1257
	B. amyloliquefaciens IT-45	*Phytophthora citrophtora*, *P. nicotianae* var parasitica	Orange, lemon, clementine	C, I	1333
	B. amyloliquefaciens strain FZB24	*Pseudoperonospora* spp., *P. infestans*, *B. cinerea*	Cucurbits, potatoes and grapevine	C, B, I	1197
	B.amyloliquefaciens strain MBI 600	*Fusarium* spp., *Pythium* spp., *Rhizoctonia* spp.	Cereals, soybeans, cotton, legumes	C	1198
	B. amyloliquefaciens subsp. plantarum D747	*Fusarium* spp., *Pythium* spp., *Rhizoctonia* spp.	Cereals, soybeans, cotton, legumes	C	1078
	B. subtilis strain IAB/BS03	*Fusarium* spp., *Pythium* spp., *Rhizoctonia* spp.	Wide range of crops and ornamentals	C	1278

Genera	Strain	Target Pathogen	Host Plamt	Mode of action	Active Substance ID
	B. thuringiensis subsp. Aizawai strain ABTS-1857	*Spodoptera* group of Lepidoptera; Cabbage moth (*Plutella xylostella*); Turkey moth caterpillars (*Chrysodeixis chalcites*).	Peppers, cucumbers, cabbages, lettuce	B	1269
	B. thuringiensis subsp. Aizawai strain GC-91	*Spodoptera* group of Lepidoptera	Vegetable, Fruit and others	B	1301
	B. thuringiensis subsp. Aizawai strains ABTS-1857, GC-91				431
	B. thuringiensis subsp. Israelensis (serotype H-14) strain AM65-52	Mosquito larvae, fungus gnats, blackfly larvae	Water environments, glasshouses, mushroom houses	B	861
	B. thuringiensis subsp. Kurstaki strain ABTS-351	European Grape Vine Moth (*Lobesia botrana*), European Grape Berry Moth (*Eupoecelia ambiguella*), Box moth	Grapes	B	1270

Genera	Strain	Target Pathogen	Host Plamt	Mode of action	Active Substance ID
		caterpillar (*Cydalima perspectalis*)			
	B. thuringiensis subsp. Kurstaki strain EG2348	European Grape Vine Moth (*L. botrana*), European Grape Berry Moth (*E. ambiguella)*	Grapes	B	1271
	B. thuringiensis subsp. Kurstaki strain PB 54	Fruit worms; Bollworms; Caterpillars	Tomatoes	B	1272
	B. thuringiensis subsp. Kurstaki strain SA 11	European Grape Vine Moth (*L. botrana*), European Grape Berry Moth (*E. ambiguella*)	Grapes	B	1273
	B. thuringiensis subsp. Kurstaki strain SA 12	European Grape Vine Moth (*L. botrana)*, European Grape Berry Moth (*E. ambiguella*)	Grapes	B	1463

Genera	Strain	Target Pathogen	Host Plamt	Mode of action	Active Substance ID
Pseudo monas spp.	*P. chlororaphis* strain MA342	Leaf stripe (*Drechslera graminea*), net blotch (*D. teres*), covered smut (*Ustilago hordeii*) in barley, stinking smut (*Tilletia caries)* & glume blotch (*Stagonospora nodorum*) in wheat.	Wheat, rye, triticale; carrot, peas	C	716
	Pseudomo nas sp. Strain DSMZ 13134	Soil-borne fungi	Potatoes	I	1084
Strepto myces spp.	*Streptomy ces lydicus* strain WYEC 108	*Fusarium* spp., *Alternaria* spp., *Pythium* spp., *Phytophthora* spp. and *Botyrtis* spp.	Glasshouse vegetables, turf, nursery crops and ornamentals	C, B	1081
	Streptomy ces strain K61 (formerly S. griseoviridis)	*Fusarium* spp., *Alternaria* spp., *Pythium* spp., *Phytophthora* spp. and *Botyrtis* spp.	Glasshouse vegetables, turf, nursery crops and ornamentals	C, B	1411
	P. nishizawae Pn1	*Heterodera schachtii*	Sugar beet	P	1309

Note: In the 'Mode of Action' column, 'B' represents bioactive metabolites, 'I' represents induced systemic resistance, 'C' represents competition for resources, and 'P' represents Parasitism. 'Active Substance ID' refers to the unique code used in the EU Pesticides Database to identify each approved substance.

Bacillus spp. could form endospores to resist adverse environment, making them promising candidates for the development of BCAs. They could produce various valuable bioactive compounds against pathogens, including ribosomally synthesized peptides bacteriocins and non-ribosomally synthesized cyclic lipopeptides (CLPs). For example, the circular bacteriocin amylocyclicin, produced by *B. amyloliquefaciens* FZB42*,* can strongly inhibit the growth of the bacterial canker disease pathogen *Clavibacter michiganensis* NCPPB382 (Scholz et al., 2014). CLPs, a large group of amphiphilic compounds, can be classified into surfactin, iturin and fengycin (Ongena & Jacques, 2008). For instance, surfactin and fengycin, produced by the *B. subtilis* strains BBG125, BBG131, and Bs2504, have shown possible ability in inducing plant resistance and thereby protecting wheat from pathogen *Zymoseptoria tritici* (Mejri et al., 2018; Theatre et al., 2021).

Pseudomonas spp. could act as BCA via competition for nutrients and niches. For example, by enriching competitive colonizers at the avocado root tips, *P. pseudoalcaligenes* strain AVO110 demonstrated a 45% reduction in *Rosellinia necatrix* infection (Pliego et al., 2007). These bacteria could produce various bioactive compounds to inhibit a wide range of pathogens, including phenazines (Morrison et al., 2017), phloroglucinols (Weller et al., 2007), dialkylresorcinols (Shi et al., 2020), pyoluteorin (Cui et al., 2023), pyrrolnitrin (Pellicciaro et al., 2022), and CLPs (Christiansen et al., 2020). In addition, they could also control plant diseases through induced systemic resistance. The CLP orfamide, derived from *Pseudomonas* spp., could trigger induced systemic resistance (ISR) responses in rice against *Cochliobolus miyabeanus* in rice (Ma et al., 2017).

Streptomycetes spp. exist in diverse environments from deep ocean to high mountain (Quinn et al., 2020). This characteristic enables them to colonize diverse environments as biological control agents. Their potential as BCAs is mainly attributed to their ability to generate a diverse array of bioactive compounds. The crude extract of *S. chrestomyceticus* STR-2 could inhibit *Magnaporthe oryzae* by reducing the mycelial growth (Rahila et al., 2023). The fermentation broth of *Streptomyces* sp. AN090126 was characterized with the ability of reducing tomato bacterial wilt caused by *Ralstonia solanacearum*, red pepper leaf spot caused by *X. euvesicatoria*, and creeping bentgrass dollar spot caused by *Sclerotinia homoeocarpa* (Le et al., 2022).

2.1.2. Fungal biological control agents

Fungi serve as BCAs mainly through the following mechanisms: competition for nutrients and space, mycoparasitism, production of bioactive metabolites, mycovirus-mediated cross-protection, and ISR (Ghorbanpour et al., 2018). Several fungi species, such as *Trichoderma* spp. (Harman et al., 2004), *Beauveria* spp. (Fernandez et al., 2023), *Metarhizium* spp. (Iwanicki et al., 2019), and *Purpureocillium lilacinum*

(Wang et al., 2016) have been extensively studied and applied in agriculture for their ability to control plant diseases. In the European Union, a total of 39 fungi have been officially approved for use as pesticides, of which 14 belong to *Trichoderma* spp.. Additionally, eight strains of Beauveria bassiana, one Metarhizium spp., and two strains of *P. lilacinum* have also been approved as pesticides (Table 1-4) (https://food.ec.europa.eu/plants/pesticides/eu-pesticides-database_en, accessed March 1, 2024).

Table 1-3: Fungal-Derived Bio-control Agents (BCAs) Approved as Biopesticides in the European Union (EU Pesticides Database, accessed 1 May 2025).

Genera	Strain	Target Pathogen	Host Plamt	Mode of action	Active Substance ID
Trichoderm spp.	*T. afroharzianum* (formerly *T. harzianum*) strain T-22	*Pythium*, *Rhizoctonia*, *Fusarium*, *Botrytis*	Vegetables, ornamentals, soybean, rice, sugarcane, maize	C, B	1403
	T. afroharzianum (formerly *T. harzianum*) strain T-22 and *atrobrunneum* (formerly *T. harzianum*) strain ITEM 908				169
	T. asperellum (formerly *T. harzianum)* strain ICC012	*Pythium*, *Rhizoctonia*, *Fusarium* spp.	Tomatoes, cucumbers	C	1396
	T. asperellum (formerly *T. harzianum*) strains ICC012, *T. asperellum* (formerly *T. viride*) T25 and *T. asperellum* (formerly *T. viride*) TV1				165

Genera	Strain	Target Pathogen	Host Plamt	Mode of action	Active Substance ID
	T. asperellum (formerly *T. viride*) strain T-25	*Pythium*, *Rhizoctonia*, *Fusarium* spp.	Tomatoes, Cucumbers, Peppers, Courgettes, Strawberry, Lettuce	C	1397
	T. asperellum (formerly *T. viride*) strain TV-1	*Pythium*, *Rhizoctonia*, *Fusarium* spp.	Tomatoes	C	1398
	T. asperellum strain T34	Fusarium wilt disease (caused by *F. oxysporium* f. Sp. Dianthi), damping-off and rot	Tomatoes, cucumbers, carnations.	C, parasitism	674
	T. atrobrunneum (formerly *T. harzianum*) strain ITEM 908	*Pythium*, *Rhizoctonia*, *Fusarium*, *Botrytis*	Tomatoes, cucumbers	C	1402
	T. atroviride (formerly *T. harzianum*) strain T11	*Pythium*, *Rhizoctonia*, *Fusarium*, *Botrytis*	Tomatoes, cucumbers	C	1298
	T. atroviride AGR2	*Sclerotinia sclerotiorum*	Oilseed rape	C, B, I	1231
	T. atroviride AT10	*Sclerotinia* spp.	Lettuce	C, B	1268
	T. atroviride strain I-1237	*Eutypa lata*	Vines, vegetable crops, top fruit	C, P	167
	T. atroviride strain SC1	*Phaeoacremonium aleophilum*, *E. lata,* also vine wood diseases	Vines	C	1205

Genera	Strain	Target Pathogen	Host Plamt	Mode of action	Active Substance ID
	T. gamsii (formerly *T. viride*) strain ICC080	*Rhizoctonia*, *Pythium*, *Armillaria*	Tomatoes, lettuc, vegetables, cereals, potatoes, citrus, soybean, sugarcane, grape	P, B	168
Beauveria spp.	*B. bassiana* strain 147	Palm borer *Paysandia archon*, red palm weevil *Rhynchophorus ferrugineus*	Ornamental palm trees	P	1183
	B. bassiana strain 203	Red palm weevil *R. ferrugineus*	Red palms	P	1336
	B. bassiana strain ATCC 74040	Whiteflies, thrips, aphids, capsids, crickets and other sucking insects	Vegetables, maize, ornamentals, cotton, turf, sugarcane, strawberries, tobacco	P	1275
	B. bassiana strain GHA	Whiteflies, thrips, aphids, capsids, crickets and other sucking insects	Vegetables, maize, ornamentals, cotton, turf, sugarcane, strawberries, tobacco	P	1339
	B. bassiana strain IMI389521	*Oryzaephilus surinamensis*, *Sitophilus granarius*, *Cryptolestes ferrugineus*	Post-harvest storage	P	1282

Genera	Strain	Target Pathogen	Host Plamt	Mode of action	Active Substance ID
	B. bassiana strain NPP111B005	Banana weevil *Cosmopolites sordidus*, red palm weevil *R. ferrugineus*	Banana trees and ornamental pines	P	1184
	B. bassiana strain PPRI 5339	Thrips; Whitefly; Potato tuber moth; Red spider mite; Mites	Glasshouse and field crops	P	1281
	B. bassiana strains ATCC 74040 and GHA				1215
Metarhizium spp.	*M. brunneum* strain Ma 43 (formerly *M. anisopliae* var anisopliae)	*Elateridae* and *Curculionidae* (scarabs and weevils)	Vines, maize, fruit, grassland, sports fields, glasshouses	P	1319
Purpureocillium spp.	*P. lilacinum* PL 11	Nematodes		P	1285
	P. lilacinum strain 251 (former *Paecilomyces lilacinus* strain 251)	Nematodes	vegetables, tomato, cucumber, potatoes, tropical & soft fruit, ornamentals, tobacco and cotton	P	864
Phlebiopsis spp.	*Phlebiopsis gigantea* strain FOC PG 410.3	*Heterobasidion annosum*	Pine and spruce trees	C	1294
	P. gigantea strain VRA 1835	*H. annosum*	Pine and spruce trees	C	1295
	P. gigantea strain VRA 1984	*H. annosum*	Pine and spruce trees	C	1296

Genera	Strain	Target Pathogen	Host Plamt	Mode of action	Active Substance ID
	Aureobasidium pullulans (strains DSM 14940 and DSM 14941)	*Erwinia amylovora*	Apples and pears and some other members of the Roasaceae family	C, I	417
	Candida oleophila strain O	Grey mold (*B. cinerea*) and blue mold (*Penicillium expansum*)	Top fruit	C	501
	Clonostachys rosea strain J1446 (*Gliocladium catenulatum* strain J1446)	*B. cinerea*, *Rhizoctonia* spp., *Pythium* spp.	Vegetables, herbs, ornamentals, turf and tree seedlings	P, B	766
	Coniothyrium minitans Strain CON/M/91-08 (DSM 9660)	*S.sclerotiorum*, *S. minor*	Oilseed rape, salads, strawberry, protected crops	P	569
	Isaria fumosorosea Apopka strain 97 (formerly *Paecilomyces fumosoroseus*)	Whiteflies, thrips, aphids, and spider mites.	Food and nonfood crops in greenhouses and on agricultural sites as approved.	P	938
	Metschnikowia fructicola strain NRRL Y-27328	*B. rot*	Grapes, soft and stone fruits	C, B	1306
	P. fumosoroseus strain Fe 9901	Aphids, thrips, mealybugs, leafhoppers, spidermites, weevils and grasshoppers	Ornamentals and food crops in glasshouses	P	939

Genera	Strain	Target Pathogen	Host Plamt	Mode of action	Active Substance ID
	Saccharomyces cerevisiae strain LAS02	*Monilinia fructigena*, *M. laxa*, *M. fructicola*, *Botrytis* spp., *B. cinerea*, *Alternaria* spp. *Neofabraea alba*, *Penicillium* spp.	Fruit	C	1196
	Verticillium albo-atrum (formerly *V. dahliae)* strain WCS850	Dutch Elm Disease	Elm trees	I	192

Note: In the 'Mode of Action' column, 'B' represents bioactive metabolites, 'I' represents induced systemic resistance, 'C' represents competition for resources, and 'P' represents Parasitism. 'Active Substance ID' refers to the unique code used in the EU Pesticides Database to identify each approved substance.

Among these beneficial fungi, *Trichoderma* spp. stands out due to their high adaptability, which enables them to colonize diverse environments (Chaverri et al., 2003). They function as BCAs mainly through parasitism, bioactive metabolites (including secondary metabolites, volatile organic compounds), competition for resources and ISR (Woo et al., 2023). The degradation of prey cell walls is a crucial step in mycoparasitism, and is facilitated by enzymes, such as chitinase, glycoside hydrolase, β-1,3-glucanases, chitosanases (Kubicek et al., 2011). *Trichoderma* spp. could produce abundant secondary metabolites, including terpenes, pyrones, polyketides (PKs), and non-ribosomal peptides (NRPs), that have antibiotic activity to against fungi (Rubio et al., 2009), oomycetes (Bae et al., 2016) and bacteria (Baazeem et al., 2021). VOCs produced by *Trichoderma* spp. could increase the efficacy of predators in parasitizing their pest targets (Contreras-Cornejo et al., 2018). *Trichoderma* spp. suppress the growth of pathogens by competing for nutrients (Sarrocco et al., 2009), dominating the rhizosphere (Guzmán-Guzmán et al., 2017), and colonizing plant tissues (Sarrocco et al., 2021). Additionally, *Trichoderma* spp. can protect plants from *Rhizoctonia solani* by boosting plant resistance (Leonetti et al., 2017).

B. bassiana, *Metarhizium anisopliae*, and *P. lilacinum* are entomopathogenic fungi that also act as antagonists to plant pathogens because of their ability to act as natural enemies of pathogens. *B. bassiana* and *M. anisopliae* are particularly effective BCAs because of their ability to synthesize abundant secondary metabolites that could inhibit different types of pathogens, including bacteria, fungi, and insects. These metabolites include bassianolides (Xu et al., 2009), bassianolone (Oller-López et al., 2005), beauvericin (Xu et al., 2007), oosporein (Feng et al., 2015), cytochalasins (Götz et al., 1997), destruxins (Odier et al., 1992), and serinocyclins (Krasnoff et al., 2007). In addition to the production of bioactive metabolites, these fungi can colonize

plants as endophytes, enhancing plant growth and providing further protection. The underlying mechanisms could be attributed to direct competition with pathogens and ISR (Ownley et al., 2008). While *P. lilacinum* has been reported to exhibit pathogenic effects on insects (Castillo Lopez et al., 2014; Liu et al., 2022), it is more widely recognized for its ability to parasitize plant-parasitic nematodes (A. Sharma et al., 2016). The bio-control capabilities and mechanisms of *P. lilacinum* will be elaborated upon in subsequent sections.

2.2. Fungi-derived agricultural beneficial molecules

Fungal secondary metabolites are classified into four main chemical classes: PKs, NRPs, terpenes, and indole alkaloids (Keller et al., 2005). In fungi, genes responsible for synthesizing secondary metabolites are organized into clusters within the genome, known as biosynthetic gene clusters (BGCs) (Figure 1-4).

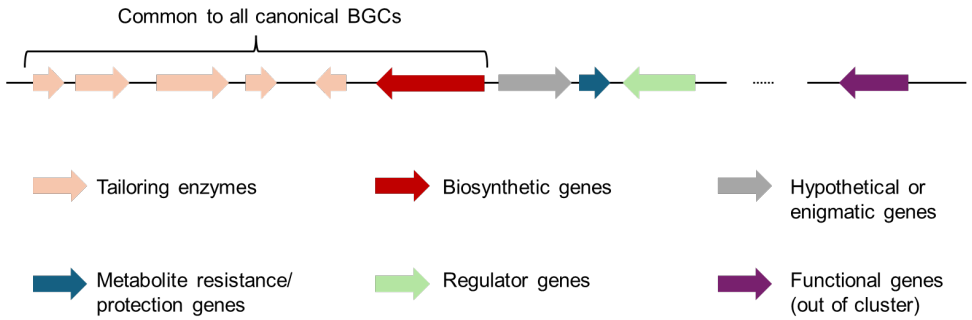

Figure 1-4: Schematic diagram of the biosynthetic gene cluster.

2.2.1. Nonribosomal peptides (NRPs)

Nonribosomal peptide synthetases (NRPSs) consist of three core domains: the adenylation (A) domain, the condensation (C) domain, and the peptidyl carrier protein (PCP) domain (Figure 1-5A). The A domain is responsible for substrate recognition and activation, the PCP domain covalently binds intermediates during synthesis, and the C domain catalyzes peptide bond formation. These domains are typically arranged in a C-A-PCP configuration (Keating & Walsh, 1999). Additional optional domains include the thioesterase (TE) domain, which terminates the elongation reaction. Du & Lou provided a detailed explanation of the mechanisms of both polyketide synthases (PKSs) and NRPSs. (Du & Lou, 2010) Furthermore, the epimerase (E) domain, cyclase (CYC) domain, methyltransferase (MT) domain, oxidase domain, reductase (KR) domain, and formylation domain modify amino acid substrates. These domains facilitate modifications such as isomerization, methylation, and acylation, resulting in a diverse array of amino acid substrates (Fischbach & Walsh, 2006).

B. bassiana is a facultative entomopathogen with a wide host range, playing a significant role in the natural regulation of insect populations. It produces the cyclooligomeric nonribosomal depsipeptides beauvericin, bassianolide, and beauverolides (Figure 1-5B) (Xu et al., 2008). The cyclic hexadepsipeptide beauvericin is used as an insecticide. The cyclic hexadepsipeptide beauvericin is used

as an insecticide and was first reported by Hamill et al. to exhibit inhibitory activity against *Artemia salina*, a model organism for studying insecticidal effects (Hamill et al., 1969). Moreover, beauvericin has demonstrated inhibitory effects against *Calliphora erythrocephala*, *Aedes aegypti* (Grove & Pople, 1980), *Lygus* spp. (Leland et al., 2005), *S. frugiperda* (fall armyworms) (Fornelli et al., 2004), and *Schizaphis graminum* (Ganassi et al., 2002). Besides, beauvericin also shows a strong antibacterial activity against various plant pathogens, the crown gall disease pathogen *A. tumefaciens*, the bacterial spot disease pathogen *X. vesicatoria* (Xu et al., 2010). The other cyclooligomeric depsipeptide product of *B. bassiana*, bassianolide, also shows insecticidal properties against *Galleria mellonella*, *S. exigua*, and *Helicoverpa zea* (Xu et al., 2009). As for the cyclic peptides beauverolides, they moderately act as insecticides against *S. litura* and *Callosobruchus chinensis* (Mochizuki et al., 2006).

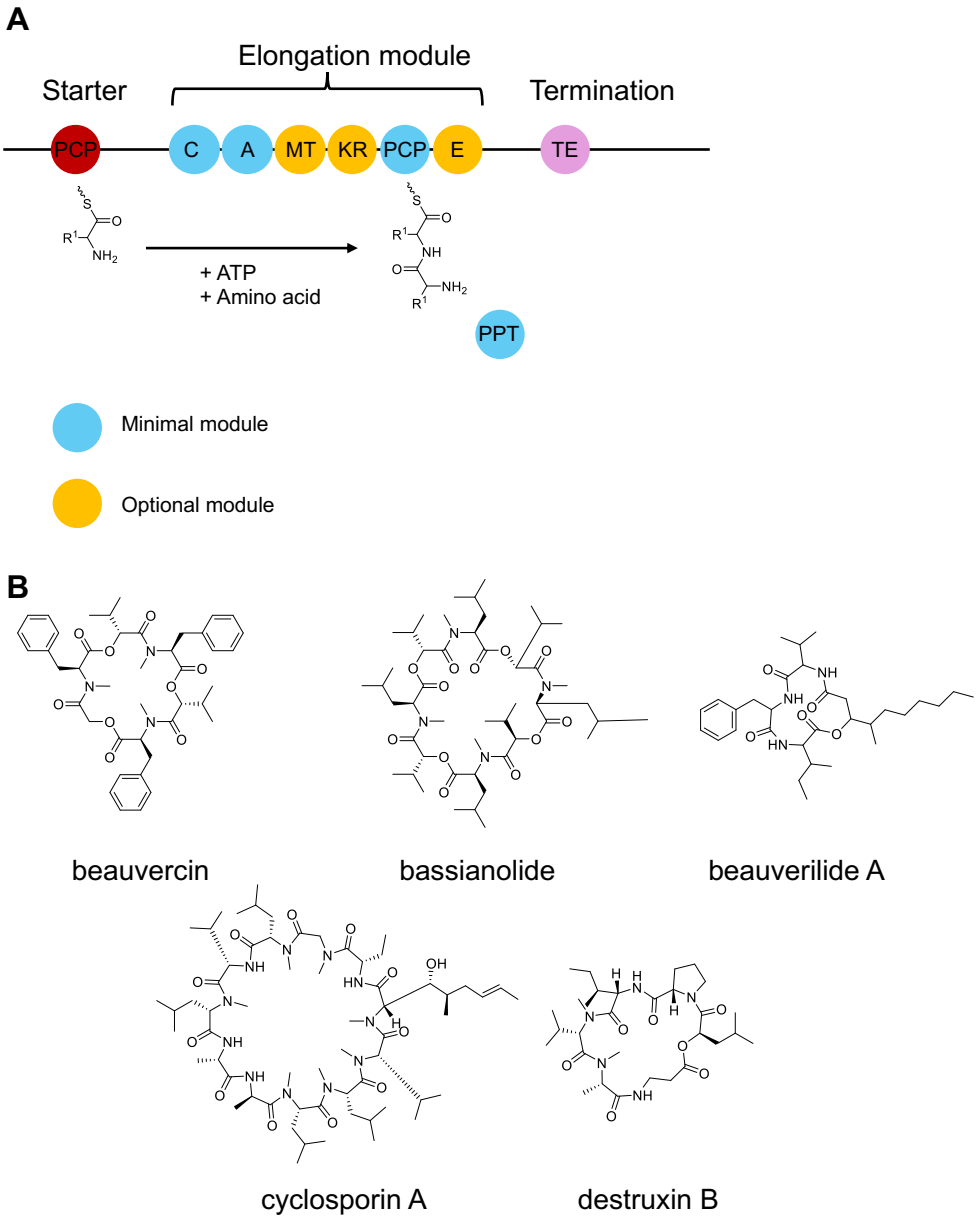

Figure 1-5: Schematic representation of nonribosomal peptide synthetase (NRPS) modules and structures of representative nonribosomal peptides (NRPs). (A) Overview of the modular organization in NRPS. C: condensation, A: adenylation, MT: methyltransferase, KR: ketoreductase, PCP: peptidyl carrier protein, E: epimerization, TE: thioesterase, PPT: Post-translational phosphopantetheinylation. (B) Chemical structures of representative NRPs.

The cyclopeptides cyclosporins are originally derived from *Tolypocladium inflatum* (Zhao et al., 1991). Cyclosporin A (CyA) (Figure 1-5B) and cyclosporin C (CyC) have a narrow spectrum of antifungal activity, such as against *Aspergillus* spp. (Schwarz & Dannaoui, 2020), and no antibacterial activity (Survase et al., 2011). It was shown that at a concentration of 200 mg/L, CsA almost completely inhibited the development of rot on grapes caused by *Aspergillus niger* in vivo (Li et al., 2023). CsA was also reported have the inhibitory affection against *H. armigera* (Wei et al., 2022), *Ostrinia furnacalis* Guenée (Lepidoptera: Pyralidae) (Sun, Li, Wang, Yin, et al., 2022), *S. frugiperda* (Sun, Li, Wang, Feng, et al., 2022).

Cyclic hexadepsipeptide destruxins (Dtxs) (Figure 1-5B) were isolated from entomopathogenic fungus *M. anisopliae* (the strain now reclassified as *M. robertsii*) (Liu et al., 2000). Bioassays show that Dtxs primarily impair insect immune function by altering Ca^{2+} balance in hemocytes and modifying the phosphorylation state of intracellular high-molecular-weight proteins, leading to immune cell apoptosis and weakened host immunity (Ruiz-Sanchez et al., 2010). Dtxs exhibit certain contact toxicity against nymphs of the whitefly (*B. tabaci*) while having minimal impact on its natural enemy, *Serangium japonicum* (Hu et al., 2009). Dtxs exhibit a wide range of biological and insecticidal activities. Destruxin B (DB) is particularly effective against *S. litura*, with an EC_{50} of 0.17 mg/mL (Rizwan-ul-Haq et al., 2009; Sree & Padmaja, 2008), and also shows insecticidal activity against *S. frugiperda* (Skrobek & Butt, 2005).

2.2.2. Other molecules

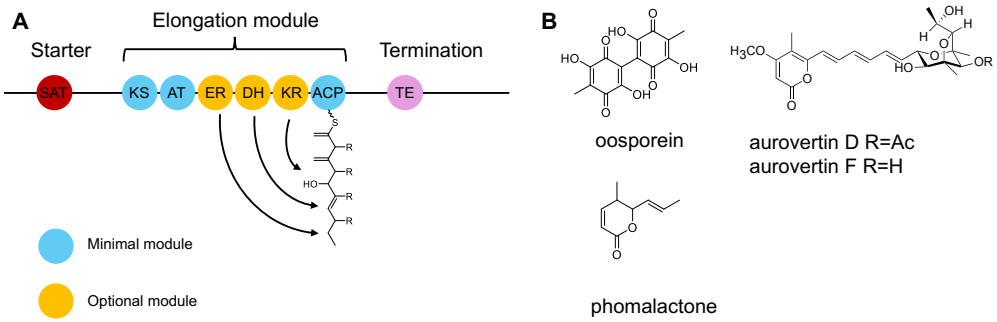

Figure 1-6: Schematic representation of polyketide synthase (PKS) modules and structures of representative polyketides (PKs). (A) Schematic diagram of the biosynthetic pathway for PKs. KS: etoacyl synthase, AT: acyltransferase, ER: enoyl reductase, DH: dehydratase, KR: ketoreductase ACP: acyl carrier protein. (B) Structures of representative PKs.

Polyketide synthases (PKSs) are modular enzymes comprising essential domains—KS for chain elongation, AT for acyl unit selection, and ACP for chain attachment—along with optional tailoring domains (e.g., DH, MT, ER, KR, TE/CYC) that modify and release the final product (Figure 1-6A) (Nguyen et al., 2008). Fungal PKSs use simple acyl-CoAs to synthesize diverse polyketide scaffolds through iterative condensation. Several polyketide-derived metabolites with demonstrated agricultural

potential include (Figure 1-6B): oosporein, an insecticidal compound; aurovertins D and F, which exhibit nematicidal activity against *Panagrellus redivivus*; and phomalactone which shows lethality toward *M. incognita* (Klingen et al., 2002; Labbe et al., 2006; Niu et al., 2010).

Fungal terpenoids identified include the sesqui-, di- and triterpenoids. They are typically biosynthesized via terpene synthases and cyclases, which build core scaffolds. Tailoring enzymes and transferases then modify these scaffolds to generate bioactive structures. Despite this diversity, all terpenoids are derived from the simple five-carbon precursor molecules dimethylallyl diphosphate (DMAPP) and isopentenyl diphosphate (IPP). In fungi, these two isomers are synthesized from acetyl-CoA through the mevalonate pathway (Miziorko, 2011). A representative terpenoid with agricultural potential is penifulvin A, which shows activity against Spodoptera frugiperda (Figure 1-7) (Shim et al., 2006).

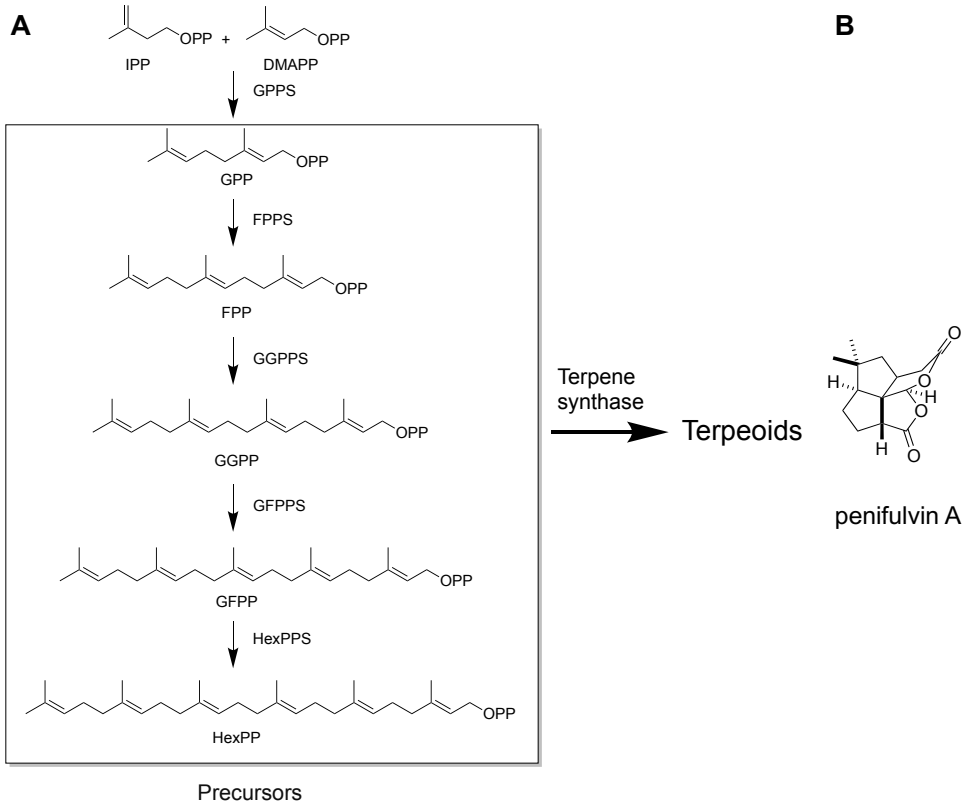

Figure 1-7: Terpenoid biosynthesis pathway and structure of penifulvin A. A) The biosynthetic pathway of terpenoids. Geranyl pyrophosphate (GPP), catalyzed by geranyl pyrophosphate synthase (GPPS); Farnesyl pyrophosphate (FPP), catalyzed by farnesyl pyrophosphate synthase (FPPS); Geranylgeranyl pyrophosphate (GGPP), catalyzed by geranylgeranyl pyrophosphate synthase (GGPPS); Geranylfarnesyl pyrophosphate (GFPP), catalyzed by geranylfarnesyl pyrophosphate synthase (GFPPS); Hexaprenyl pyrophosphate

(HexPP), catalyzed by hexaprenyl pyrophosphate synthase (HexPPS). B) The structure of penifulvin A.

Indole alkaloids are among the most extensive classes of nitrogen-containing secondary metabolites. Fungi, particularly ascomycetes, are widely known to produce indole alkaloids. These alkaloids are derived from prenylated tryptophan. The dimeric indole piperazine alkaloid campesines G exhibits inhibitory activity against the global honeybee pest *G. mellonella* (Figure 1-8) (He et al., 2024).

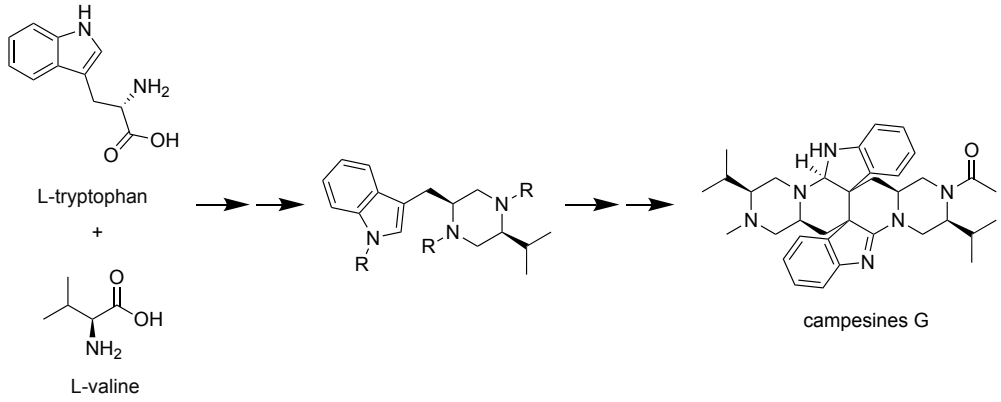

Figure 1-8: Biosynthesis pathway of campesines G.

In addition to the four main types of secondary metabolites, hybrid secondary metabolites exist, containing structural features from two or more of these categories. For example, tenuazonic acid (TeA), synthesized by an NRPS–PKS hybrid, inhibits *G. mellonella*, while indole-diterpenoids like penitrems A–D and F affect *Oncopeltus fasciatus* and *Ceratitis capitata* (Figure 1-9) (González et al., 2003; Yun et al., 2015).

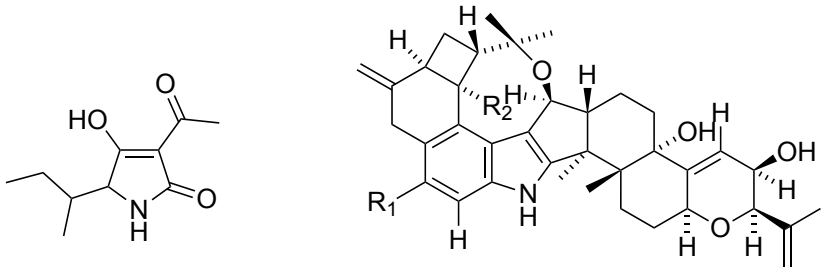

tenuazonic acid

penitrem A: R_1=Cl R_2=OH
penitrem B: R_1=H R_2=H
penitrem C: R_1=Cl R_2=H
penitrem D: R_1=H R_2=H
penitrem E: R_1=H R_2=OH
penitrem F: R_1=Cl R_2=H

Figure 1-9: Structures of tenuazonic acid and penitrems.

2.3. Fungal post-modifying enzymes

Core biosynthetic enzymes, such as PKS and NRPS, synthesize the core skeleton of fungal natural products. However, these compounds often require further modifications by tailoring enzymes to become biologically active. These tailoring enzymes are usually co-located with the core biosynthetic enzymes within the same gene cluster.

2.3.1. Glycosyltransferase

Glycosylation is a crucial and widespread biotransformant process to modulate the physicochemical and biological properties of natural products (Liang et al., 2015). It is related to the pharmacodynamics and pharmacokinetics of many clinically significant natural products, including vancomycin, erythromycin, and adriamycin (Chen, 2011; Fujita et al., 1986; Losey et al., 2001). The mechanism by which glycosylation influences molecular properties is largely attributed to the multiple hydroxyl groups provided by the sugar moiety. These hydroxyl groups can enhance the molecular interactions between drug-like compounds and their target proteins through non-covalent hydrogen bonds (Chen, 2011). Besides, glycosylation can significantly enhance the aqueous solubility of these molecules and facilitate their transport within and between cells (Chen, 2011; Liang et al., 2015).

Xie et al. reported a glycosyltransferase (GT) family from *B. bassiana* could produce glycosylated benzenediol lactones unprecedented in nature and enhance their cell line-specific antiproliferative activity or cancer cell–matrix attachment inhibitory activity (Xie et al., 2018). They also characterized a glycosyltransferase-methyltransferase derived from Hypocreales fungi substantially enhance the insecticidal activity against the larvae of oriental armyworm *Mythimna separata* (Walker) of kaempferol (Xie et al., 2019). Besides, there is another publication described a C-GT from *Epicoccum nigrum* could yield epipyon A (Figure 1-10), a

compound exhibiting 5.7-fold higher activity against *F. fujikuroi* compared to its unglycosylated form (Fan et al., 2024).

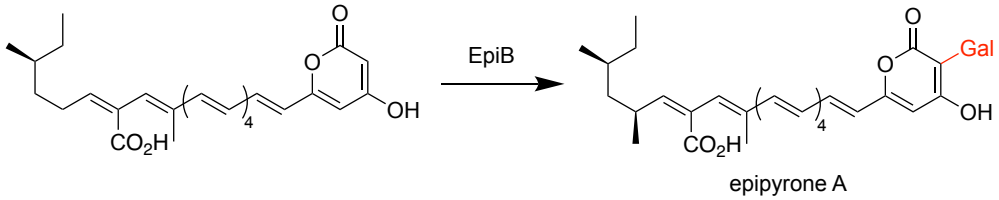

Figure 1-10: The glycosylation reaction catalyzed by the glycosyltransferase EpiB.

2.3.2. Acyltransferase

Acylation is a fundamental reaction in the formation of core frameworks of natural products, such as aromatic esters, macrolides, and antibiotics, which exhibit important biological activities, including antitumor, antiviral, and antibacterial properties.

Harzianum A, an antifungal trichothecene analog with an octa-2,4,6-trienedioyl acyl group, is produced by *T. arundinaceum*. Its biosynthesis requires two acyltransferases: TRI3, which catalyzes the 4-O-acetylation of trichodermol, and TRI18, which replaces the acetyl group with the octa-2,4,6-trienedioyl moiety to yield Harzianum A (Figure 1-11). Homologous genes of TRI18 have also been identified in other trichothecene-producing species, including *Fusarium* spp., indicating that acyltransferases play a crucial role in trichothecenes biosynthesis not only in biological control agents like *Trichoderma* spp. but also in pathogenic fungi (Lindo et al., 2019).

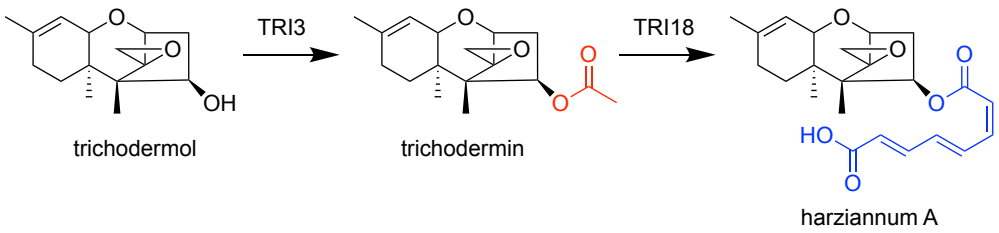

Figure 1-11: Two-step acylation reactions in the biosynthesis of harzianum A in Trichoderma arundinaceum. TRI3 catalyzes 4-O-acetylation of trichodermol to form trichodermin, and TRI18 subsequently replaces the acetyl group with an octa-2,4,6-trienedioyl moiety, yielding harzianum A.

Penicillin G acylase (PGA), a significant enzyme, was first discovered in *P. chrysogenum* Q176 (Sakaguchi & Murao, 1950). It is widely used in the pharmaceutical industry, particularly in the production of β-lactam antibiotics. PGA hydrolyzes penicillin G to produce 6-aminopenicillanic acid (6-APA), a key intermediate in β-lactam synthesis. In addition, it catalyzes the synthesis of novel semi-synthetic penicillins and cephalosporins by acylating intermediates such as 6-

APA, 7-aminocephalosporanic acid (7-ACA), or 7-amino-desacetoxycephalosporanic acid (7-ADCA) with new acyl groups (Figure 1-12) (Srirangan et al., 2013).

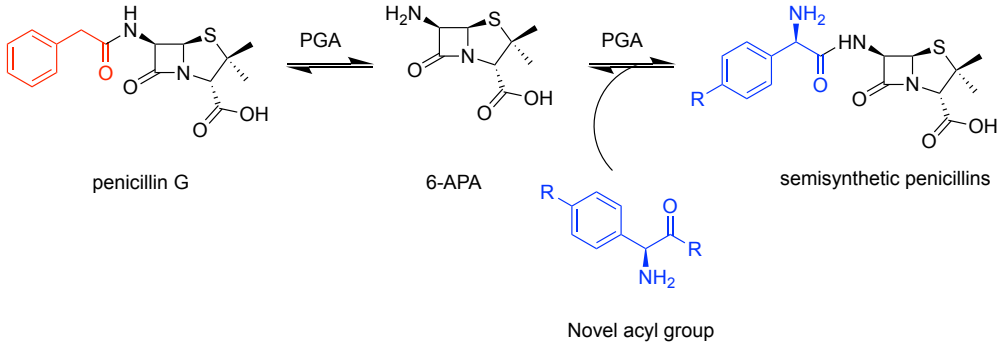

Figure 1-12: Deacylation and acylation reaction catalyzed by penicillin G acylase (PGA).

2.3.3. Oxidoreductases

Redox modifications can significantly enhance the structural complexity of natural products, improve their biological activity, and increase their water solubility. Redox modifications are mediated by various redox enzymes, such as cytochrome P450, α-ketoglutarate-dependent oxidases, and NAD(P)H/NAD(P)+ or flavin-dependent oxidoreductases. These enzyme-mediated chemical modifications, which may include the rearrangement of molecular scaffolds, significantly contribute to the structural diversity of natural products.

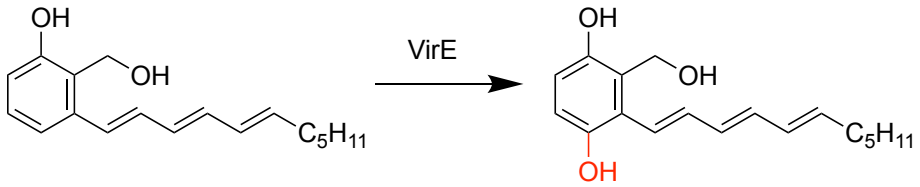

Figure 1-13: Hydroxylation reaction catalyzed by cytochrome P450 VirE.

Cytochrome P450 VirE (Figure 1-13) was characterized from the biosynthetic pathway of trichoxide in the bio-control fungus *T. virens*. It catalyzes the hydroxylation of the *p*-hydroxyl group onto the phenol substrate (Liu et al., 2019). MalC (Figure 1-14), identified from *Malbranchea aurantiaca*, is a bifunctional NADPH-dependent reductase/Diels-Alderase. It plays a crucial role in catalyzing the enantioselective cycloaddition reaction during the biosynthesis of the bicyclo[2.2.2]diazaoctane core of the anthelmintic compound paraherquamides (Dan et al., 2019).

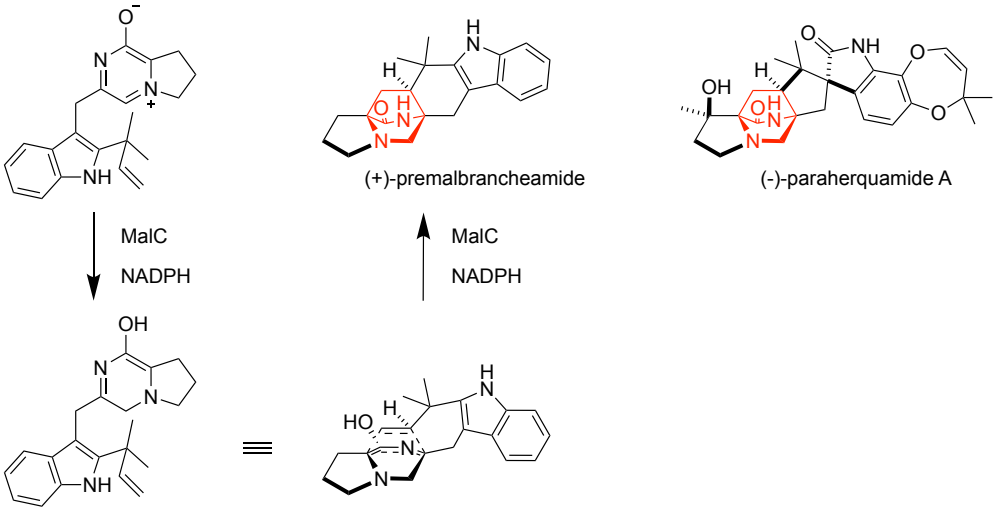

Figure 1-14: Biosynthesis of the bicyclo[2.2.2]diazaoctane core in paraherquamides catalyzed by the bifunctional NADPH-dependent reductase/Diels-Alderase MalC.

2.3.4. Methyltransferase

Methyltransferases play a pivotal role in the structural diversification and functional enhancement of fungal secondary metabolites. By introducing methyl groups at various atomic positions—most commonly at oxygen or nitrogen atoms—they profoundly enhance pharmacokinetic and physicochemical properties, including polarity, membrane permeability, and metabolic stability, thereby improving bioavailability and efficacy (Beck et al., 2012). In addition, they influence the biological activities of natural products, such as antimicrobial, antiparasitic, and insecticidal effects (Lee et al., 2013; Schwarzer et al., 2003; Velkov et al., 2011).

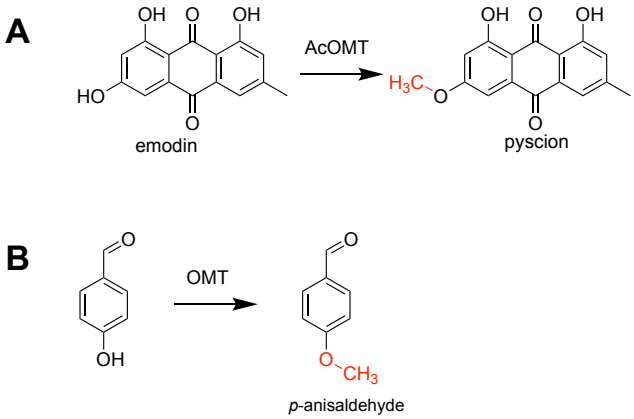

Figure 1-15: Catalytic reactions of two O-methyltransferases (OMTs). (A) The AcOMT catalyzes the transfer of a methyl group to the C-6 hydroxyl of emodin, producing physcion.

(B) An OMT mediates the formation of the flavor compound p-anisaldehyde through methylation.

The *O*-methyltransferase (OMT) from *A. chevalieri* can transfer a methyl group to the *C*-6 hydroxyl of emodin forming the plant-derived fungicide physcion (Figure 1-15A) (Yao et al., 2023). Likewise, an OMT from *Pleurotus sapidus* was confirmed to participate in the formation of flavor *p*-anisaldehyde, which exhibits lethal and repellent effects on *Musca domestica* (houseflies) (Figure 1-15B) (Brescia et al., 2024; Showler & Harlien, 2018).

N-methyltransferases (NMTs) typically function as a domain within NRPSs (Labby et al., 2015; Mori et al., 2018; Weckwerth et al., 2000; Xu et al., 2019), and their catalytic sites are usually located on the main chain peptide bonds or active side chains of NRPs. A few NMTs are known as freestanding enzymes that catalyze the methylation of NRPs. For instance, in the production of bioactive pentapeptides known as cycloaspeptides, the NRPS lacks NMT domains. Instead, an independent NMT is partnered with the NRPS to supply methylated substrates, preferentially incorporating methylated amino acids at two specific positions within the cycloaspeptides. However, there are few reports on the terminal *N*-methylation of NRPs (de Mattos-Shipley et al., 2018). The literature reviewed primarily focuses on single-site *N*-methylation within NRP structures. One study explores the *N*-methylation of the pipecolic acid moiety, which serves as the initial substrate for tubulysin synthesis (Figure 1-16). This methylation process is catalyzed by the NMT domain within the A-domain of its respective NRPS (Sandmann et al., 2004). To our knowledge, the termini of NRPs have never before been shown to undergo a discrete NMT-catalyzed iterative *N*-methylation.

These findings demonstrate the potential of methyltransferases as valuable tools for optimizing the activity of natural products used in the management of agricultural pests and diseases. Accordingly, they represent promising targets for both understanding fungal metabolite diversification and advancing synthetic biology strategies to boost compound efficacy.

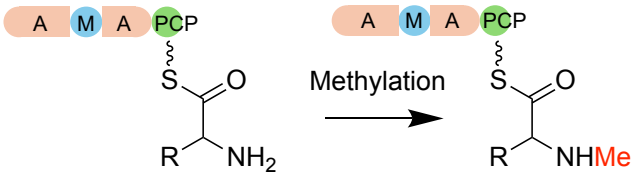

Figure 1-16: Methylation catalyzed by the NMT domain in tubulysin biosynthesis. A: A-domain, M: methylation domain, PCP: peptidyl carrier protein domain.

2.4. Fungal transcription factor

Transcription factors in fungi play an important role in controlling gene expression and metabolic activities. These factors regulate multiple signaling pathways by interacting with specific DNA sequences or transcription factors. They are crucial in processes such as growth, the secondary metabolism (including antibiotics and toxins),

and stress responses. Understanding the mechanisms of these transcription factors is crucial for the development of antifungal agents, improving industrial fermentation efficiency, and managing fungal infections.

2.4.1. Light-responsive regulator

LaeA and velvet proteins are key global transcription factors generally regulated by light (Yu et al., 2023). LaeA is a nuclear protein widely present in filamentous fungi. It was first reported in *Aspergillus* spp. (Bok & Keller, 2004). The velvet protein, synthesized by the *veA* gene, acts as a negative regulator of asexual development and antibiotic production in fungi. Light exposure prevents its entry into the nucleus. VeA is mainly expressed in darkness. During sexual development, it binds to VelB and enters the nucleus. There, it interacts with LaeA to form the VelB/VeA/LaeA *velvet* complex (Bayram et al., 2008).

As a global regulator, LaeA influences fungal primary metabolism and seconday metabolism. LaeA, as an epigenetic modifier and methyltransferase, indirectly modulates the expression of secondary metabolite genes through chromatin remodeling in fungi (Zhang et al., 2024). It has been reported to regulate colony morphology and spore development in various filamentous fungi, including *A. fumigatus* (Bok et al., 2005), *P. chrysogenum* (Kosalková et al., 2009), *T. atroviride* (Karimi Aghcheh et al., 2013), and so on. Besides, LaeA has been shown to affect fungal virulence (Bok et al., 2005; Karimi Aghcheh et al., 2013). In *Aspergillus* spp., deletion of LaeA blocks the production of secondary metabolites such as sterigmatocystin and penicillin G in *A. nidulans*, gliotoxin and endocrocin in *A. fumigatus*, and lovastatin in *A. terreus*. Additionally, this study found that LaeA primarily regulates the synthesis of secondary metabolites in *Aspergillus* spp., with a relatively minor impact on fungal morphological development (Bok & Keller, 2004). Subsequently, researchers identified LaeA homologs in other filamentous fungi beyond *Aspergillus* spp., which also regulate secondary metabolite production. This includes the regulation of penicillin biosynthesis in the industrially relevant *P. chrysogenum* and toxin production in the plant pathogen *F. fujikuroi* (Hoff et al., 2010; Wiemann et al., 2010). Moreover, LaeA was found to positively regulate conidiation in *P. chrysogenum* (Hoff et al., 2010).

The velvet protein VeA plays a critical role in red light-induced conidiation (Mooney & Yager, 1990). It impacts on the growth, development, and morphological changes of fungal strains. For instance, the lack of VeA in *A. parasiticus* could result in the blockage of sclerotial formation. (Calvo et al., 2004) The deletion of VeA in *A. cristatus* leads to the increase of conidial production and the reduction of sexual sporulation (Tan et al., 2018). Subsequent studies found that VeA also affects the production of secondary metabolites in fungi. Deletion of VeA in *A. nidulans* results in the loss of sterigmatocystin and penicillin production (Kato et al., 2003).

2.4.2. Nitrogen regulator

In all studied fungal species, the GATA transcription factor AreA and its co-repressor Nmr play central roles in the nitrogen regulation network. AreA transcription factor functions mainly as a positive regulator of nitrogen metabolism,

activating the expression of genes involved in utilizing secondary nitrogen sources under nitrogen-limiting conditions (Tollervey & Arst, 1982). Additionally, the GATA family transcription factor AreB also participates in this regulatory network. There is an interaction between AreA and AreB: AreA and AreB can regulate certaib genes cooperatively, while also independently controlling other genes. Unlike in other fungi, where AreB acts as a negative regulator or a competing factor to AreA (Wong et al., 2009), AreB is not only a potential negative regulator of nitrogen catabolism but also functions as both a repressor and activator of gene transcription in *F. fujikuroi* (Michielse et al., 2014).

Among these nitrogen metabolism-related regulators, AreA was the most studied. AreA and its orthologs were reported to be needed by the full virulence of some pathogens. The disruption of the AreA homolog Fnr1 in *F. oxysporum* significantly delayed its infection rate of tomato seedlings, compared to the wild type (Divon et al., 2006). The Δ*areA* mutant strain of *Gibberella zeae* exhibited a markedly reduced ability to cause disease on wheat heads in comparison to the wild-type strain (Min et al., 2012). Following the injection of *B. bassiana AreA* knockdown mutants into *G. mellonella* larvae for 36 hours, hyphal growth of the mutants was nearly eliminated. Compared to the wild-type strain after 36 hours of infection, overall fungal growth in the hemocoel of the mutants decreased by 20% (Luo et al., 2023). However, in the study by Wang et al., deletion of the *AwAreA* gene in *A. westerdijkiae* led to increased infectivity towards pear, salted meat, and cheese (Wang et al., 2022). In addition to regulating the use and metabolization of non-preferred nitrogen sources and virulence, AreA also influences secondary metabolism in fungi. Kim et al. proved AreA is necessary for the biosynthesis of fumonisin B1 in *F. verticillioides* (Kim & Woloshuk, 2008). In *G. zeae*, the *areA* knock-out of reduced the yield of trichothecene but did not influence that of zearalenone (Min et al., 2012). The disruption of *AwAreA* could impact yield of chratoxin A in *A. westerdijkiae* (Wang et al., 2022). In the case of *B. bassiana*, the knockdown of *AreA* resulted in more production of oosporein and the production of yellow pigments (Luo et al., 2023).

2.4.3. pH-responsive regulator

Environmental pH is one of the important physiological factors influencing the growth and development, stress response, secondary metabolism and pathogenicity of fungi (Luo et al., 2017). For filamentous fungi, PacC is a conserved pH-specific genetic regulator which first reported in *A. nidulans* (Prusky & Yakoby, 2003). PacC acts through a signaling pathway composed of six pal gens (palA, palB, palC, palF, palH and palI), which was usually called PacC/Pal pathways (Penalva et al., 2008). When the ambient pH changes from neutral to alkaline, the activation of the full-length form of *A. nidulans* PacC (72-kD $PacC^{72}$) would undergo two successive proteolytic cleavages to yield $PacC^{53}$ and $PacC^{27}$ (Orejas et al., 1995). 7-transmembrane domain (TMD) protein PalH, 3-TMD protein PalI, and the arrestin-like protein PalF constitute a plasma membrane complex participating in the ambient pH signal transition. PalI assists in the plasma membrane localization of PalH (Calcagno-Pizarelli et al., 2007), and both act as putative pH sensors. PalF becomes multiply ubiquitylated and phosphorylated in an alkaline ambient pH after binding to

PalH. PalA, PalB, and PalC function downstream of the ubiquitylation and phosphorylation of PalF (Penalva et al., 2008). The ubiquitylated PalF strongly interacts with the endosomal sorting complex required for transcript (ESCRT) I component (Vps23), and recruit Vps23 to the plasma membrane, linking the ESCRT machinery to the receptor–arrestin complex. PalA and PalC are subsequently recruited to plasma membrane by Vps32/Vps20 (ESCRT-III components). The signaling protease PalB is recruited and possibly activated by Vps24 (ESCRT-III components) and mediated the generation of PacC53 from PacC72. PacC53 is further removed ~245 residues to generate PacC, the active form that suppresses the expression of acidic genes while promoting the expression of alkaline genes. As a global regulator, PacC can control many cellular metabolisms, including fungal development, pathogenicity, and secondary metabolite production.

Chapter 2

Thesis Objectives, hypothesis, and experimental design

1. Objective

Among the various bio-control agents, *Purpureocillium lilacinum* has emerged as a highly promising fungus in agriculture for combating plant pathogens. Its secondary metabolite, particularly leucinostatin, has attracted significant attention due to its close association with bio-control activity.

Previous structure–activity relationship (SAR) studies have indicated the importance of the C-terminal structure in determining the biological activity of leucinostatins. Chemical profiling of *P. lilacinum* strain PLBJ-1 revealed that its four major leucinostatins (LeuA, LeuB, LeuC, LeuK0) differ in the degree of C-terminal methylation, a modification known to influence bioactivity. Genome analysis of *P. lilacinum* PLBJ-1identified a putative methyltransferase, LcsG, embedded within the leucinostatin biosynthetic gene cluster. In this study, we aimed to determine whether LcsG is responsible for the C-terminal methylation of leucinostatins and whether this methylation modulates their biological activity. The minimum inhibitory concentration (MIC) against *Cryptococcus neoformans* H99 was used as the primary indicator of bioactivity.

For further application and development of leucinostatins, enhancing their production is essential. However, no studies to date have explicitly focused on optimizing the culture conditions of P. lilacinum PLBJ-1 to improve leucinostatin yield. Therefore, we aim to identify the key environmental and regulatory factors that influence leucinostatin biosynthesis, elucidate their underlying molecular mechanisms, and apply this knowledge to enhance production efficiency. The relative peak areas of four major leucinostatins in fermentation broth, quantified via LC-MS analysis, were used as the metric for evaluating production yield.

This work aims to enhance the utility of leucinostatin in sustainable agriculture by strategically optimizing both activity and yield.

2. Hypothesis

1. We hypothesize that methyltransferase LcsG, located within the leucinostatin biosynthetic gene cluster, catalyzes C-terminal methylation of leucinostatins and regulates the bioactivity of this compound.
2. We hypothesize that the culture conditions of *P. lilacinum* significantly influence the yield of leucinostatin.

3. Experimental design

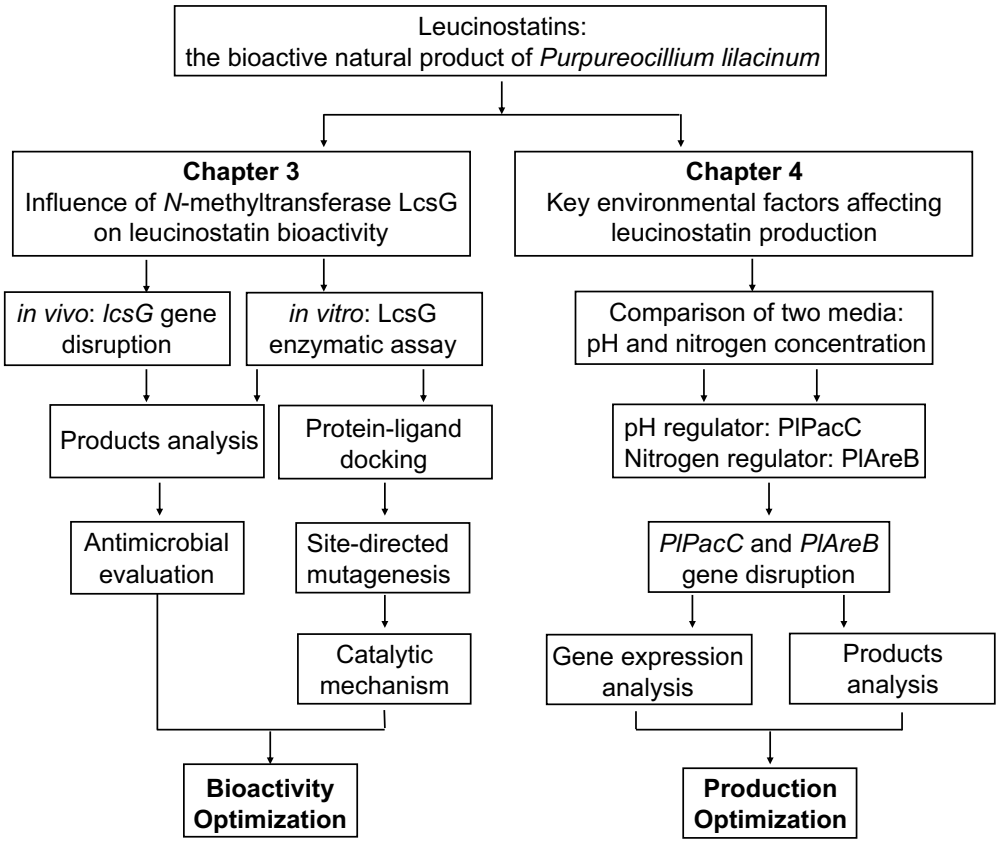

Figure 2-1: Technical route of this research.

Chapter 3

Characterization of a methyltransferase for iterative *N*-methylation at the leucinostatin termini in *Purpureocillium lilacinum*

Adapted from:

Li Z#, Jiao Y#, Ling J, Zhao J, Yang Y, Mao Z, Zhou K, Wang W, Xie B, Li Y. Characterization of a methyltransferase for iterative *N*-methylation at the leucinostatin termini in *Purpureocillium lilacinum*. **Commun Biol.** 2024 Jun 22;7(1):757.

Author Contribution:

Li Z: Conceptualization, Methodology (protein purification, fungal fermentation, compounds isolation, structure elucidation, LC-MS analysis, in vivo genetic and in vitro biochemical experiments), Software, Writing – original draft, Writing – review & editing

Jiao Y: Methodology (gene disruption, LC-MS analysis, assisted in protein purification and in vitro biochemical experiments)

Ling J and Zhao J: Methodology (genomic analysis)

Mao Z and Yang Y: Resources (strains for the test of antimicrobial activity)

Zhou K: Methodology (assisted in structure elucidation and chemical synthesis)

Wang W: Methodology (LC-MS analysis and LC-HRESI-MS-MS analysis)

Li Y and Xie B: Conceptualization, Funding acquisition, Writing – review & editing

1. Abstract

N-methyltransferase (NMT)-catalyzed methylation at the termini of nonribosomal peptides (NRPs) has rarely been reported. Here, we discover a fungal NMT LcsG for the iterative terminal *N*-methylation of a family of NRPs, leucinostatins. Gene deletion results suggest that LcsG is essential for leucinostatins methylation. Results from in vitro assays and HRESI-MS-MS analysis reveal the methylation sites as NH_2, $NHCH_3$ and $N(CH_3)_2$ in the C-terminus of various leucinostatins. LcsG catalysis yields new lipopeptides, some of which demonstrate effective antibiotic properties against the human pathogen *Cryptococcus neoformans* and the plant pathogen *Phytophthora infestans*. Multiple sequence alignments and site-directed mutagenesis of LcsG indicate the presence of a highly conserved SAM-binding pocket, along with two possible active site residues (D368 and D395). Molecular dynamics simulations show that the targeted N can dock between these two residues. Thus, this study suggests a method for increasing the variety of natural bioactivity of NPRs and a possible catalytic mechanism underlying the *N*-methylation of NRPs.

2. Introduction

Nonribosomal peptides (NRPs), such as the antifungal agent echinocandins (Cacho et al., 2012), the immunosuppressant cyclosporines (Bills et al., 2014; Yang et al., 2018), and the insecticide bassianolide (Xu et al., 2008), are a class of natural products with considerable biological and pharmaceutical potential. One common structural modification in these molecules is *N*-methylation. *N*-methylations contribute substantially to the properties of NRPs by modifying their structures (Beck et al., 2012) and influencing their bioactivities (Lee et al., 2013; Schwarzer et al., 2003; Velkov et al., 2011). For example, the anthelmintic activities of cyclooctadepsipeptides with increased lipophilicity result from the introduction of homologous *N*-alkyl groups, which depend strongly on their nature of the *N*-methyl amino acid (Scherkenbeck et al., 1998). *N*-methylation of cyclosporin A may help increase oral availability (Räder et al., 2018) and stabilize the main conformation (Velkov et al., 2011).

N-methyltransferases (NMTs) typically function as a domain within nonribosomal peptide synthetases (NRPSs) (Labby et al., 2015; Mori et al., 2018; Weckwerth et al., 2000; Xu et al., 2019), and their catalytic sites are usually located on the main chain peptide bonds or active side chains of NRPs. A few NMTs are known as freestanding enzymes that catalyze the methylation of NRPs. For instance, in the production of bioactive pentapeptides known as cycloaspeptides, the NRPS lacks NMT domains. Instead, an independent NMT is partnered with the NRPS to supply methylated substrates, preferentially incorporating methylated amino acids at two specific positions within the cycloaspeptides. However, there are few reports on the terminal *N*-methylation of NRPs (de Mattos-Shipley et al., 2018). The literature reviewed primarily focuses on single-site *N*-methylation within NRP structures. One study explores the *N*-methylation of the pipecolic acid moiety, which serves as the initial substrate for tubulysin synthesis. This methylation process is catalyzed by the NMT domain within the A-domain of its respective NRPS (Sandmann et al., 2004). To our

knowledge, the termini of NRPs have never before been shown to undergo a discrete NMT-catalyzed iterative *N*-methylation.

Leucinostatins are a family of lipopeptide antibiotics, derived from *Purpureocillium lilacinum* (Arai et al., 1973). They exhibit a wide range of biological activities that affect multiple pathogens. (Fukushima et al., 1983). Furthermore, leucinostatins have been studied as potential anticancer agents and potent antiprotozoal agents (Brand et al., 2021; Kawada et al., 2010; Kil et al., 2020), and their bioactivities inhibit mitochondrial function (Momose et al., 2019; Shima et al., 1990). At least 24 leucinostatin homologs have been isolated and characterized (Martinez & Moraes, 2015). Their backbone chains are assembled by an NRPS with nine amino acids and an atypical amino moiety at the C-terminus, linked by peptide linkages (Isogai et al., 1992). The C-termini of leucinostatins are methylated to varying degrees. Specifically, the C-terminus of leucinostatin C (**1**, LeuC) is propane-1,2-diamine (PD), while those of leucinostatin B (**2**, LeuB) and leucinostatin A (**3**, LeuA) are protected by *N*-methylpropane-1,2-diamine (MPD), and N_1,N_1-dimethylpropane-1,2-diamine (DMPD), respectively (Figure 3-1A). However, the biosynthetic mechanisms involved in the generation of diverse C-termini remain unknown.

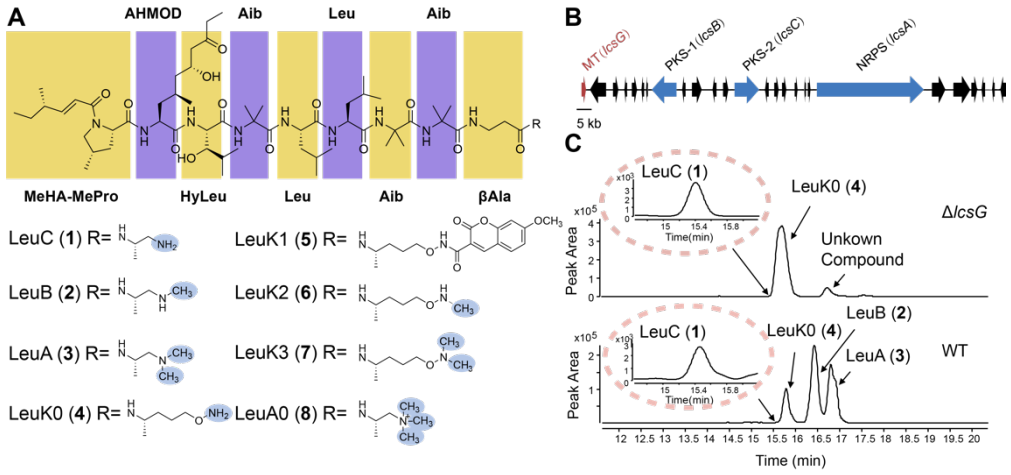

Figure 3-1: Identification of the predicted methyltransferase LcsG. (A) Structures of leucinostatins (1-8). MeHA: methylhex-2-enoic acid; MePro: 4-methyl-proline; AHMOD: 2-amino-6-hydroxy-4-methyl-8-oxodecanoic acid; HyLeu: hydroxyleucine; Aib: aminoisobutyric acid; Leu: leucine; βAla: β-alanine. (B) Genetic organization of the leucinostatin BGC in *P. lilacinum* PLBJ-1. MT: methyltransferase; PKS: polyketide synthase; NRPS: nonribosomal peptide synthetase. (C) LC–MS analysis of the lcsG knockout (ΔlcsG) mutant and the wild-type (WT) strain. Extracted ion chromatograms (EICs) were obtained for m/z 1190.8 ± 0.5 (LeuC (**1**)), 1204.8 ± 0.5 (LeuB (**2**)), 1218.8 ± 0.5 (LeuA(**3**)), and 1234.8 ± 0.5 (LeuK0 (**4**)) in positive ionization mode.

In this work, we identify a discrete NMT, LcsG, from the biological control fungus *Purpureocillium lilacinum* PLBJ-1 that catalyzes the incorporation of a unique moiety located at the terminus of an NRP (Wang et al., 2016). Deleting the *lcsG* gene led to

the disappearance of leucinostatins with methylated terminus. Subsequent in vitro enzyme activity assays and structural elucidation of the products demonstrated that LcsG is involved in the iterative methylation of terminal-free amines in leucinostatins. Moreover, structure–function relationship analysis provided a probable insight into the catalytic mechanism of LcsG. Additionally, we obtained new leucinostatins from the LcsG-catalyzed reaction, that can inhibit the growth of the human pathogen *Cryptococcus neoformans* and the plant pathogen *Phytophthora infestans*.

3. Results

3.1. Identification of LcsG from Purpureocillium lilacinum

Our previous studies demonstrated that the *P. lilacinum* PLBJ-1 strain harbors the leucinostatin biosynthesis-related gene cluster (BGC), and the *lcsG* gene, which was predicted to function as a methyltransferase attracted our interest (Figure 3-1B) (Wang et al., 2016). LcsG is equipped with the Methyltransf_2 domain, which is commonly found in *O*-methyltransferases (OMTs). The top hit in its pBLAST search shared 31.65% sequence identity with an OMT called VdtC (A0A443HJY8.1) (Urquhart et al., 2019). However, despite this prediction, we did not find any *O*-methylated units in leucinostatins. This inconsistency prompted us to investigate the function of LcsG.

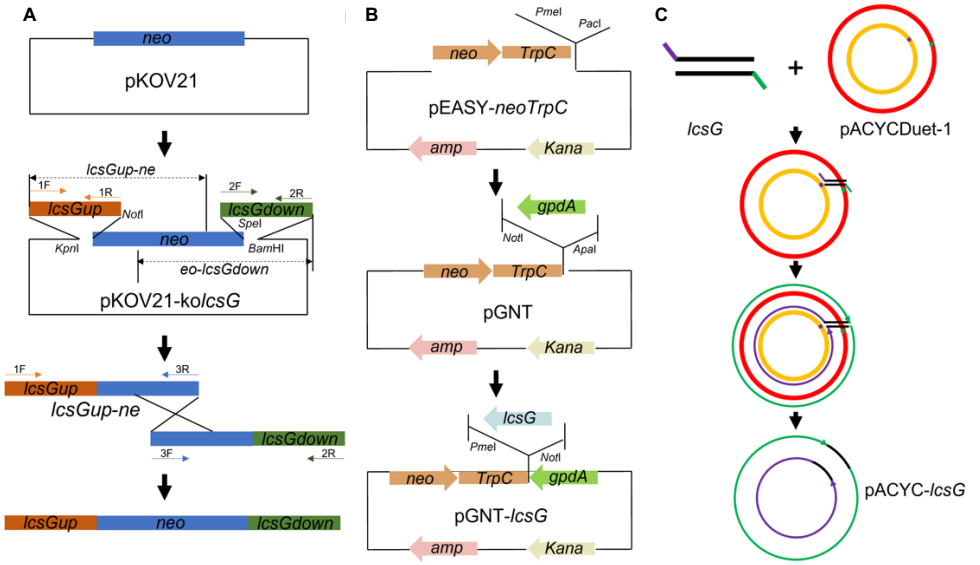

Figure 3-2: The scheme of plasmids construction. (A) Construction of the *lcsG* deletion vector pKOV21-ko*lcsG,* and schematic diagram of split-mark to disrupt the gene. 1F: *lcsG*up-f, 1R: *lcsG*up-r; 2F: *lcsG*down-f, 2R: *lcsG*down-r; 3R: *lcsGup-ne*-r 3F: *eo-lcsGdown*-f. (B) Construction of the *lcsG* overexpression vector pGNT-*lcsG.* (C) Construction of the recombinant protein LcsG expression vector pACYC-*lcsG.* The recombinant plasmid was constructed by using the quick-change method.

To determine the function of LcsG in leucinostatin biosynthesis, we constructed deletion mutants (Δ*lcsG*) and overexpression mutants (OE*lcsG*) of *P. lilacinum* PLBJ-

1 (Figures 3-2 and 3-3). For overexpression, a plasmid carrying the fungal strong promoter *gpdA* fused to the lcsG coding sequence was randomly integrated into the genome of the wild-type strain (WT). Two PCR-confirmed positive transformants, designated OE1 and OE2, were randomly selected for further analysis of *lcsG* expression levels by qRT-PCR. Both exhibited an over 100-fold increase in *lcsG* transcript levels, confirming successful overexpression. (Figure 3-4A). Following growth on a productive medium and production extraction, LC–MS analysis was performed, revealing obvious differences between the deletion mutant and WT (Figure 3-1C); in contrast, there were no obvious differences between the OE2 and the WT (Figure 3-4B).

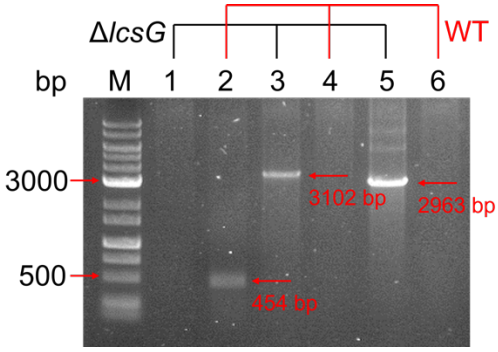

Figure 3-3: Confirmation of the *lcsG* deletions in *P. lilacinum* strain PLBJ-1. Marker was FastGene 1 kb DNA Marker Plus (NIPPON Genetics). Lane 1, 3, 5 showed PCR products from the *lcsG* knock-out strain. Lane 2, 4, 6 showed PCR products from PLBJ-1 (WT). Lane 1, 2 were amplified with primer pair *lcsG* check-f and *lcsG* check-r. Lane 3, 4 were amplified with primer pair *lcsG* up-f and *lcsGup-ne*-r. Lane 5, 6 were amplified with primer pair *eo-lcsGdown*-f and *lcsG*down-r.

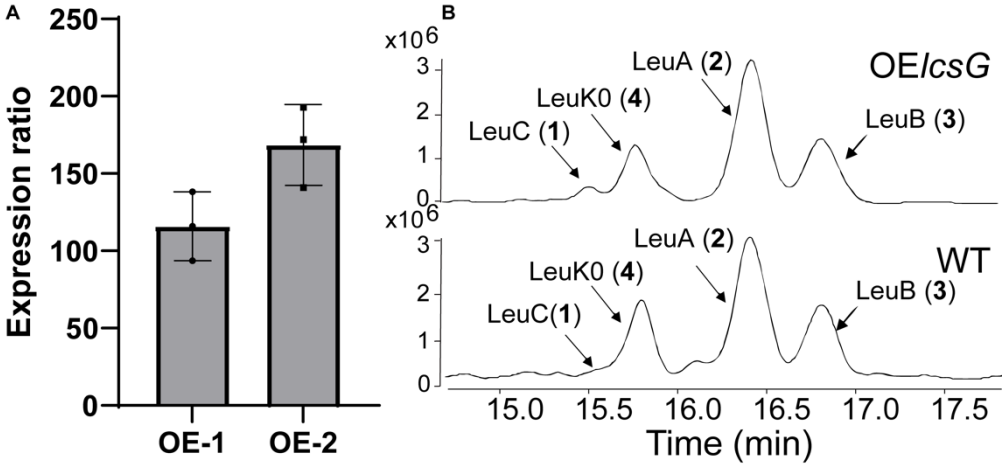

Figure 3-4: (A) Quantitative analysis of *lcsG* gene expression in overexpression (OE) mutants by quantitative real- time PCR. The gene expression level of *lcsG* in OE-1 and OE-2 demonstrate 115.69-fold and 168.56-fold upregulation, respectively. All data represent the

mean of n = 3 biologically independent samples and error bars show standard deviation. (B) LC-MS analysis of leucinostatin C (LeuC, **1**), LeuB (**2**), LeuA (**3**), and LeuK0 (**4**) of the *lcsG* overexpression (OE*lcsG*) mutant and WT. Extracted ion chromatograms (EICs) were obtained for m/z 1190.8 ± 0.5 (LeuC (**1**)), 1204.8 ± 0.5 (LeuB (**2**)), 1218.8 ± 0.5 (LeuA(**3**)), and 1234.8 ± 0.5 (LeuK0 (4)) in positive ionization mode.

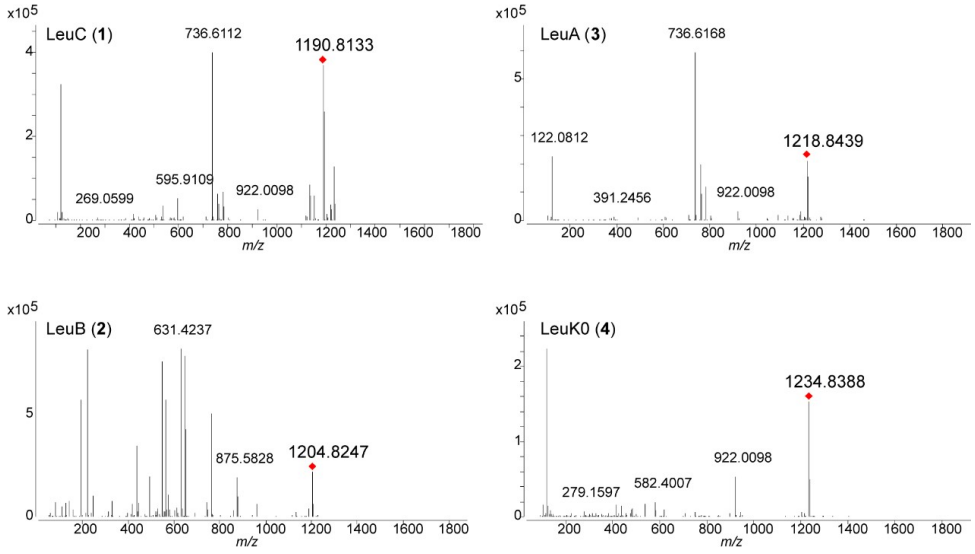

Figure 3-5: HRESI-MS spectrum of LeuC (1), LeuB (2), LeuA (3), and LeuK0 (4).

Table 3-1: Comparison of the reported fragment ions (m/z) in ESI-MS-MS spectra of leucinostatins in this study.

	B1	**A2**	**B2**	**B3**	**B4**	**B5**	**B6**	**B7**	**B8**	**B9**	**C10**	**Y5**	**Y4**	**Y3**	**Y2**
LeuA	111	194	222	435	564	649	762	875	960	1045	1173	457	344	259	174
LeuB	111	194	222	435	564	649	762	875	960	1045	1173	443	330	245	160
LeuC	111	194	222	435	564	649	762	875	960	1045	1173				
LeuA0	111	194	222	435	564	649	762	875	960	1045	1173				
LeuK0	111	194	222	435	564	649	762	875	960	1045	1173	473	360	275	190
Unknown compound	111	194	222	417	546	613	744	857	942	1027	1155	473	360	275	190
LeuK1	111	194	222	435	564	649	762	875	960	1045	1173	675	562	477	392
LeuK2	111	194	222	435	564	649	762	875	960	1045	1173	487	374	289	204
LeuK3	111	194	222	435	564	649	762	875	960	1045	1173				

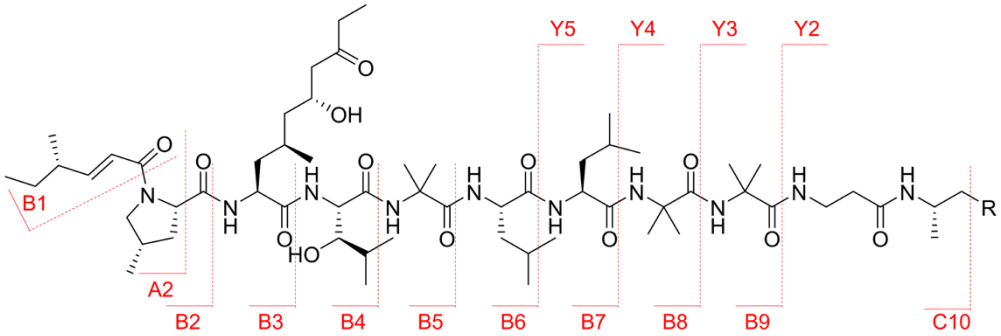

Figure 3-6: Fragmentation types observed in MS-MS spectra of leucinostatins.

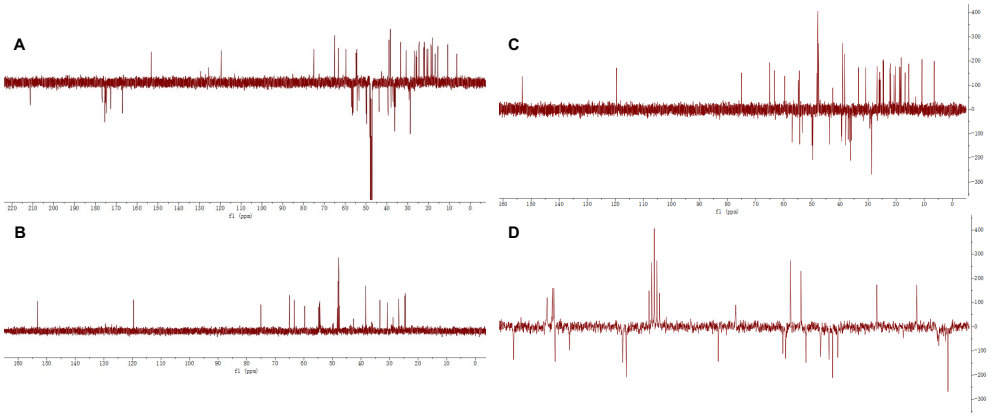

Figure 3-7: ^{13}C-NMR of LeuK0 in CD_3OD. (A) ^{13}C-NMR (APT) of LeuK0 in CD_3OD. It revealed that LeuK0 possessed total of 62 carbons, including 18 methyl groups (-CH_3), 14 methylenes (-CH_2), 16 methines (-CH), and 14 sp^3 quaternary carbons. (B) 13C-NMR (DEPT-90) of LeuK0 in CD3OD. The 13C-NMR DEPT-90 spectrum of LeuK0 indicated it contains 16 -CH units. (C) ^{13}C-NMR (DEPT-135) of LeuK0 in CD_3OD (global view). The ^{13}C-NMR DEPT-135 data of LeuK0 indicated it contains 14 -CH_2 units and 34 -CH/CH_3 units. (D) ^{13}C-NMR (DEPT-135) of LeuK0 in CD_3OD (local view).

LC–MS analysis of the WT extracts revealed that the *m/z* $[M+H]^+$ values of the four peaks (**1**-**4**) were 1190.8133, 1218.8439, 1204.8247, and 1234.8388, respectively (Figure 3-5). High-resolution electrospray ionization mass spectrometry (HRESI-MS-MS) analysis (Table 3-1 and Figure 3-6) confirmed that peaks **1**-**3** were attributed to the LeuC, LeuB, and LeuA, respectively. Based on the HRESI-MS-MS results and the same molecular weight obtained, peak **4** was initially presumed to be leucinostatin K (LeuK), a compound isolated from *Paecilomyces lilacinus* (synonym *Purpureocillium lilacinum*) (Mikami et al., 1989). However, the NMR analysis suggested that peak **4** was not the known compound LeuK but rather a compound derived from LeuC whose C-terminus was -NH-CH_2-CH_2-OH or -CH_2-CH_2-O-NH_2. As its structure was not fully consistent with that of LeuC, the compound has not been previously reported, we designated it as leucinostatin K0 (**4**, LeuK0) since the name

"K0" was unclaimed (Figures 3-7). A specific *N*-hydroxysuccinimide (NHS)-ester reaction was employed to verify the free amine in LeuK0, and then the product compound LeuK1 (**5**) with NHS ester labeling was detected (Figure 3-8), which confirmed the structure of LueK0 (**4**) as shown in Figure 3-1A. The deletion of *lcsG* led to the abolishment of LeuB and LeuA, both of which have methylated termini, suggesting that the deletion blocked the formation of the methylated C-terminal amines. Moreover, LeuK0 and an unidentified compound that shared the same C-terminus (Table 3-1) persisted in the deletion mutant (Figure 3-1C). Therefore, LcsG was inferred to play an essential role in the biosynthesis of terminal amines of leucinostatins.

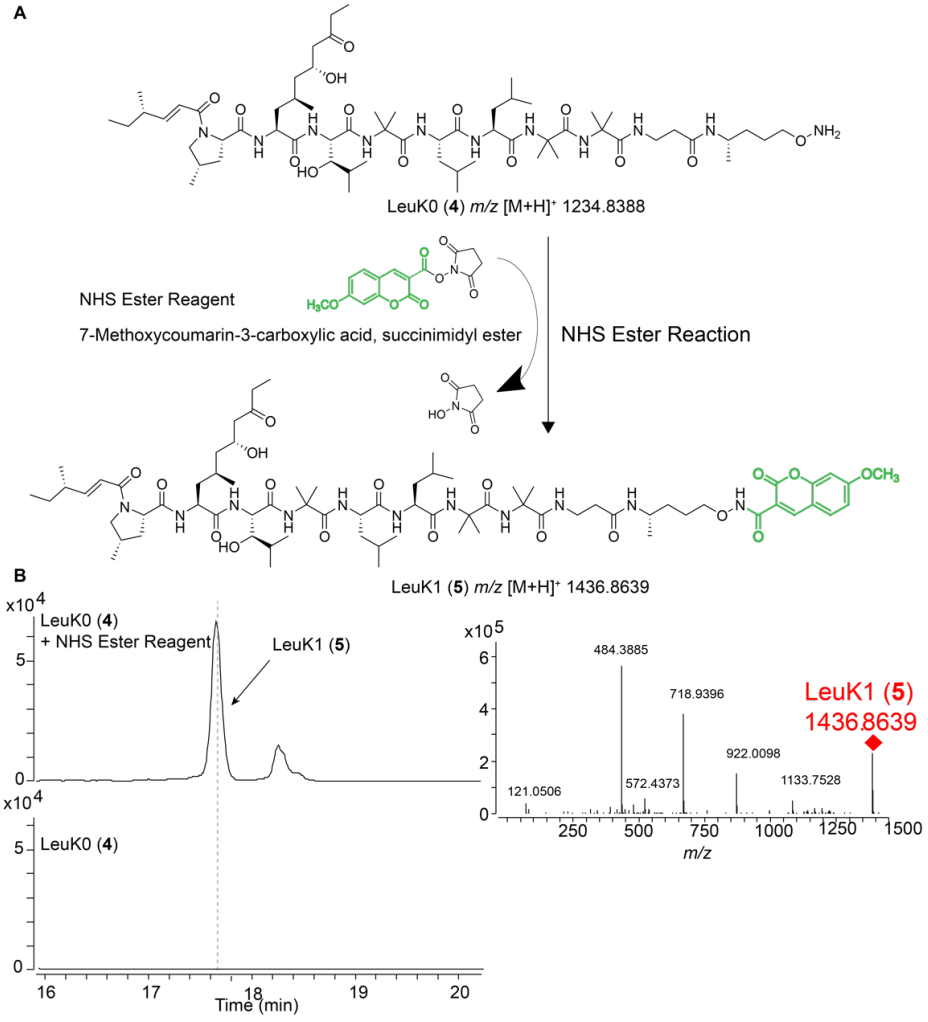

Figure 3-8: NHS ester reaction scheme. (A) NHS ester reaction scheme for chemical conjugation to LeuK0 (**4**). 7-Methoxycoumarin-3-carboxylic acid succinimidyl ester was employed as the NHS ester reagent. (B) LC- MS analysis of LeuK0 (**4**) and NHS ester

reaction with LeuK0. EICs was obtained for m/z 1436.8 ± 0.5, corresponding to LeuK1 (**5**), in positive ionization mode. EIS at m/z 1436.8469 refers to [M+H]+ ion of product LeuK1 (**5**).

3.2. LcsG functions as a SAM-dependent methyltransferase

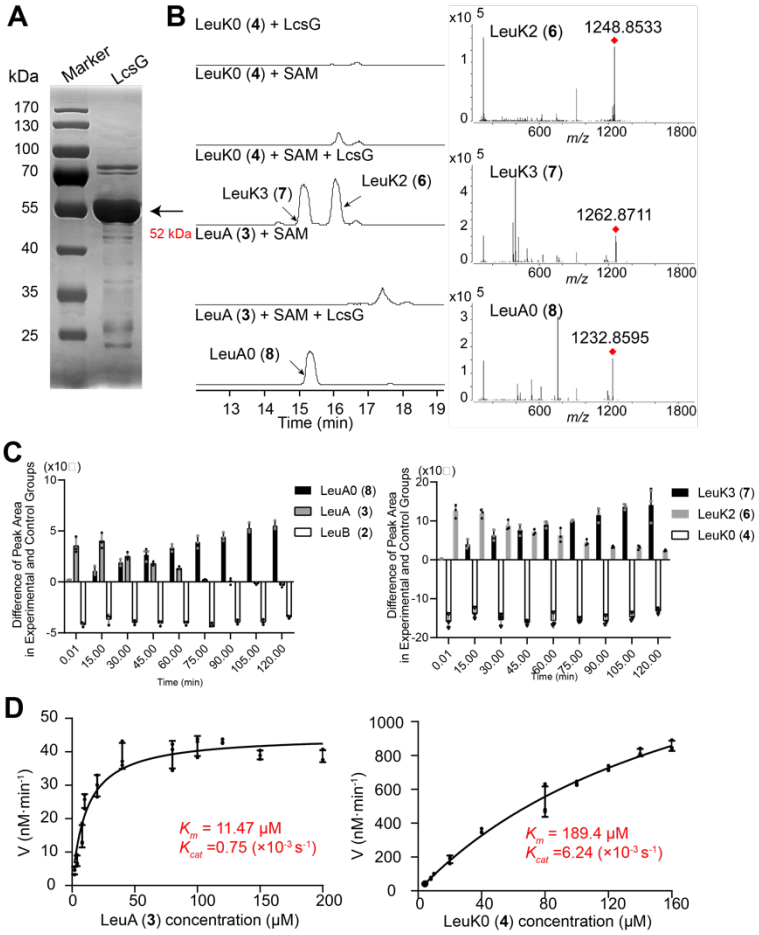

Figure 3-9: Verification that LcsG is involved in the methylation of leucinostatins. (A) SDS–PAGE analysis of the recombinant protein LcsG. (B) In vitro LcsG activity analysis using LeuK0 (4) and LeuA (3) as the substrates and the $[M+H]^+$ ions of three new product peaks at positions 6-8. (C) Time dependency of the variations in each component. (D) Kinetic analysis of LcsG using LeuA (3, top) and LeuK0 (4, bottom) as substrates. All the data are represented as the means of n = 3 biologically independent samples, and the error bars show the standard deviations (C, D).

Sequence analysis suggested that LcsG is an *S*-adenosyl-L-methionine (SAM)-dependent methyltransferase. To clarify its biochemical function, we expressed *lcsG* in *E. coli* ArcticExpress (DE3) and purified the recombinant protein LcsG, which was

tagged with His_6 at both the N and C termini, using nickel affinity chromatography (Figure 3-9A). Obtaining pure LeuB and LeuC in the laboratory is exceptionally difficult. The enzymatic activity was assayed by using LeuK0 (**4**) and LeuA (**3**) as the substrates. The S-adenosyl-$_L$-homocysteine (SAH) and three new product peaks, LeuK2 (**6**), LeuK3 (**7**) and LeuA0 (**8**), were detected only in the presence of the substrate, LcsG, and SAM (Figure 3-10 and Figure 3-9B). In contrast, omitting LcsG or SAM resulted in no product formation. LC–MS analysis confirmed that the $[M+H]^+$ values of the **6-8** ions were 1248.8533, 1262.8711, and 1232.8595, respectively (Figure 3-9B). These molecular weights indicated that LeuK2 (**6**) and LeuA0 (**8**) are the methylated products of LeuK0 (**4**) and LeuA (**3**), respectively, and that LeuK3 (**7**) is the dimethylated product of LeuK0 (**4**). These results indicated that LcsG is likely a SAM-dependent methyltransferase.

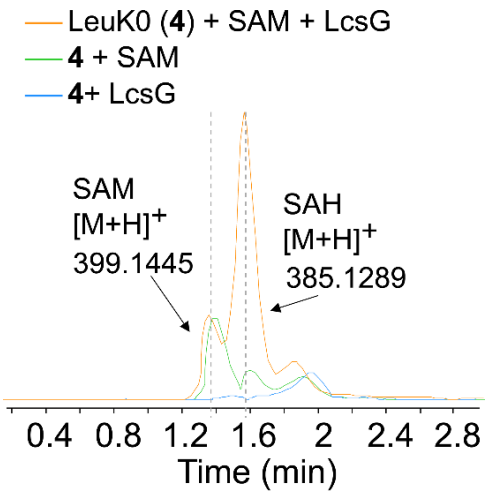

Figure 3-10: LC-MS detection of SAM and SAH of LcsG-catalyzed reactions.

The kinetic activity of LcsG was analyzed to gain further insight into its methylation activity. We conducted several single-factor enzymatic assays. The ethyl acetate (EtOAc) extracts of the WT PLBJ-1 strain cultures, which inherently contained LeuB (**2**), LeuA (**3**), and LeuK0 (**4**), served as substrates. We also established a control group without the addition of LcsG and employed LC–MS analysis to quantify each component in the experimental and control groups. The variations in component levels between the experimental and control groups were compared to characterize the changes induced by LcsG catalysis. Positive values indicate that a component's level in the experimental group is greater than that in the control group, suggesting that a component accumulates during catalysis. Conversely, negative values suggest that the level of the component in the experimental group was lower than that in the control group, indicating that a component is consumed during catalysis. The time dependency of the LcsG-catalyzed reaction showed that LeuA0 (**8**) and LeuK3 (**7**) accumulated nearly linearly with time and appeared almost immediately after the

reaction started. LeuB (**2**) and LeuK0 (**4**) were nearly completely consumed after the beginning of the reaction, while the amount of LeuA (**3**) and LeuK2 (**6**) increased early on and decreased (Figure 3-9C). These results suggested that LcsG is an iterative methyltransferase, and the reaction sequences could be LeuB-LeuA-LeuA0 and LeuK0-LeuK2-LeuK3. The optimal pH and temperature for producing the final products LeuA0 and LeuK3 were determined (Figure 3-11), followed by measurements of the initial rates at substrate concentrations ranging from 0-200 μM. Standard curves correlating concentration with peak area were established for LeuA0 (**8**) and LeuK3 (**7**) using LC–MS (Figure 3-12). The initial rate data were measured by LC–MS and fitted to the Michaelis–Menten equation to determine the kinetic parameters (Figure 3-9D). The K_{cat}/K_m values obtained for LeuA (**3**) and LeuK0 (**4**) were 65.39 $s^{-1}M^{-1}$ and 32.94 $s^{-1}M^{-1}$, respectively.

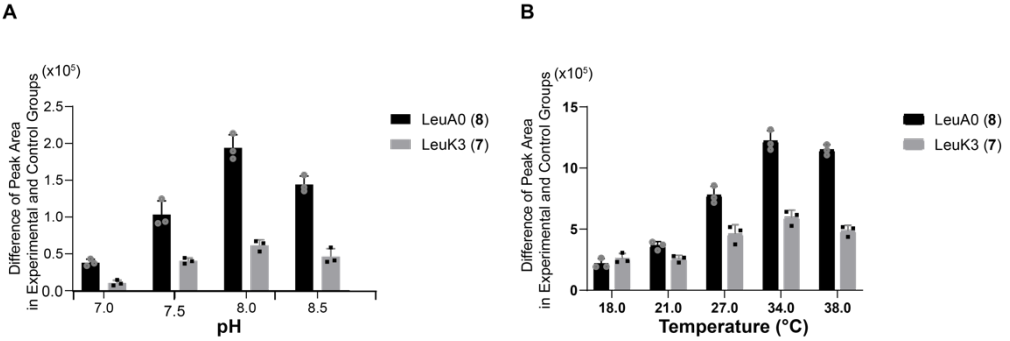

Figure 3-11: (A**)** Effect of pH (pH 7.0, pH 7.5. pH 8.0, pH 8.5) on the production of LeuA0 (**8**) and LeuK3 (**7**) by LcsG- catalyzed. LcsG showed a pH optimum of 8.0. (B) Effect of temperature (18°C, 21°C, 27°C, 34°C, 38°C) on the production of LeuA0 (**8**) and LeuK3 (**7**) by LcsG-catalyzed. LcsG showed a temperature optimum of 34 °C. All data represent the mean of n = 3 biologically independent samples and error bars show standard deviation (A, B).

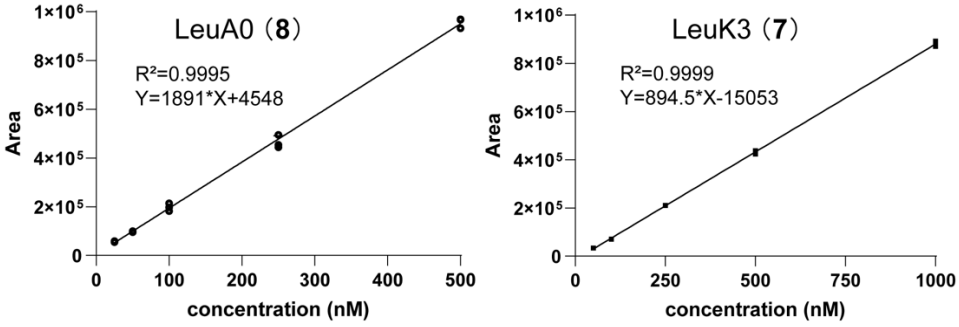

Figure 3-12: Standard curve of concentration and peak area of LeuA0 (**8**) and LeuK3 (**7**) determined by LC-MS. All data represent the mean of n = 3 biologically independent samples and error bars show standard deviation.

3.3. Characterizations of the products of the LcsG-catalyzed reaction

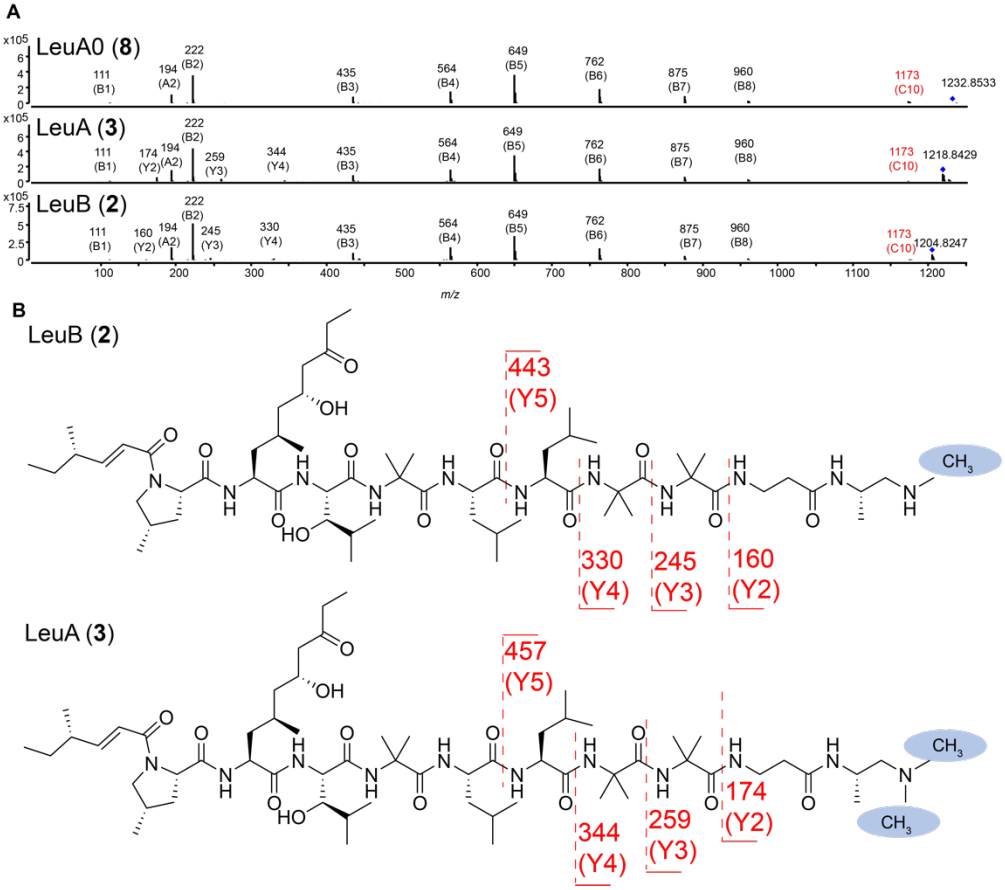

Figure 3-13: (A) Ions from the HRESI-MS-MS data of LeuB (**2**), LeuA (**3**), and LeuA0 (**8**). (B) Predicted fragments and their calculated *m/z* for observed ions got from HRESI- MS-MS of LeuB (**2**), LeuA (**3**).

Next, we performed HRESI-MS-MS analysis to elucidate the structures of compounds LeuK2 (**6**), LeuK3 (**7**) and LeuA0 (**8**), we turned to HRESI-MS-MS analysis. The *m/z* values of the fragments of each leucinostatin are presented in Table 3-1. Comparisons of the MS-MS data of LeuA0 (**8**) with those of LeuA (**3**) and LeuB (**2**) revealed that the spectrum of LeuA0 (8) showed remarkably similar fragments to those of LeuA (**3**) and LeuB (**2**) (Figure 3-13). Specifically, they shared one fragment with a *m/z* value of 1173. This ion was deduced to be the $[M+H]^+$ ion of fragment C10, indicating the possible methylation site of the C-terminal amine. Therefore, LeuA0 (**8**) was concluded to be a trimethylammonium compound in which the terminal amine carried a positive charge and three methyl groups. This predicted structure is identical to a previously identified structure (Mori et al., 1983), which was obtained by treating

LeuA (**3**) with methyl iodide. This reaction afforded the same product as the enzymatic reaction (Figure 3-14A), confirming the structure of LeuA0 (Figure 3-14C). Combined with its molecular weight, LeuA0 (**8**) was assigned the molecular formula $C_{63}H_{114}N_{11}O_{13}^{+}$.

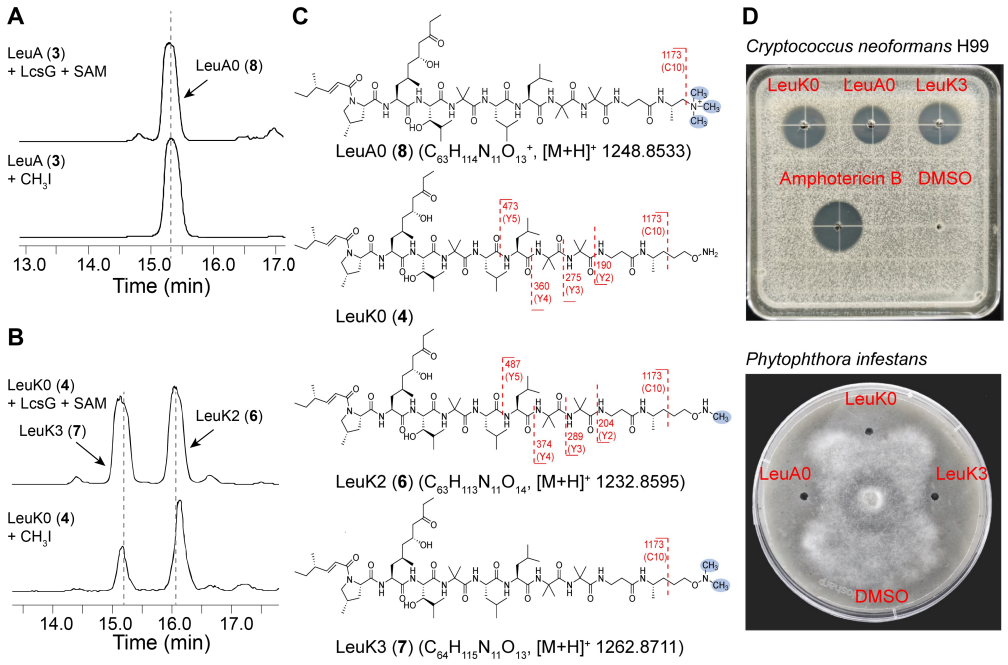

Figure 3-14: Structural elucidation of LeuA0 (**8**), LeuK2 (**6**), and LeuK3 (**7**). (A) LC–MS analysis of the N-methylation of LeuA (**3**) to the same trimethylammonium compound (**8**, LeuA0) by LcsG and CH_3I. (B) LC–MS analysis of two methylation reactions using LeuK0 (**4**) as the substrate and LcsG and CH_3I. (C) Structures and the HERSI-MS-MS data of LeuA0 (**8**), LeuK0 (**4**), LeuK2 (**6**), and LeuK3 (**7**). (D) Growth inhibition of eukaryotic microorganisms by 25 µg/well LeuK0 (**4**), LeuA0 (**8**), and LeuK3 (**7**) according to the agar diffusion assay.

Treating LeuK0 (**4**) with methyl iodide produced LeuK2 (**6**) and LeuK3 (**7**) as shown in Figure 3-14B. Based on their HRESIMS data, LeuK2 (**6**) and LeuK3 (**7**) have molecular formulas of $C_{63}H_{113}N_{11}O_{14}$ and $C_{64}H_{115}N_{11}O_{14}$, respectively. MS-MS experiments revealed similar fragments to LeuK0, with differences in Y-type fragments. Notably, the Y-type fragments in LeuK2 (**6**) are +14 mass units larger than those in LeuK0 (**4**). For example, *m/z* values of 190 and 204 correspond to $[M+H]^+$ ions of Y2 fragments in LeuK0 and LeuK2 (**6**), respectively. Furthermore, LeuK2 (**6**) and LeuK3 (**7**) produced an ion at *m/z* 1173 (C10), indicating that the terminal amine of LeuK2 was methylated LeuK2 (**6**) (Figure 3-15). These findings revealed LeuK2 (**6**) and LeuK3 (**7**) as new leucinostatins, as depicted in Figure 3-14C. Overall, these results confirm that LcsG, as an NMT, can iteratively catalyze the methylation of NRP terminal amines.

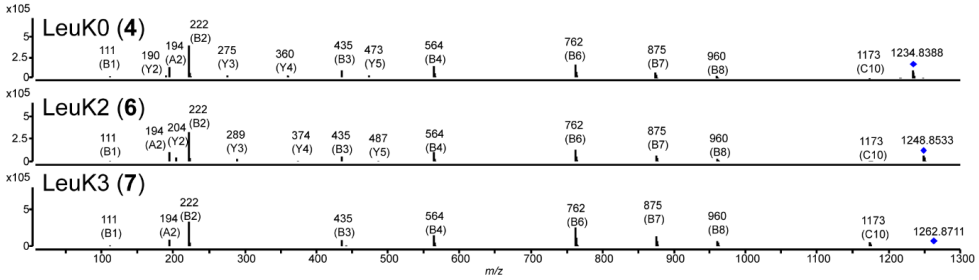

Figure 3-15: Ions from the HRESI-MS-MS data of LeuK0 (**4**), LeuK2 (**6**), and LeuK3 (**7**).

3.4. Antimicrobial evaluation of leucinostatins

Leucinostatins are well-known antibiotics. We purified these compounds by semipreparative HPLC and successfully generated LeuA0 (**8**), LeuK0 (**4**) and LeuK3 (**7**) in sufficient quantities for the antimicrobial assay. The inhibitory activity of these compounds against the drug-resistant strain *C. neoformans* H99 and the plant pathogen *P. infestans* was determined using agar diffusion assays. Notably, previous studies have demonstrated the inhibitory effects of LeuA and LeuB on both *C. neoformans* (Fukushima et al., 1983) and *P. infestans* (Wang et al., 2016). All of these leucinostatins had inhibitory effects on these pathogens (Figure 3-14D). Moreover, the anti-*C. neoformans* MICs value of the two methylated products, LeuA0 (**8**, 25.8 μg/mL) and LeuK3 (**7,** 25.8 μg/mL), were four and two times lower than those of their parent products, LeuA (**3**, 102.4 μg/mL) and LeuK0 (**4**, 51.2 μg/mL), respectively (Figure 3-16), which indicated that *N*-methylation at the terminus of leucinostatins can improve their antimicrobial efficiency.

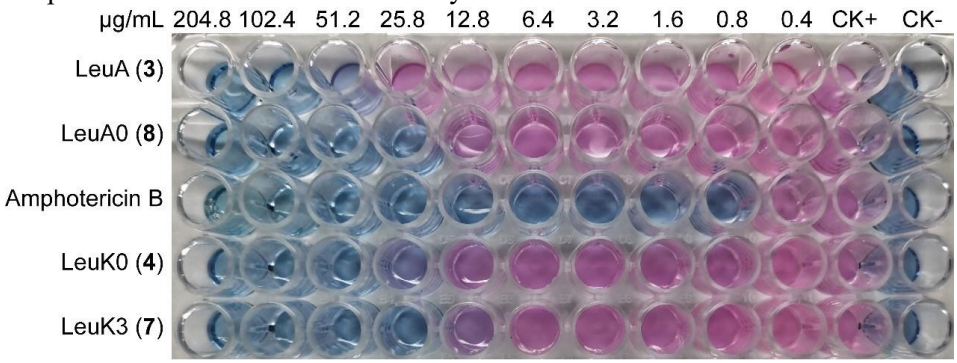

Figure 3-16: MIC (μg/mL) of leucinostatins (LeuA (**3**), LeuA0 (**8**), LeuK0 (**4**), LeuK3 (**7**)) against *Cryptococcus neoformans* strain H99 in a 2-fold liquid dilution assay. The 2-fold serial dilution of leucinostatins from 204.8 to 0.4 μg/mL was tested in 96-well plates. The positive control was amphotericin B at a 2-fold serial dilution from 204.8 to 0.4 μg/mL. The negative controls were medium (CK-) and inoculum (CK+).

3.5. Catalytic mechanism of the N-methyltransferase LcsG

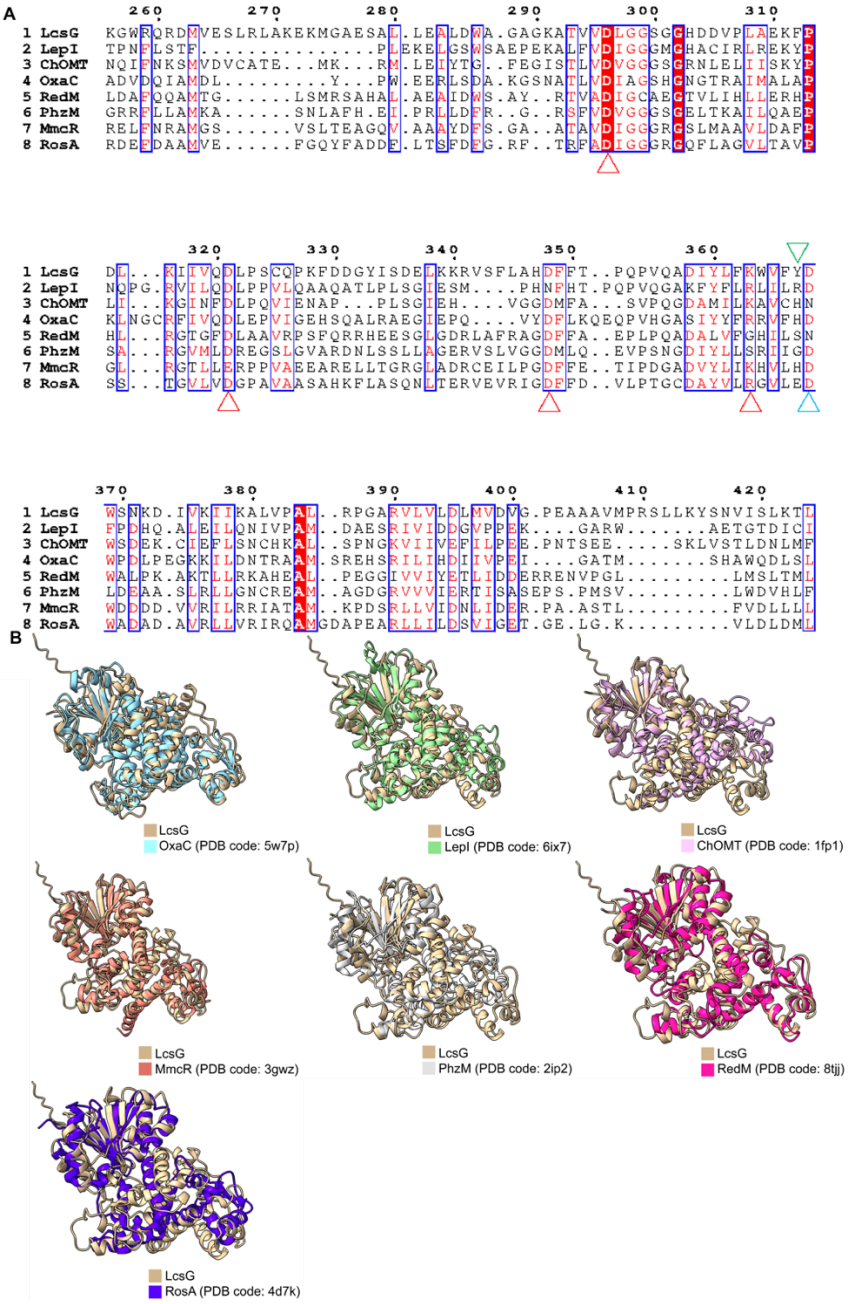

Figure 3-17: Comparison between the LcsG and its structurally characterized homologues. ChOMT (UniProt accessions number: P93324), OxaC (UniProt accessions number: A0A1B2TT09), MmcR (UniProt accessions number: Q9X5T6) were characterized as OMTs;

RedM (UniProt accessions number: O54154), PhzM (UniProt accessions number: Q9HWH2), and RosA (UniProt accessions number: K4RFM2) were characterized as NMTs; LepI (UniProt accessions number: B8NJH3) was characterized as a SAM-dependent OMT-like pericyclase-dehydratase. (A) Sequence comparison between the LcsG and these homologues. White letters on a red background indicated strictly conserved amino acid residues. Red letters in blue boxes indicated well-conserved amino acids or similar amino acids. The positions marked with red triangles are predicted to be part of the SAH binding motif; those labeled with blue triangles are predicted catalytic residues; the green triangle indicated LcsG's Y367 and its corresponding residues. (B) Structural comparison between LcsG and these homologies.

Table 3-2: The pLDDT scores of six predicted active residues.

Residues	pLDDT score
D296	0.95
D321	0.95
D348	0.94
K363	0.95
D368	0.95
D395	0.92

Table 3-3: RMSD values of LcsG and its homologies.

Name	PDB code	Pruned atom pairs		Overall	
		pairs	RSMD (Å)	pairs	RSMD (Å)
OxaC	5w7p	158	1.264	369	5.851
LepI	6ix7	124	0.946	372	6.219
ChOMT	1fp1	93	0.943	319	11.807
MmcR	3gwz	117	1.037	337	4.841
PhzM	2ip2	49	1.398	324	8.562
RedM	8tjj	84	1.424	324	5.692
RosA	4d7k	86	1.029	322	11.147

We then identified the catalytic residues in LcsG. Local multiple sequence alignments revealed that LcsG shares a conserved SAH/SAM binding motif (D296, D321, D348, and K363) and two possible catalytic residues (D368 and D395) (Figure 3-17A). Despite many attempts, we were unable to obtain a crystal of the LcsG protein suitable for X-ray crystallographic analysis. As an alternative, we employed an

artificial intelligence (AI) method, Uni-Fold, to approximate a model of LcsG. The overall structure of LcsG with color-coded pLDDT scores is presented in Figure 3-18A, and the six predicted residues are depicted in Figure 3-18C. Additionally, Table 3-2 provides the pLDDT scores for these six predicted residues. These results indicated that AI predicts the protein structure with high confidence, including the active site residues that are proposed to be relevant for substrate binding and catalysis. Structural alignments between LcsG and its homologs are shown in Figure 3-17B, with corresponding RMSD values detailed in Table 3-3. The overall structure of LcsG involved a typical Class I methyltransferase fold; the N-terminus appears to be responsible for dimerization and substrate binding and the C-terminus appears to be responsible for SAM binding (Figure 3-18B). To determine the structure–function relationship of LcsG, we conducted a molecular docking analysis using the predicted LcsG structure and SAH. SAH was docked into the LcsG structure model binding pocket, and the hydrogen bond network that mediates SAH binding was present in the final docking position.

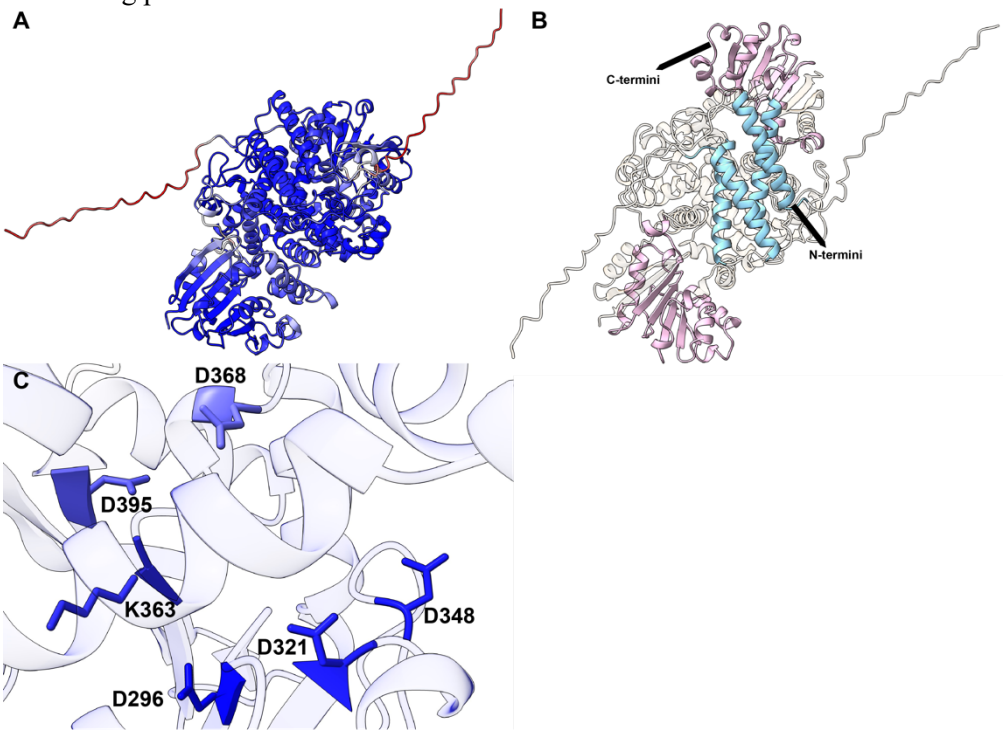

Figure 3-18: (A)The overall structure of LcsG with color-coded pLDDT scores, where a blue hue corresponds to a pLDDT score of 1.0, indicating high confidence, while a red hue signifies a pLDDT score of 0, representing lower confidence. (B) Cartoon representation of LcsG dimer. The C-terminal acceptor binding site and the N-terminal helices were depicted in pink and blue, respectively. (C) The pLDDT scores of the six predicted active site residues.

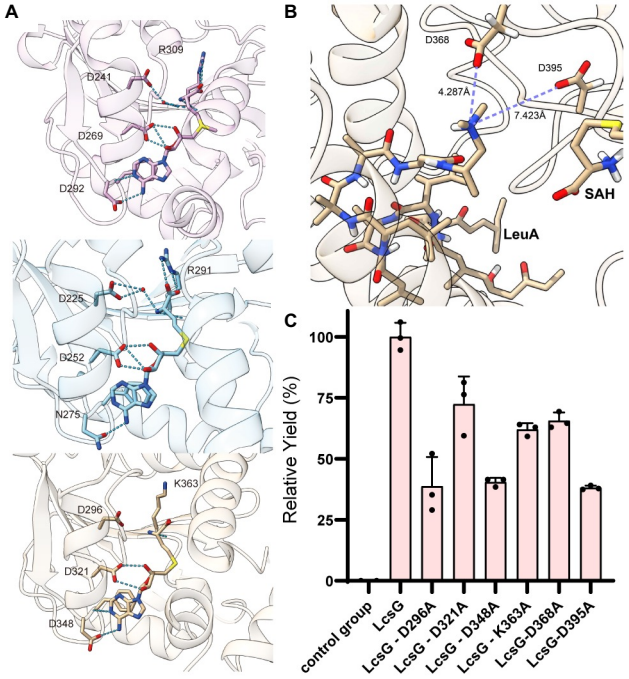

Figure 3-19: Catalytic sites of LcsG. (A) SAH binding sites of OxaC (PDB code: 5w7p, marked in pink), LepI (PDB code: 6ix7, marked in blue), and LcsG (marked in golden). (B) Modified LeuA binding sites of LcsG (Maestro, Schrödinger, LLC). (C) Comparison of wild-type LcsG and mutated LcsG-mediated methylation. The yield of the product was quantified by comparison with the peak area of the product catalyzed by LcsG (100%). All the data are represented as the means of n = 3 biologically independent samples and the error bars show the standard deviations.

As shown in Figure 3-19A, potential hydrogen bond interactions between SAH and residues D296, D321, D348, and K363 were detected, which was consistent with the results of multiple sequence alignment (Figure 3-18C). The accurate stereo-structure structures of nonpeptide leucinostatins are difficult to predict because they are composed of seven nonstandard and unusual α-amino acid residues. Based on the crystal structures of the analogs helioferin A (Brand et al., 2021) and ZHAWOC6027 (Gessmann et al., 2018) (Figure 3-20), a structural model of LeuA was predicted, and LeuA was docked into the LcsG structure via DiffDock (Corso et al., 2022). In the first ranked result, the *N* atom that becomes methylated occupies the position between D368, D395 and SAH. Subsequent molecular dynamics (MD) simulations were used to further explore the stabilities of our protein–ligand complex and the importance of catalytic site residues. After 500 ns of equilibration (Figure 3-21), 3 independent 500 ns MD simulations were performed (Table 3-4 and Figure 3-22). The results showed that the positively charged N is located between D395 and D368, and the terminal N of LcsG could form a stable complex system with D368 (Figure 3-19B). Nevertheless,

the results provided insight into the importance of D368. In some snapshots, the ligand formed salt bridges with D368 and D395 (Figure 3-23).

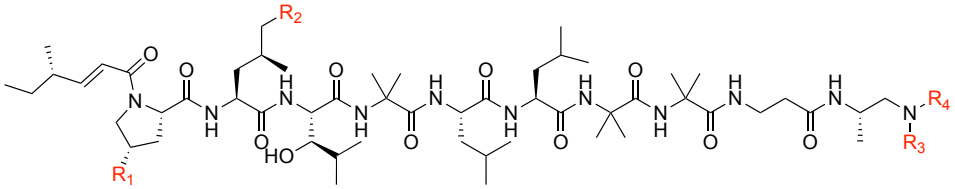

LeuA

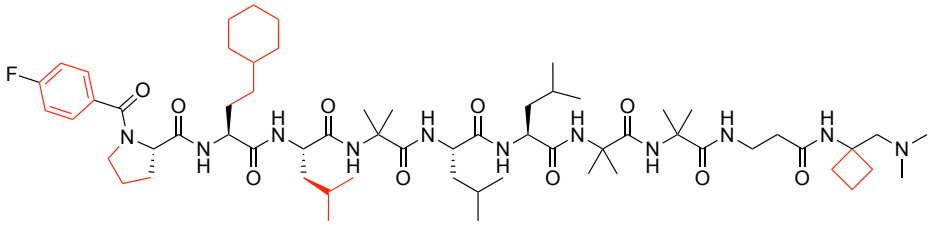

ZHAWOC6027

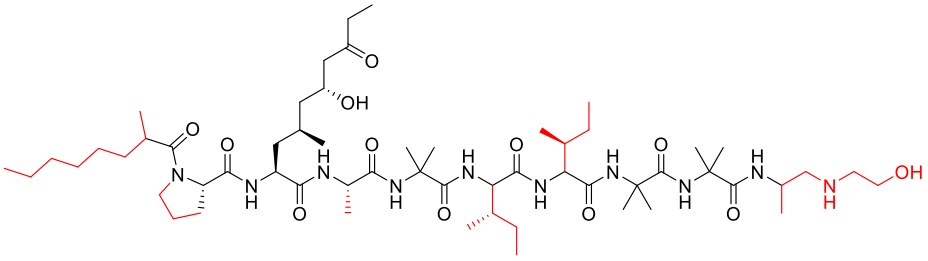

helioferin A

Figure 3-20: Formulas and sequences of LeuA, ZHAWOC6027, and helioferin A. Structural motifs that are different from LeuA are shown in red.

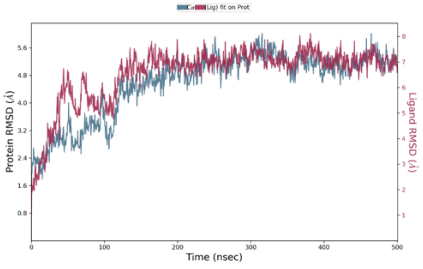

Figure 3-21: 500 ns trajectories protein & ligand RMSD. Protein and ligand were stable after 500 ns MD simulation.

Table 3-4: The system setup that includes number of simulations per system, simulation box dimensions, total number of atoms, total number of water molecules, salt concentration, liquid composition (number of molecules and type).

Num of independent run	Box dimensions (Å)	Num of atoms	Num of water	Salt concentration
3	88.124, 79.711, 74.777	52533	15062	0.15M

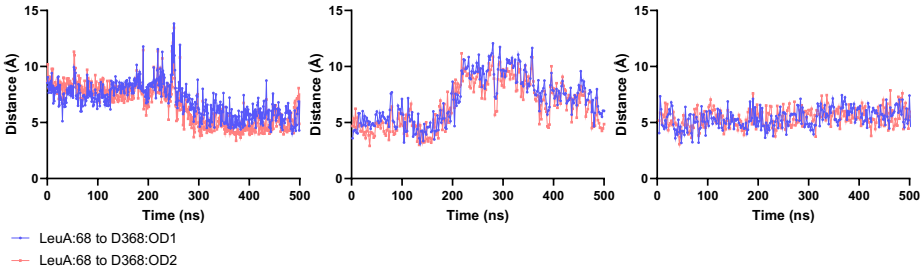

Figure 3-22: Interatomic distance between targeted N of LeuA (LeuA:68) and two O of D368 (OD1 and OD2) in 3 independent MD simulations. Following a 500 ns equilibration period, three additional independent simulations, each lasting 500 ns, were conducted.

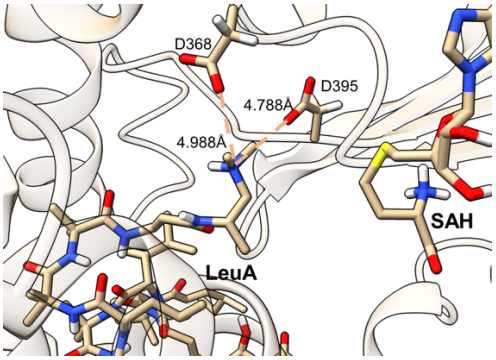

Figure 3-23: Representative snapshot from molecular dynamics simulations depicting the formation of salt bridges between the ligand and D368 and D395.

To verify this result, we mutated D296, D321, D348, K363, D368, and D395 to Ala in LcsG (Figure 3-24). Biochemical assays of these mutants were then performed using LeuA as substrate. After 1 h of incubation, the conversion of LeuA (**3**) to LeuA0 (**8**) decreased for all the mutants (Figure 3-19C). These findings are consistent with our earlier in vitro assays and docking and MD simulation results. These findings indicate that the SAM binding site of LcsG is involved in leucinostatin methylation and provide additional support that LcsG is a SAM-dependent methyltransferase.

Addtionally, D368 and D395 were shown to contribute notably to the substrate binding.

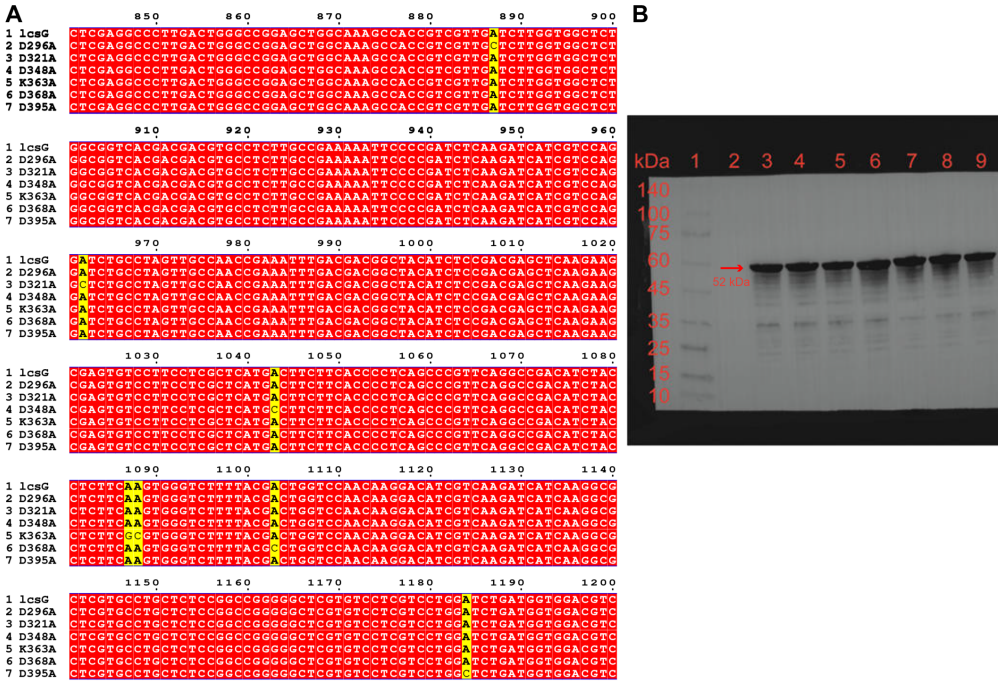

Figure 3-24: (A) The DNA sequencing of the plasmids of LcsG mutagenesis. White letters on a red background indicated same nucleotides. The black letter on a yellow background indicated the mutation site. (B) Western blot analysis of LcsG mutated proteins. The expected size of proteins (52kDa) was indicated. Lane 1: Ladder; Lane 2: the negative control strain contained blunt vector; Lane 3: LcsG wild-type protein; Lane 4: LcsG-D296A; Lane 5: LcsG-D321A; Lane 6: LcsG-D348A; Lane 7: LcsG-K363A; Lane 8: LcsG-D368A; Lane 9: LcsG- D395A.

4. Discussion

Table 3-5: Known NMTs capable of furnishing at least two methyl transfers to at least one substrate and their similarity to LcsG.

Name	UniProt accessions numbers	Coverage /Identity
EgtD	A0R5M8	No significant similarity
PfPMT	Q8IDQ9	No significant similarity
BANMT	Q84N56	22/24.07
NRMT	Q9BV86	21/21.90
PsiM	P0DPA9	No significant similarity

RosA	K4RFM2	25/26.67
RedM	A0A0F7G196	27/29.13
OxyT	Q3S8P6	25/31.67
AMNMT	Q96565	31/24.07

NMTs are important for the biotransformation of bioactive molecules. *N*-methylation can modulate the activity of signaling molecules and participate in the biosynthesis of natural products. NMTs are of great interest because site-specific modifications are crucial for the bioactivity and biosynthesis of natural products. In this study, we successfully determined the in vitro activity of the NMT LcsG, which is involved in the iterative *N*-methylation of the unique terminal unit of leucinostatins. Few NMTs are known to iteratively transfer methyl groups to natural products (Table 3-5). The NMTs EgtD (Vit et al., 2015), PfPMT (Lee et al., 2012), BANMT (Raman & Rathinasabapathi, 2003) and NRMT (Schaner Tooley et al., 2010) were reported to catalyze the *N*-trimethylation of corresponding substrates progressively. Moreover, PsiM (Fricke et al., 2017), RosA (Tongsook et al., 2016), RedM (Daniel-Ivad & Ryan, 2024), OxyT (Zhang et al., 2008), and AMNMT (Larsson et al., 2006) were shown to catalyze the two methylation reactions. Although the NMTs involved in the biosynthesis of plantazolicin-class ribosomally synthesized and posttranslationally modified peptides (RiPPs) are responsible for dimethylation, the corresponding monomethylated products have never been detected (Lee et al., 2013; Molohon et al., 2011).

Table 3-6: Annotated enzymes clustered with LcsG in the sequence similarity network.

	UniProt accessions numbers	**Description**	**Involved in the biosynthesis of**	**Organism**	**Coverage /Identity**
OMT 1	Q0UI04	*O*-methyltransferase elcB	elsinochrome C	*Phaeosphaeria nodorum* strain SN15	88/37.27
OMT 2	P0CT89	4-*O*-methyltransferase 1	4-OH phenolic compounds	*Phanerochaete chrysosporium* strain RP-78	92/32.80
OMT 3	P0CT90	3-*O*-methyltransferase 2	3-OH phenolic compounds	*Phanerochaete chrysosporium* strain RP-78	88/33.04
OMT 4	A0A1U8QH20	*O*-methyltransferase cicE	cichorine	*Emericella nidulans* strain FGSC A4	90/33.88
OMT 5	Q0CCY5	*O*-methyltransferase gedA	geodin	*Aspergillus terreus* strain NIH 2624	73/29.41
OMT 6	Q4WQZ7	*O*-methyltransferase tpcA	trypacidin	*Aspergillus fumigatus* Af293	73/29.29
OMT 7	Q9UQY0	Demethylsterigmat-ocystin 6-*O*-	aflatoxins	*Aspergillus parasiticus* SU-1	85/34.23

		methyltransferase			
OMT 8	I1RL18	*O*-methyltransferase dpfgI	pyrones	*Gibberella zeae*	81/22.43
OMT 9	A0A4P8WAD3	*O*-methyltransferase pyiA	pyrichalasin H	*Pyricularia grisea*	89/33.05
OMT 10	Q9P900	Demethylsterigmat-ocystin 6-*O*-methyltransferase	demethylsterigmatocystin, dihydrosterigmatocystin	*Aspergillus flavus* NRRL 3357	85/33.33
OMT 11	C9K2Q2	16-O-methyltransferase bsc6	brassicicene C	*Alternaria brassicicola*	82/33.33
OMT 12	S0DLP1	*O*-methyltransferase apf6	cyclic tetrapeptide apicidin F	*Gibberella fujikuroi* IMI 58289	81/24.3
OMT 13	B8NY85	*O*-methyltransferase agiB	aspergillicins	*Aspergillus flavus* NRRL 3357	71/35.11
OMT 14	B3FWS1	*O*-methyltransferase hmp5	hypothemycin	*Hypomyces subiculosus*	80/24.07
OMT 15	G3XSI5	*O*-methyltransferase aunD	aurasperone B	*Aspergillus niger*	98/34.62
OMT 16	I1RF60	*O*-methyltransferase aurJ	aurofusarin	*Gibberella zeae* PH-1	93/33.85
OMT 17	Q2I0M6	Dual *O*-methyltransferase/ FAD-dependent monooxygenase CTB3	cercosporin	*Cercospora nicotianae*	92/32.80
OMT 18	A2QBF0	*O*-methyltransferase aunD	aurasperone B	*Aspergillus niger* CBS 513.88	98/34.62
OMT 19	Q4WAW6	6-hydroxytryprostatin B *O*-methyltransferase	fumitremorgins	*Aspergillus fumigatus* Af293	91/37.07
OMT 20	S0DQQ0	*O*-methyltransferase fsr2	fusarubins	*Gibberella fujikuroi* IMI 58289	94/40.98
OMT 21	S0E608	*O*-methyltransferase bik3	bikaverin	*Gibberella fujikuroi* IMI 58289	80/47.57
OMT 22	Q0UI02	*O*-methyltransferase elcB	elsinochrome C	*Phaeosphaeria nodorum* SN15	82/37.27

OMT 23	D3H5H5	Chlorophenol *O*-methyltransferase	chlorophenol	Trichoderma longibrachiatum	89/42.98
OMT 24	A0A443HJY8	*O*-methyltransferase VdtC	viriditoxin	*Byssochlamys spectabilis*	93/46.77
OMT 25	L0MXX3	*O*-methyltransferase PaMT	fusicoccins	*Phomopsis amygdali*	94/41.18
OMT 26	D7PI16	*O*-methyltransferase gsfB	griseofulvin	*Penicillium aethiopicum*	80/47.57
OMT 27	A0A1U9YI02	*O*-methyltransferase verK	11'-deoxyverticillin A	*Clonostachys rogersoniana*	99/26.87
OMT 28	Q2UPA6	*O*-methyltransferase aclU	aspirochlorine	*Aspergillus oryzae* RIB 40	92/22.48
OMT 29	Q2UPB3	*O*-methyltransferase aclM	aspirochlorine	*Aspergillus oryzae* RIB 40	86/30.71
OMT 30	Q4WMJ5	*O*-methyltransferase gliM	gliotoxin	*Aspergillus fumigatus* Af293	86/28.81
OMT 31	P55790	Sterigmatocystin 8-*O*-methyltransferase	sterigmatocystin	*Aspergillus flavus* NRRL 3357	84/33.33
OMT 32	Q12120	Sterigmatocystin 8-*O*-methyltransferase	sterigmatocystin	*Aspergillus parasiticus* SU-1	84/34.26
OMT 33	A0A142C7A1	*O*-methyltransferase phnC	atrovenetin	*Penicillium herquei*	79/22.94
OMT 34	D7PI17	*O*-methyltransferase gsfC	griseophenone D	*Penicillium aethiopicum*	79/27.45
OMT 35	D7PI18	*O*-methyltransferase gsfD	desmethyl-dehydrogriseofulvin	*Penicillium aethiopicum*	85/31.25
OMT 36	A0A067Z9B6	*O*-methyltransferase af390-400	fumagillin	*Aspergillus fumigatus* Af293	25/32.81
OMT 37	A0A0C1E5J2	*O*-methyltransferase opaF	oxepinamides	*Aspergillus ustus*	40/31.48
OMT 38	A0A0B5L781	*O*-methyltransferase mpaG	mycophenolic acid	*Penicillium brevicompactum*	94/33.87
OMT 39	B8N8R1	*O*-methyltransferase afvC	aflavarin	*Aspergillus flavus* NRRL 3357	81/26.79

EqxD	S4W780	Methyltransferase eqxD	equisetin	*Fusarium heterosporum*	78/26.92
Fsa4	A0A0E3VJW8	Methyltransferase fsa4	fusarisetin A	*Fusarium* sp. strain FN080326	81/26.17
PynC	A5ABG3	Methyltransferase pynC	pyranonigrins	*Aspergillus niger* CBS 513.88	90/28.24
Phm5	A0A2Z5XAK6	Methyltransferase phm5	phomasetin	*Pyrenochaetopsis* sp.	83/29.46
NanE	A0A6G9KJC3	*N*-methyltransferase nanE	nanangelenin	*Aspergillus nanangensis*	82/31.13

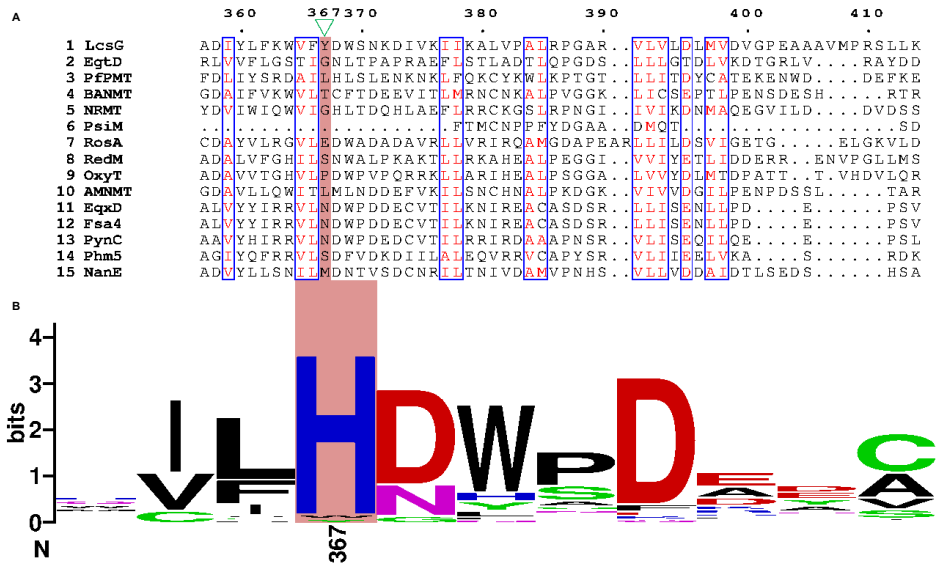

Figure 3-25: Sequence comparison between the LcsG and other identified NMTs and OMTs. The residues corresponding to Y367 in LcsG were indicated with the red background and green triangle. (A) Sequence comparison between the LcsG and NMTs. Red letters in blue boxes indicated well-conserved amino acids or similar amino acids. (B) Generated WebLogo for the LcsG and OMTs listed in Table 3-6.

In functional OMTs, the charge relay system involving the His-Glu catalytic dyad is highly conserved (Jansson et al., 2005). The His serves as the general base, facilitating the deprotonation of the substrate nucleophile, typically the hydroxyl group (Cai et al., 2019).Taking the proteins analyzed in our previous multiple sequence alignments as examples (Figure 3-17A), the basic residues in ChOMT (Zubieta et al., 2001), MmcR (Singh et al., 2011), and OxaC (H278, H259, H313) contrast with LcsG's Y (at position 367). Among the identified structural homologs of LcsG in the PDB database, RosA and RedB are the only two NMTs with reported crystal structures and active sites; RosA and RedB feature S253 and E255 as their

corresponding residues, respectively. To expand the search, we selected fungal-derived methyltransferases similar to LcsG, annotated by the same Pfam (PF00891), for analysis (Table 3-6). Sequence comparison of OMTs and NMTs mentioned in Table 3-5 and Table 3-6 revealed that most of these OMTs have basic residues, while NMTs exhibit neutral or acidic residues at the corresponding positions (Figure 3-25). As hypothesized in our study, in the LcsG-catalyzed *N*-methyl transfer reaction, which involves a nucleophilic attack by the terminal N lone electron pair of leucinostatin on the reactive sulfonium methyl group of SAM, the *N*-methyl transfer reaction may not require a basic residue for deprotonation.

To elucidate the relationship between LcsG and other methyltransferases, we constructed a phylogenetic tree that included LcsG and experimentally confirmed similar MT sequences and NMTs listed in Table 3-5 (Figure 3-26a). This tree is divided into four main phylogenetic groups representing genes from fungi, bacteria, animals, and plants. Notably, OMTs and NMTs did not form distinct evolutionary groups, with LcsG appearing on an independent branch. An exception was observed in *Streptomyces* sp., in which OMT (P16559) and NMT (RosA) showed a close phylogenetic relationship and high similarity in sequences (Figure 3-26b); this result indicated that a gene duplication event may have led to divergence of OMT and NMT after the speciation of *Streptomyces*. Consistent with previous findings, the residue corresponding to Y367 in LcsG is H in OMT and E in NMT. (Figure 3-26b). Further investigation revealed a sequence similarity network (SSN) for LcsG and sequences mentioned in Table 3-6 (Figure 3-27A). The SSN findings were consistent with the phylogenetic tree, showing no clear separation between OMTs and NMTs. In the network, NMTs, including LcsG, exhibited more connections with OMTs. Specifically, NMT Fsa4 clustered with three other NMTs (PynC, EqxD, and Phm5), likely due to similarities in their substrates (Figure 3-27B). Apart from LcsG, we propose that some sequences annotated as OMTs in genomic databases may actually be NMTs. Differences in some specific acidic residues at key positions in OMTs and NMTs, such as Y versus H, can serve as an indicator. This bioinformatic analysis indicated a possible evolutionary link between OMTs and NMTs, and also emphasized the important functions of those specific amino acids in OMTs and NMTs.

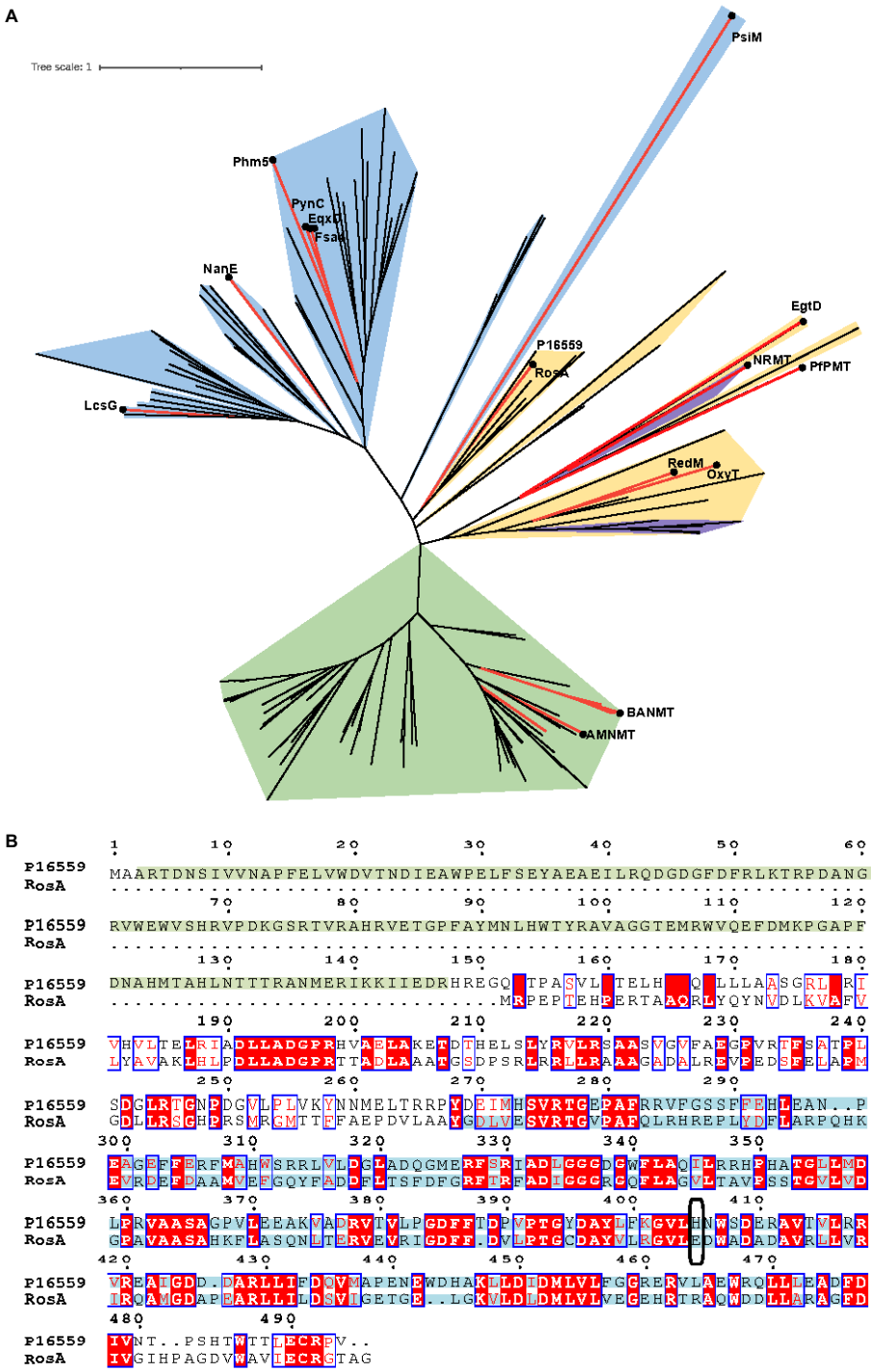
A
Tree scale: 1
PsiM
Phm5
PyncEqxDFsaB
NanE
LcsG
P16559
RosA
EgtD
NRMT
PfPMT
RedM
OxyT
BANMT
AMNMT
B
P16559 MAARTDNSIVVNAPFELVWDVTNDIEAWPELFSEYAEAEILRQDGDGFDFRLKTRPDANG
RosA --
P16559 RVWEWVSHRVPDKGSRTVRAHRVETGPFAYMNLHWTYRAVAGGTEMRWVQEFDMKPGAPF
RosA --
P16559 DNAHMTAHLNTTTRANMERIKKIIEDRHREGQLTPASVLLTELHQLLLAASGRLRRI
RosA ----------------------------MRPEPTEHPERTAAQRLYQYNVDLKVAFV
P16559 VHVLTELRIADLLADGPRHVAELAKETDTHELSLYRVLRSAASVGVFAEGPVRTFSATPL
RosA LYAVAKLHLPDLLADGPRTTADLAAATGSDPSRLRRLLRAAAGADALREVPEDSFELAPM
P16559 SDGLRTGNPDGVLPLVKYNNMELTRRPYDEIMHSVRTGEPAFRRVFGSSFFEHLEAN..P
RosA GDLLRSGHPRSMRGMTTFFAEPDVLAAYGDLVESVRTGVPAFQLRHREPLYDFLARPQHK
P16559 EAGEFFERFMAHWSRRLVLDGLADQGMERFSRIADLGGGDGWFLAQILRRHPHATGLLMD
RosA EVRDEFDAAMVEFGQYFADDFLTSFDFGRFTRFADIGGGRGQFLAGVLTAVPSSTGVLVD
P16559 LPRVAASAGPVLEEAKVADRVTVLPGDFFTDPVPTGYDAYLFKGVLHNWSDERAVTVLRR
RosA GPAVAASAHKFLASQNLTERVEVRIGDFF.DVLPTGCDAYVLKGVLEDWADADAVRLLVR
P16559 VREAIGDD.DARLLIFDQVMAPENEWDHAKLLDIDMLVLFGGRERVLAEWRQLLLEADFD
RosA IRQAMGDAPEARLLILDSVIGETGE..LGKVLDLDMLVLVEGEEHRTRAQWDDLLARAGFD
P16559 IVNT..PSHTWTTLECRPV..
RosA IVGIHPAGDVWAVIECRGTAG

Figure 3-26: (A) A phylogenetic tree showing the relationships between LcsG and other methyltransferases. The black and red lines represent OMT and NMT, respectively. Sequence origins are color-coded as follows: blue for fungi, yellow for bacteria, purple for animals and humans, green for plants, and white for protozoa. (B) Alignment sequences of OMT (P16559) and NMT (RosA). White letters on a red background indicated strictly conserved amino acid residues. Red letters in blue boxes indicated well-conserved amino acids or similar amino acids. Additionally, the N-terminal aromatase/cyclase domain of the multifunctional protein P16559 is delineated with a green background, whereas the Methyltransf_2 domain is highlighted in blue. The black frame indicated the residue corresponding to Y367 in LcsG.

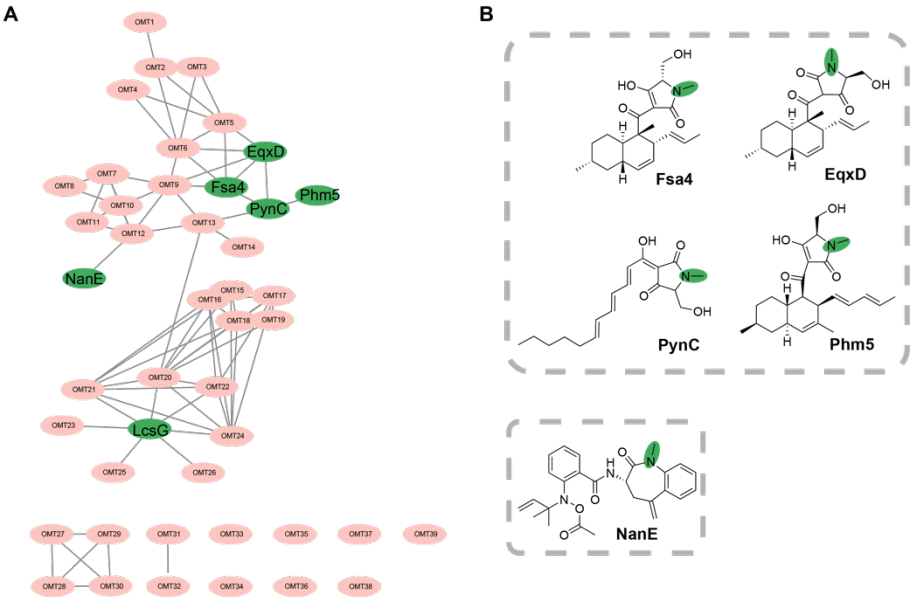

Figure 3-27: (A) Sequence similarity network (SSN) of LcsG and other fungi-derived methyltransferases from PF00891 (alignment score ≥10). (B) Substrates of the NMT FsaA, PynC, EqxD, and Phm5. Catalytic sites are highlighted in green.

Regarding the enzymatic mechanism of methyltransferases, numerous studies have proposed a reaction mechanism for OMT, involving a His/Glu dyad and an Asp residue. The Glu residue was placed near the His residue, and the His residue was activated to deprotonate the hydroxyl group in the substrate. The Asp residue was shown to interact with the substrate to improve binding. The deprotonated hydroxyl group functions as a good nucleophile to attack SAM (Newmister et al., 2018), which is a methyl donor, to form the *O*-methylation product. In the case of NMT, similar but different mechanisms have been proposed (Mahmoodi et al., 2020). A QM/MM study on the catalytic mechanism of phenylethanolamine NMT (Hou et al., 2012) revealed that unlike OMT, a Glu residue was employed to deprotonate the protonated amine in the substrate to form a nucleophile. Then, the methyl group was transferred from the

methyl-donor SAM to the deprotonated amine group. Unlike reactions catalyzed by OMT, a His/Glu dyad was not needed for NMT. The lone electron pair of the *N* atom on the dimethylamine group can undergo a nucleophilic attack. We proposed that the protonated dimethylamine group in leucinostatins might be coordinated and deprotonated by two negatively charged residues (D368 and D395). A nucleophilic attack between dimethylamine and SAM followed, and the methyl group was transferred from SAM to leucinostatins. Compared to wild-type LcsG, the D368A and D395A mutants exhibited markedly obvious decreased methylation (Figure 3-19C), highlighting the importance of these residues in substrate binding. For LcsG, the mutation data, docking results and MD simulation results collectively gave a hint that its reaction mechanism is similar to that of phenylethanolamine NMT.

NRPSs are well-known megaenzymes that consist of sequential domains. The peptide is elongated, followed by release from the terminal module, which includes condensation domains (C_T), reductase domains (R), Dieckmann cyclase domains (D), and thioesterase domains (TE) (Zhang et al., 2023). According to the analysis of the antiSMASH 2.0 and pBLAST results (Table 3-7), the terminal module of the NRPS in the biosynthesis-related gene cluster (LcsA) should be an R domain that can release the peptide from the NRPS by reduction; thus, the C-terminus of leucinostatins is normally an aldehyde group (Berry et al., 2019; Schracke et al., 2005; Tanaka et al., 2005; Yeh et al., 2016) or a hydroxyl group (Chiang et al., 2016; Jia et al., 2019; Li et al., 2018) (Figure 3-28). However, we have not observed these similar structures among the existing characterized leucinostatins. Based on these reports and the NMR results of LeuK0, we initially deduced the C-terminus of LeuK0 to be -NH-CH_2-CH_2-OH, but this hypothesis was rejected by subsequent NHS ester reactions and enzyme assays.

Table 3-7: Non-ribosomal peptide synthetases (NRPSs) contained terminal modules similar to that of LcsG.

Name	**UniProt Accession No.**	**Gene cluster**	**Organism**	**Terminal Module Coverage /Identity**
InpA	Q5B7I5	Fellutamide B	*Aspergillus nidulans* FGSC A4	100/41.57
ApmA	A0A1W6BT53	Asperphenamate	*Penicillium brevicompactum*	100/42.35
AtnA	Q5AUZ6	Aspercryptin	*Aspergillus nidulans* FGSC A4	100/42.16
NRPS 5	I1SAJ7	Fusaoctaxin A	*Fusarium graminearum* PH-1	92/40.69
PpzA	A0A166YZW0	Pyrrolopyrazine	*Metarhizium rileyi* RCEF 4871	100/40.24
PerA	Q4H424	Peramine	*Epichloe festucae* Fl1	96/41.49
LgrD	Q70LM4	Linear gramicidin	*Brevibacillus parabrevis*	89/33.62

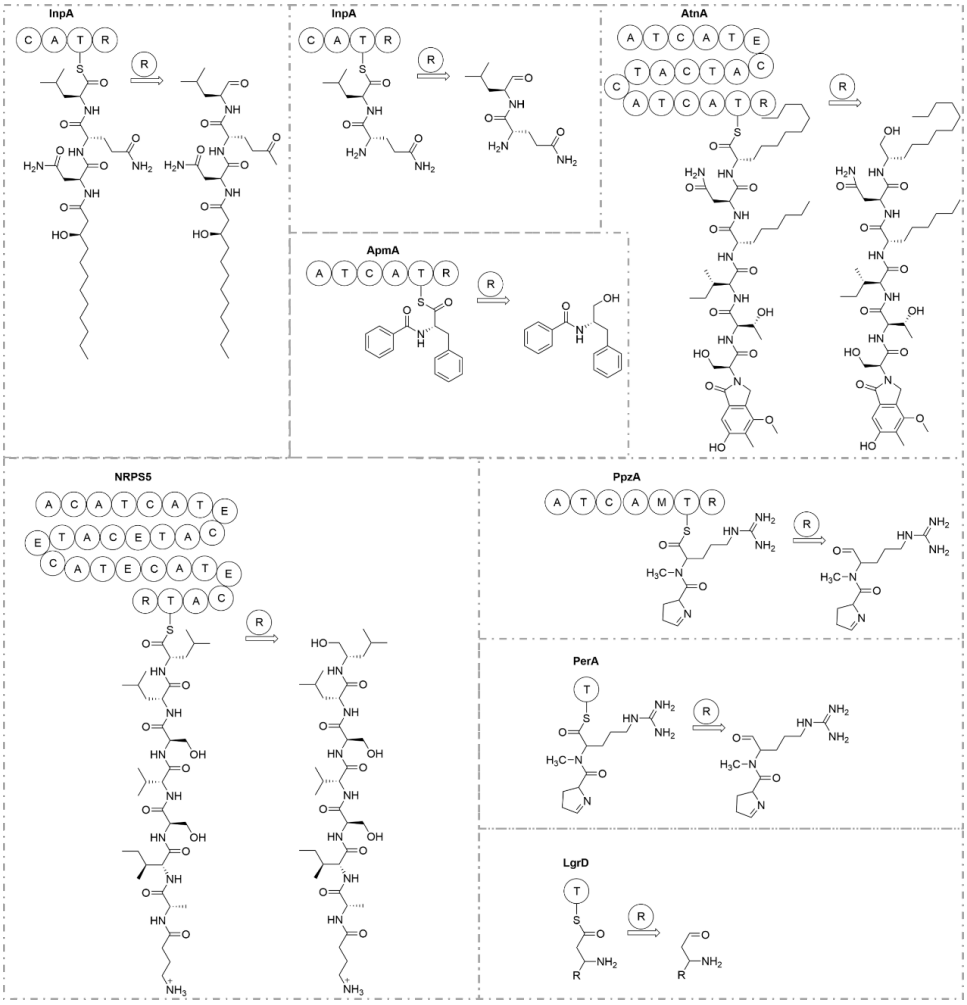

Figure 3-28: The termination step mediated by the reductase (R) domain in the biosynthesis of NRPs whose gene contained similar terminal modules with that of LcsG.

5. Conclusion

In conclusion, an OMT-like enzyme from *P. lilacinum*, LcsG, was identified as a discrete SAM-dependent NMT that can iteratively catalyze the formation of primary amines, secondary amines, and tertiary amines in the unique terminal unit of leucinostatins. Furthermore, one new secondary metabolite (LeuK0) and two enzymatic products (LeuK2 and LeuK3) were identified as new leucinostatins. In addition, the methylated compounds were observed to display greater antimicrobial activity than that of their parent molecules. To our knowledge, LcsG is a rare NMT that can methylate the terminal residues of NRPs. We expect that the results of this study will provide deeper insights into the mechanisms underlying the *N*-methylation

of peptides and increase the possibility of engineering new methylated molecules for exploring more potent antibiotics.

6. Materials and methods

6.1. Strains and culture conditions

The strains used in this study are listed in Table 3-8. *Purpureocillium lilacinum* strain PLBJ-1 (CGMCC3.17492) (Jiao et al., 2019; Liu et al., 2020; Wang et al., 2016), was isolated from tomato roots in Beijing, and its transformants were cultured at 28 °C in potato dextrose agar (PDA) or potato dextrose broth (PDB) supplemented with 400 μg/mL geneticin (G418). *Escherichia coli* Trelief 5α (Tsingke, China) was cultured at 37 °C in Luria–Bertani (LB) broth supplemented with appropriate antibiotics. *E. coli* ArcticExpress (DE3) (Agilent Technologies) was used to express LcsG proteins. *E. coli* ArcticExpress (DE3) was cultivated at 37 °C in LB broth supplemented with appropriate antibiotics for growth, followed by growth at 11 °C to induce the recombinant protein.

Table 3-8: Plasmids and strains used in this study.

Plasmids/Strains	Description	Reference
pKOV21	geneticin (*neo*, G418) resistance vector, Amp	Shen, B. et al. Development of a high-efficiency gene knockout system for *Pochonia chlamydosporia*
pEASY	*LacZα*, T7 promoter, Kan^r, Amp	TransGen Biotech
pACYCDuet-1	*lacI*, T7 promoter-1, T7 promoter-2, Cm^r	Novagen
KSTNP	*TrpC* terminator and *neo* contained vector	Wang, G. et al. Biosynthesis of Antibiotic Leucinostatins in Bio-control Fungus *Purpureocillium lilacinum* and Their Inhibition on *Phytophthora* Revealed by Genome Mining

PCH-sGFP	*gpdA(p)* contained vector	Liang, L. et al. A high efficiency gene disruption strategy using a positive–negative split selection marker and electroporation for *Fusarium oxysporum*
pGNT	*neo*, *TrpC*, *gpdA(p)* in pEASY	This study
pKOV21-ko*lcsG*	*lcsG* deletion cassette in pKOV21	This study
pGNT-*lcsG*	*lcsG* overexpression cassette in pGNT	This study
pACYC-*lcsG*	*lcsG* expression cassette in pACYCDuet-1	This study
Purpureocillium lilacinum strain PLBJ-1 (CGMCC3.17492)	Wild type	This study
Escherichia coli DH5α		Tsingke
Escherichia coli ArcticExpress (DE3)	*E. coli* B F$^-$ *ompT hsdS*(r_B^- m_B^-) *dcm*$^+$ Tet^r *gal* λ(DE3) *endA* Hte [*cpn10 cpn60* Gent^r]	Agilent Technologies
PLBJ-Δ*lcsG*	Δ*lcsG*::*neo* in *P. lilacinum* PLBJ-1	This study
PLBJ-OE*lcsG*	*neo, gpdA*::*lcsG*::*TrpC* in *P. lilacinum* PLBJ-1	This study
E. coli ArcticExpress (DE3)-*lcsG*	*E. coli* ArcticExpress (DE3) pACYC-*lcsG*	This study

6.2. DNA and RNA isolation

The mycelia of PLBJ-1 and the mutants were harvested via filtration after cultivation in 2 mL of potato dextrose broth (PDB) at 28 °C for 24 hours. The genomic DNA was extracted using a Qiagen DNeasy Kit. RNA was extracted using a TRIzol reagent (Takara, Japan) following the manufacturer's protocol. Fungal samples used for RNA extraction was cultivated on PDA at 28 °C for 3 days.

6.3. Gene cloning and plasmid construction

The oligonucleotide sequences for PCR primers are listed in Table 3-9. PCRs were performed using 2 × Phanta Max Master Mix Polymerase (P525, Vazyme Biotech Co., Ltd, China) and Q5 High-Fidelity DNA Polymerase (New England Biolabs, USA). The plasmids used are listed in Table 3-8. To construct the deletion cassette of *lcsG*,

approximately 1 kb DNA fragments located upstream and downstream of the *lcsG* coding region were amplified from the gDNA of PLBJ-1 and named *lcsGup* and *lcsGdown*, respectively. Two fragments and the selection marker gene *neo* were integrated into the *Kpn*I/*Bam*HI-cleaved vector pKOV21 via the digestion-ligation method by using T4 DNA Ligase (Thermo Fisher Scientific, USA) to generate the deletion plasmid pKOV21-ko*lcsG*.

For the overexpression of *lcsG* in PLBJ-1, the *lcsG* gene was amplified from the cDNA of PLBJ-1. The selection marker gene *neo* and the terminator *TrpC* were amplified from the KSTNP vector. This fragment and two restriction enzyme cutting sites, *Pme*I and *Pac*I, were integrated into the pEASY vector by using the *pEASY*®-Blunt cloning Kit (TransGen Biotech, China) to generate the intermediate vector pEASY-*neoTrpC*. Then the strong promoter *gpdA* was amplified from the PCH-sGFP vector and integrated into the *Not*I/*Apa*I-cleaved vector pEASY-*neoTrpC* via the digestion-ligation method by using DNA T4 ligase to generate the vector pGNT. Afterward, the *lcsG* gene was integrated into the *Pme*I/*Not*I-cleaved vector pGNT by using *pEASY*®-Basic Seamless Cloning and Assembly Kit (TransGen Biotech, China) to create the overexpression vector pGNT-*lcsG*. The recombinant protein LcsG expression vector pACYC-*lcsG* was generated by integrating the *lcsG* gene from the PLBJ-1 cDNA into the protein expression vector pACYCDuet-1 by using the quick-change method (Bok & Keller, 2012). The mutated LcsG protein vectors were obtained by using a QuickMutation™ Site-Directed Mutagenesis Kit (D02065, Beyotime Biotechnology, China) following the manufacturer's instructions. The following sites were used for mutagenesis of the pACYC-*lcsG* plasmid: D296A (AGT to GCT), D321A (GAT to GCT), D348A (GAC to GCC), K363A (CAA to CGC), D368A (GAC to GCC), and D395A (GAT to GCT). Mutations were confirmed by sequencing.

Table 3-9: Primers used in this study.

Primers name	**Sequence (5′ to 3′)**
*lcsG*up-f	TCCCCGCGGAAGTCGGGTAGACAGGGTGAAAT
*lcsG*up-r	AAGGAAAAAAGCGGCCGCACAGATGAAGCTGCGTTTACGAC
*lcsG*down-f	GACTAGTGCTGCGATAGTCGCTACTAAAGC
*lcsG*down-r	CGCGGATCCGCCTTGAGCAACATTCTGGC
lcsGup-ne-r	CGTAAAGCACGAGGAAGCG
eo-lcsGdown-f	GACTGGGCACAACAGACAATCG
p*lcsG*KO SCR-f	AAGCTCATCAAACGGTCAAACAT
p*lcsG*KO SCR-r	CACTCACCAAGTCAGTGCTCCTC
*lcsG*check-f	CCCTGAAAGAGCGACTGGAG
*lcsG*check-r	GGCTCAAAGATGCGGTTGCTA
QC-*lcsG*-f	gatataccatgggcagcagccatcaccatcatcaccacATGGGAGACAACG

	TTCAGTCC
QC-*lcsG*-r	gcgccgagctcgaattcggatcctggctTCAGTGGTGGTGGTGGTGGT GGCCACGCCAAACAGCCTC
	GA
pEASY-*neoTtrpC*-f	ttaattaagtttaaacACTTAACGTTACTGAAATCATCAAA
pEASY-*neoTtrpC*-r	TCTAGATTAACGCTTACAATTTCCA
pGNT-*gpdA*-f	CATGgggcccGCCATTCAGGCTGCGCAACTGTTGG
Pgnt-*gpdA*-r	AAGGAAAAAAgcggccgcGGTGATGTCTGCTCAAGCGGG GTAG
OE-*lcsG*-f	AGCAGACATCACCGCATGGGAGACAACGTTCAGTC
OE-*lcsG*-r	CAGTAACGTTAAGTgCTAGCCACGCCAAACAGCCTC
OE-*lcsG*-SCR-f	GTTGACAAGGTCGTTGCGTC
OE-*lcsG*-SCR-r	GATAGCCTCAACCGCCTCCTG
Actin-f	GCCCTCTGTCCTGGGTCTT
Actin-r	ACAGGGAGGCGAGAATGGA
qp-*lcsG*-f	CTCGTGTCCTCGTCCTGGATCTG
qp-*lcsG*-r	GATCATCCGCTGCCTTGAAGAGATC
mutant-D296-F	CAAAGCCACCGTCGTTGcTCTTGGTGGCTCTGGC
mutant-D296-R	GCCAGAGCCACCAAGAgCAACGACGGTGGCTTTG
mutant-D321-F	CAAGATCATCGTCCAGGcTCTGCCTAGTTGCCAA
mutant-D321-R	TTGGCAACTAGGCAGAgCCTGGACGATGATCTTG
mutant-D348-F	TCCTTCCTCGCTCATGcCTTCTTCACCCCTCAG
mutant-D348-R	CTGAGGGGTGAAGAAGgCATGAGCGAGGAAGGA
mutant-K363-F	CGACATCTACCTCTTCgcGTGGGTCTTTTACGACT
mutant-K363-R	AGTCGTAAAAGACCCACgcGAAGAGGTAGATGTCG
mutant-Y367-F	CTTCAAGTGGGTCTTTgcCGACTGGTCCAACAAG
mutant-Y367-R	CTTGTTGGACCAGTCGgcAAAGACCCACTTGAAG
mutant-D368-F	CAAGTGGGTCTTTTACGcCTGGTCCAACAAGGAC
mutant-D368-R	GTCCTTGTTGGACCAGgCGTAAAAGACCCACTTG
mutant-D395-F	CGTGTCCTCGTCCTGGcTCTGATGGTGGACGTC
mutant-D395-R	GACGTCCACCATCAGAgCCAGGACGAGGACACG
mutant-K431-F	GCTGTTTGGACATACCgcGCAGGCGACGAAGAAG
mutant-K431-R	CTTCTTCGTCGCCTGCgcGGTATGTCCAAACAGC

6.4. PEG-mediated fungal transformation

The split-marker strategy was used to disrupt the *lcsG* gene. The DNA fragments *lcsGup-ne* (*lcsGup* and the first half of *neo*) and *eo-lcsGdown* (the second half of *neo*

and *lcsGdown*) were amplified from pKOV21-ko*lcsG*. The two fragments of *neo* overlapped by 667 bp. For polyethylene glycol (PEG)-mediated fungal transformation, 10^8 spores of PLBJ-1 was cultured in 200 mL of PDB medium at 28 °C and 150 rpm for 18 hours. The fungal germlings were harvested using a 4-layer Miracloth filter (Solarbio, China). After washing with 0.7 M NaCl, the mycelia were treated with 2 μg/mL driselase (Sigma) at 28 °C and 150 rpm for 4 hours to obtain protoplasts. Microscopic examination was conducted to assess the protoplast status. Following filtration with the 4-layer Miracloth and thorough washing with STC buffer, the protoplasts were collected by centrifugation at 4 °C, 4000 rpm for 15 minutes, and resuspended to a concentration of 10^6/mL in STC buffer. Five microgram of the two DNA fragments were transformed into 100 μL of PLBJ-1 protoplasts. G418-resistant colonies were selected after culture on PDA at 28 °C for 1 day. The candidate transformants were picked and inoculated onto new PDA plates supplemented with 400 μg/mL G418 (Inalco, USA) for 3-5 days. These transformants were verified via diagnostic PCR with primers. For the overexpression of *lcsG*, the plasmid pGNT-*lcsG* and the empty vector pGNT were transformed into PLBJ-1 to construct the overexpression and control strains, respectively.

6.5. qRT–PCR analysis of the lcsG overexpression strain

For cDNA synthesis, approximately 1 μg of DNase-treated, RNase-cleaned RNA was used as the template by using HiScript III RT SuperMix for qPCR (+gDNA wiper) (R312, Vazyme Biotech Co., Ltd, China). Three biological replicates were measured for each analysis of the relative expression levels. The housekeeping gene *actin* (GenBank number VFPBJ_07912) was used as a control. qRT–PCR was performed with ChamQ Universal SYBR qPCR Master Mix (Q711, Vazyme Biotech Co., Ltd, China) on a Bio-Rad CFX96 (Bio-Rad). The relative expression values were calculated using the $2^{-\Delta\Delta Ct}$ method (Livak & Schmittgen, 2001). The primers used are listed in Table 3-9.

6.6. Culture extraction

Cultures of 1×10^5 conidia per mL of PLBJ-1 and its mutants were cultured in PDB media at 28 °C and 220 rpm for 14 days. The fermentation mixture was extracted with an equal volume of ethyl acetate (EtOAc) three times (every 1 hour) to efficiently extract leucinostatins and EtOAc was evaporated under reduced pressure. The extract was redissolved in acetonitrile (MeCN) for further experiments.

6.7. Product purification of LeuK0, LeuA0, and LeuK3

LeuK0, LeuA0, and LeuK3 were purified by semipreparative HPLC from the crude extracts mentioned above. The UV absorption of leucinostatins was monitored at 214 nm with HPLC DAD. The samples were separated on an Agilent 1260 Infinity II HPLC system with a Kromasil 100-5-C18 column (10 mm × 250 mm), and eluted with a linear gradient of MeCN-water, starting at 20% MeCN and reaching 70% MeCN over 25 min at a flow rate of 2 mL/min. The retention times of LeuK0, LeuA0, and LeuK3 were 23.8 min, 21.6 min, and 22.3 min, respectively. LeuK0 (18 mg, purity ≥ 95%) was obtained from the crude extract of Δ*lcsG* mutant (570 mg). LeuA0 (13

mg, purity ≥ 95%) and LeuK3 (11 mg, purity ≥ 95%) were isolated from chemically methylated WT (390 mg) and Δ*lcsG* mutant crude extracts (500 mg), respectively.

6.8. Chemical methylation of LeuA and LeuK0

For the chemical methylation pilot study of LeuA and LeuK0, diisopropylethylamine (15 μL) and iodomethane (55 μL) were successively added to solutions of LeuA and LeuK0 (10 mg) in dry tetrahydrofuran (THF) (0.6 mL), respectively. These mixtures were stirred at room temperature at 800 rpm for 46 hours, and volatile constituents were evaporated at room temperature by using nitrogen blowdown evaporator (Langlois & Le Nguyen, 2004). To isolate LeuA0 and LeuK3 in bulk, the WT and Δ*lcsG* mutant crude extracts were used as substrates, respectively.

6.9. Structural characterization of LeuK0

LeuK0 was assigned a molecular formula of $C_{62}H_{111}N_{11}O_{14}$ based on its HRESIMS data (*m/z* 1234.8383 $[M+H]^+$). ESI-MS-MS data were compared with those of previously reported leucinostatins A—C, revealing identical structural features (from B1 to C10) but a distinct C-terminal unit (C_2H_6NO) in LeuK0. Analysis of its ^{13}C-NMR APT, DEPT-135, and DEPT-90 spectroscopic data revealed a total of 62 carbons, including 18 methyl groups (-CH_3), 14 methylenes (-CH_2), 16 methines (-CH), and 14 sp^3 quaternary carbons. Since the known unit (from B1 to C10) already contains 18 -CH_3, 12 -CH_2, 16 -CH, and 14 sp^3 quaternary carbons, the C-terminal unit (C_2H_6NO) in LeuK0 was thought to be -NH-CH_2-CH_2-OH or -CH_2-CH_2-O-NH_2.

6.10. N-hydroxysuccinimide (NHS)-ester reaction

7-methoxycoumarin-3-carboxylic acid N-succinimidyl ester (4 mg) and diisopropylethylamine (6 μL) were successively added to a solution of LeuK0 (15 mg) in dimethylformamide (DMF) (200 μL). These mixtures were stirred at room temperature at 800 rpm for 3 hours, and the volatile constituents were evaporated at room temperature by using nitrogen blowdown evaporator.

6.11. Protein expression and purification

For the expression of LcsG, *E. coli* ArcticExpress (DE3) carrying pACYC-*lcsG* was cultured. The *E. coli* cells were grown at 37 °C in 1 L of LB medium supplemented with the appropriate antibiotics. The culture was supplemented with IPTG (at a final concentration of 0.1 mM) when the OD_{600} reached 0.6-0.8, after which the induced *E. coli* were grown at 11 °C for 24 hours. The cells were harvested by centrifugation (5000 rpm, 15 min, 4 °C), resuspended in 20 mL of lysis buffer (50 mM NaH_2PO_4, pH 8.0, 300 mM NaCl, 10 mM imidazole) and lysed by sonication on ice (200 W, 10 s, 10 s, 20 min) with an ultrasonic homogenizer SCIENTZ-IID (SCIENTZ, China). The lysate was centrifuged (12000 × g, 1 hour, 4 °C), and the supernatant was collected and filtered through a 0.45 μm membrane (Sartorius Stedim Biotech, Germany) to remove residual cellular debris. A nickel affinity chromatography column was prepared with 2 mL of Ni-NTA resin (Trans Gen Biotech, China) loaded into a gravity column (Sangon, China) and used to separate the filtered supernatant. After the samples were washed with wash buffer (50 mM NaH_2PO_4, pH 8.0, 300 mM

NaCl, and 20/40/60 mM imidazole), His-tagged proteins were eluted with elution buffer (50 mM NaH_2PO_4, pH 8.0, 300 mM NaCl, and 250 mM imidazole). Purified proteins were concentrated in storage buffer (50 mM Tris-HCl, pH 7.5, 20% glycerol), and flash frozen. The purity of the protein was confirmed by SDS–PAGE. The mutant proteins were purified via a procedure similar to that used for LcsG. The expression of the mutated proteins was verified by Western blotting using an anti-His antibody (TransGen Biotech Ltd., Beijing, China).

6.12. In vitro enzyme assay for LcsG and its mutants

For the benchmark experimental conditions, the enzyme assays (50 μL) contained Tris-HCl buffer (50 mM, pH 7.5), SAM (2 mM), LeuA or LeuK0 (10 μM), and purified recombinant LcsG (10 μM). The reactions were incubated at 28 °C for 120 min. For single-factor experiments, the enzyme assays (50μL) contained Tris-HCl buffer (50 mM), SAM (2 mM), PLBJ-1 WT crude extract (200 μg), and purified recombinant LcsG (10 μM). For the reaction time course assay, LcsG was tested with Tris-HCl buffer (pH 7.5) at 28 °C for 0.01 min, 15 min, 30 min, 45 min, 60 min, 75 min, 90 min, 105 min, and 120 min. For the reaction pH course assay, LcsG was tested at 28 °C for 120 min with Tris-HCl buffer at different pH values (pH 7.0, pH 7.5, pH 8.0, pH 8.5). For the reaction temperature course assay, LcsG was tested with Tris-HCl buffer (pH 8.0) for 120 min at 18 °C, 21 °C, 27 °C, 34 °C, and 38 °C. To determine the function of mutated LcsG, 50 μL reaction mixtures were prepared with 500 nM mutant catalysts, 2 mM SAM, 100 mM Tris-HCl buffer (pH 8.0), and 10 μM substrates. The reactions were incubated at 34 °C for 120 min. The above enzymatic reactions were quenched by adding 50 μL cold acetonitrile and 10 μL was analyzed by LC–MS.

6.13. Calibration curves of LeuA0 and LeuK3

The compounds were quantified by an external standard method and calibration curves were constructed using LeuA0 and LeuK3. In this study, LeuA0 was diluted to concentrations of 25, 50, 100, 250, and 500 nM. LeuK3 was also diluted to concentrations of 50, 100, 250, 500, and 1000 nM. Dilutions were prepared in MeCN, and calibration curves were constructed using the software GraphPad Prism 9.

6.14. Michaelis–Menten enzyme kinetics

The kinetic constants of LcsG were determined by the following approach: 1 μM LcsG was assayed against different specific concentrations of the substrates LeuA (2 μM, 4 μM, 8 μM, 10 μM, 20 μM, 40 μM, 80 μM, 100 μM, 120 μM, 150 μM, and 200 μM) and LeuK0 (4 μM, 8 μM, 10 μM, 20 μM, 40 μM, 80 μM, 100 μM, 120 μM, 140 μM, and 160 μM). The initial rate of the reaction was measured by monitoring the formation of products (LeuA0 or LeuK3) at 34 °C for 30 minutes. The rates were plotted against substrate concentration using the Michaelis–Menten kinetics equation by nonlinear regression analysis with the software GraphPad Prism 9, and K_m and K_{cat} constants were generated from the resulting Michaelis–Menten plot.

6.15. LC–MS analysis

LC–MS analyses were performed on an Agilent 1290 Infinity II HPLC with an Agilent Infinity Lab single quadrupole mass selective detector by using an Agilent Zorbax Eclipse Plus C18 reversed-phase column (2.1 × 100 mm, 2.7 μm). Water (A) with 0.1% (v/v) formic acid and acetonitrile (B) were used as the solvents at a flow rate of 0.25 mL min^{-1}. The substances were eluted with 10% (v/v) B for 1 min, subjected to a linear gradient from 10 to 100% (v/v) B for 12 min, washed with 100% solvent B for 5 min, and equilibrated with 5% solvent B for 10 min at a flow rate of 0.25 mL/min. The mass spectrometer was set in electrospray positive ion mode for ionization.

LC-HRESI-MS-MS analyses were performed on an Agilent HPLC 1260 Infinity II system equipped with an Agilent G6510A mass spectrometer by using an Agilent Zorbax SB-C18 reversed-phase column (4.6 × 150 mm, 5 μm). A linear gradient analytical method was used (10–100% MeCN in water with 0.1% formic acid for 20 min at a flow rate of 1.0 mL/min). The Q-TOF was operated in positive electrospray ionization mode with a capillary voltage of 1800 V and a drying gas flow rate of 1 μL/min at 300 °C. The MS scan range was 80–2000 *m/z*, and the MS-MS scan range was 40–1400 *m/z*. The fixed collision energy was 65 V.

6.16. Microbial growth inhibition assays

The growth inhibition of *C. neoformans* H99 by leucinostatins (LeuK0, LeuK3, LeuA0) with was assessed on PDA media with agar diffusion assays. Overnight cultures of *C. neoformans* grown in PDB broth at 28 °C were diluted with PDB broth to an OD_{600} of 0.1. One milliliter aliquots of the resulting mixture were combined with 30 mL aliquots of PDA at 45 °C. The test wells (4 mm diameter) were aspirated from the solidified medium using the tip of a sterilized Luer-lock syringe, and 10 μL of each compound (25 μg) was added to each well. The plate was incubated at 28 °C. Zones of inhibition were photographed after 36 hours, and leucinostatins and amphotericin B (Solarbio, China) were dissolved in DMSO. The growth inhibition of *P. infestans* by leucinostatins (LeuK0, LeuK3, LeuA0) with was assessed on rye agar medium in 9-cm Petri plates. *P. infestans* was incubated on the center of plates and cultured at 18 °C for 3 d, followed by incubation in aspiration test wells (4 mm diam) at the colony edges.

According to the National Committee for Clinical Laboratory Standards (NCCLS) recommendations (Li et al., 2016), the minimal inhibitory concentration (MIC) was determined with three replicates using the serial dilution method in 96-well plates with YM (1% maltose extract, 0.2% yeast extract) as the test medium. Amphotericin B was used as the positive control. Test compounds were dissolved in DMSO and serially diluted in a growth medium. The visual endpoint and optical density of the microplate wells were measured relative to those of the positive and negative controls. The *C. neoformans* H99 strains were incubated at 25 °C, and the MICs were determined at 48 hours. Viability was determined with the aid of a plate reader using PrestoBlue resazurin dye (Life Technologies) as the viability indicator. The spectrophotometric MIC value was defined as the lowest concentration of a test compound that resulted

in a culture with a density equal to 100% inhibition compared to the growth of the untreated control.

6.17. Structure prediction of LcsG

Uni-Fold (https://github.com/dptech-corp/Uni-Fold) was used to predict the LcsG dimer structure. A fasta file of two lcsG sequences was uploaded, and a predicted structure was returned. The average pLDDT score was 0.88.

6.18. Structure and sequence alignment

Homologous protein structures were searched via HHpred. ChimeraX was used to estimate the structural alignment and plot the figures. Multiple sequences were aligned by MAFFT, and ESpript3 (https://espript.ibcp.fr/ESPript/cgi-bin/ESPript.cgi) was subsequently used to export the sequence alignment results.

6.19. DiffDock

The structure of leucinostatin A was modified from the structures of its analogs ZHAWOC6027(PDB: 8a19) and helioferin A (PDB: 6evh). The DiffDock webserver (https://huggingface.co/spaces/simonduerr/diffdock) was used to simulate the dock. The predicted LcsG dimer structure, and leucinostatin A structure were uploaded to initiate the docking process, and the website's backend algorithms were used to process the data and predict the ligand's binding poses to the protein. The model was then chosen from the final docking poses as well as the top-ranked docking pose.

6.20. Molecular dynamic simulation

Molecular dynamics simulations were performed using Desmond (Bowers et al., 2006). The protein–ligand complex was used as an input for the system builder. The OPLS4 force field was employed, the water model used was SPC, and the concentration of NaCl was 0.15 M. The final system was composed of a protein–ligand complex, 15062 water, 53 Na^+ and 42 Cl^-. The output of the system builder was then loaded into the Energy Minimization panel. After energy minimization, the system was then loaded into the Molecular Dynamics panel. The simulation was carried out with the default NPT run settings in Desmond; the temperature was 300 K, the pressure was 1 bar and the simulation time was 500 ns. Later, we extract the last frame of the simulation and run 3 more independent 500 ns simulations.

6.21. Bioinformatics analysis and phylogenetic tree construction

In total, 130 sequences of methyltransferases with annotated functions were downloaded from the NCBI database. The conserved domain architecture of these methyltransferases was characterized using the SMART domain prediction tool (http://smart.embl-heidelberg.de/). The specific parameters for domain prediction (Letunic et al., 2021) were set to include the PFAM and SMART domain databases. For phylogenetic analysis, a maximum likelihood tree was estimated utilizing IQ-TREE software version 1.6.12 (Trifinopoulos et al., 2016) with a bootstrap of 1000. The resulting tree was visualized using the Interactive Tree of Life (ITOL, http://itol.embl.de/).

6.22. Sequence similarity networks

A search for sequences similar to LcsG was performed using the NCBI BLASTp tool, setting the expectation threshold at 0.05. This search specifically identified sequences from fungi within the same Pfam (PF00891) with LcsG that have been demonstrated by experiments. These selected sequences were then analyzed using the EFI-EST enzyme similarity tool (Zallot et al., 2019). A sequence similarity network (SSN) was constructed for the domains of LcsG and these related sequences. For visualization purposes, an alignment score cutoff of 10 was employed, and sequences with ≥40% identity were combined into representative nodes. This SSN was subsequently visualized using Cytoscape version 3.9.1.

6.23. Statistics and Reproducibility

Every experiment was conducted with a minimum of three independent biological replicates. Data are presented as the mean ± standard deviation (SD). Data points in figures represent biological replicates. Each graph displays individual data points. Statistical analyses (mean and SD) were performed using GraphPad Prism 9 software. Detailed information on all reagents and resources can be found in Methods section.

Chapter 4

The pH-Responsive Regulator PlPacC and GATA Transcription Factor PlAreB are Involved in the Regulation of the Biosynthesis of the Antifungal Lipopeptaibols Leucinostatins in *Purpureocillium lilacinum*

Adapted from a manuscript currently under review:

Li Z, Jiao Y, Tang J, Dong X, Thomas R, Xie B, Li Y, Jacques P. The pH-Responsive Regulator PlPacC and GATA Transcription Factor PlAreB are Involved in the Regulation of the Biosynthesis of the Antifungal Lipopeptaibols Leucinostatins in *Purpureocillium lilacinum*. Microbiol Res (Under review)

Author Contribution:

Zixin Li: Conceptualization, Methodology (fungal cultivation, RT-qPCR, protein sequence analysis, gene disruption), Formal analysis, Writing – original draft

Yang Jiao: Methodology (yeast-one-hybrid), Funding acquisition, Writing – review and editing

Jiawei Tang: Methodology (assistant in yeast-one-hybrid)

Xin Dong and Romain Thomas: Methodology (LC-MS analysis)

Bingyan Xie: Supervision

Yan Li: Conceptualization, Writing – review & editing, Supervision, Funding acquisition

Philippe Jacques: Conceptualization, Writing – review & editing, Supervision

1. Abstract

The bio-control fungus *Purpureocillium lilacinum* PLBJ-1 produces leucinostatins, a class of non-ribosomal peptides (NRPSs) with broad-spectrum antimicrobial activities. However, the molecular mechanisms underlying the optimization of culture conditions for leucinostatin production remain unexplored. Previous research showed that that PLBJ-1 synthesizes leucinostatins more effectively in hand-made Potato Dextrose Broth (PDB-M) than in commercially available PDB (PDB-C). Elementary analysis of these two media indicated that difference in leucinostatin yield was correlated with variations in pH dynamics and nitrogen content. Subsequent experiments under different initial pH and nitrogen levels confirmed that an alkaline environment and reduced nitrogen availability could enhance leucinostatin production. To investigate the regulators involved, CRISPR-Cas9-mediated gene disruptions were performed on the pH-responsive transcription factor PlPacC and the nitrogen regulator PlAreB. The disruption of either PlPacC or PlAreB resulted in a marked reduction in biomass and sporulation in *P. lilacinum* PLBJ-1. Specifically, PlPacC disruption impaired environmental pH regulation and significantly decreased leucinostatin production. In contrast, PlAreB disruption led to an increased leucinostatin yield. Overall, these findings demonstrate that environmental pH and nitrogen availability are the critical factors governing leucinostatin biosynthesis, acting through two key transcriptional regulators, PlPacC and PlAreB. This study lays a molecular foundation for future large-scale optimization of leucinostatin fermentation.

Key words: PacC, AreB, PDB, leucinostatins, *Purpureocillium lilacinum*, CRISPR-Cas9

2. Introduction

The filamentous fungus *Purpureocillium lilacinum* (formerly known as *Paecilomyces lilacinus*) is widely recognized for its role in biological control (Luangsa-Ard et al., 2011). It exhibits potent bio-control activity against a variety of plant pathogens, including fungi (Elsherbiny et al., 2021; Lan et al., 2017), insect pests (Goffre & Folgarait, 2015; Liu et al., 2022; Panyasiri et al., 2022; Sani et al., 2023), particularly nematodes (Khan & Tanaka, 2023; Mhatre et al., 2022; Silva et al., 2022). Two strains of *P. lilacinum* (PL11 and 251) have been approved as pesticides in the European Union. Beyond its parasitization of nematode eggs (Xu et al., 2021) and enzymatic degradation of cell membranes (Elsherbiny et al., 2021), *P. lilacinum* produces leucinostatins, a class of antifungal lipopeptides with broad-spectrum bioactivity (Wang et al., 2016). These compounds were assembled by nonribosomal peptide synthetases (NRPS). Beyond their agricultural applications as nematicidal agents and anti-*Phytophthora* agents, leucinostatins have also shown potential in inhibiting cancer cells and protozoa (Brand et al., 2021; Kawada et al., 2010; Kil et al., 2020). In recent years, our group has extensively explored *P. lilacinum* PLBJ-1 and its leucinostatin metabolites. The biosynthetic gene cluster responsible for leucinostatin production was elucidated, revealing 20 genes involved in its

biosynthesis (Wang et al., 2016).. Based on this, the function of the transcription factor within this cluster was characterized (Jiao et al., 2019). In parallel, chemical analyses revealed that *P. lilacinum* PLBJ-1 predominantly produces four major leucinostatins: A, B, C, and K0. Additonally, the role of a rare free-strand N-methyltransferase at the NRPs terminus has been elucidated, revealing its influence on leucinostatins' antimicrobial activity (Li et al., 2024). Obviously, enhancing leucinostatins yield is important to facilitate its industrial application.

Modifying cultivation conditions (for example temperature, pH, oxygen availability) or adjusting medium composition (including carbon sources, nitrogen sources, and trace elements) can significantly influence fungal metabolism (Bode et al., 2002). Potato Dextrose Agar (PDA) and Potato Dextrose Broth (PDB) are widely used fungal culture media. Depending on their origin, these culture media can differ in their composition which can strongly influence fungal growth. Differences in copper content among PDA brands directly influenced fungal growth (Griffith et al., 2007). Additionally, *Fusarium oxysporum* formed more bud cells and produced greater fungal biomass on PDB-M than on PDB-C, likely due to the higher molecular weight carbohydrates (molecular weight >20 MDa) present in PDB-M (Yokota et al., 2010). Regarding *P. lilacinum* PLBJ-1, it produced leucinostatins in PDB-M but almost none in PDB-C (Wang et al., 2016). However, to our knowledge, the genetic mechanisms underlying these differences remain unexplored.

Environmental pH is one of the important physiological factors influencing fungal growth and development, stress response, secondary metabolism and pathogenicity (Luo et al., 2017). PacC is a conserved pH-specific genetic regulator which was first reported in *Aspergillus nidulans*. (Prusky & Yakoby, 2003) Under alkaline condition, the full-length form of PacC (72-kD $PacC^{72}$) would undergo two successive proteolytic cleavages to yield $PacC^{53}$ (53-kD PacC) and the active form $PacC^{27}$(27-kD PacC), which suppresses the expression of acid-expressed genes while promoting the expression of alkaline-expressed genes (Diez et al., 2002; Orejas et al., 1995; Penas et al., 2007; Rodriguez-Galan et al., 2009). As a global regulator, PacC can control fungal development (Trushina et al., 2013), pathogenicity (Caracuel et al., 2003; Tilburn et al., 1995), and secondary metabolite production (Barda et al., 2020). For example, deletion of PacC completely abolished oosporein biosynthesis in *Beauveria bassiana* (Chen et al., 2022). Nitrogen availability and type also play a crucial role in fungal physiology. In ascomycetes, nitrogen metabolism is primarily regulated by the GATA family transcription factors AreA and AreB. Filamentous fungi preferentially utilize $NH4^+$ and glutamine as energetically favorable nitrogen sources (Marzluf, 1997). AreA expression increases under nitrogen-limiting conditions (Caddick et al., 1994; Michielse et al., 2014), activating the expression of genes for secondary nitrogen sources (Macios et al., 2012), while AreB acts as a negative regulator by competing with AreA for promoter binding sites (Wong et al., 2009). Studies in *A. nidulans*, *F. fujikuroi*, and *Metarhizium acridum* demonstrated their regulatory roles in regulating growth, metabolism, and virulence (Guan et al., 2017; Li et al., 2021; Macios et al., 2012; Michielse et al., 2014; Zhi et al., 2024). Notably, loss of *areB* in *A. flavu*s leads to a significant upregulation of aflatoxin

production. (Zhi et al., 2024) However, the functions of PacC and AreB remain poorly understood in *P. lilacinum*.

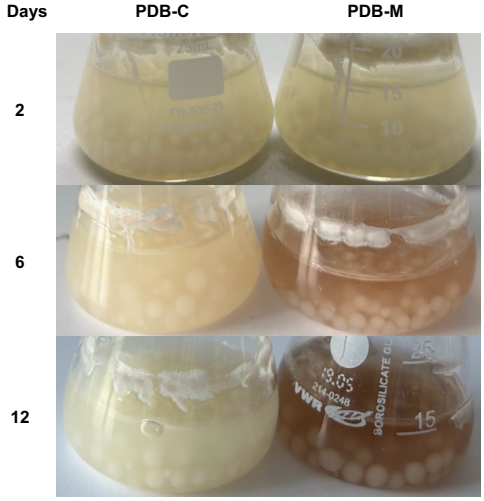

Figure 4-1: Differential Growth Performance of *P. lilacinum* PLBJ-1 on PDB-C and PDB-M Media at 2, 6, and 12 Days

In this study, pH dynamics and nitrogen availability were identified as key environmental factors influencing *P. lilacinum* PLBJ-1's physiology and metabolic activity through comparative analysis of growth kinetics and medium composition in both of PDB-C and PDB-M (Figure 4-1). Additional cultivation experiments under varied conditions confirmed that both the initial pH and nitrogen levels in the culture medium influence leucinostatin production. Finally, CRISPR-Cas9-mediated gene disruption experiments established that pH-responsive regulator PlPacC and the nitrogen regulator PlAreB play essential roles in fungal development and leucinostatin biosynthesis. Moreover, understanding their regulatory mechanisms provides a foundation for optimizing fermentation conditions to enhance leucinostatins production and improving the broader application of *P. lilacinum* in bio-control strategies.

3. Results

3.1. Differential pH dynamics, growth, and leucinostatin production of P. lilacinum PLBJ-1 in PDB-M and PDB-C

In this and subsequent analyses, we extracted four types of leucinostatins from the crude extracts of PLBJ-1, leucinostatin A, B, C, and K0, and calculated the peak integration areas to quantify their production levels. After inoculating *P. lilacinum* PLBJ-1 in PDB-M and PDB-C (purchased from Sigma) for 12 days, leucinostatins were detected in the PDB-M culture but were nearly undetectable in PDB-C (Figure 4-2A). This result was consistent with previous findings, which reported a similar trend using PDB-M and PDB-C (purchased from BD) (Wang et al., 2016). To

investigate the key factors influencing the production of leucinostatin compounds, the elemental composition of these two media was analyzed by Bureau Environnement et Analyses de Gembloux (B.E.A.Gx.) (Table 4-1). The most notable difference between the two media was that PDB-C contained higher levels of phosphate, sodium, and total nitrogen, whereas PDB-M had a higher concentration of potassium. However, adding K^+ to PDB-C had no significant impact on leucinostatin production and biomass (Figure 4-3), suggesting that K^+ is not a limiting factor.

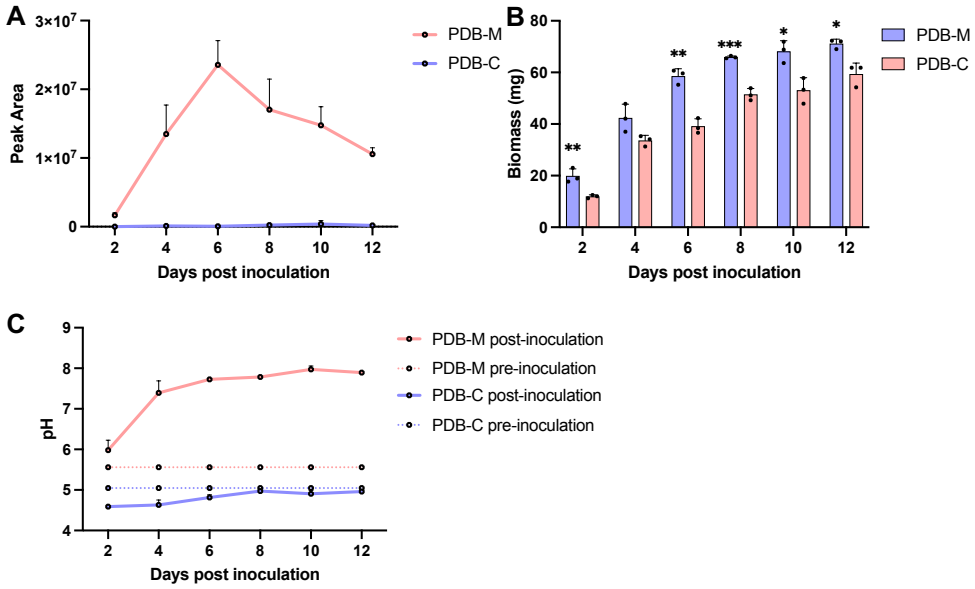

Figure 4-2. Leucinostatins production (A), biomass (B), and pH value dynamic (C) of *P. lilacinum* PLBJ-1 wild-type (WT) on PDB-C and PDB-M media over a period of 2 to 12 days. Data were analysed according to the paired T-Test. Mean values with asterisks indicate significanc: $p < 0.05$ (one asterisk), $p < 0.01$ (two asterisks), and $p < 0.001$ (three asterisks). All the data are represented as the means of $n = 3$ biologically independent samples, and the error bars show the standard deviations.

Table 4-1: Comprehensive chemical analysis of PDB-M and PDB-C

mg/L	**PDB-M**	**PDB-C**
$N_{kjeldahl}$	97	231
P_2O_5	50.6	109.1
CaO	64.6	33.8
MgO	38.7	43.7
K_2O_T	425.3	44
NaO	15.7	78.4
Fer	0.38	0.18

Mangnanese (Mn)	0.08	0.01
Sulfates (SO_4^{2-})	57	177
Chlorures (Cl^-)	20	<1
Carbone Organique Total	290	294

Phosphate and sodium are the primary components of classical phosphate buffer systems. Given their higher concentrations in PDB-C compared to PDB-M, we speculated that PDB-C may contain a phosphate-based pH buffering system. We conducted growth kinetic studies using PDB-M and PDB-C media. Over a 12-day cultivation period, significant differences were observed in leucinostatin yield (Figure 4-2A), biomass (Figure 4-2B), and culture medium pH dynamic (Figure 4-2C). After 6 days of inoculation, the pH of the PDB-M culture medium increased by more than 2 units, whereas the pH of the PDB-C medium remained stable at approximately its initial value of pH 5 (Figure 4-2C). The distinct pH changes observed following the cultivation of PDB-C and PDB-M have prompted the hypothesis that leucinostatin production and the growth of *P. lilacinum* PLBJ-1 might be influenced by pH of culture medium.

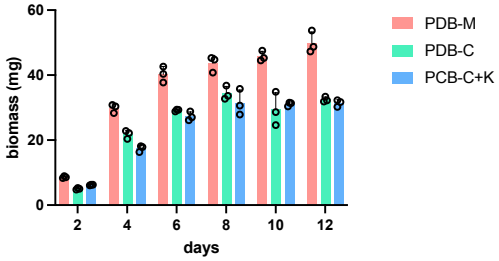

Figure 4-3: Biomass of the WT strain on PDB-M, PDB-C, and PDB-C supplemented with 100mM KCl. All the data are represented as the means of n = 3 biologically independent samples, and the error bars show the standard deviations.

3.2. Impact of environmental pH to the growth and leucinostatin production of P. lilacinum

Table 4-2: pH changes of the PDB-M with different initial pH on 10-days post inoculation.

Before inoculation	**After 10 days of culture**
5.5	5.78
6.0	6.16
6.5	6.63
7.0	6.96

7.5	6.93
8.0	7.47

To investigate the effect of pH on leucinostatin production, *P. lilacinum* PLBJ-1 was inoculated in PDB-M medium buffered to various pH levels (pH 5.0, 5.5, 6.0, 6.5, 7.0, 7.5, and 8.0), and their pH dynamics before and after inoculation showed in Table 4-2. The leucinostatin production was compared across different pH values, revealing a strong impact of pH on yield. Within initial pH ranged from 5.5 to 8.0, leucinostatin production exhibited a positive correlation with pH; higher pH values led to increased leucinostatin yield (Figure 4-4A). On the sixth day post-inoculation, the biomass of the culture was measured, and the results indicated that after 6-days culture an initial medium pH range of 7.0–7.5 was more favorable (Figure 4-4B), indicating that pH also influences the growth of *P. lilacinum* PLBJ-1.

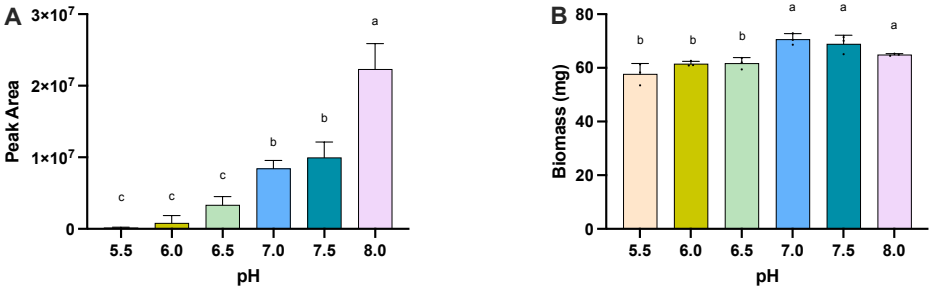

Figure 4-4 Effect of different pH on leucinostatins production and growth of WT strain. Data were analyzed according to the Tukey's HSD. Values with different letters (a, b, c, d) are significantly different from each other ($p < 0.05$). Identical letters indicate no significant difference. All the data are represented as the means of n = 3 biologically independent samples, and the error bars show the standard deviations. A) Leucinostatins production of WT strain under different initial pH after 6-days growth. B) Biomass of WT strain under different initial pH after 6-days growth.

3.3. Identification of the pH-responsive regulator PlPacC

Regarding the response to environmental pH, fungi possess a conserved PacC/Pal signaling pathway mediated by the regulator PacC. Based on the results of a BLASTp analysis using the PacC sequence from *A. nidulans*, the gene *VPFBJ_03549* in *P. lilacinum* PLBJ-1 was identified as the putative *PacC* and named *PlPacC*. The PlPacC gene (2012 bp) encodes a 600-amino acid protein. Compared with the well-characterized PacC protein sequence, multiple sequence alignment analysis showed that the PlPacC protein contains three conserved Cys2His2 zinc finger protein structural domain (Figure 4-5A). Besides, PlPacC has three highly conserved regions, including region A, B and C from N-terminal to C-terminal. As previous description, the interaction between regions A and B can facilitate the formation of a structural configuration that associates with region C, thereby locking PacC protein into a “closed” and functionally inaccessible conformation. Changes in environmental pH,

in most cases involving an alkaline signal, disrupt the interaction between regions A and B, thereby triggering the conversion of PacC into an “open”, accessible state (Espeso et al., 2000). Region A possesses a PacC processing proteolytic cleavage site. (Hervas-Aguilar et al., 2007; Li et al., 2022) A putative nuclear localization signal (NLS) was predicted to partially overlap with region A, and the conserved signaling protease box of PacC was also identified (Figure 4-5A). The 2000 bp sequence upstream of PlPacC contains a putative promoter region between 356-405 bp, eight PacC DNA binding sites ‘GCCARG’ (Espeso et al., 1997) between 1147-1713 bp, one core promoter elements TATA-box, and six enhancer elements CAAT-box (Figure 4-6). Phylogenetic analysis of PlPacC and its experimentally verified fungal homologs revealed that PlPacC is closely related to the PacC protein in *F. oxysporum* f. sp. lycopersici 4287 and *Hapsidospora chrysogena*, with sequence identities of 71.31% and 69.78%, respectively (Figure 4-5B).

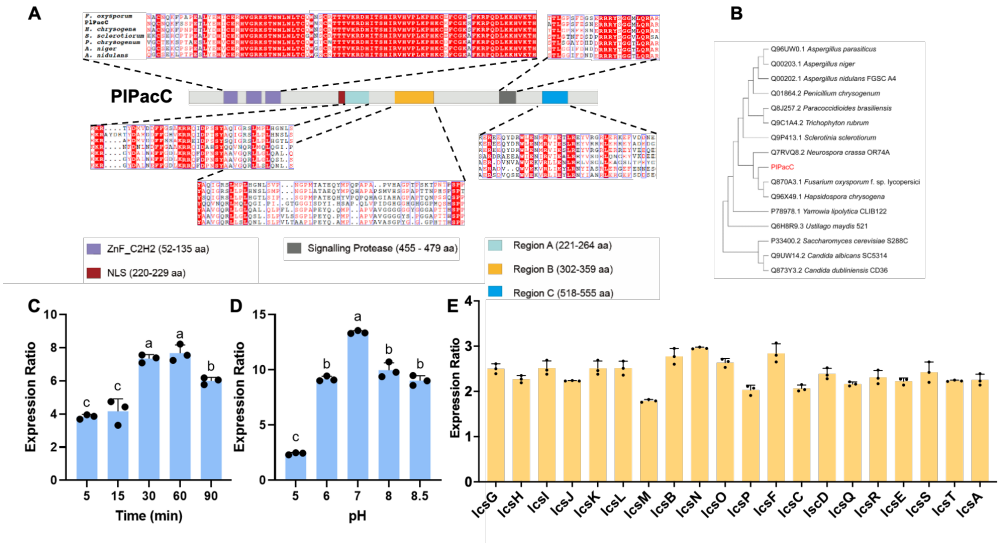

Figure 4-5: Identification of the putative pH regulator PlPacC. Data were analysed according to the Tukey's HSD. Values with different letters (a, b, c, d) are significantly different from each other ($p < 0.05$). Identical letters indicate no significant difference. All the data are represented as the means of $n = 3$ biologically independent samples, and the error bars show the standard deviations. A) Conserved domain arrangements of the PlPacC and its orthologues in other fungal species. Multiple sequence alignment of PacC from *P. lilacinum* and other species. White letters on a red background indicated strictly conserved amino acid residues. Red letters in blue boxes indicated well-conserved amino acids or similar amino acids. B) Phylogenetic tree of PlPacC and other species. C) Gene expression of PlPacC in short-term responses to ambient pH shift. D) Gene expression of PlPacC under different pH conditions. E) Expression ratios of genes involved in leucinostatins biosynthesis in *P. lilacinum* PLBJ-1 cultured in pH7-adjusted CY medium was compared to pH 4-adjusted CY medium.

Figure 4-6: The 2000 bp sequence upstream of PlPacC. The green letters indicated the putative promoter region predicted by BDGP. The blue letters indicated PacC DNA binding sites. The red letters with black box indicated CAAT box or TAAT box predicted by Plant CARE.

pH shift experiments were conducted to evaluate the expression level of *PlPacC* gene at different time points after transferring to an alkaline environment and at different pH levels. To investigate the short-term response and the expression level of *PlPacC* gene, mycelia of *P. lilacinum* PLBJ-1 strain was transferred from CY medium of pH 4 to pH 8 for shaking for 5, 15, 30, 60, and 90 min. RT-qPCR analysis showed that the expression level of PlPacC significantly quickly increased 4-folds in alkaline conditions at 5 min after the shift and reached its peak at 60 min (8-folds) (Figure 4-5C). To evaluate the expression level of *PlPacC* gene under different pH, the mycelia of *P. lilacinum* PLBJ-1 strain was transferred from CY medium of pH 4 to pH 4.0, 5.0, 6.0, 7.0, 8.0, 8.5 for shaking for 60 min. Compared to pH 4, the relative expression of *PlPacC* increased as the ambient pH rose, reaching a peak at pH 7.0 (13-folds) before decreasing at pH 8.0 and pH 8.5 (Figure 4-5D). Meanwhile, genes located in leucinostatins biosynthetic gene cluster (BGC) were also upregulated in pH 7.0-adjusted CY medium compared to those in pH 4.0-adjusted CY medium (Figure 4-5E). These results suggest environmental pH shifts can rapidly induce transcriptional activation of PlPacC and the leucinostatin BGC.

3.4. PlPacC is requied for growth, environmental pH elevation, and leucinostatin biosynthesis

The *PlPacC* gene was disrupted in the wild-type PLBJ-1 strain by inserting an eGFP sequence using the CRISPR-Cas9 strategy. Successful transformants (KOPlPacC)

were identified through fluorescence screening and diagnostic PCR (Figure 4-6). The wild-type and KOPlPacC strains were cultured separately in PDB-M and PDB-C media for 6 days. The culture of KOPlPacC exhibited a lighter color than WT in PDB-M, while no significant changes in PDB-C (Figure 4-7).

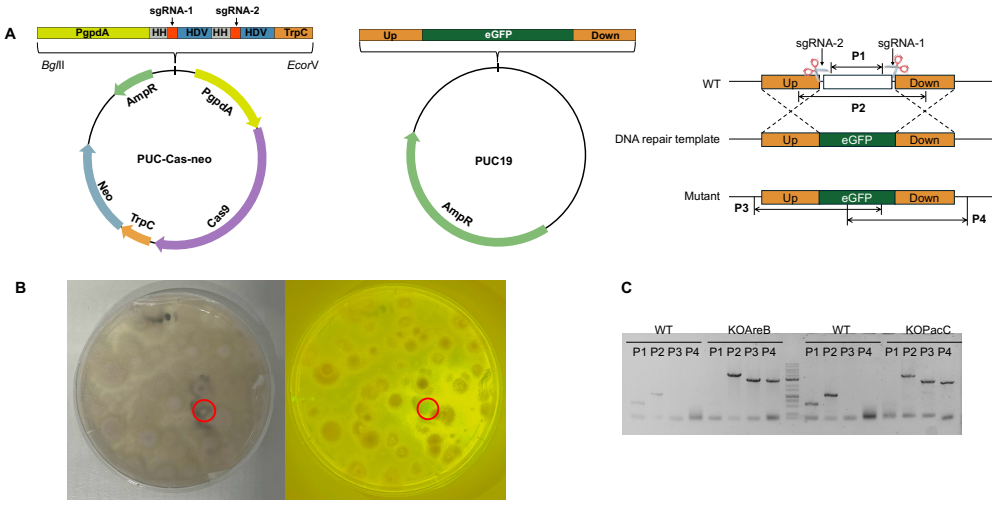

Figure 4-7: Generation of gene disruption mutants in *P. lilacinum.* (A)Scheme illustration of disruption of genes in *P. lilacinum*. Four pairs of primers including P1, P2, P3, and P4. P1 was amplified with primer PlPacC (PlAreB)-check2-F and PlPacC (PlAreB)-check2-R; P2 was amplified with primer PlPacC (PlAreB)-check-F and PlPacC (PlAreB)-check-R; P3 was amplified with primer PlPacC (PlAreB)- -out-F and gfp-check-R; P4 was amplified with primer gfp-check-F and PlPacC (PlAreB)-out-R. (B) Fungal transformation plates observed under visible light (left) and at a wavelength of 488 nm (right) using a handheld fluorescence device. Colonies marked with red circles exhibited green fluorescence under 488 nm excitation, and subsequent PCR validation confirmed these as the correct mutant strains. (C) Comfirmation of Δ*PlPacC* strains by diagnostic PCR. In the Δ*PlPacC* strains, the specific bands (about 3939 bp, 2900 bp, and 2500 bp) were detected in mutant using the P2, P3, and P4 primers but not in WT. The PlPacC gene was detected in WT using P1 primers, but not in the mutant strains.

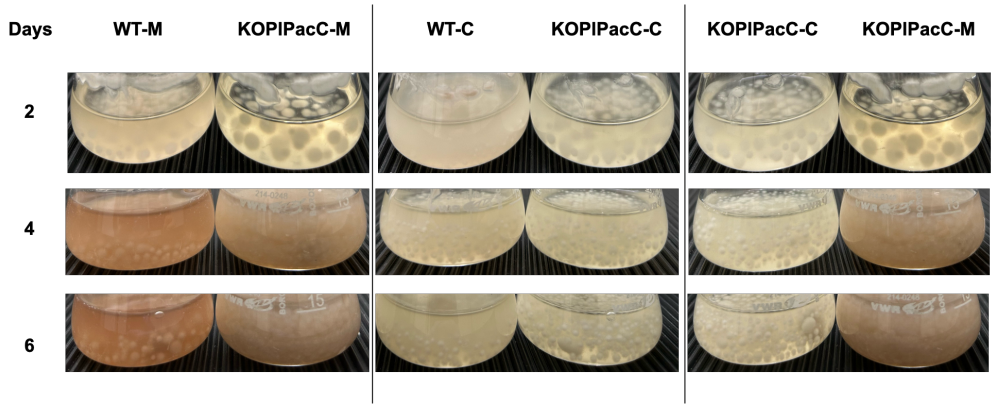

Figure 4-8: Growth of *P. lilacinum* PLBJ-1 WT strain and KOPlPacC strain on PDB-C (C) and PDB-M (M) media for 2, 4, and 6 days.

Compared to the wild-type strain, KOPlPacC produced significantly lower biomass (Figure 4-9A), fewer conidia (Figure 4-9B), a smaller increase in culture medium pH (Figure 4-9C), and reduced levels of leucinostatins (Figure 4-9D). RT-qPCR analysis showed that 19 of the 20 leucinostatin-related genes exhibited reduced transcriptional levels in KOPlPacC compared to WT (Figure 4-4E). Furthermore, when the absolute leucinostatin production was normalized to mycelial biomass, KOPlPacC still showed a significantly reduced yield per unit biomass compared to the WT, indicating that the decline in leucinostatin production was not solely attributable to reduced fungal growth (Figure 4-10). These results indicated PlPacC plays a positive regulatory role in growth, environmental pH elevation, and leucinostatins biosynthesis in *P. lilacinum* PLBJ-1.

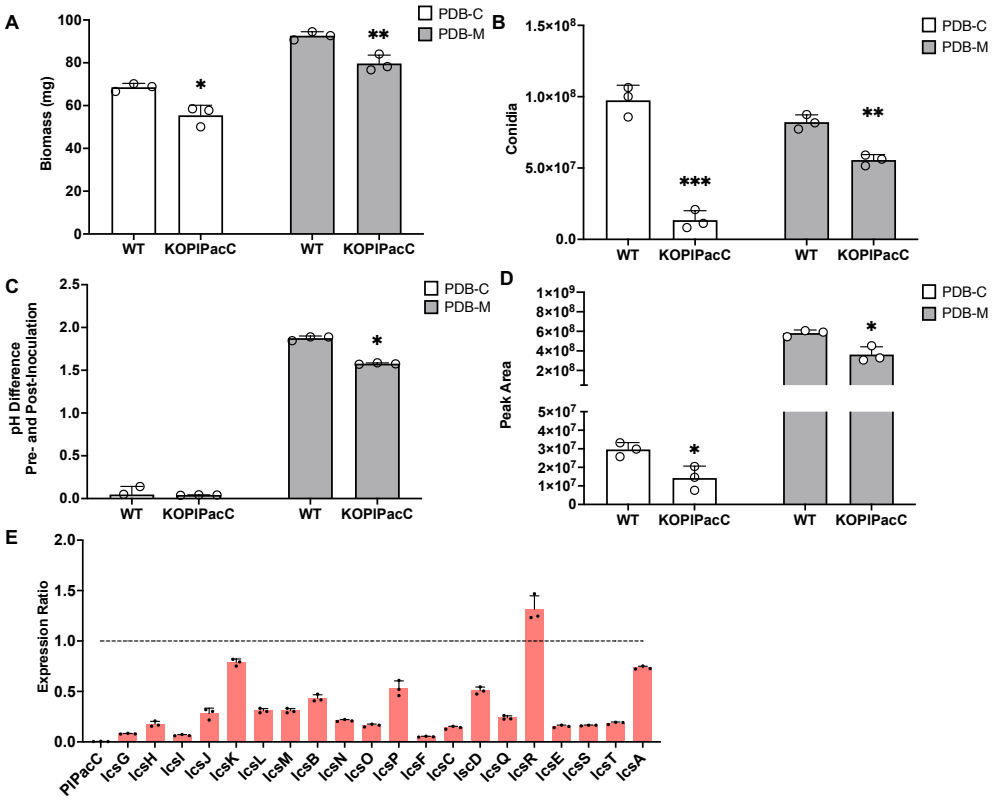

Figure 4-9. PlPacC involved in growth, environmental pH regulation, and leucinostatins biosynthesis. Biomass (A), conidial yield (B), environmental pH changes before and after inoculation (C), and leucinsotatins of the WT, KOPlPacC strains on PDB-C and PDB-M (D). E) Relative expression levels of leucinsotatins biosynthesis-related genes in KOPlPacC compared to WT. Data were analysed according to the paired T-Test. Mean values with asterisks indicate significanc: $p < 0.05$ (one asterisk), $p < 0.01$ (two asterisks), and $p < 0.001$ (three asterisks). All the data are represented as the means of $n = 3$ biologically independent samples, and the error bars show the standard deviations.

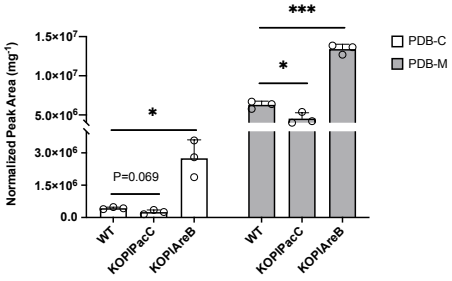

Figure 4-10: Normalized leucinostatin production in KOPlPacC and KOPlAreB strains compared to the WT grown on PDB-C medium and PDB-M. Leucinostatin production was

normalized to mycelial biomass and expressed as micrograms per milligram of dry weight in both mutant and WT strains. Data were analysed according to the paired T-Test. Mean values with asterisks indicate significanc: $p < 0.05$ (one asterisk), $p < 0.01$ (two asterisks), and $p < 0.001$ (three asterisks). All the data are represented as the means of $n = 3$ biologically independent samples, and the error bars show the standard deviations.

3.5. Identification of the GATA transcription factor PlAreB

PDB-C and PDB-M were researched for composition. When peptone was added to the PDB-M medium to increase its total nitrogen content to match that of PDB-C, the leucinostatins yield decreased (Figure 4-11A) while biomass increased (Figure 4-11B). These observations suggest that differences in nitrogen content between PDB-M and PDB-C may be another factor influencing the differential performance of *P. lilacinum* PLBJ-1 in these two media.

AreA and AreB are nitrogen metabolism regulatory transcription factors widely found in filamentous fungi. In *P. lilacinum* PLBJ-1, the corresponding genes are predicted to be *VPFBJ_00440* and *VPFBJ_01061*, which were named PlAreA and PlAreB, respectively. To investigate the impact of nitrogen supplementation on gene expression, qRT-PCR was performed to assess the transcriptional responses of *PlAreA*, *PlAreB*, and the leucinostatin BGC. As nitrogen concentration increased, the transcript levels of *PlAreA* and the leucinostatin BGC were downregulated while *PlAreB* showed transcriptional upregulation (Figure 4-11C). However, only the PlAreB gene disruption mutant was successfully constructed, and thus, subsequent studies focused on PlAreB. Based on comparisons with experimentally validated AreB transcription factors sequences in other fungi, PlAreB was found to contain conserved structural domains. The N-terminal zinc finger DNA-binding domain was highly conserved, and the C-terminal leucine zipper domain exhibited moderate conservation (Figure 4-11D).

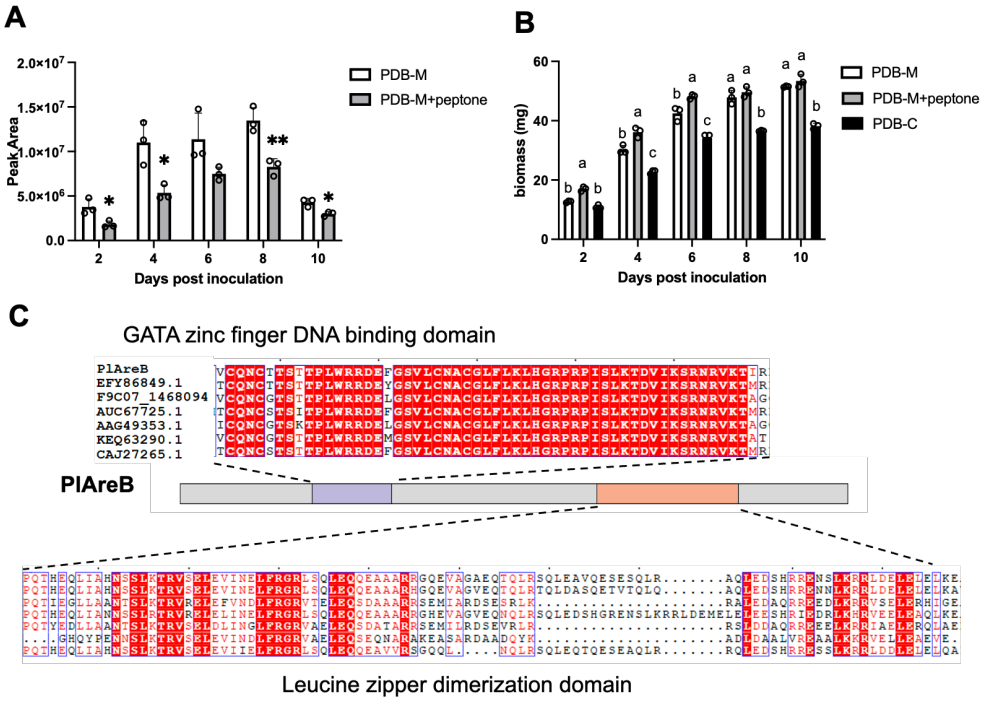

Figure 4-11. Identification of the putative nitrogen regulator PlAreB. A) Leucinostatins yield measured in PDB-M medium and PDB-M medium supplemented with 200mg/L peptone. Data were analysed according to the unpaired T-Test. Data are expressed as means ± standard deviations (n = 3). Asterisks indicate statistically significant differences (*P < 0.05, **P < 0.01) between groups at the same time points. B) Biomass of *P. lilacinum* PLBJ-1 in PDB-M medium, PDB-M medium supplemented with peptone, and PDB-C medium. Data were analysed according to the Tukey's HSD. Different letters indicate significant differences among treatments (P < 0.05). C) Expression ratios of genes involved in leucinostatins biosynthesis in *P. lilacinum* PLBJ-1 cultured in peptone-supplemented PDB-M medium was compared to PDB-M medium. D) Predicted conserved domains in the PlAreB transcription factor. The N-terminal zinc finger DNA-binding domain (purple) and the C-terminal leucine zipper dimerization domain (orange) are highlighted. Multiple sequence alignment of AreB from *P. lilacinum* and other species. White letters on a red background indicated strictly conserved amino acid residues. Red letters in blue boxes indicated well-conserved amino acids or similar amino acids.

3.6. Roles of PlAreB in growth and leucinostatins biosynthesis

To investigate the role of PlAreB in *P. lilacinum* PLBJ-1, CRISPR-Cas9 system was also employed to construct PlAreB disruption mutants (KOPlAreB) in the wild-type (WT) background. The successful construction of these mutants was confirmed through diagnostic PCR (Figure 4-7). The culture color of KOPlAreB exhibited no significant changes compared to WT in neither PDB-M nor PDB-C (Figure 4-12).

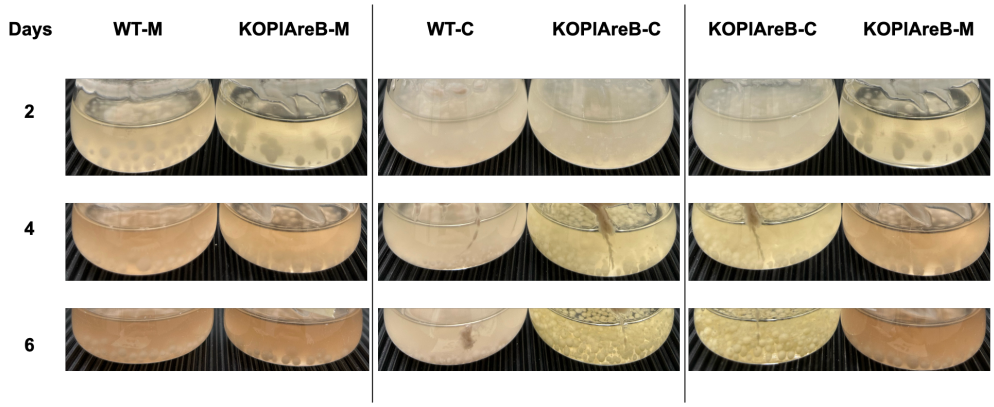

Figure 4-12: Growth of *P. lilacinum* PLBJ-1 WT strain and KOPlAreB strain on PDB-C (C) and PDB-M (M) media for 2, 4, and 6 days. In both media, the KOPlAreB strain exhibited a marked reduction in sporulation compared to the WT strain.

Additionally, the biomass and conidia production of KOPlAreB were significantly reduced compared to WT, regardless of whether they were cultured in PDB-C or PDB-M (Figure 4-13A and B). For KOPlAreB, the changes in environmental pH before and after inoculation in PDB-C and PDB-M media showed no significant differences compared to WT, thereby ruling out the possibility that the CRISPR-Cas9 system interfered with *P. lilacinum* PLBJ-1's ability to elevate environmental pH (Figure 4-13C). In contrast of KOPlPacC, KOPlAreB showed a significant increase in leucinostatins production in both PDB-C and PDB-M (Figure 4-13D). Furthermore, when the absolute leucinostatin production was normalized to mycelial biomass, KOPlPacC showed a significantly reduced yield per unit biomass compared to the WT (Figure 4-10). Further analysis of 20 leucinostatins biosynthesis-related genes revealed that their expression levels were almost entirely significantly upregulated in KOPlAreB, compared to WT (Figure 4-6E). These results indicate that PlAreB plays important roles in promoting the growth and conidial production of *P. lilacinum* PLBJ-1 but acts as a negative regulator of leucinostatins biosynthesis.

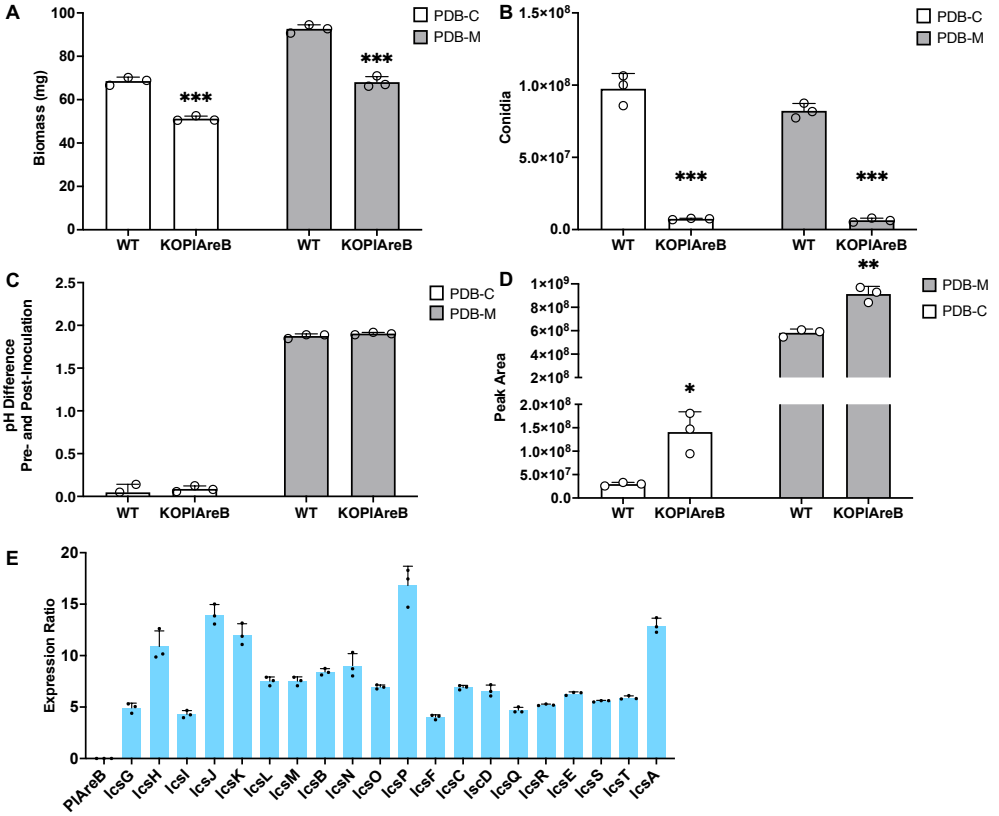

Figure 4-13. PlAreB involved in growth, environmental pH regulation, and leucinostatins biosynthesis. Biomass (A), conidial yield (B), environmental pH changes before and after inoculation (C), and leucinsotatins of the WT, KOPlPacC strains on PDB-C and PDB-M (D). E) Relative expression levels of leucinsotatins biosynthesis-related genes in KOPlAreB compared to WT. Data were analysed according to the paired T-Test. Mean values with asterisks indicate significanc: $p < 0.05$ (one asterisk), $p < 0.01$ (two asterisks), and $p < 0.001$ (three asterisks). All the data are represented as the means of $n = 3$ biologically independent samples, and the error bars show the standard deviations.

4. Disucussion

Fungal secondary metabolites are generally not essential for fungal survival and are often associated with considerable metabolic costs (Calvo et al., 2002). Among them, fungal-derived antibiotics can inhibit the growth of surrounding bacteria, fungi, and protozoa, thereby reducing ecological competition. The natural production of antibiotics by fungi is therefore considered a strategy to suppress microbial competitors in their habitat. The biosynthesis of these compounds is highly sensitive to environmental cues. A systematic variation of culture conditions, or the application of stressors, has been widely adopted to stimulate secondary metabolite production (Scherlach & Hertweck, 2021).

Environmental pH is a critical factor influencing cellular metabolism and secondary metabolite biosynthesis. In our study, we confirmed that culture pH directly affects the biosynthesis of leucinostatin in *P. lilacinum* PLBJ-1, with significantly lower production observed at pH 5.5 compared to pH 8.0. Similar trends have been reported in other fungal species: for instance, penicillin production by *A. nidulans* is optimized under alkaline conditions (Shah et al., 1991). The insect-pathogenic fungus *B. bassiana* fonly produces the antibiotic oosporein under alkaline pH (8.0) when cultured in Sabouraud Dextrose Broth (Chen et al., 2022). Compared to other organisms, fungi often dominate in acidic environments (Wang & Kuzyakov, 2024). In such conditions, the energetic cost of antibiotic production may not be justified due to reduced microbial competition, which may lead fungi to downregulate secondary metabolite biosynthesis. The production of antagonistic compounds under biological competition pressure may reflect an adaptive ecological strategy employed by fungi.

Nutrient starvation is another major environmental cue that strongly induces secondary metabolite biosynthesis in fungi (Zehetbauer et al., 2022). Under stress conditions such as metal, carbon, or nitrogen starvation, fungi undergo profound changes in their developmental programs, resulting in the activation of SM biosynthetic pathways (Lim et al., 2018; Németh et al., 2016). This adaptive response enhances fungal survival under adverse conditions until more favorable environment return (Umar et al., 2024). Transcriptomic analyses of nutrient-depleted wild-type *A. nidulans* cells revealed a distinct shift in gene expression: genes involved in primary metabolism were strongly downregulated, while those associated with the biosynthesis of carbon storage compounds (for energy conservation), conidiation (for reproduction), and secondary metabolites (for defense) were significantly upregulated (Zehetbauer et al., 2022). Our results demonstrated that *P. lilacinum* strain PLBJ-1 produces less leucinostatin and accumulates more biomass under nitrogen-rich conditions. This finding aligns with observations in *Penicillium chrysogenum*, where the availability of preferred nitrogen sources and favorable growth conditions leads to reduced penicillin biosynthesis (Brakhage, 1998).. Similarly, in *F. fujikuroi*, the production of bikaverin—a secondary metabolite that evolved to protect the fungus from endosymbiotic bacteria—is specifically induced upon nitrogen exhaustion (Rodríguez-Ortiz et al., 2009). Additionally, *A. nidulans* produces two novel polyketide antibiotics, sanghaspirodins A and B, under limited nitrogen supply, both of which exhibit moderate activity against Gram-positive bacteria (Scherlach et al., 2011). Taken together, our findings suggest that the enhanced leucinostatin production by *P. lilacinum* PLBJ-1 under alkaline and nitrogen-limited conditions may represent a survival strategy, enabling the fungus to optimize its metabolic investment and increase its fitness in competitive or nutrient-scarce environments.

To further understand how environmental conditions influence fungal secondary metabolism, it is essential to identify the transcription factors that mediate this regulation. Our study demonstrated that culturing *P. lilacinum* PLBJ-1 in CY medium at pH 4.0 for 24 hours followed by transfer to CY medium at pH 7.0 induced transcriptional upregulation of pH-responsive regulator PlPacC. Yeast one-hybrid (Y1H) assays was conducted to validate PlPacC's ability to bind promoters of

leucinostatin biosynthesis related genes. The coding sequence of PlPacC and 20 putative promoters were cloned. Y1H analysis showed that PlPacC could bind 12 putative promoters (Figure 4-14). Among them, *lcsG* encodes an enzyme responsible for *N*-methylation at the C-terminus of leucinostatins, which influences their bioactivity (Li et al., 2024). *lcsH* and *lcsO* are predicted to encode ABC transporters, while *lcsJ* encodes a thioesterase-like enzyme. *lcsK* and *lcsN* are predicted as cytochrome P450 enzymes. *lcsB* is predicted to encode a polyketide synthase (PKS) responsible for PK side-chain synthesis in leucinostatins, while *lcsD*, predicted as an acyl-CoA ligase, is essential for leucinostatins biosynthesis, as its disruption leads to complete loss of the compounds. *lcsQ* is predicted as a tRNA synthetase, and *lcsT* as an epimerase (Wang et al., 2016). These findings gave a hint that PlPacC plays a direct role in regulating the biosynthesis of leucinostatins (Chen et al., 2023). Previous studies have shown that PacC can bind transcription factors within BGCs to mediate secondary metabolite regulation (Chen et al., 2022; Chen et al., 2023). However, in our study, Y1H assays did not detect binding between PlPacC and the two cluster-situated promoters of transcription factors *lcsL* and *lcsF*. Additionally, the presence of PacC binding sites in the PlAreB promoter suggests a potential interaction between PlPacC and PlAreB (Figure 4-15). Nevertheless, we cannot exclude the possibility that PlPacC may regulate LcsL and LcsF indirectly through interaction with other transcription factors.

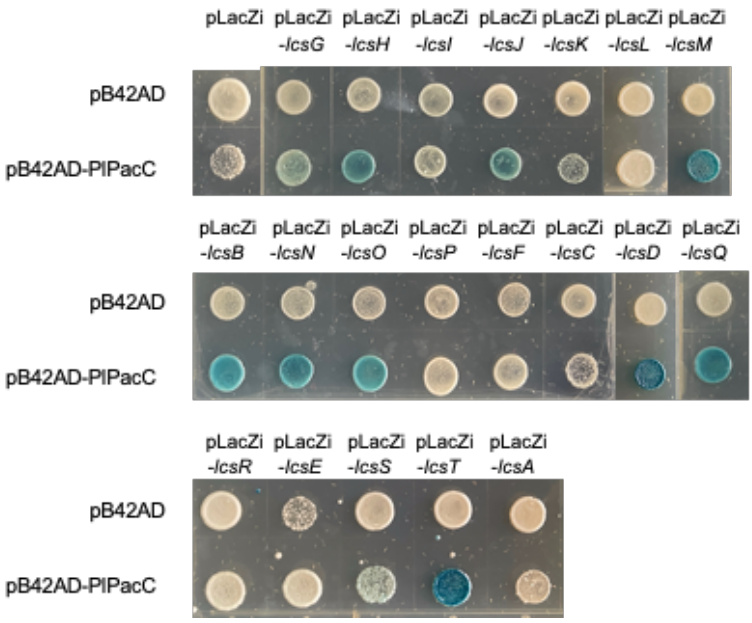

Figure 4-14: Y1H analysis reveals the interaction of PlPacC and promoters of leucinostatins biosynthesis-related genes. Yeast strain EGY48 was co-transformed with either the pB42AD-PlPacC or empty pB42AD vector (control) along with pLacZi-putative promoters of leucinostatins-related genes or empty pLacZi (control). Blue colonies indicate a

positive interaction between PlPacC and the respective promoter region. Controls with empty pB42AD showed no blue coloration, confirming the specificity of PlPacC-promoter interactions.

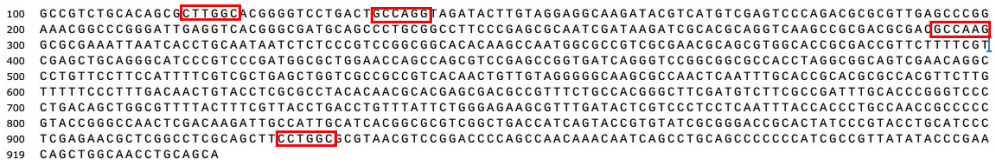

Figure 4-15: Putative promoter of PlAreB. The red box indicated PacC DNA binding sites, suggesting a potential interaction between PlAreB and PlPacC.

Here, we employed a CRISPR-Cas9 system incorporating G418 resistance and eGFP fluorescence as selectable markers to individually disrupt PlPacC and PlAreB in *P. lilacinum* PLBJ-1. However, while G418 resistance is available for wild-type strains (Jiao et al., 2019; Wang et al., 2016), no selectable marker exists for post-knockout complementation. Previous studies used pyrG mutants or hygromycin B selection (Alimu et al., 2022; Binh et al., 2021), but these approaches are yet to be validated in PLBJ-1. To mitigate potential off-target effects, we used the same system to individually knock out two genes and observed that the two mutants exhibited opposite effects on leucinostatins production. This phenomenon, to some extent, serves as an internal control, mitigating concerns about the influence of knockout system itself.

In this study, we identified the transcriptional response of PlPacC to changes in culture medium pH and demonstrated, through gene disruption, its regulatory role in various metabolic processes in *P. lilacinum* PLBJ-1, including the biosynthesis of leucinostatins. However, we observed that adjusting the culture medium pH had a greater effect on leucinostatin production than disruption of PlPacC. Although PacC is known to play a critical role in the alkaline pH response, the regulatory effects exerted by environmental pH likely involve a broader spectrum of cellular processes beyond the PacC pathway. This observation is consistent with findings in Trichoderma virens, where approximately 5% of genes (650 out of 12,427 predicted protein-coding transcripts) were differentially expressed solely in response to ambient pH changes, while only 157 genes were regulated directly or indirectly by PacC (Trushina et al., 2013).

We demonstrated that alkaline and low-nitrogen environments favor the biosynthesis of leucinostatins in *P. lilacinum* PLBJ-1. However, this study did not further explore the optimization of fermentation conditions for enhancing compound yield. Optimizing culture conditions and nutrient composition is crucial for enhancing microbial product yields. Studies in *P. lilacinum* have applied response surface methodology (RSM) to enhance biomass (Mousumi Das et al., 2020), chitosanase yield (Nidheesh et al., 2015), protease activity (Yu et al., 2015), and phosphorus solubilization (Wang et al., 2023), yet research on maximizing leucinostatin production in *P. lilacinum* remains limited. In this study, we examined only PlAreB's response to total organic nitrogen, but future research should explore how specific

nitrogen sources, such as glutamine and nitrate. Identifying optimal optimal medium components and fermentation strategies could provide valuable insights for enhancing biomass and leucinostatin production and broaden agricultural and pharmaceutical applications of *P. lilacinum* and its metabolites.

5. Conclusion

Overall, this work confirmed PDB-C and PDB-M can cause different performance of *P. lilacinum* PLBJ-1. Among the key factors, both pH and nitrogen content played crucial roles. Specifically, an alkaline environment and the lower nitrogen content were more conducive to leucinostatins production in *P. lilacinum* PLBJ-1. Two regulators, the pH transcription factor PlPacC and the nitrogen regulator PlAreB, are proven to be responsible for fungal growth and leucinostatins production.

6. Materials and methods

6.1. Fungal strain and growth conditions

The strains used in this study are listed in Table 4-3. *P. lilacinum* strain PLBJ-1 (CGMCC3.17492), isolated from tomato roots in Beijing, was cultured at 25 °C in potato dextrose agar (PDA) or potato dextrose broth (PDB). The formulation of leucinostatins-inducing PDB-M is as follows: 200 g of potatoes were boiled for 30 min, and then 20 g of glucose were dissolved into the filtrate and diluted to 1 L. The non-inducing PDB-C medium (PDA-C) came from NutriSelect (Sigma-Aldrich, USA) or Becton, Dickinson and Company (NJ, USA). The formulation of CY medium, used in pH shift experiments, is as follows: K_2HPO_4 1 g/L, Yeast extract 5 g/L, sucrose 30 g/L, czapek concentrate (comprising 30 g/L $NaNO_3$, 5 g/L KCl, 5 g/L $MgSO_4 \cdot 7H_2O$, 0.1 g/L $FeSO_4 \cdot 7H_2O$, 0.1 g/L $ZnSO_4 \cdot 7H_2O$, and 0.05 g/L $CuSO_4 \cdot 5H_2O$) 10 ml/L, agar 15 g/L. The formulation of T-Top medium for fungal transformation is as follows: KCl (0.5 g/L), MgSO4▪$7H_2O$ (0.5 g/L), KH2PO4 (1 g/L), NaNO3 (2 g/L), sucrose (200 g/L), glucose (20 g/L), agar (10 g/L).

Table 4-3: Strains used in this study.

Plasmids/Strains	Description
Purpureocillium lilacinum strain PLBJ-1 (CGMCC3.17492)	Wild type
PLBJ-KOPlPacC	Δ*PlPacC*::eGFP in *P. lilacinum* PLBJ-1
PLBJ- KOPlAreB	*ΔPlAreB::eGFP in P. lilacinum PLBJ-1*
Saccharomyces cerevisiae EGY48	*MATα*, *ura3*, *his3*, *trp1*, *LexAop (x6)-LEU2*

For pH-variable experiments, PDB medium adjusted to different pH values using 50 mM MES (pH 5.5-7.0) and 50 mM HEPES (pH 7.0-8.0) or 0.2 M Na_2HPO_4 -0.1 M citric acid (pH 4.0-8.0) and 0.1 M Tris-HCl (pH 8.5-9.0).

The pH shift experiment was conducted following the methodology outlined by Chen et al. (Chen et al., 2018) To investigate the short-term response, cultures of 1×10^6 conidia per ml of *P. lilacinum* PLBJ-1 were cultured at 25°C in CY medium

buffered at pH 4.0 for 24 h with shaking at 150 rpm, then shifted to media at pH 8.0 for 5 min, 15 min, 30 min, 60 min, and 90 min. To evaluate the effect of different pH, *P. lilacinum* PLBJ-1 was transferred to media buffered at pH 4.0-8.5 for 1 h after culture in CY medium of pH 4 for 24 h.

6.2. Detection of leucinostatins production by LC-MS analysis

P. lilacinum PLBJ-1 and its related mutants were grown in PDB medium at 25 °C on a shaker at 150 rpm for the required duration. The fermentation broth was extracted with an equal volume of ethyl acetate (EtOAc) two times (every 1 h) to efficiently extract leucinostatins. The EtOAc was evaporated under reduced pressure.

LC–MS analyses for cultures of PLBJ-1 under different conditions were performed on an UPLC Waters Acquity H Class MS SQ detector by using an acquity BEH C18 (2.1× 50 mm, 1.7 μm). A linear gradient analytical method was used: the mobile phase was composed of 0.1% trifluoroacetic acid (TFA) in water (solvent A) and acetonitrile (solvent B) at a flow rate of 0.6 mL/min. The gradient program was as following: 0–2 min, 15% solvent B; 2–7 min, increase to 95% solvent B; 7–9.5 min, maintain 95% solvent B. The MS scan range was 2–2047m/z. The mass spectrometer was set in ES+ mode for ionization.

LC- MS analyses for cultures of PLBJ-1 and its related mutants (3.6 section) were performed on an Agilent HPLC 1260 Infinity II system equipped with an Agilent G6510A mass spectrometer by using an Agilent Zorbax SB-C18 reversed-phase column (4.6 × 150 mm, 5 μm). A linear gradient analytical method was used: the mobile phase was composed of 0.1% trifluoroacetic acid (TFA) in water (solvent A) and acetonitrile (solvent B) at a flow rate of 1 mL/min. The gradient program was as following: 0–2 min, 10% solvent B; 2–20 min, increase to 100% solvent B; 20–28 min, maintain 100% solvent B. The Q-TOF was operated in positive electrospray ionization mode with a capillary voltage of 1800 V and a drying gas flow rate of 1 μl/min at 300 °C. The MS scan range was 80–2000 m/z.

6.3. Biomass dry weight determination

The culture samples were centrifuged for10 min at 6000 ×g. The remaining cell pellets were washed by resuspending them in distilled water followed by centrifugation. After the centrifugation, the supernatant was discarded, and the remaining cell pellet was filled into a pre-weighted aluminum cup. The biomass sample in the aluminum cup was dried in the oven at 105 °C and weighed after 48 h to determine the corresponding cell dry weight.

6.4. Bioinformatics analysis of PlPacC and PlAreB

Multiple sequences were aligned by MAFFT, and ESpript3 (https://espript.ibcp.fr/ESPript/cgi-bin/ESPript.cgi) was subsequently used to export the sequence alignment results. Phylogenetic tree was constructed by neighbour-Joining in MEGA X. Structural domains of PacC and AreB proteins were predicted using the NCBI Conserved Domain Search analysis (https://www.ncbi.nlm.nih.gov/Structure/cdd/wrpsb.cgi), and their schematic diagram were illustrated by using IBS 2.0 (https://ibs.renlab.org/#/server). (Xie et al.,

2022) Nuclear localization signals of PacC proteins were predicted using DeepLoc-2.0 (https://services.healthtech.dtu.dk/services/DeepLoc-2.0/) and cNLS Mapper (https://nls-mapper.iab.keio.ac.jp/cgi-bin/NLS_Mapper_form.cgi). BDGP (http://www.fruitfly.org/seq_tools/promoter.html) and Promoter - 2.0 (https://services.healthtech.dtu.dk/services/Promoter-2.0/) were used to predict the promoter transcription start site. JASPAR online analysis (https://jaspar.elixir.no/) was used to analyze transcription factor binding sites. Plant CARE (http://bioinformatics.psb.ugent.be/webtools/plantcare/html/) was used to predict promoter cis-acting elements. (Lescot et al., 2002)

6.5. DNA and RNA extraction

The mycelia of *P. lilacinum* PLBJ-1 WT and the mutant strains were harvested via filtration after cultivation in 2 ml of potato dextrose broth (PDB) at 25°C for 24 h for DNA isolation. The genomic DNA was extracted using Plant/Fungi DNA Isolation Kits (Norgen Biotek) according to the manufacturer's instructions. RNA was extracted using RNeasy Plant Mini Kit (QIAGEN) following the manufacturer's protocol. Nanodrop was used to evaluate nucleic acid concentrations, and agarose gel electrophoresis was performed to assess RNA integrity.

6.6. RT–qPCR analysis

The primers used for RT–qPCR analysis are listed in Table 4-4. For RT–qPCR analysis, 50 ng of RNA was used as the template by using Luna® Universal One-Step RT-qPCR Kit (E3005, New England Biolabs) following the manufacturer's protocol on a QuantStudio™ 3 Real-Time PCR System (Thermo Fisher Scientific). The housekeeping actin gene designed from *VFPBJ_07912*, which was similar to the reported GU299860.1, was used for normalization. Three biological replicates were measured for each analysis of the relative expression levels. The relative expression values were calculated using the $2^{-\Delta\Delta Ct}$ method. (Livak & Schmittgen, 2001)

Table 4-4: Primers used for qRT-PCR.

Primer name	Sequence (5′ to 3′)
Actin-F	GCCCTCTGTCCTGGGTCTT
Actin-R	ACAGGGAGGCGAGAATGGA
PlPacC-F	AGAGCACCAATAACCTGAACC
PlPacC-R	AGCCTGTGTTCTGTAGTTGAG
PlAreA-F	GTCAGACAGGCGACACAGAA
PlAreA-R	ACTTGATGGGAATGGCCGAG
PlAreB-F	GATGAGTTTGGTTCCGTTCTGTG
PlAreB-R	GCTGTTGTTGCTGCTTCTTCTT

lcsA-F	CGACTCGGACTCGGTTCAG
lcsA-R	TGCCGTGATGGTAGACAAGAG
lcsC-F	CCCAGATGCCCTCACTTTT
lcsC-R	GACCACCGACTTGAACCAA
lcsD-F	GCCAAAGTGAGAAGGGACA
lcsD-R	CCGCTGGATGAAGTATGAG
lcsE-F	TACAGACGCCACCATCAGG
lcsE-R	TCAACACGACACGGCTTTC
lcsF-F	CACAAAGAGGAGGGTTCGG
lcsF-R	CTCGCCATGTTCGTGCTAG
lcsG -F	GGCTCGTGTCCTCGTCCTG
lcsG-R	TCGTCGCCTGCTTGGTATG
lcsH -F	ATGAGGCAACCACAACACT
lcsH-R	AGACGACCAGCATCCAAGA
lcsI -F	GGTCCATCCTTCAAGCAGA
lcsI-R	AAGCACGAACAGTTCCACATA
lcsJ -F	GTCAAGGGACGACCAGCAC
lcsJ-R	CTCACGAACCAGGAACCAA
lcsK -F	CCCTGCCGCCGTGGCTGTAT
lcsK-R	TCGCCCGCTTCGTGTCCG
lcsL -F	TGGAAATGACGGATGGGGATG
lcsL-R	GAGGCGAAGCCAGGAAAGG
lcsM-F	GAAACCGTCTTTCCGCCTTTA
lcsM-R	AGCGAGCCGTACCGTGATG
lcsB-F	GCACGAAGCAATCACCTCT
lcsB-R	AATCCCACCTCACCCATAA
lcsN-F	ACACGAAGCCGTTTACCTA
lcsN-R	GAAGACGATCATCATTTGC
lcsO-F	GAGATGACGGTCAGG
lcsO-R	CGCTCCACCAGAACG

lcsP-F	TAGGCTGGACCGTTGAGAA
lcsP-R	GCGCTTTGGTAGAGGAATT
lcsQ-F	ACTCGGCGTATGTCAACTT
lcsQ-R	CAATTCCTCTTCACTCCAAA
lcsR-F	CGCATCTGGAATCACCGAC
lcsR-R	CGAGGCAACTGACCACGAC
lcsS-F	CGATGGGTGCGAGTCTAAG
lcsS-R	GTGGGAGGTAACCGATGAA
lcsT-F	CCGAGCAAGCGTTTGGAGA
lcsT-R	TCAATAAGTGCGGGGCGTA

6.7. Gene cloning and plasmid construction

PCRs were performed using Q5® High-Fidelity DNA Polymerase (M0491, New England Biolabs) according to manufacturer's instructions. The plasmid recombinations were performed by using the ClonExpress MultiS One Step Cloning Kit (Vayzme, China).

The primers used for constructing Cas9 plasmid and homologous repair plasmid are listed in Table 4-5. Disruption of PlPacC and PlAreB genes was done byCRISPR-Cas9 technic using two recombinant plasmids: the CRISPR-Cas9-PlPacC (or CRISPR-Cas9-PlAreB) plasmid and the plasmid for homologous repair templates. (Jiao et al., 2019) The CHOPCHOP website (http://chopchop.cbu.uib.no) was used to design the targeted sequence of *PlPacC* and *PlAreB*. To enhance the efficiency of gene manipulation, the two highest-ranked targeted sequences were simultaneously employed. The sequences of sgRNAs of *PlPacC* were 5′-TCGGCATCCAGCAACAACAG -3′ (sgRNA-1) and 5′-CCAAGCTACTATGATCACAA -3′ (sgRNA-2). The sequences of sgRNAs of *PlAreB* were 5′- CCACAGACACCGATGAACAC -3′ (sgRNA-1) and 5′-TCTTTGAAGCCAGGTCCGGG -3′ (sgRNA-2). Hammerhead (HH), sgRNA-1, liver hepatic delta virus (HDV) ribozymes, HH, sgRNA-2, and HDV ribozymes were sequentially synthesized to form the sgRNA expression cassette from Liuhe BGI Tech Solutions Co., Limited (Beijing, China). The strong promoter *gpdA*, sgRNA expression cassette, and the terminator *trpC* were obtained by PCR and sequentially inserted into PUC-Cas9-neo-gRNA plasmid which linearized by *EcoR*V and *Bgl*II (New England Biolabs, USA).

The plasmids containing the homologous repair template were constructed by incorporating an upstream homology region, a GFP screening marker, and a downstream homology arm. For *PlPacC*, the homology regions flanking the sgRNA target sites were designed to ensure precise genome editing, spanning 1392 bp upstream and 1452 bp downstream of the PlPacC locus. For *PlAreB*, the upstream homology arm corresponds to the 1351 bp region upstream of the sgRNA-2 target site,

while the downstream homology arm corresponds to the 1631 bp region downstream of the sgRNA-1 target site.

The primers used for yeast-one-hybrid are listed in Table 4-5. To construct the pLacZi-promoter and pB42AD-PlPacC plasmids for yeast one-hybrid assays, promoter sequences of leucinostatin gene cluster were amplified by PCR and cloned into the *Xho*I restriction sites of the pLacZi reporter vector. To construct pB42AD-PlPacC vector, the full-length coding sequence (CDS) of PlPacC was amplified by PCR and inserted into the *EcoR*I sites of the pB42AD activation domain vector.

Table 4-5: Primers used for plasmids construction.

Primer name	**Sequence (5′ to 3′)**
CRISPR-gpdA-F	aatgcgtcgagatgaagatctGCCATTCAGGCTGCGCAA
CRISPR-gpdA-R	atcgagaGGTGATGTCTGCTCAAGCGG
sgRNA-F	agcagacatcaccTCTCGATCCGCAGTGTCTTGC
sgRNA-R	acgttaagtCGTCTCGGTTGGCAGTGACT
CRISPR-trpC-F	caaccgagacgACTTAACGTTACTGAAATCATCAAACAG
CRISPR-trpC-R	cgcagcctgaatggcgatatcAAGAAGGATTACCTCTAAACAAGT GTACC
gpdA-check	ATCTGTAGGGCGTCCAAATATCG
trpC-check	ATCTGGAAGAGGTAAACCCGAAAC
puc-F	ACTGGCCGTCGTTTTACAACG
puc-R	AAGTTGGGTAACGCCAGGGT
PlPacC-up-F	gctatgaccatgattacgccGCGTAGGTGGGAGCGGTG
PlPacC-up-R	caatcTTGTTGCTGGATGCCGATG
PlPacC-GFP-F	ggcatccagcaacaaGATTGTACTGAGAGTGCACCATATGG
PlPacC-GFP-R	atttggccgttgGCCATTCAGGCTGCGCAA
PlPacC-down-F	tgaatggcCAACGGCCAAATCCGAGG
PlPacC-down-R	gttgtaaaacgacggccagtTTGGACGCCCATCACTTCA
PlPacC-check-F	ATTCCGCTCGCCCTTTCTC
PlPacC-check-R	GTGTTCAGAGGAGGCTGGTTG
PlPacC-check2-F	CAACTTGACCTGCCGTTGG
PlPacC-check2-R	TGCTGCAATGCCAGTCAGC
PlPacC-out-F	CAAGGGAAGGATGCACCGCTG

gfp-check-R	GACAAGGTCGTTGCGTCAGTC
gfp-check-F	CTCATGGCGATTGCAGTCCTC
PlPacC-out-R	GATGCGAACCGTCACCTCTC
PlAreB-up-F	gctatgaccatgattacgccGCCACGTAACCAGGCAGTGC
PlAreB-up-R	atcTTCATCGGTGTCTGTGGTGCT
PlAreB-GFP-F	ccacagacaccgatgaaGATTGTACTGAGAGTGCACCATATGG
PlAreB-GFP-R	tcttctttgaagccaggtccGCCATTCAGGCTGCGCAA
PlAreB-down-F	GGACCTGGCTTCAAAGAAGAAG
PlAreB-down-R	gttgtaaaacgacggccagtGAGGCCGCCAACCGAGAC
PlAreB-check-F	GCAACCCTCCACTCCAGGC
PlAreB-check-R	GACGGTGCCATTCGCATTC
PlAreB-check2-F	AGCACCACAGACACCGATGAAC
PlAreB-check2-R	ATTGCACAGAACGGAACCAAAC
PlAreB-out-F	CTGTCCATCCTCGTGATGGTTG
PlAreB-out-R	CTGCGATACGGAAATGCAGCTTC

6.8. PEG-mediated fungal transformation

For polyethylene glycol (PEG)-mediated fungal transformation, 200 ml of PDB medium containing 10^8 spores of *P. lilacinum* PLBJ-1 was cultured in at 25 °C and 150 rpm for 18 h. The fungal germlings were harvested using a 4-layer of sterile lens tissue filter. After washing with 0.7 M NaCl, the germlings were treated with 2 μg/ml driselase (Sigma) at 25 °C and 150 rpm for about 4 h to obtain protoplasts. Microscopic examination was conducted to assess the protoplast status. Following filtration with the 4-layer sterile lens tissue and thorough washing with cold STC buffer (0.8 M sorbitol, 0.05 M $CaCl_2 \cdot H_2O$, 0.01 M Tris-HCl), the protoplasts were collected by centrifugation at 4 °C, 4000 ×g for 15 min, and resuspended to a concentration of 10^6/ml in cold STC buffer. A total of 100 μl of *P. lilacinum* PLBJ-1 protoplast suspension was mixed with 5 μg of each transformation DNA which was adjusted to a final volume of 60 μl with TEC buffer (0.01 M HCl-Tris, 0.001 M EDTA, 0.04 M $CaCl_2 \cdot H_2O$) following by incubating on ice for 30 minutes. Subsequently, the mixture was incubated at room temperature for 20 minutes after adding 60 μl of 60% PEG4000 solution (60% PEG, 0.6 M MOPS). Following this incubation, 1 ml of STC solution was added, and the contents were gently mixed. The suspension was centrifuged, and the supernatant was discarded to remove PEG4000. The protoplast pellet was resuspended in 100 μl of STC solution. For plating, 20 μl of the resuspended protoplast solution was mixed with 5 ml of molten T-Top medium, evenly spread onto PDA plates, and incubated overnight at 28°C. On the following day, 10 ml of T-Top

medium containing 400 μg/ml G418 (geneticin) (Sigma) was overlaid onto each plate. These plates were incubated at 28°C for further selection and growth.

6.9. Identification of transformant by using fluorescence observation

Candidate colonies were selected after culture on PDA at 28 °C for 2 days. By using a handheld instrument (CZ-JF488YGDB, China) with a 488-nm excitation filter (yellow glasses), the colonies contained eGFP reporter were picked and inoculated onto new PDA plates supplemented with 400 μg/ml G418 (Sigma) for 3–5 days at 28°C. These transformants were verified via diagnostic PCR after being lysed using the Plant Direct PCR Kit (PD105, Vazyme Biotech Co., Ltd, China).

6.10. Conidia counting in different strains

P. lilacinum PLBJ-1 and its transformants were grown at 25°C on 100 ml PDB and 150 rpm for 8 days. Three replicates were performed for each culture. The culture broth was filtered using lens tissue to obtain a spore suspension, which was then centrifuged at 8000 ×g for 10 minutes. The supernatant was discarded, and the pellet was resuspended to a final volume of 2 ml. And the number of conidia from different mutants and WT were determined by blood cell counting plate. Each strain was cultured in triplicate, with cell counts performed three times for each replicate.

6.11. Yeast one-hybrid screening

For the yeast one-hybrid (Y1H) assay, pB42AD-PlPacC and pLacZi-promoters were cotransformed into yeast strain EGY48, and transformants were selected and grown on SD/-Trp-Ura dropout medium. The empty pB42AD and pLacZi-promoters vectors were co-transformed in parallel as negative controls. The primers used for Y1H assay were listed in Table 4-6. Positive transformants were verified and selected for growth on medium containing 1% raffinose (Coolaber, cat. no. SL0990) and 80 mg/L X-gal (Coolaber, cat. no. CX11921) for blue color reactions after approximately 2–3 days.

Table 4-6: Primers used for yeast one hybrid.

Primer name	Sequence (5′ to 3′)
PB42AD-PlPacC-F	TGCCTCTCCCGAATTCATGGCCGCCCAGGTCTC
PB42AD-PlPacC-R	CGAGTCGGCCGAATTCTCAAGACCCCGGTACCGG
Pb42ADseq-F	ACCAGCCTCTTGCTGAGTGGAGATGCC
Pb42ADseq-R	GAAGTGTCAACAACGTATCTA
LACZlcsG-F	ATCTGTCGACCTCGAGGGGTCGCAGGGGTGTGATG
LACZlcsG-R	GAGCACATGCCTCGAGGGTGAGTAGCGTGCTGTCAGTTAC

LACZlcsH-F	ATCTGTCGACCTCGAGTGCCTCTCCCGAATTCGGGTGACAGTGATAAATGCACG
LACZlcsH-R	GAGCACATGCCTCGAGTGTCGGACTCTACACAGAGCCAC
LACZlcsI-F	ATCTGTCGACCTCGAGGTCGGGGAGGCCGGTG
LACZlcsI-R	GAGCACATGCCTCGAGGTTGTTGAGCCGCGCTACTATG
LACZlcsJ-F	ATCTGTCGACCTCGAGATCCTCCTCGCTTAAAAGGCTC
LACZlcsJ-R	GAGCACATGCCTCGAGTGTAACTGTAGATGAGTGCACTTGC
LACZlcsK-F	ATCTGTCGACCTCGAGTCGCGGCCTTTATACTCGAC
LACZlcsK-R	GAGCACATGCCTCGAGCATATGGCTCTTGATATGGAACACT
LACZlcsL-F	ATCTGTCGACCTCGAGGACTGCTCCTGATTCTAGAAACTAG
LACZlcsL-R	GAGCACATGCCTCGAGTGTGAAAGCAGCCGGCCTG
LACZlcsM-F	ATCTGTCGACCTCGAGAATATGAGACCCAAACGCAGATC
LACZlcsM-R	GAGCACATGCCTCGAGGCACGGGTGCCGATTGG
LACZlcsB-F	ATCTGTCGACCTCGAGAGCGCAACTGAAGGGACGAC
LACZlcsB-R	GAGCACATGCCTCGAGTTTGTTCTCTTTGCTAGAATAAGCG
LACZlcsN-F	ATCTGTCGACCTCGAGATGGTGACCATATATATCTACGTCA
LACZlcsN-R	GAGCACATGCCTCGAGTCCCGGTGGGTTTTTCTCATC
LACZlcsO-F	ATCTGTCGACCTCGAGCAGCCATACTGGTAGACGAAGTGTC
LACZlcsO-R	GAGCACATGCCTCGAGATTGACATATATCGGTGTCACCAAA
LACZlcsP-F	ATCTGTCGACCTCGAGGCGGAGTTGATGGAGCTCG
LACZlcsP-R	GAGCACATGCCTCGAGGTTCCTCCAAGCAATCAAATAGTG
LACZlcsF-F	ATCTGTCGACCTCGAGATCCAGGGTGTATTAAGGCCG
LACZlcsF-R	GAGCACATGCCTCGAGTGTTTGGATGCAAAAGGGTG
LACZlcsC-F	ATCTGTCGACCTCGAGATAGTCATACGAAAAATGGTCGCC
LACZlcsC-R	GAGCACATGCCTCGAGGATTGCTGAAAGTCGTCCGCAG

LACZlcsD-F	ATCTGTCGACCTCGAGCAGGCATGCTATAAATGCTAACAG
LACZlcsD-R	GAGCACATGCCTCGAGGACGCTTTTCTGGAGCATATATGA G
LACZlcsQ-F	ATCTGTCGACCTCGAGAGCTACTGTTGGCGAAAGACG
LACZlcsQ-R	GAGCACATGCCTCGAGCACCTCGCAGAGACCAAAAG
LACZlcsR-F	ATCTGTCGACCTCGAGATTCACGTCTGCATACAGGCG
LACZlcsR-R	GAGCACATGCCTCGAGTTCGGTATCCTTTCAAAACGTG
LACZlcsE-F	ATCTGTCGACCTCGAGGGCGTTGGCTTTTAAAGGC
LACZlcsE-R	GAGCACATGCCTCGAGTCTTGAGATCACCTAGGCAGCC
LACZlcsS-F	ATCTGTCGACCTCGAGAATCGGGTTGTAATAAAGACCACT C
LACZlcsS-R	GAGCACATGCCTCGAGGAATCGCTTTTGCAACGACC
LACZlcsT-F	ATCTGTCGACCTCGAGCAGCTGGTTGTTAAAAAGCTCG
LACZlcsT-R	GAGCACATGCCTCGAGCGCAAAGCTCACACTCGGG
LACZlcsA-F	ATCTGTCGACCTCGAGAGGCAGATGCTTGGGCG
LACZlcsA-R	GAGCACATGCCTCGAGGATATCGACCGTTGCGTATAGTC
PLacZ2U-F	GAATTCGAGCTCGGTACCC
PLacZ2U-R	GGACCTAATGTATAAGGAAAG

6.12. Statistics and reproducibility

Every experiment was conducted with a minimum of three independent biological replicates. Data are presented as the mean ± standard deviation (SD). Data points in figures represent biological replicates. Each graph displays individual data points. Statistical analyses (mean and SD) were performed using GraphPad Prism 10 software.

Chapter 5

General discussion

leucinostatins, a class of nonribosomal peptide (NRP) natural products with broad-spectrum bioactivity, are produced by the bio-control fungus *Purpureocillium lilacinum*. In addition to their potential as antimalarial and antitumor pharmaceutical precursors, they have shown promising applications in agricultural bio-control (Brand et al., 2021; Liu et al., 2020; Park et al., 2004; L. Rimle et al., 2025). To further application of *P. lilacinum* in the production of leucinostatins, two critical challenges must be addressed: enhancing the bioactivity and increasing the yield.

In **Chapter 3** of this study, we report the identification and characterization of LcsG, a freestanding N-methyltransferase encoded within the leucinostatin biosynthetic gene cluster. LcsG catalyzes iterative N-methylation at the C-terminal amino group of leucinostatins, marking the first example of a discrete enzyme performing terminal methylation of NRPs. Traditionally, N-methylations in NRPs are catalyzed by methyltransferase domains embedded within NRPS modules; therefore, our discovery expands the current paradigm of peptide tailoring mechanisms. Interestingly, LcsG was initially predicted to be an O-methyltransferase based on pBLAST analysis. To address this apparent discrepancy, we performed comparative sequence alignment and phylogenetic analysis of LcsG alongside several well-characterized O-methyltransferases and N-methyltransferases, which hinted at a potential evolutionary relationship between these two enzyme classes. Furthermore, through protein-ligand docking analysis and site-directed mutagenesis verification, we identified the key catalytic residues required for LcsG activity, providing a foundation for future enzyme engineering aimed at expanding its substrate specificity. This paves the way for structure-guided molecular editing of NRPs via enzyme-assisted terminal modifications. Notably, the LcsG-mediated methylation enhanced antimicrobial activity, demonstrating the importance of terminal modifications in the structure–activity relationship (SAR) of leucinostatins. This insight contributes to the rational design of more potent leucinostatin derivatives and provides a model system for the SAR-guided optimization of other bioactive NRPs.

Since the extraction of leucinostatins from *P. lilacinum* fermentation remains the predominant production method, enhancing their yield is essential for facilitating both fundamental research and practical applications of these bioactive compounds (Niu et al., 2024). As a critical first step toward production optimization, it is necessary to identify the key environmental parameters that govern leucinostatin biosynthesis. **Chapter 4** examines the differences between leucinostatin-inducing and non-inducing media, revealing that pH and total nitrogen content are crucial factors for leucinostatin production. These findings not only provide a theoretical basis for the future fermentation optimization of leucinostatins but also serve as a methodological reference for defining culture conditions critical to the production of other valuable natural products. Additionally, the characterization of transcription factors in *P. lilacinum* PLBJ-1 that respond to these environmental factors establishes a verifiable model for dissecting environment–transcription factor–metabolite regulatory pathways in filamentous fungi.

These results build the theoretical foundation for future modification and large-scale production of leucinostatins.

1.1. Integration of leucinostatin biosynthesis research and advances in mechanistic understanding

In this study, we identified a freestanding N-methyltransferase gene, *lcsG*, within the leucinostatin biosynthetic gene cluster of *P. lilacinum* PLBJ-1 and demonstrated its essential role in catalyzing N-methylation at the C-terminal amine of leucinostatins. The wild-type strain produces three major leucinostatins: LeuA, LeuB, and LeuK0. In the *lcsG* knockout mutant, the leucinostatins with N-methylated terminus (LeuA and LeuB) were almost completely abolished, while the leucinostatin with free amine (LeuK0) remained detectable. Based on the structural comparison of these compounds, we inferred that LcsG acts on the free amine at the C-terminus of leucinostatins.

This study collectively indicates the broad substrate specificity of LcsG toward members of the leucinostatin family. In vitro enzymatic assays further confirmed the catalytic activity of LcsG. It was able to sequentially methylate LeuB (terminal –$NHCH_3$) to LeuA (–$N(CH_3)_2$), and to LeuA0, which possesses a trimethylated quaternary ammonium group –$N(CH_3)_3^+$. Similarly, LcsG catalyzed the iterative methylation of LeuK0 to generate LeuK2 and LeuK3. In addition to these published results, ou in vitro enzymatic assays and further high-resolution ESI-MS/MS analysis also revealed that LcsG is capable of methylating additional leucinostatins, including LeuF (*m/z* $[M+H]^+$=1104.8), LeuD (*m/z* $[M+H]^+$=1118.8), and LeuH (*m/z* $[M+H]^+$=1234.8) (unpublished data, Figure 5-1, Table 5-1). These two compounds share the same nonribosomal peptide (NRP) backbone as LeuA and LeuK0, respectively, but differ in their AHMOD (2-amino-6-hydroxy-4-methyl-8-oxodecanoic acid) residue.

LcsG functions as an NMT capable of iteratively methylating the terminal nitrogen atom at the C-terminus of the NRP. In most cases, NRPS-associated N-methylation occurred in specific positions along the peptide backbone or amino acid residues, as observed in cyclosporin and pyochelin biosynthesis (Patel & Walsh, 2001; Weber et al., 1994). This modification is typically typically catalyzed by an NMT domain embedded within NRPSs. Reports on the functional characterization of free-standing NMTs involved in NRPSs biosynthesis remain limited. Notable exceptions include MtfA, which is involved in the biosynthesis of glycopeptide antibiotics such as vancomycin (Shi et al., 2009), and a discrete NMT responsible for the incorporation of methylated amino acids at two specific positions within cycloaspeptides (de Mattos-Shipley et al., 2018).

The lipopeptide antibiotics leucinostatins contain terminal N-methylations. Furthermore, their biosynthetic gene cluster includes a potential free-standing NMT, LcsG. These attracted our interest in exploring the function and influence of LcsG. To our knowledge, this is the first report of an NMT-catalyzed iterative *N*-methylation specifically targeting the terminus of NRPs, broadening our understanding of NRP modifications. Moreover, the broad substrate promiscuity exhibited by LcsG highlights its potential utility in engineering methylated analogs of other NRP-derived natural products, making it a promising candidate for future synthetic biology applications.

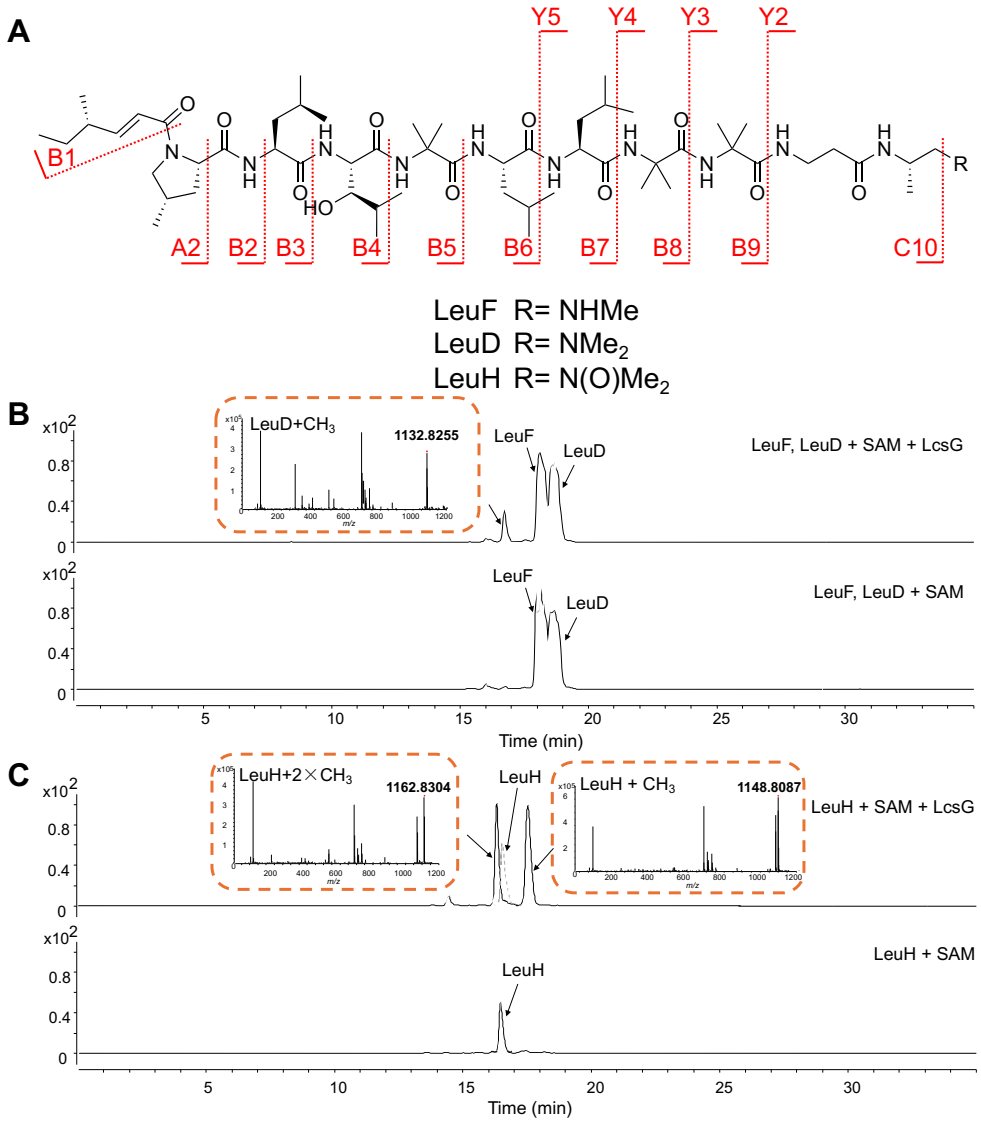

Figure 5-1: (A) strucutres of LeuF, LeuD, and LeuH. (B) In vitro enzymatic assay of LcsG using LeuF and LeuD as substrates. The $[M + H]^+$ ions of the newly detected product peaks are shown: LeuD + CH_3. Extracted ion chromatograms (EICs) were obtained for m/z 1104.8 ± 0.5 (LeuF), 1118.8 ± 0.5 (LeuD), 1132.8 ± 0.5 (LeuD + CH_3) in positive ionization mode. (C) In vitro enzymatic assay of LcsG using LeuH as substrate. The $[M + H]^+$ ions of two newly detected product peaks are shown: LeuH + CH_3, and LeuH + 2×CH_3.Extracted ion chromatograms (EICs) were obtained for m/z 1134.8 ± 0.5 (LeuH), 1148.8 ± 0.5 (LeuH + CH_3), 1162.8 ± 0.5 (LeuH + 2×CH_3) in positive ionization mode.

Table 5-1: Comparison of the reported fragment ions (m/z) in ESI-MS-MS spectra of LeuF, LeuD and their catalytic products

	B1	**A2**	**B2**	**B3**	**B4**	**B5**	**B6**	**B7**	**B8**	**B9**	**C10**	**Y5**	**Y4**	**Y3**	**Y2**
LeuF	111	194	222	335	464	549	662	775	860	945	1073	443	330	245	160
LeuD	111	194	222	335	464	549	662	775	860	945	1073	457	344	259	174
LeuD+CH_3	111	194	222	335	464	549	662	775	860	945	1073				
LeuH	111	194	222	335	464	549	662	775	860	945	1073	473	360	275	190
LeuH+CH_3	111	194	222	335	464	549	662	775	860	945	1073	487	374	289	204
LeuH+ 2×CH_3	111	194	222	335	464	549	662	775	860	945	1073				

1.2. Rationally engineering LcsG for broader biocatalytic applications

This terminal modification, catalyzed by LcsG, significantly enhances the antimicrobial activity of leucinostatins, consistent with the so-called “magic methyl effect” in drug discovery, wherein the introduction of a methyl group can markedly improve biological activity (Pinheiro et al., 2023). LcsG’s unique ability makes it a promising biocatalyst for late-stage peptide functionalization. Rational engineering of LcsG may enable broader applications by enhancing its catalytic efficiency, expanding its substrate scope, and facilitating diverse alkyl group transfer.

Structural predictions suggest that LcsG contains a canonical Class I methyltransferase fold, with conserved SAM-binding residues and catalytic residues. Inspired by recent engineering of the SAM-dependent carbon methyltransferase SgvM, where flexible loop remodeling effectively expanded the substrate-binding pocket and enabled highly efficient enantioselective methylation, a similar strategy could be applied to LcsG (Ju et al., 2023). Guided by this approach, active-site remodeling may improve LcsG’s ability to accommodate larger or non-natural substrates.

Given that LcsG is a SAM-dependent enzyme, its active site may be amenable to engineering to accommodate and transfer bulkier alkyl groups beyond the native methyl. A report indicated that both plant-derived N- and O-methyltransferases have been successfully engineered to utilize synthetic SAM analogues, such as S-adenosyl-ethionine (SAE) for ethyl transfer and S-adenosyl-allyl-L-methionine (SAA) for allyl transfer, thereby enabling the installation of non-native alkyl groups onto diverse substrates (Jockmann et al., 2023). This publication suggests that rational design or screening of LcsG variants may enable the effective use of SAM analogues bearing ethyl, allyl, propargyl, or other functionalized alkyl chains. Such modifications could significantly expand the chemical diversity of terminally alkylated leucinostatins or other natural product-related compounds (NPRCs), potentially enhancing or diversifying their bioactivities.

1.3. Structure–activity relationship between the chemical structure of leucinostatins and their biological activities

In this study, we employed an enzyme-catalyzed strategy to introduce specific N-methylation at the C-terminal amino group of leucinostatin analogs and evaluated the impact of this modification on their antifungal activity against the drug-resistant strain *Cryptococcus neoformans* H99. The results demonstrated that N-methylation significantly enhanced bioactivity: the minimum inhibitory concentrations (MICs) of the methylated products LeuA0 and LeuK3 were significatntly lower than those of their respective parent compounds LeuA and LeuK0, highlighting the influence of C-terminal modification in antifungal efficacy.

This result reveals an important principle in the structure–activity relationship (SAR) of peptide-based bioactive compounds: N-methylation often significantly enhances their activity against pathogenic organisms. This trend is consistent with previous SAR studies on LeuA and its derivatives. In one study, structural modifications of LeuA demonstrated that the structural state of the C-terminus played a decisive role in biological activity. Notably, LeuA exhibited enhanced antifungal potency in its hydrochloride salt form, likely due to the presence of a positive charge—a finding that aligns well with our observation that methylated LeuA0 displays superior activity (Vertuani et al., 1995). Another study introduced substituents at the C-terminal amine, such as morpholine and difluoroethylmethylamine and found that increasing amine basicity correlated with reduced antiprotozoal efficacy (Brand et al., 2021). This supports our conclusion that LeuK3, bearing a more basic dimethylamine group, exhibits stronger antifungal activity than LeuK0, which has a free primary amine. Similar SAR patterns have also been reported in other natural products, such as the antileishmanial compound almiramide, whose C-terminal N-methylation led to a marked increase in bioactivity (Das et al., 2017). The ribosomally synthesized and post-translationally modified peptides (RiPPs) cypemycin and plantazolicin lost their antibiotic activity upon the removal of N-methylation (Claesen & Bibb, 2010; Lee et al., 2013).

Moreover, the leucinostatin BGC harbors numerous uncharacterized tailoring enzymes, including cytochrome P450 monooxygenases, aminotransferases, and epimerases, which are known to play crucial roles in the structural diversification and activity regulation of other bioactive natural products. P450 enzymes are known to be essential in the hydroxylation and cyclization of natural products such as erythromycin (Andersen & Hutchinson, 1992), rifamycin (Qi et al., 2018), and paclitaxel (Song et al., 2024), modulating their bioactivity. Aminotransferases participate in the biosynthesis of aminoglycoside antibiotics (Kudo & Eguchi, 2016) and dendrobine (Li et al., 2017). Meanwhile, epimerases play a key role in the stereochemical modifications of austinol (Lo et al., 2012) and neosartorin (Yang et al., 2021). Based on these findings, we reasonably postulate that these enzymes may also regulate antimicrobial potency through hydroxylation, amination, or chiral rearrangement of leucinostatins.

From the perspectives of drug discovery and biopesticide development, this study underscores the central role of SAR analysis. Rational modification of key structural motifs—especially through biocatalytic approaches enabling site-specific functionalization of the C-terminus—can significantly improve the pharmacological profiles of leucinostatin-type compounds. The successful functional characterization of LcsG not only expands the toolkit for structural remodeling of leucinostatins but also establishes a biosynthetic platform to explore other promising tailoring enzymes within the BGC, illustrating the great potential of enzyme-assisted structural optimization in natural product development.

1.4. Potential crosstalk between pH adaptation and nitrogen metabolism

In this study, we elucidated the relationship between environmental pH, the transcriptional regulation of the putative pH-responsive transcription factor PlPacC, and leucinostatin production. Furthermore, we investigated how nitrogen availability and the putative nitrogen regulator PlAreB influence leucinostatin yield. These findings confirm that PlPacC and PlAreB independently modulate leucinostatin production.

The presence of a putative PacC binding site in the promoter region of PlAreB suggest a potential interaction between these two regulators. Currently, only one study has reported a link between PacC and AreB, in which RNA sequencing data analysis in *Colletotrichum gloeosporioides* suggested that PacC activates AreB expression (Ment et al., 2015). In previous studies investigating the cooperative regulation of fungal metabolism by PacC and other transcription factors, their interactions have been demonstrated through double knockout mutants or direct physical interaction assays such as yeast two-hybrid (Y2H), GST pull-down, and bimolecular fluorescence complementation (BiFC) (Chen et al., 2022; Chen et al., 2023).

If the regulatory link between PlPacC and PlAreB can be confirmed through future experiments, it would not only enhance our understanding of fungal environmental adaptation but also offer new leverage points for rational engineering of metabolic pathways. Specifically, coordinated manipulation of both pH and nitrogen signaling components could lead to more robust control over leucinostatin production. Moreover, uncovering the molecular basis of this potential crosstalk could provide broader insights into the modularity and plasticity of transcriptional networks governing fungal development and secondary metabolism.

1.5. Fermentation optimization of leucinostatins for potential industrial application

Leucinostatins exhibit great potential in pharmaceutical and bio-control applications. Industrial fermentation optimization plays a pivotal role in fully utilizing their therapeutic and agricultural value, as it not only maximizes metabolite production but also reduces overall production costs.

In this study, we identified environmental pH and nitrogen availability as key factors influencing leucinostatin biosynthesis. Several strategies can be applied to optimize

these parameters, including traditional one-factor-at-a-time (OFAT) methods, Plackett–Burman design (PBD) for screening significant variables, and response surface methodology (RSM) for multi-factorial optimization. Notably, RSM has been shown to significantly improve yields of various secondary metabolites in microbial fermentation (R. Sharma et al., 2016). Future research may build on these findings by applying RSM or other statistical tools to systematically refine culture conditions, thereby boosting leucinostatin yield and production efficiency.

In addition, synthetic biology approaches targeting biosynthetic genes and regulatory elements present another promising strategy for enhancing yield. Previous studies have shown that two cluster-associated transcription factors, LcsF and LcsL, positively regulate leucinostatin production (Jiao et al., 2019; Wang et al., 2016). In the present work, we further identified two additional regulators: the pH-responsive activator PlPacC and the nitrogen-responsive repressor PlAreB. Rational engineering of these regulatory components could serve as a powerful strategy to achieve strain improvement for industrial-scale leucinostatin production.

1.6. Bio-control potential of P. lilacinum: from lab to field application

Although current EU risk assessments on leucinostatins have not yet provided sufficient in situ data on their yield, toxicological profiles, or environmental persistence under field condition, *P. lilacinum* strain 251 and PL11 has been approved by the The European Food Safety Authority (EFSA) as a biological nematicide with a favorable safety profile for practical application. (Anastassiadou et al., 2022; Anastassiadou et al., 2020). This study demonstrates that a slightly alkaline environment (pH 7.0–8.0) and higher total nitrogen could promote the growth of wild-type *P. lilacinum* PLBJ-1. These findings offer valuable insights into optimizing the environmental conditions for the field deployment of these approved *P. lilacinum*-based biopesticides.

Based on our results, future systematic analyses of these two environmental conditions may establish a foundation for the field application of *P. lilacinum*. By regulating microecological environment in agricultural fields, such as adjusting pH, optimizing the carbon-to-nitrogen ratio, and improving soil structure, it is possible to enhance the survival environment and production of *P. lilacinum*. These modifications may increase colonization efficiency and bio-control activity of *P. lilacinum* and thereby reinforce its stability and efficacy within the agricultural ecosystem.

Previous studies have shown that optimizing the soil microecology can effectively increase the abundance and stability of beneficial microorganisms. For instance, in tea plantations in Pu'er, Yunnan, China, soils under organic management exhibited significantly higher fungal diversity and evenness indices compared to conventionally managed soils. This indicates that organic management contributes to the stabilization of beneficial microbial communities and enhancement of soil ecological functions (Huang et al., 2023). In another publication, organic fertilizer substitution for chemical fertilizers has been shown to lower soil pH and bulk density, significantly

enhance soil enzyme activity and nutrient content, and ultimately improve rhizosphere microbial community structure, thereby promoting crop growth and increasing yield (Nie et al., 2024). These findings suggest that scientific microecological regulation can create optimal conditions for beneficial fungi such as *P. lilacinum*, enhancing their adaptability and bio-control efficacy in agricultural fields.

Chapter 6

Conclusions and perspective

1. Conclusion

1.1. The unique catalytic function of N-methyltransferase LcsG in the biosynthesis of NRPs

lcsG was predicted as a methyltransferase located in the biosynthetic gene cluster of leucinostatins. The disruption of *lcsG* in *P. lilacinum* PLBJ-1 resulted in the abolishment of leucinostatins with terminal N-methylation (mainly LeuA and LeuB), while didn't influence the persistence of leucinostatins with free amine terminus (mainly LeuK0). Further *in vitro* enzymatic assays revealed LcsG could SAM-dependently catalyzes the following reaction sequences: LeuB-LeuA-LeuA0 (the methylated product of LeuA) and LeuK0-LeuK2 (the methylated product of LeuK0)-LeuK3 (the dimethylated product of LeuK0).

This study revealed the rare catalytic function of N-methyltransferase LcsG in *P. lilacinum* PLBJ-1: LcsG functions as a discrete SAM-dependent NMT that can iteratively catalyze the formation of primary amines, secondary amines, and tertiary amines in the unique terminal unit of leucinostatins. Besides, LeuK2 and LeuK3 were identified as new leucinostatins, further expanding the diversity of leucinostatins.

1.2. The active pocket and key residues of LcsG

Through protein-ligand docking analysis, the conserved SAH/SAM-binding motif (D296, D321, D348, and K363) and two possible catalytic residues (D368 and D395) were predicted and validated by further site-directed mutagenesis experiments. Subsequent molecular dynamics (MD) simulations showed that the positively charged N is located between D395 and D368, and the terminal N of LcsG could form a stable complex system with D368, and the ligand formed salt bridges with D368 and D395 in some snapshots. This result gave a hint that its reaction mechanism is similar to that of phenylethanolamine NMT.

1.3. The N-methylated products (LeuA0 and LeuK3) exhibited higher anti-microbial activities

The *N*-methylated products LeuA0 and LeuK3 exhibited inhibitory activities against the drug-resistant strain *Cryptococcus neoformans* H99 and the plant pathogen *Phytophthora infestans*. Notably, the anti-*C. neoformans* MICs value of the two methylated products, LeuA0 (25.8 μg/ml) and LeuK3 (25.8 μg/ml), were four and two times lower than those of their parent products, LeuA (102.4 μg/ml) and LeuK0 (51.2 μg/ml), respectively. This result demonstrates that *N*-methylation at the terminus of leucinostatins can improve their antimicrobial efficacy.

1.4. Effects of medium pH and nitrogen concentration on leucinostatin production and biomass in P. lilacinum PLBJ-1

The composition of the growth medium strongly impacts fungi's growth and metabolism. In this study, the hand-made PDB (PDB-M) could induce more biomass and the leucinostatins production, while commercial PDB (PDB-C) could barely induce leucinostatins production. By comparing the growth kinetic of *P. lilacinum*

PLBJ-1 by using these two media respectively, a significant difference in pH was observed. Over the 12-day culture period, the pH of PDB-C remained stable at about pH5, whereas the pH of PDB-M fluctuated from pH 5.5 to pH 8. Subsequent pH adjustments of PDB-M strongly influenced leucinostatin yield, indicating that leucinostatin biosynthesis favors a slightly alkaline environment.

Besides, the difference in total nitrogen content was detected between these two media: the leucinostatins-inducing medium, PDB-M, contained a lower level of total nitrogen. Supplementing PDB-M medium with additional peptoneled to a decrease in yield of leucinostatins.

These results suggested the production of leucinosatin in *P. lilacinum* PLBJ-1prefers a slight alkaline and lower total nitrogen content environment.

1.5. Characterization of the transcription factors responding to the environmental pH and total nitrogen content: PlPacC and PlAreB

Using the reported homologous sequences as queries, *VFPBJ_03549* and *VFPBJ_01061* were identified as potential pH-responsive factors (PlPacC) and potential nitrogen regulators (PlAreB), respectively. qRT-PCR analysis was conducted on cultures grown in media with different pH levels, and in a separate experiment, cultures were grown in media with different nitrogen levels. The results confirmed their involvement in responding to these environmental fluctuations.

1.6. The regulatory role of PlPacC and PlAreB in growth and leucinostatins production

Further CRISPR-Cas9 mediated gene disruptions confirmed that the absence of either PlPacC or PlAreB reduced biomass and conidia formation of *P. lilacinum* PLBJ-1. However, their effects on leucinostatin production were opposite: PlPacC deficiency reduced the yield, while PlAreB deficiency increased the yield.

2. Further perspectives

This study provides a theoretical foundation for promoting bioactivity and yield of leucinostatins. It uncovers the critical role of N-methylation at the C-terminus of leucinostatins in determining their biological activity, as well as the influence of environmental pH and total nitrogen content on leucinostatins production.

Based on this research, further work can expanse surrounding the following points:

2.1. Rational engineering to enhance catalytic efficiency and substrate promiscuity of LcsG

In recent years, rational design strategies have been increasingly employed to enhance the catalytic performance of enzymes. In this study, site-directed mutagenesis was used to verify the putative catalytic site of LcsG, demonstrating the feasibility of targeted enzyme modification and laying the groundwork for future rational engineering efforts to enhance its catalytic efficiency.

2.2. Exploring the role of tailoring enzymes in leucinostatin biosynthesis

The influence of other tailoring enzymes on leucinostatins' biological activity remains to be fully understood. Future research could be investigated through targeted gene knockout experiments, comprehensive in vitro enzymatic assays, and structural biology investigations to elucidate their catalytic mechanisms.

2.3. Exploring the crosstalk between PlPacC and PlAreB

To investigate potential interactions between PlPacC and PlAreB, future work could employ yeast two-hybrid (Y2H), GST pull-down, or BiFC assays to test for direct protein–protein interactions. If physical interaction is confirmed, further experiments can involve culturing the KOPlPacC mutant under varying nitrogen conditions and the KOPlAreB mutant under different pH conditions, followed by transcriptomic profiling to determine whether and how each regulator influences the other's pathway.

2.4. Optimal culture conditions for leucinostatins production

While environmental pH and total nitrogen content have been identified as key factors influencing leucinostatin production, the effects of other parameters remain to be explored. In this study, we utilized the complex organic nitrogen source peptone to assess its impact; however, the specific effects of individual nitrogen sources remain unknown. Additionally, variations in carbon sources, the presence of trace elements, and other environmental factors may also play a crucial role in production. Once the most influential variables are identified, response surface methodology (RSM) can be applied to systematically optimize culture conditions, ultimately improving leucinostatin yield and production efficiency.

References

Abe, H., Ouchi, H., Sakashita, C., Kawada, M., Watanabe, T., & Shibasaki, M. (2017). Catalytic Asymmetric Total Synthesis and Stereochemical Revision of Leucinostatin A: A Modulator of Tumor–Stroma Interaction. *Chemistry – A European Journal*, *23*(49), 11792-11796.

Alabouvette, C., & Steinberg, C. (2006). THE SOIL AS A RESERVOIR FOR ANTAGONISTS TO PLANT DISEASES. In J. Eilenberg & H. M. T. Hokkanen (Eds.), *An Ecological and Societal Approach to Biological Control* (pp. 123-144). Springer Netherlands.

Alimu, Y., Kusuya, Y., Yamamoto, T., Arita, K., Shigemune, N., Takahashi, H., & Yaguchi, T. (2022). Mechanism of Polyhexamethylene Biguanide Resistance in *Purpureocillium lilacinum* Strains. *Biocontrol Science*, *27*(3), 117-130.

Anastassiadou, M., Arena, M., Auteri, D., Brancato, A., Bura, L., Carrasco Cabrera, L., Castoldi, A., Chaideftou, E., Chiusolo, A., Crivellente, F., De Lentdecker, C., Egsmose, M., Fait, G., Greco, L., Ippolito, A., Istace, F., Jarrah, S., Kardassi, D., Leuschner, R., . . . Villamar-Bouza, L. (2022). Peer review of the pesticide risk assessment of the active substance *Purpureocillium lilacinum* strain PL11. *Efsa j*, *20*(5), e06393.

Anastassiadou, M., Arena, M., Auteri, D., Brancato, A., Bura, L., Carrasco Cabrera, L., Chaideftou, E., Chiusolo, A., Crivellente, F., De Lentdecker, C., Egsmose, M., Fait, G., Greco, L., Ippolito, A., Istace, F., Jarrah, S., Kardassi, D., Leuschner, R., Lostia, A., . . . Villamar-Bouza, L. (2020). Peer review of the pesticide risk assessment of the active substance *Purpureocillium lilacinum* strain 251. *Efsa j*, *18*(9), e06238.

Andersen, J. F., & Hutchinson, C. R. (1992). Characterization of Saccharopolyspora erythraea cytochrome P-450 genes and enzymes, including 6-deoxyerythronolide B hydroxylase. *Journal of Bacteriology*, *174*(3), 725-735.

Arai, T., Mikami, Y., Fukushima, K., Utsumi, T., & Yazawa, K. (1973). A new antibiotic, leucinostatin, derived from *Penicillium lilacinum*. *J Antibiot (Tokyo)*, *26*(3), 157-161.

Baazeem, A., Almanea, A., Manikandan, P., Alorabi, M., Vijayaraghavan, P., & Abdel-Hadi, A. (2021). In Vitro Antibacterial, Antifungal, Nematocidal and Growth Promoting Activities of *Trichoderma hamatum* FB10 and Its Secondary Metabolites. *J Fungi (Basel). 7*(5), 331.

Bae, S.-J., Mohanta, T. K., Chung, J. Y., Ryu, M., Park, G., Shim, S., Hong, S.-B., Seo, H., Bae, D.-W., Bae, I., Kim, J.-J., & Bae, H. (2016). Trichoderma metabolites as biological control agents against Phytophthora pathogens. *Biological Control*, *92*, 128-138.

Barda, O., Maor, U., Sadhasivam, S., Bi, Y., Zakin, V., Prusky, D., & Sionov, E. (2020). The pH-Responsive Transcription Factor PacC Governs

Pathogenicity and Ochratoxin A Biosynthesis in *Aspergillus carbonarius*. *Front Microbiol*, *11*, 210.

Barra, P., Etcheverry, M., & Nesci, A. (2015). Improvement of the Insecticidal Capacity of Two *Purpureocillium Lilacinum* Strains against *Tribolium Confusum*. *Insects*, *6*(1), 206-223.

Bayram, Ö., Krappmann, S., Ni, M., Bok, J. W., Helmstaedt, K., Valerius, O., Braus-Stromeyer, S., Kwon, N.-J., Keller, N. P., Yu, J.-H., & Braus, G. H. (2008). VelB/VeA/LaeA Complex Coordinates Light Signal with Fungal Development and Secondary Metabolism. *Science*, *320*(5882), 1504-1506.

Beck, J. G., Chatterjee, J., Laufer, B., Kiran, M. U., Frank, A. O., Neubauer, S., Ovadia, O., Greenberg, S., Gilon, C., Hoffman, A., & Kessler, H. (2012). Intestinal permeability of cyclic peptides: common key backbone motifs identified. *J Am Chem Soc*, *134*(29), 12125-12133.

Berry, D., Mace, W., Rehner, S. A., Grage, K., Dijkwel, P. P., Young, C. A., & Scott, B. (2019). Orthologous peramine and pyrrolopyrazine-producing biosynthetic gene clusters in *Metarhizium rileyi*, *Metarhizium majus* and *Cladonia grayi*. *Environmental Microbiology*, *21*(3), 928-939.

Bills, G., Li, Y., Chen, L., Yue, Q., Niu, X. M., & An, Z. (2014). New insights into the echinocandins and other fungal non-ribosomal peptides and peptaibiotics. *Nat Prod Rep*, *31*(10), 1348-1375.

Binh, C. T., Thai, H. D., Ha, B. T. V., & Tran, V. T. (2021). Establishment of a new and efficient Agrobacterium-mediated transformation system in the nematicidal fungus *Purpureocillium lilacinum*. *Microbiological Research*, *249*, 126773.

Bode, H. B., Bethe, B., Höfs, R., & Zeeck, A. (2002). Big effects from small changes: possible ways to explore nature's chemical diversity. *Chembiochem*, *3*(7), 619-627.

Bok, J. W., Balajee, S. A., Marr, K. A., Andes, D., Nielsen, K. F., Frisvad, J. C., & Keller, N. P. (2005). LaeA, a regulator of morphogenetic fungal virulence factors. *Eukaryot Cell*, *4*(9), 1574-1582.

Bok, J. W., & Keller, N. P. (2004). LaeA, a regulator of secondary metabolism in Aspergillus spp. *Eukaryot Cell*, *3*(2), 527-535.

Bok, J. W., & Keller, N. P. (2012). Fast and easy method for construction of plasmid vectors using modified quick-change mutagenesis. *Methods in Molecular Biology*, *944*, 163-174.

Bonaterra, A., Badosa, E., Daranas, N., Francés, J., Roselló, G., & Montesinos, E. J. M. (2022). Bacteria as biological control agents of plant diseases. *10*(9), 1759.

Bowers, K. J., Chow, E., Xu, H., Dror, R. O., Eastwood, M. P., Gregersen, B. A., Klepeis, J. L., Kolossvary, I., Moraes, M. A., & Sacerdoti, F. D. (2006). Scalable algorithms for molecular dynamics simulations on commodity clusters. Proceedings of the 2006 ACM/IEEE Conference on Supercomputing,

Brakhage, A. A. (1998). Molecular regulation of beta-lactam biosynthesis in filamentous fungi. *Microbiol Mol Biol Rev*, *62*(3), 547-585.

Brand, M., Wang, L., Agnello, S., Gazzola, S., Gall, F. M., Raguz, L., Kaiser, M., Schmidt, R. S., Ritschl, A., Jelk, J., Hemphill, A., Maser, P., Butikofer, P., Adams, M., & Riedl, R. (2021). Antiprotozoal Structure-Activity Relationships of Synthetic Leucinostatin Derivatives and Elucidation of their Mode of Action. *Angew Chem Int Ed Engl*, *60*(28), 15613-15621.

Brescia, F. F., Korf, L., Essen, L. O., Zorn, H., & Ruehl, M. (2024). A Novel O- and S-Methyltransferase from *Pleurotus sapidus* Is Involved in Flavor Formation. *J Agric Food Chem*, *72*(12), 6471-6480.

Cacho, R. A., Jiang, W., Chooi, Y. H., Walsh, C. T., & Tang, Y. (2012). Identification and characterization of the echinocandin B biosynthetic gene cluster from *Emericella rugulosa* NRRL 11440. *J Am Chem Soc*, *134*(40), 16781-16790.

Caddick, M. X., Peters, D., & Platt, A. (1994). Nitrogen regulation in fungi. *Antonie Van Leeuwenhoek*, *65*(3), 169-177.

Cai, Y., Hai, Y., Ohashi, M., Jamieson, C. S., Garcia-Borras, M., Houk, K. N., Zhou, J., & Tang, Y. (2019). Structural basis for stereoselective dehydration and hydrogen-bonding catalysis by the SAM-dependent pericyclase LepI. *Nature Chemistry*, *11*(9), 812-820.

Calcagno-Pizarelli, A. M., Negrete-Urtasun, S., Denison, S. H., Rudnicka, J. D., Bussink, H. J., Munera-Huertas, T., Stanton, L., Hervas-Aguilar, A., Espeso, E. A., Tilburn, J., Arst, H. N., Jr., & Penalva, M. A. (2007). Establishment of the ambient pH signaling complex in *Aspergillus nidulans*: PalI assists plasma membrane localization of PalH. *Eukaryot Cell*, *6*(12), 2365-2375.

Calvo, A. M., Bok, J., Brooks, W., & Keller, N. P. (2004). veA is required for toxin and sclerotial production in *Aspergillus parasiticus*. *Appl Environ Microbiol*, *70*(8), 4733-4739.

Calvo, A. M., Wilson, R. A., Bok, J. W., & Keller, N. P. (2002). Relationship between secondary metabolism and fungal development. *Microbiol Mol Biol Rev*, *66*(3), 447-459, table of contents.

Caracuel, Z., Roncero, M. I., Espeso, E. A., Gonzalez-Verdejo, C. I., Garcia-Maceira, F. I., & Di Pietro, A. (2003). The pH signalling transcription factor PacC controls virulence in the plant pathogen *Fusarium oxysporum*. *Molecular Microbiology*, *48*(3), 765-779.

Castillo Lopez, D., Zhu-Salzman, K., Ek-Ramos, M. J., & Sword, G. A. (2014). The entomopathogenic fungal endophytes *Purpureocillium lilacinum* (formerly *Paecilomyces lilacinus*) and Beauveria bassiana negatively affect cotton aphid reproduction under both greenhouse and field conditions. *PloS One*, *9*(8), e103891.

Cavello, I., & Cavalitto, S. (2013). Optimization of keratinolytic protease production by *Purpureocillium lilacinum* LPS# 876 as a sustainable management of tannery hair waste. *Journal Of The American Leather Chemists Association*, *108*(08), 300-310.

Chaverri, P., Castlebury, L. A., Overton, B. E., & Samuels, G. J. (2003). Hypocrea/Trichoderma: species with conidiophore elongations and green conidia. *Mycologia*, *95*(6), 1100-1140.

Chen, X. (2011). Fermenting next generation glycosylated therapeutics. *ACS Chem Biol*, *6*(1), 14-17.

Chen, X., Zhang, W., Wang, J., Zhu, S., Shen, X., Chen, H., & Fan, Y. (2022). Transcription Factors BbPacC and Bbmsn2 Jointly Regulate Oosporein Production in *Beauveria bassiana*. *Microbiol Spectr*, *10*(6), e0311822.

Chen, Y., Cao, Y., Jiao, C., Sun, X., Gai, Y., Zhu, Z., & Li, H. (2023). The Alternaria alternata StuA transcription factor interacting with the pH-responsive regulator PacC for the biosynthesis of host-selective toxin and virulence in citrus. *Microbiol Spectr*, *11*(6), e0233523.

Chen, Y., Li, B., Xu, X., Zhang, Z., & Tian, S. (2018). The pH-responsive PacC transcription factor plays pivotal roles in virulence and patulin biosynthesis in *Penicillium expansum*. *Environmental Microbiology*, *20*(11), 4063-4078.

Chiang, Y. M., Ahuja, M., Oakley, C. E., Entwistle, R., Asokan, A., Zutz, C., Wang, C. C., & Oakley, B. R. (2016). Development of genetic dereplication strains in Aspergillus nidulans results in the discovery of aspercryptin. *Angew Chem Int Ed*, *55*(5), 1662-1665.

Christiansen, L., Alanin, K. S., Phippen, C. B. W., Olsson, S., Stougaard, P., & Hennessy, R. C. (2020). Fungal-Associated Molecules Induce Key Genes Involved in the Biosynthesis of the Antifungal Secondary Metabolites Nunamycin and Nunapeptin in the Biocontrol Strain *Pseudomonas fluorescens* In5. *Appl Environ Microbiol*, *86*(21).

Claesen, J., & Bibb, M. (2010). Genome mining and genetic analysis of cypemycin biosynthesis reveal an unusual class of posttranslationally modified peptides. *Proc Natl Acad Sci U S A*, *107*(37), 16297-16302.

Contreras-Cornejo, H. A., del-Val, E., Macías-Rodríguez, L., Alarcón, A., González-Esquivel, C. E., & Larsen, J. (2018). *Trichoderma atroviride*, a maize root associated fungus, increases the parasitism rate of the fall armyworm

Spodoptera frugiperda by its natural enemy Campoletis sonorensis. *Soil Biology and Biochemistry*, *122*, 196-202.

Corso, G., Stärk, H., Jing, B., Barzilay, R., & Jaakkola, T. (2022). Diffdock: Diffusion steps, twists, and turns for molecular docking. *arXiv preprint arXiv:2210.01776*.

Cui, Y., Song, K., Jin, Z. J., Lee, L. H., Thawai, C., & He, Y. W. (2023). Fructose promotes pyoluteorin biosynthesis via the CbrAB-CrcZ-Hfq/Crc pathway in the biocontrol strain *Pseudomonas* PA1201. *Synth Syst Biotechnol*, *8*(4), 618-628.

Dan, Q., Newmister, S. A., Klas, K. R., Fraley, A. E., McAfoos, T. J., Somoza, A. D., Sunderhaus, J. D., Ye, Y., Shende, V. V., Yu, F., Sanders, J. N., Brown, W. C., Zhao, L., Paton, R. S., Houk, K. N., Smith, J. L., Sherman, D. H., & Williams, R. M. (2019). Fungal indole alkaloid biogenesis through evolution of a bifunctional reductase/Diels-Alderase. *Nature Chemistry*, *11*(11), 972-980.

Daniel-Ivad, P., & Ryan, K. S. (2024). Structure of methyltransferase RedM that forms the dimethylpyrrolinium of the bisindole reductasporine. *J Biol Chem*, *300*(1), 105520.

Das, D., Khan, H. P., Shivahare, R., Gupta, S., Sarkar, J., Siddiqui, M. I., Ampapathi, R. S., & Chakraborty, T. K. (2017). Synthesis, SAR and biological studies of sugar amino acid-based almiramide analogues: N-methylation leads the way. *Org Biomol Chem*, *15*(15), 3337-3352.

de Mattos-Shipley, K. M. J., Greco, C., Heard, D. M., Hough, G., Mulholland, N. P., Vincent, J. L., Micklefield, J., Simpson, T. J., Willis, C. L., Cox, R. J., & Bailey, A. M. (2018). The cycloaspeptides: uncovering a new model for methylated nonribosomal peptide biosynthesis. *Chem Sci*, *9*(17), 4109-4117.

Diez, E., Alvaro, J., Espeso, E. A., Rainbow, L., Suarez, T., Tilburn, J., Arst, H. N., Jr., & Penalva, M. A. (2002). Activation of the Aspergillus PacC zinc finger transcription factor requires two proteolytic steps. *Embo Journal*, *21*(6), 1350-1359.

Divon, H. H., Ziv, C., Davydov, O., Yarden, O., & Fluhr, R. (2006). The global nitrogen regulator, FNR1, regulates fungal nutrition-genes and fitness during *Fusarium oxysporum* pathogenesis. *Mol Plant Pathol*, *7*(6), 485-497.

Du, L., & Lou, L. (2010). PKS and NRPS release mechanisms. *Nat Prod Rep*, *27*(2), 255-278.

Elsherbiny, E. A., Taher, M. A., Abd El-Aziz, M. H., & Mohamed, S. Y. (2021). Action mechanisms and biocontrol of *Purpureocillium lilacinum* against green mould caused by *Penicillium digitatum* in orange fruit. *J Appl Microbiol*, *131*(3), 1378-1390.

Espeso, E. A., Roncal, T., Díez, E., Rainbow, L., Bignell, E., Alvaro, J., Suárez, T., Denison, S. H., Tilburn, J., Arst, H. N., Jr., & Peñalva, M. A. (2000). On how a transcription factor can avoid its proteolytic activation in the absence of signal transduction. *Embo J*, *19*(4), 719-728.

Espeso, E. A., Tilburn, J., Sanchez-Pulido, L., Brown, C. V., Valencia, A., Arst, H. N., Jr., & Penalva, M. A. (1997). Specific DNA recognition by the *Aspergillus nidulans* three zinc finger transcription factor PacC. *J Mol Biol*, *274*(4), 466-480.

Fan, A., Zhong, B., Liu, D., Lu, Y., Wu, M., Jin, H., Shi, X. M., Ren, J., Zhang, B., Su, X. D., Ma, M., Li, S. M., & Lin, W. (2024). Biosynthesis of Epipyrone A Reveals a Highly Specific Membrane-Bound Fungal C-Glycosyltransferase for Pyrone Galactosylation. *Org Lett*, *26*(6), 1160-1165.

Fang, W., Feng, J., Fan, Y., Zhang, Y., Bidochka, M. J., Leger, R. J., & Pei, Y. (2009). Expressing a fusion protein with protease and chitinase activities increases the virulence of the insect pathogen *Beauveria bassiana*. *J Invertebr Pathol*, *102*(2), 155-159.

Feng, P., Shang, Y., Cen, K., & Wang, C. (2015). Fungal biosynthesis of the bibenzoquinone oosporein to evade insect immunity. *Proc Natl Acad Sci U S A*, *112*(36), 11365-11370.

Fernandez, K. X., Pokorny, S., Ishangulyeva, G., Ullah, A., Todorova, S. I., Erbilgin, N., Carroll, A. L., & Vederas, J. C. (2023). *Beauveria bassiana* exhibits strong virulence against Dendroctonus ponderosae in greenhouse and field experiments. *Appl Microbiol Biotechnol*, *107*(10), 3341-3352.

Fischbach, M. A., & Walsh, C. T. (2006). Assembly-line enzymology for polyketide and nonribosomal Peptide antibiotics: logic, machinery, and mechanisms. *Chem Rev*, *106*(8), 3468-3496.

Fornelli, F., Minervini, F., & Logrieco, A. (2004). Cytotoxicity of fungal metabolites to lepidopteran (*Spodoptera frugiperda*) cell line (SF-9). *J Invertebr Pathol*, *85*(2), 74-79.

Fricke, J., Blei, F., & Hoffmeister, D. (2017). Enzymatic synthesis of psilocybin. *Angew Chem Int Ed*, *56*(40), 12352-12355.

Fujita, H., Ogawa, K., Tone, H., Iguchi, H., Shomura, T., & Murata, S. (1986). Pharmacokinetics of doxorubicin, (2"R)-4'-O-tetrahydropyranyl-adriamycin and aclarubicin. *Jpn J Antibiot*, *39*(5), 1321-1336.

Fukushima, K., Arai, T., Mori, Y., Tsuboi, M., & Suzuki, M. (1983). Studies on peptide antibiotics, leucinostatins. I. Separation, physico-chemical properties and biological activities of leucinostatins A and B. *J Antibiot (Tokyo)*, *36*(12), 1606-1612.

Ganassi, S., Moretti, A., Bonvicini Pagliai, A. M., Logrieco, A., & Agnese Sabatini, M. (2002). Effects of beauvericin on *Schizaphis graminum* (Aphididae). *J Invertebr Pathol*, *80*(2), 90-96.

Gao, F., Yuan, Y., Yu, X., Jiang, Q., Zhang, Z., Hu, X., Zhao, C., & Cheng, Z. (2023). Optimization of *Purpureocillium lilacinum* Derived from Spent Mushroom Substrate and Its Potential to Control Soybean Cyst Nematode. *Waste Biomass Valor*, *14*(5), 1637-1647.

Gessmann, R., Brückner, H., Berg, A., & Petratos, K. (2018). The crystal structure of the lipoaminopeptaibol helioferin, an antibiotic peptide from *Mycogone rosea*. *Acta Crystallogr D Struct Biol*, *74*(Pt 4), 315-320.

Ghorbanpour, M., Omidvari, M., Abbaszadeh-Dahaji, P., Omidvar, R., & Kariman, K. (2018). Mechanisms underlying the protective effects of beneficial fungi against plant diseases. *Biol Control*, *117*, 147-157.

Girardi, N. S., Sosa, A. L., Etcheverry, M. G., & Passone, M. A. (2022). In vitro characterization bioassays of the nematophagous fungus *Purpureocillium lilacinum*: Evaluation on growth, extracellular enzymes, mycotoxins and survival in the surrounding agroecosystem of tomato. *Fungal Biol*, *126*(4), 300-307.

Goffre, D., & Folgarait, P. J. (2015). *Purpureocillium lilacinum*, potential agent for biological control of the leaf-cutting ant Acromyrmex lundii. *J Invertebr Pathol*, *130*, 107-115.

González, M. C., Lull, C., Moya, P., Ayala, I., Primo, J., & Primo Yúfera, E. (2003). Insecticidal activity of penitrems, including penitrem G, a new member of the family isolated from *Penicillium crustosum*. *J Agric Food Chem*, *51*(8), 2156-2160.

Götz, P., Matha, V., & Vilcinskas, A. (1997). Effects of the entomopathogenic fungus *Metarhizium anisopliae* and its secondary metabolites on morphology and cytoskeleton of plasmatocytes isolated from the greater wax moth, *Galleria mellonella*. *J Insect Physiol*, *43*(12), 1149-1159.

Griffith, G. W., Easton, G. L., Detheridge, A., Roderick, K., Edwards, A., Worgan, H. J., Nicholson, J., & Perkins, W. T. (2007). Copper deficiency in potato dextrose agar causes reduced pigmentation in cultures of various fungi. *Fems Microbiol Lett*, *276*(2), 165-171.

Grove, J. F., & Pople, M. (1980). The insecticidal activity of beauvericin and the enniatin complex. *Mycopathologia*, *70*(2), 103-105.

Guan, F., Pan, Y., Li, J., & Liu, G. (2017). A GATA-type transcription factor AcAREB for nitrogen metabolism is involved in regulation of cephalosporin biosynthesis in *Acremonium chrysogenum*. *Sci China Life Sci*, *60*(9), 958-967.

Guzmán-Guzmán, P., Alemán-Duarte, M. I., Delaye, L., Herrera-Estrella, A., & Olmedo-Monfil, V. (2017). Identification of effector-like proteins in Trichoderma spp. and role of a hydrophobin in the plant-fungus interaction and mycoparasitism. *BMC Genet*, *18*(1), 16.

Hamill, R. L., Higgens, C., Boaz, H., & Gorman, M. (1969). The structure op beauvericin, a new depsipeptide antibiotic toxic to *Artemia salina*. *Tetrahedron Lett*, *10*(49), 4255-4258.

Harman, G. E., Howell, C. R., Viterbo, A., Chet, I., & Lorito, M. (2004). Trichoderma species — opportunistic, avirulent plant symbionts. *Nat Rev Microbiol*, *2*(1), 43-56.

He, Q., Zhang, H. R., & Zou, Y. (2024). A Cytochrome P450 Catalyzes Oxidative Coupling Formation of Insecticidal Dimeric Indole Piperazine Alkaloids. *Angew Chem Int Ed Engl*, *63*(22), e202404000.

Hervas-Aguilar, A., Rodriguez, J. M., Tilburn, J., Arst, H. N., Jr., & Penalva, M. A. (2007). Evidence for the direct involvement of the proteasome in the proteolytic processing of the *Aspergillus nidulans* zinc finger transcription factor PacC. *J Biol Chem*, *282*(48), 34735-34747.

Hoff, B., Kamerewerd, J., Sigl, C., Mitterbauer, R., Zadra, I., Kürnsteiner, H., & Kück, U. (2010). Two components of a velvet-like complex control hyphal morphogenesis, conidiophore development, and penicillin biosynthesis in *Penicillium chrysogenum*. *Eukaryot Cell*, *9*(8), 1236-1250.

Hou, Q., Wang, J., Gao, J., Liu, Y., & Liu, C. (2012). QM/MM studies on the catalytic mechanism of phenylethanolamine N-methyltransferase. *Biochim Biophys Acta Proteins Proteom*, *1824*(4), 533-541.

Hu, Q. B., An, X. C., Jin, F. L., Freed, S., & Ren, S. X. (2009). Toxicities of destruxins against Bemisia tabaci and its natural enemy, *Serangium japonicum*. *Toxicon*, *53*(1), 115-121.

Huang, X., Zheng, Y., Li, P., Cui, J., Sui, P., Chen, Y., & Gao, W. (2023). Organic management increases beneficial microorganisms and promotes the stability of microecological networks in tea plantation soil. *Front Microbiol*, *19*(14), 1237842.

Isaac, G. S., El-Deriny, M. M., & Taha, R. G. (2021). Efficacy of *Purpureocillium lilacinum* AUMC 10149 as biocontrol agent against root-knot nematode Meloidogyne incognita infecting tomato plant. *Braz J Biol*, *84*, e253451.

Isogai, A., Nakayama, J., Takayama, S., Kusai, A., & Suzuki, A. (1992). Structural elucidation of minor components of peptidyl antibiotic P168s (leucinostatins) by tandem mass spectrometry. *Biosci Biotechnol Biochem*, *56*(7), 1079-1085.

Iwanicki, N. S. A., Pereira, A. A., Botelho, A., Rezende, J. M., Moral, R. A., Zucchi, M. I., & Delalibera Junior, I. (2019). Monitoring of the field application of

Metarhizium anisopliae in Brazil revealed high molecular diversity of *Metarhizium* spp in insects, soil and sugarcane roots. *Sci Rep*, *9*(1), 4443.

Jansson, A., Koskiniemi, H., Erola, A., Wang, J., Mäntsälä, P., Schneider, G., & Niemi, J. (2005). Aclacinomycin 10-hydroxylase is a novel substrate-assisted hydroxylase requiring S-adenosyl-L-methionine as cofactor. *J Biol Chem*, *280*(5), 3636-3644.

Jia, L. J., Tang, H. Y., Wang, W. Q., Yuan, T. L., Wei, W. Q., Pang, B., Gong, X. M., Wang, S. F., Li, Y. J., Zhang, D., Liu, W., & Tang, W. H. (2019). A linear nonribosomal octapeptide from *Fusarium graminearum* facilitates cell-to-cell invasion of wheat. *Nat Commun*, *10*(1), 922.

Jiao, Y., Li, Y., Li, Y., Cao, H., Mao, Z., Ling, J., Yang, Y., & Xie, B. (2019). Functional genetic analysis of the leucinostatin biosynthesis transcription regulator lcsL in *Purpureocillium lilacinum* using CRISPR-Cas9 technology. *Appl Microbiol Biotechnol*, *103*(15), 6187-6194.

Jockmann, E., Subrizi, F., Mohr, M. K. F., Carter, E. M., Hebecker, P. M., Popadić, D., Hailes, H. C., & Andexer, J. N. (2023). Expanding the Substrate Scope of N- and O-Methyltransferases from Plants for Chemoselective Alkylation. *ChemCatChem*, *15*(22), e202300930.

Ju, S., Kuzelka, K. P., Guo, R., Krohn-Hansen, B., Wu, J., Nair, S. K., & Yang, Y. (2023). A biocatalytic platform for asymmetric alkylation of α-keto acids by mining and engineering of methyltransferases. *Nat Commun*, *14*(1), 5704.

Karimi Aghcheh, R., Druzhinina, I. S., & Kubicek, C. P. (2013). The putative protein methyltransferase LAE1 of *Trichoderma atroviride* is a key regulator of asexual development and mycoparasitism. *PloS One*, *8*(6), e67144.

Kato, N., Brooks, W., & Calvo, A. M. (2003). The expression of sterigmatocystin and penicillin genes in *Aspergillus nidulans* is controlled by veA, a gene required for sexual development. *Eukaryot Cell*, *2*(6), 1178-1186.

Kawada, M., Inoue, H., Ohba, S., Masuda, T., Momose, I., & Ikeda, D. (2010). Leucinostatin A inhibits prostate cancer growth through reduction of insulin-like growth factor-I expression in prostate stromal cells. *Int J Cancer*, *126*(4), 810-818.

Keating, T. A., & Walsh, C. T. (1999). Initiation, elongation, and termination strategies in polyketide and polypeptide antibiotic biosynthesis. *Curr Opin Chem Biol*, *3*(5), 598-606.

Keller, N. P., Turner, G., & Bennett, J. W. (2005). Fungal secondary metabolism - from biochemistry to genomics. *Nat Rev Microbiol*, *3*(12), 937-947.

Khan, M., & Tanaka, K. (2023). *Purpureocillium lilacinum* for plant growth promotion and biocontrol against root-knot nematodes infecting eggplant. *PloS One*, *18*(3), e0283550.

Kil, Y. S., Risinger, A. L., Petersen, C. L., Mooberry, S. L., & Cichewicz, R. H. (2020). Leucinostatins from *Ophiocordyceps* spp. and *Purpureocillium* spp. Demonstrate Selective Antiproliferative Effects in Cells Representing the Luminal Androgen Receptor Subtype of Triple Negative Breast Cancer. *J Nat Prod*, *83*(6), 2010-2024.

Kim, H., & Woloshuk, C. P. (2008). Role of AREA, a regulator of nitrogen metabolism, during colonization of maize kernels and fumonisin biosynthesis in *Fusarium verticillioides*. *Fungal Genet Biol*, *45*(6), 947-953.

Klingen, I., Meadow, R., & Aandal, T. (2002). Mortality of *Delia floralis*, *Galleria mellonella* and *Mamestra brassicae* treated with insect pathogenic hyphomycetous fungi. *J Appl Entomol*, *126*(5), 231-237.

Kosalková, K., García-Estrada, C., Ullán, R. V., Godio, R. P., Feltrer, R., Teijeira, F., Mauriz, E., & Martín, J. F. (2009). The global regulator LaeA controls penicillin biosynthesis, pigmentation and sporulation, but not roquefortine C synthesis in *Penicillium chrysogenum*. *Biochimie*, *91*(2), 214-225.

Krasnoff, S. B., Keresztes, I., Gillilan, R. E., Szebenyi, D. M., Donzelli, B. G., Churchill, A. C., & Gibson, D. M. (2007). Serinocyclins A and B, cyclic heptapeptides from *Metarhizium anisopliae*. *J Nat Prod*, *70*(12), 1919-1924.

Kubicek, C. P., Herrera-Estrella, A., Seidl-Seiboth, V., Martinez, D. A., Druzhinina, I. S., Thon, M., Zeilinger, S., Casas-Flores, S., Horwitz, B. A., Mukherjee, P. K., Mukherjee, M., Kredics, L., Alcaraz, L. D., Aerts, A., Antal, Z., Atanasova, L., Cervantes-Badillo, M. G., Challacombe, J., Chertkov, O., . . . Grigoriev, I. V. (2011). Comparative genome sequence analysis underscores mycoparasitism as the ancestral life style of Trichoderma. *Genome Biol*, *12*(4), R40.

Kudo, F., & Eguchi, T. (2016). Aminoglycoside Antibiotics: New Insights into the Biosynthetic Machinery of Old Drugs. *Chem Rec*, *16*(1), 4-18.

Kuwata, S., Nakanishi, A., Yamada, T., & Miyazawa, T. (1992). Total synthesis of Leucinostatin D. *Tetrahedron Lett*, *33*(46), 6995-6998.

Labbe, R. M., Cloutier, C., & Brodeur, J. (2006). Prey selection by *Dicyphus hesperus* of infected or parasitized greenhouse whitefly. *Biocontrol Sci Technol*, *16*(5), 485-494.

Labby, K. J., Watsula, S. G., & Garneau-Tsodikova, S. (2015). Interrupted adenylation domains: unique bifunctional enzymes involved in nonribosomal peptide biosynthesis. *Nat Prod Rep*, *32*(5), 641-653.

Lan, X., Zhang, J., Zong, Z., Ma, Q., & Wang, Y. (2017). Evaluation of the Biocontrol Potential of *Purpureocillium lilacinum* QLP12 against *Verticillium dahliae* in Eggplant. *Biomed Res Int*, *2017*, 4101357.

Langlois, N., & Le Nguyen, B. K. (2004). Diastereoselective syntheses of deoxydysibetaine, dysibetaine, and its 4-epimer. *J Org Chem*, *69*(22), 7558-7564.

Larsson, K. A., Zetterlund, I., Delp, G., & Jonsson, L. M. (2006). N-Methyltransferase involved in gramine biosynthesis in barley: cloning and characterization. *Phytochemistry*, *67*(18), 2002-2008.

Le, K. D., Yu, N. H., Park, A. R., Park, D. J., Kim, C. J., & Kim, J. C. (2022). *Streptomyces* sp. AN090126 as a Biocontrol Agent against Bacterial and Fungal Plant Diseases. *Microorganisms*, *10*(4).

Lee, J., Hao, Y., Blair, P. M., Melby, J. O., Agarwal, V., Burkhart, B. J., Nair, S. K., & Mitchell, D. A. (2013). Structural and functional insight into an unexpectedly selective N-methyltransferase involved in plantazolicin biosynthesis. *Proc Natl Acad Sci U S A*, *110*(32), 12954-12959.

Lee, S. G., Kim, Y., Alpert, T. D., Nagata, A., & Jez, J. M. (2012). Structure and reaction mechanism of phosphoethanolamine methyltransferase from the malaria parasite *Plasmodium falciparum*: an antiparasitic drug target. *J Biol Chem*, *287*(2), 1426-1434.

Leland, J. E., McGuire, M. R., Grace, J. A., Jaronski, S. T., Ulloa, M., Park, Y.-H., & Plattner, R. D. (2005). Strain selection of a fungal entomopathogen, *Beauveria bassiana*, for control of plant bugs (Lygus spp.)(Heteroptera: Miridae). *Biol Control*, *35*(2), 104-114.

Leonetti, P., Zonno, M. C., Molinari, S., & Altomare, C. (2017). Induction of SA-signaling pathway and ethylene biosynthesis in *Trichoderma harzianum*-treated tomato plants after infection of the root-knot nematode *Meloidogyne incognita*. *Plant Cell Rep*, *36*(4), 621-631.

Lescot, M., Dehais, P., Thijs, G., Marchal, K., Moreau, Y., Van de Peer, Y., Rouze, P., & Rombauts, S. (2002). PlantCARE, a database of plant cis-acting regulatory elements and a portal to tools for in silico analysis of promoter sequences. *Nucleic Acids Res*, *30*(1), 325-327.

Letunic, I., Khedkar, S., & Bork, P. (2021). SMART: recent updates, new developments and status in 2020. *Nucleic Acids Res*, *49*(D1), D458-d460.

Li, B., Chen, Y., & Tian, S. (2022). Function of pH-dependent transcription factor PacC in regulating development, pathogenicity, and mycotoxin biosynthesis of phytopathogenic fungi. *FEBS J*, *289*(7), 1723-1730.

Li, C., Zhang, Q., Xia, Y., & Jin, K. (2021). MaAreB, a GATA Transcription Factor, Is Involved in Nitrogen Source Utilization, Stress Tolerances and Virulence in *Metarhizium acridum*. *J Fungi (Basel)*, *7*(7).

Li, F., Lv, Z., Zhong, Z., Mao, L., Chua, L. S., Xu, L., & Huang, R. (2023). The Effect of Cyclosporin A on *Aspergillus niger* and the Possible Mechanisms Involved. *Foods*, *12*(3).

Li, Q., Ding, G., Li, B., & Guo, S.-X. (2017). Transcriptome Analysis of Genes Involved in Dendrobine Biosynthesis in *Dendrobium nobile* Lindl. Infected with Mycorrhizal Fungus MF23 (Mycena sp.). *Sci Rep*, *7*(1), 316.

Li, W., Fan, A., Wang, L., Zhang, P., Liu, Z., An, Z., & Yin, W. B. (2018). Asperphenamate biosynthesis reveals a novel two-module NRPS system to synthesize amino acid esters in fungi. *Chem Sci*, *9*(9), 2589-2594.

Li, Y., Yue, Q., Krausert, N. M., An, Z., Gloer, J. B., & Bills, G. F. (2016). Emestrins: Anti-Cryptococcus Epipolythiodioxopiperazines from *Podospora australis*. *J Nat Prod*, *79*(9), 2357-2363.

Li, Z., Jiao, Y., Ling, J., Zhao, J., Yang, Y., Mao, Z., Zhou, K., Wang, W., Xie, B., & Li, Y. (2024). Characterization of a methyltransferase for iterative N-methylation at the leucinostatin termini in *Purpureocillium lilacinum*. *Commun Biol*, *7*(1), 757.

Liang, D.-M., Liu, J.-H., Wu, H., Wang, B.-B., Zhu, H.-J., & Qiao, J.-J. (2015). Glycosyltransferases: mechanisms and applications in natural product development. *Chem Soc Rev*, *44*(22), 8350-8374.

Lim, F. Y., Won, T. H., Raffa, N., Baccile, J. A., Wisecaver, J., Rokas, A., Schroeder, F. C., & Keller, N. P. (2018). Fungal Isocyanide Synthases and Xanthocillin Biosynthesis in *Aspergillus fumigatus*. *MBio*, *9*(3).

Lindo, L., McCormick, S. P., Cardoza, R. E., Busman, M., Alexander, N. J., Proctor, R. H., & Gutiérrez, S. (2019). Requirement of Two Acyltransferases for 4-O-Acylation during Biosynthesis of Harzianum A, an Antifungal Trichothecene Produced by Trichoderma arundinaceum. *J Agric Food Chem*, *67*(2), 723-734.

Liu, B. L., Chen, J. W., & Tzeng, Y. M. (2000). Production of cyclodepsipeptides destruxin A and B from *Metarhizium anisopliae*. *Biotechnol Prog*, *16*(6), 993-999.

Liu, L., Tang, M. C., & Tang, Y. (2019). Fungal Highly Reducing Polyketide Synthases Biosynthesize Salicylaldehydes That Are Precursors to Epoxycyclohexenol Natural Products. *J Am Chem Soc*, *141*(50), 19538-19541.

Liu, R., Khan, R. A. A., Yue, Q., Jiao, Y., Yang, Y., Li, Y., & Xie, B. (2020). Discovery of a new antifungal lipopeptaibol from *Purpureocillium lilacinum* using MALDI-TOF-IMS. *Biochem Biophys Res Commun*, *527*(3), 689-695.

Liu, Z., Liu, F.-F., Li, H., Zhang, W.-T., Wang, Q., Zhang, B.-X., Sun, Y.-X., & Rao, X.-J. (2022). Virulence of the Bio-Control Fungus *Purpureocillium lilacinum* Against *Myzus persicae* (Hemiptera: Aphididae) and S*podoptera frugiperda* (Lepidoptera: Noctuidae). *J Econ Entomol*, *115*(2), 462-473.

Livak, K. J., & Schmittgen, T. D. (2001). Analysis of relative gene expression data using real-time quantitative PCR and the 2(-Delta Delta C(T)) Method. *Methods*, *25*(4), 402-408.

Lo, H. C., Entwistle, R., Guo, C. J., Ahuja, M., Szewczyk, E., Hung, J. H., Chiang, Y. M., Oakley, B. R., & Wang, C. C. (2012). Two separate gene clusters encode the biosynthetic pathway for the meroterpenoids austinol and dehydroaustinol in *Aspergillus nidulans*. *J Am Chem Soc*, *134*(10), 4709-4720.

Losey, H. C., Peczuh, M. W., Chen, Z., Eggert, U. S., Dong, S. D., Pelczer, I., Kahne, D., & Walsh, C. T. (2001). Tandem action of glycosyltransferases in the maturation of vancomycin and teicoplanin aglycones: novel glycopeptides. *Biochemistry*, *40*(15), 4745-4755.

Luangsa-Ard, J., Houbraken, J., van Doorn, T., Hong, S. B., Borman, A. M., Hywel-Jones, N. L., & Samson, R. A. (2011). Purpureocillium, a new genus for the medically important *Paecilomyces lilacinus*. *Fems Microbiol Lett*, *321*(2), 141-149.

Luo, Z., Chen, Q., Su, Y., Hu, S., Keyhani, N. O., Wang, J., Zhu, C., Zhou, T., Pan, Y., Bidochka, M. J., & Zhang, Y. (2023). The AreA Nitrogen Catabolite Repression Activator Balances Fungal Nutrient Utilization and Virulence in the Insect Fungal Pathogen *Beauveria bassiana*. *J Agric Food Chem*, *71*(1), 646-659.

Luo, Z., Ren, H., Mousa, J. J., Rangel, D. E., Zhang, Y., Bruner, S. D., & Keyhani, N. O. (2017). The PacC transcription factor regulates secondary metabolite production and stress response, but has only minor effects on virulence in the insect pathogenic fungus *Beauveria bassiana*. *Environ Microbiol*, *19*(2), 788-802.

Ma, Z., Ongena, M., & Hofte, M. (2017). The cyclic lipopeptide orfamide induces systemic resistance in rice to *Cochliobolus miyabeanus* but not to *Magnaporthe oryzae*. *Plant Cell Rep*, *36*(11), 1731-1746.

Macios, M., Caddick, M. X., Weglenski, P., Scazzocchio, C., & Dzikowska, A. (2012). The GATA factors AREA and AREB together with the co-repressor NMRA, negatively regulate arginine catabolism in *Aspergillus nidulans* in response to nitrogen and carbon source. *Fungal Genet Biol*, *49*(3), 189-198.

Mahmoodi, N., Harijan, R. K., & Schramm, V. L. (2020). Transition-State Analogues of Phenylethanolamine N-Methyltransferase. *J Am Chem Soc*, *142*(33), 14222-14233.

Martinez, A. F., & Moraes, L. A. (2015). Liquid chromatography-tandem mass spectrometry characterization of five new leucinostatins produced by *Paecilomyces lilacinus* CG-189. *J Antibiot (Tokyo)*, *68*(3), 178-184.

Marzluf, G. A. (1997). Genetic regulation of nitrogen metabolism in the fungi. *Microbiol Mol Biol Rev*, *61*(1), 17-32.

Mascarin, G. M., Jackson, M. A., Kobori, N. N., Behle, R. W., Dunlap, C. A., & Delalibera Júnior, Í. (2015). Glucose concentration alters dissolved oxygen levels in liquid cultures of *Beauveria bassiana* and affects formation and bioefficacy of blastospores. *Appl Microbiol Biotechnol*, *99*, 6653-6665.

Mejri, S., Siah, A., Coutte, F., Magnin-Robert, M., Randoux, B., Tisserant, B., Krier, F., Jacques, P., Reignault, P., & Halama, P. (2018). Biocontrol of the wheat pathogen Zymoseptoria tritici using cyclic lipopeptides from Bacillus subtilis. *Environ Sci Pollut Res Int*, *25*(30), 29822-29833.

Ment, D., Alkan, N., Luria, N., Bi, F. C., Reuveni, E., Fluhr, R., & Prusky, D. (2015). A Role of AREB in the Regulation of PACC-Dependent Acid-Expressed-Genes and Pathogenicity of *Colletotrichum gloeosporioides*. *Mol Plant Microbe Interact s*, *28*(2), 154-166.

Mhatre, P. H., Divya, K. L., Venkatasalam, E. P., Watpade, S., Bairwa, A., & Patil, J. (2022). Management of potato cyst nematodes with special focus on biological control and trap cropping strategies. *Pest Manag Sci*, *78*(9), 3746-3759.

Michielse, C. B., Pfannmüller, A., Macios, M., Rengers, P., Dzikowska, A., & Tudzynski, B. (2014). The interplay between the GATA transcription factors AreA, the global nitrogen regulator and AreB in *Fusarium fujikuroi*. *Mol Microbiol*, *91*(3), 472-493.

Mikami, Y., Yazawa, K., Fukushima, K., Arai, T., Udagawa, S.-i., & Samson, R. A. (1989). Paecilotoxin production in clinical or terrestrial isolates of *Paecilomyces lilacinu*s strains. *Mycopathologia*, *108*, 195-199.

Min, K., Shin, Y., Son, H., Lee, J., Kim, J. C., Choi, G. J., & Lee, Y. W. (2012). Functional analyses of the nitrogen regulatory gene areA in Gibberella zeae. *FEMS Microbiol Lett*, *334*(1), 66-73.

Miziorko, H. M. (2011). Enzymes of the mevalonate pathway of isoprenoid biosynthesis. *Arch Biochem Biophys*, *505*(2), 131-143.

Mochizuki, K., Ohmori, K., Tamura, H., Shizuri, Y., Nishiyama, S., Miyoshi, E., & Yamamura, S. (2006). The Structures of Bioactive Cyclodepsipeptides, Beauveriolides I and II, Metabolites of Entomopathogenic Fungi *Beauveria* sp. *Bull Chem Soc Jpn*, *66*(10), 3041-3046.

Molohon, K. J., Melby, J. O., Lee, J., Evans, B. S., Dunbar, K. L., Bumpus, S. B., Kelleher, N. L., & Mitchell, D. A. (2011). Structure determination and interception of biosynthetic intermediates for the plantazolicin class of highly discriminating antibiotics. *ACS Chem Biol*, *6*(12), 1307-1313.

Momose, I., Onodera, T., Doi, H., Adachi, H., Iijima, M., Yamazaki, Y., Sawa, R., Kubota, Y., Igarashi, M., & Kawada, M. (2019). Leucinostatin Y: A Peptaibiotic Produced by the Entomoparasitic Fungus *Purpureocillium lilacinum* 40-H-28. *J Nat Prod*, *82*(5), 1120-1127.

Mooney, J. L., & Yager, L. N. (1990). Light is required for conidiation in *Aspergillus nidulans*. *Genes Dev*, *4*(9), 1473-1482.

Mori, S., Pang, A. H., Lundy, T. A., Garzan, A., Tsodikov, O. V., & Garneau-Tsodikova, S. (2018). Structural basis for backbone N-methylation by an interrupted adenylation domain. *Nat Chem Biol*, *14*(5), 428-430.

Mori, Y., Suzuki, M., Fukushima, K., & Arai, T. (1983). Structure of leucinostatin B, an uncoupler on mitochondria. *The Journal of Antibiotics*, *36*(8), 1084-1086.

Morrison, C. K., Arseneault, T., Novinscak, A., & Filion, M. (2017). Phenazine-1-Carboxylic Acid Production by *Pseudomonas fluorescens* LBUM636 Alters Phytophthora infestans Growth and Late Blight Development. *Phytopathology*, *107*(3), 273-279.

Mousumi Das, M., Haridas, M., & Sabu, A. (2020). Process development for the enhanced production of bio-nematicide *Purpureocillium lilacinum* KU8 under solid-state fermentation. *Bioresour Technol*, *308*, 123328.

Németh, Z., Molnár Á, P., Fejes, B., Novák, L., Karaffa, L., Keller, N. P., & Fekete, E. (2016). Growth-Phase Sterigmatocystin Formation on Lactose Is Mediated via Low Specific Growth Rates in *Aspergillus nidulans*. *Toxins*, *8*(12).

Newmister, S. A., Romminger, S., Schmidt, J. J., Williams, R. M., Smith, J. L., Berlinck, R. G. S., & Sherman, D. H. (2018). Unveiling sequential late-stage methyltransferase reactions in the meleagrin/oxaline biosynthetic pathway. *Org Biomol Chem*, *16*(35), 6450-6459.

Nguyen, T., Ishida, K., Jenke-Kodama, H., Dittmann, E., Gurgui, C., Hochmuth, T., Taudien, S., Platzer, M., Hertweck, C., & Piel, J. (2008). Exploiting the mosaic structure of trans-acyltransferase polyketide synthases for natural product discovery and pathway dissection. *Nat Biotechnol*, *26*(2), 225-233.

Nidheesh, T., Pal, G. K., & Suresh, P. V. (2015). Chitooligomers preparation by chitosanase produced under solid state fermentation using shrimp by-products as substrate. *Carbohydr Polym*, *121*, 1-9.

Nie, M., Yue, G., Wang, L., & Zhang, Y. (2024). Short-term organic fertilizer substitution increases sorghum yield by improving soil physicochemical characteristics and regulating microbial community structure. *Front Plant Sci*, *15*.

Niu, G., Wang, X., Hao, Y., Kandel, S., Niu, G., Raptis, R. G., & Li, J. (2021). A novel fungal metabolite inhibits *Plasmodium falciparum* transmission and infection. *Parasites Vectors*, *14*(1), 177.

Niu, G., Wang, X., & Li, J. (2024). Leucinostatins target *Plasmodium mitochondria* to block malaria transmission. *Parasit Vectors*, *17*(1), 524.

Niu, X. M., Wang, Y. L., Chu, Y. S., Xue, H. X., Li, N., Wei, L. X., Mo, M. H., & Zhang, K. Q. (2010). Nematodetoxic aurovertin-type metabolites from a root-knot nematode parasitic fungus *Pochonia chlamydosporia*. *J Agric Food Chem*, *58*(2), 828-834.

Odier, F., Vey, A., & Bureau, J. P. (1992). In vitro effect of fungal cyclodepsipeptides on leukemic cells: study of destruxins A, B and E. *Biol Cell*, *74*(3), 267-271.

Oller-López, J. L., Iranzo, M., Mormeneo, S., Oliver, E., Cuerva, J. M., & Oltra, J. E. (2005). Bassianolone: an antimicrobial precursor of cephalosporolides E and F from the entomoparasitic fungus *Beauveria bassiana*. *Org Biomol Chem*, *3*(7), 1172-1173.

Ongena, M., & Jacques, P. (2008). Bacillus lipopeptides: versatile weapons for plant disease biocontrol. *Trends Microbiol*, *16*(3), 115-125.

Orejas, M., Espeso, E. A., Tilburn, J., Sarkar, S., Arst, H. N., Jr., & Penalva, M. A. (1995). Activation of the Aspergillus PacC transcription factor in response to alkaline ambient pH requires proteolysis of the carboxy-terminal moiety. *Genes Dev*, *9*(13), 1622-1632.

Ownley, B. H., Griffin, M. R., Klingeman, W. E., Gwinn, K. D., Moulton, J. K., & Pereira, R. M. (2008). Beauveria bassiana: Endophytic colonization and plant disease control. *J Invertebr Pathol*, *98*(3), 267-270.

Panyasiri, C., Supothina, S., Veeranondha, S., Chanthaket, R., Boonruangprapa, T., & Vichai, V. (2022). Control Efficacy of Entomopathogenic Fungus *Purpureocillium lilacinum* against Chili Thrips (*Scirtothrips dorsalis*) on Chili Plant. *Insects*, *13*(8).

Park, J. O., Hargreaves, J. R., McConville, E. J., Stirling, G. R., Ghisalberti, E. L., & Sivasithamparam, K. (2004). Production of leucinostatins and nematicidal activity of Australian isolates of *Paecilomyces lilacinu*s (Thom) Samson. *Lett Appl Microbiol*, *38*(4), 271-276.

Patel, H. M., & Walsh, C. T. (2001). In vitro reconstitution of the Pseudomonas aeruginosa nonribosomal peptide synthesis of pyochelin: characterization of backbone tailoring thiazoline reductase and N-methyltransferase activities. *Biochemistry*, *40*(30), 9023-9031.

Pellicciaro, M., Padoan, E., Lione, G., Celi, L., & Gonthier, P. (2022). Pyoluteorin Produced by the Biocontrol Agent Pseudomonas protegens Is Involved in the Inhibition of *Heterobasidion* Species Present in Europe. *Pathogens*, *11*(4).

Penalva, M. A., Tilburn, J., Bignell, E., & Arst, H. N., Jr. (2008). Ambient pH gene regulation in fungi: making connections. *Trends Microbiol*, *16*(6), 291-300.

Penas, M. M., Hervas-Aguilar, A., Munera-Huertas, T., Reoyo, E., Penalva, M. A., Arst, H. N., Jr., & Tilburn, J. (2007). Further characterization of the signaling proteolysis step in the *Aspergillus nidulans* pH signal transduction pathway. *Eukaryot Cell*, *6*(6), 960-970.

Pimentel, D., Acquay, H., Biltonen, M., Rice, P., Silva, M., Nelson, J., Lipner, V., Giordano, S., Horowitz, A., & D'Amore, M. (1992). Environmental and Economic Costs of Pesticide Use. *Bioscience*, *42*(10), 750-760.

Pinheiro, P. S. M., Franco, L. S., & Fraga, C. A. M. (2023). The Magic Methyl and Its Tricks in Drug Discovery and Development. *Pharmaceuticals (Basel)*, *16*(8).

Pliego, C., Cazorla, F. M., Gonzalez-Sanchez, M. A., Perez-Jimenez, R. M., de Vicente, A., & Ramos, C. (2007). Selection for biocontrol bacteria antagonistic toward *Rosellinia necatrix* by enrichment of competitive avocado root tip colonizers. *Res Microbiol*, *158*(5), 463-470.

Prusky, D., & Yakoby, N. (2003). Pathogenic fungi: leading or led by ambient pH? *Mol Plant Pathol*, *4*(6), 509-516.

Qi, F., Lei, C., Li, F., Zhang, X., Wang, J., Zhang, W., Fan, Z., Li, W., Tang, G.-L., Xiao, Y., Zhao, G., & Li, S. (2018). Deciphering the late steps of rifamycin biosynthesis. *Nat Commun*, *9*(1), 2342.

Quinn, G. A., Banat, A. M., Abdelhameed, A. M., & Banat, I. M. (2020). Streptomyces from traditional medicine: sources of new innovations in antibiotic discovery. *J Med Microbiol*, *69*(8), 1040-1048.

Räder, A. F. B., Reichart, F., Weinmüller, M., & Kessler, H. (2018). Improving oral bioavailability of cyclic peptides by N-methylation. *Bioorg Med Chem*, *26*(10), 2766-2773.

Radics, L., Kajtar-Peredy, M., Casinovi, C. G., Rossi, C., Ricci, M., & Tuttobello, L. (1987). Leucinostatins H and K, two novel peptide antibiotics with tertiary amine-oxide terminal group from *Paecilomyces marquandii* isolation, structure and biological activity. *J Antibiot (Tokyo)*, *40*(5), 714-716.

Rahila, R., Harish, S., Kalpana, K., Anand, G., Arulsamy, M., & Kalaivanan, R. (2023). Antifungal Metabolites of *Streptomyces chrestomyceticus* STR-2 Inhibits *Magnaporthe oryzae*, the Incitant of Rice Blast. *Curr Microbiol*, *80*(4), 107.

Raman, S. B., & Rathinasabapathi, B. (2003). beta-alanine N-methyltransferase of *Limonium latifolium*. cDNA cloning and functional expression of a novel N-methyltransferase implicated in the synthesis of the osmoprotectant beta-alanine betaine. *Plant Physiol*, *132*(3), 1642-1651.

Rimle, L., Pliatsika, D., Arnold, N., Kurth, S., Kaiser, M., Mäser, P., Kemmler, M., Adams, M., Riedl, R., & von Ballmoos, C. (2025). Dissecting Structural

Requirements of Leucinostatin A Derivatives for Antiprotozoal Activity and Mammalian Toxicity. *J Med Microbiol*, *68*(4), 4237-4258.

Rimle, L., Pliatsika, D., Arnold, N., Kurth, S., Kaiser, M., Mäser, P., Kemmler, M., Adams, M., Riedl, R., & von Ballmoos, C. (2025). Dissecting Structural Requirements of Leucinostatin A Derivatives for Antiprotozoal Activity and Mammalian Toxicity. *J Med Chem*, *68*(4), 4237-4258.

Rizwan-ul-Haq, M., Hu, Q. B., Hu, M. Y., Zhong, G., & Weng, Q. (2009). Study of destruxin B and tea saponin, their interaction and synergism activities with Bacillus thuringiensis kurstaki against *Spodoptera exigua* (Hübner)(Lepidoptera: Noctuidae). *Appl Entomol Zool*, *44*(3), 419-428.

Rodriguez-Galan, O., Galindo, A., Hervas-Aguilar, A., Arst, H. N., Jr., & Penalva, M. A. (2009). Physiological involvement in pH signaling of Vps24-mediated recruitment of Aspergillus PalB cysteine protease to ESCRT-III. *J Biol Chem*, *284*(7), 4404-4412.

Rodríguez-Ortiz, R., Limón, M. C., & Avalos, J. (2009). Regulation of carotenogenesis and secondary metabolism by nitrogen in wild-type *Fusarium fujikuroi* and carotenoid-overproducing mutants. *Appl Environ Microbiol*, *75*(2), 405-413.

Rossi, C., Tuttobello, L., Ricci, M., Casinovi, C. G., & Radics, L. (1987). Leucinostatin D, a novel peptide antibiotic from *Paecilomyces marquandii*. *J Antibiot (Tokyo)*, *40*(1), 130-133.

Rubio, M. B., Hermosa, R., Reino, J. L., Collado, I. G., & Monte, E. (2009). Thctf1 transcription factor of Trichoderma harzianum is involved in 6-pentyl-2H-pyran-2-one production and antifungal activity. *Fungal Genet Biol*, *46*(1), 17-27.

Ruiz-Sanchez, E., Lange, A. B., & Orchard, I. (2010). Effects of the mycotoxin destruxin A on *Locusta migratoria* visceral muscles. *Toxicon*, *56*(6), 1043-1051.

Sakaguchi, K., & Murao, S. (1950). A Prcliminary Report on a New Enzyme,"Penicillin-amidase". *Nippon Nogeikagaku Kaishi*, *23*(9), 411-411.

Sandmann, A., Sasse, F., & Müller, R. (2004). Identification and analysis of the core biosynthetic machinery of tubulysin, a potent cytotoxin with potential anticancer activity. *Chem Biol*, *11*(8), 1071-1079.

Sani, I., Jamian, S., Saad, N., Abdullah, S., Mohd Hata, E., Jalinas, J., & Ismail, S. I. (2023). Inoculation and colonization of the entomopathogenic fungi, Isaria javanica and *Purpureocillium lilacinum*, in tomato plants, and their effect on seedling growth, mortality and adult emergence of *Bemisia tabaci* (Gennadius). *PloS One*, *18*(5), e0285666.

Sarrocco, S., Esteban, P., Vicente, I., Bernardi, R., Plainchamp, T., Domenichini, S., Puntoni, G., Baroncelli, R., Vannacci, G., & Dufresne, M. (2021). Straw Competition and Wheat Root Endophytism of *Trichoderma gamsii* T6085 as Useful Traits in the Biological Control of Fusarium Head Blight. *Phytopathology*, *111*(7), 1129-1136.

Sarrocco, S., Guidi, L., Fambrini, S., Degl'Innocenti, E., & Vannacci, G. J. J. o. P. P. (2009). Competition for cellulose exploitation between Rhizoctonia solani and two Trichoderma isolates in the decomposition of wheat straw. *J Plant Path*, 331-338.

Savary, S., Willocquet, L., Pethybridge, S. J., Esker, P., McRoberts, N., & Nelson, A. (2019). The global burden of pathogens and pests on major food crops. *Nat Ecol Evol*, *3*(3), 430-439.

Schaner Tooley, C. E., Petkowski, J. J., Muratore-Schroeder, T. L., Balsbaugh, J. L., Shabanowitz, J., Sabat, M., Minor, W., Hunt, D. F., & Macara, I. G. (2010). NRMT is an α-N-methyltransferase that methylates RCC1 and retinoblastoma protein. *Nature*, *466*(7310), 1125-1128.

Scherkenbeck, J., Harder, A., Plant, A., & Dyker, H. (1998). PF1022A--a novel anthelmintic cyclooctadepsipeptide. Modification and exchange of the N-methyl leucine residues. *Bioorg Med Chem Lett*, *8*(9), 1035-1040.

Scherlach, K., & Hertweck, C. (2021). Mining and unearthing hidden biosynthetic potential. *Nat Commun*, *12*(1), 3864.

Scherlach, K., Sarkar, A., Schroeckh, V., Dahse, H. M., Roth, M., Brakhage, A. A., Horn, U., & Hertweck, C. (2011). Two induced fungal polyketide pathways converge into antiproliferative spiroanthrones. *Chembiochem*, *12*(12), 1836-1839.

Scholz, R., Vater, J., Budiharjo, A., Wang, Z., He, Y., Dietel, K., Schwecke, T., Herfort, S., Lasch, P., & Borriss, R. (2014). Amylocyclicin, a novel circular bacteriocin produced by *Bacillus amyloliquefaciens* FZB42. *J Bacteriol*, *196*(10), 1842-1852.

Schracke, N., Linne, U., Mahlert, C., & Marahiel, M. A. (2005). Synthesis of linear gramicidin requires the cooperation of two independent reductases. *Biochemistry*, *44*(23), 8507-8513.

Schwarz, P., & Dannaoui, E. (2020). In Vitro Interaction between Isavuconazole and Tacrolimus, Cyclosporin A, or Sirolimus against *Aspergillus Species*. *J Fungi (Basel)*, *6*(3).

Schwarzer, D., Finking, R., & Marahiel, M. A. (2003). Nonribosomal peptides: from genes to products. *Nat Prod Rep*, *20*(3), 275-287.

Shah, A. J., Tilburn, J., Adlard, M. W., & Arst, H. N., Jr. (1991). pH regulation of penicillin production in *Aspergillus nidulans*. *FEMS Microbiol Lett*, *61*(2-3), 209-212.

Sharma, A., Sharma, S., Mittal, A., & Naik, S. N. (2016). Evidence for the involvement of nematocidal toxins of Purpureocillium lilacinum 6029 cultured on Karanja deoiled cake liquid medium. *World J Microbiol Biotechnol*, *32*(5), 82.

Sharma, R., Singh, V. P., Singh, D., Yusuf, F., Kumar, A., Vishwakarma, R. A., & Chaubey, A. (2016). Optimization of nonribosomal peptides production by a psychrotrophic fungus: *Trichoderma velutinum* ACR-P1. *Appl Microbiol Biotechnol*, *100*(21), 9091-9102.

Shi, R., Lamb, S. S., Zakeri, B., Proteau, A., Cui, Q., Sulea, T., Matte, A., Wright, G. D., & Cygler, M. (2009). Structure and Function of the Glycopeptide N-methyltransferase MtfA, a Tool for the Biosynthesis of Modified Glycopeptide Antibiotics. *Chem Biol*, *16*(4), 401-410.

Shi, Y., Zaleta-Pinet, D. A., & Clark, B. R. (2020). Isolation, Identification, and Decomposition of Antibacterial Dialkylresorcinols from a Chinese *Pseudomonas aurantiaca* Strain. *J Nat Prod*, *83*(2), 194-201.

Shim, S. H., Swenson, D. C., Gloer, J. B., Dowd, P. F., & Wicklow, D. T. (2006). Penifulvin A: a sesquiterpenoid-derived metabolite containing a novel dioxa[5,5,5,6]fenestrane ring system from a fungicolous isolate of *Penicillium griseofulvum*. *Org Lett*, *8*(6), 1225-1228.

Shima, A., Fukushima, K., Arai, T., & Terada, H. (1990). Dual inhibitory effects of the peptide antibiotics leucinostatins on oxidative phosphorylation in mitochondria. *Cell Struct Funct*, *15*(1), 53-58.

Showler, A. T., & Harlien, J. L. (2018). Lethal and Repellent Effects of the Botanical p-Anisaldehyde on *Musca domestica* (Diptera: Muscidae). *J Econ Entomol*, *112*(1), 485-493.

Silva, D. M., de Souza, V. H. M., Moral, R. A., Delalibera Junior, I., & Mascarin, G. M. (2022). Production of *Purpureocillium lilacinum* and *Pochonia chlamydosporia* by Submerged Liquid Fermentation and Bioactivity against *Tetranychus urticae* and *Heterodera glycines* through Seed Inoculation. *J Fungi (Basel)*, *8*(5).

Singh, S., Chang, A., Goff, R. D., Bingman, C. A., Grüschow, S., Sherman, D. H., Phillips Jr, G. N., & Thorson, J. S. (2011). Structural characterization of the mitomycin 7‐O‐methyltransferase. *Proteins*, *79*(7), 2181-2188.

Skrobek, A., & Butt, T. M. (2005). Toxicity testing of destruxins and crude extracts from the insect-pathogenic fungus *Metarhizium anisopliae*. *FEMS Microbiol Lett*, *251*(1), 23-28.

Song, X., Wang, Q., Zhu, X., Fang, W., Liu, X., Shi, C., Chang, Z., Jiang, H., & Wang, B. (2024). Unraveling the Catalytic Mechanism of Taxadiene-5α-hydroxylase from Crystallography and Computational Analyses. *ACS Catalysis*, *14*(6), 3912-3925.

Sree, K. S., & Padmaja, V. (2008). Destruxin from *Metarhizium anisopliae* induces oxidative stress effecting larval mortality of the polyphagous pest *Spodoptera litura*. *J Appl Entomol*, *132*(1), 68-78.

Srirangan, K., Orr, V., Akawi, L., Westbrook, A., Moo-Young, M., & Chou, C. P. (2013). Biotechnological advances on Penicillin G acylase: Pharmaceutical implications, unique expression mechanism and production strategies. *Biotechnol Adv*, *31*(8), 1319-1332.

Sun, C., Li, S., Wang, K., Feng, H., Tian, C., Liu, X., Li, X., Yin, X., Wang, Y., Wei, J., & An, S. (2022). Cyclosporin A as a Source for a Novel Insecticidal Product for Controlling *Spodoptera frugiperda*. *Toxins*, *14*(10).

Sun, C., Li, S., Wang, K., Yin, X., Wang, Y., Du, M., Wei, J., & An, S. (2022). Cyclosporin A as a Potential Insecticide to Control the Asian Corn Borer Ostrinia furnacalis Guenée (Lepidoptera: Pyralidae). *Insects*, *13*(10).

Survase, S. A., Kagliwal, L. D., Annapure, U. S., & Singhal, R. S. (2011). Cyclosporin A — A review on fermentative production, downstream processing and pharmacological applications. *Biotechnol Adv*, *29*(4), 418-435.

Tan, Y., Wang, H., Wang, Y., Ge, Y., Ren, X., Ren, C., Wang, Y., Ren, X., Liu, Y., & Liu, Z. (2018). The role of the veA gene in adjusting developmental balance and environmental stress response in *Aspergillus cristatus*. *Fungal Biol*, *122*(10), 952-964.

Tanaka, A., Tapper, B. A., Popay, A., Parker, E. J., & Scott, B. (2005). A symbiosis expressed non-ribosomal peptide synthetase from a mutualistic fungal endophyte of perennial ryegrass confers protection to the symbiotum from insect herbivory. *Mol Microbiol*, *57*(4), 1036-1050.

Theatre, A., Cano-Prieto, C., Bartolini, M., Laurin, Y., Deleu, M., Niehren, J., Fida, T., Gerbinet, S., Alanjary, M., Medema, M. H., Leonard, A., Lins, L., Arabolaza, A., Gramajo, H., Gross, H., & Jacques, P. (2021). The Surfactin-Like Lipopeptides From *Bacillus* spp.: Natural Biodiversity and Synthetic Biology for a Broader Application Range. *Front Bioeng Biotechnol*, *9*, 623701.

Tilburn, J., Sarkar, S., Widdick, D. A., Espeso, E. A., Orejas, M., Mungroo, J., Penalva, M. A., & Arst, H. N., Jr. (1995). The Aspergillus PacC zinc finger transcription factor mediates regulation of both acid- and alkaline-expressed genes by ambient pH. *Embo J*, *14*(4), 779-790.

Tollervey, D. W., & Arst, H. N., Jr. (1982). Domain-wide, locus-specific suppression of nitrogen metabolite repressed mutations in Aspergillus nidulans. *Curr Genet*, *6*(1), 79-85.

Tongsook, C., Uhl, M. K., Jankowitsch, F., Mack, M., Gruber, K., & Macheroux, P. (2016). Structural and kinetic studies on RosA, the enzyme catalysing the methylation of 8-demethyl-8-amino-d-riboflavin to the antibiotic roseoflavin. *FEBS J*, *283*(8), 1531-1549.

Trifinopoulos, J., Nguyen, L. T., von Haeseler, A., & Minh, B. Q. (2016). W-IQ-TREE: a fast online phylogenetic tool for maximum likelihood analysis. *Nucleic Acids Res*, *44*(W1), W232-235.

Trushina, N., Levin, M., Mukherjee, P. K., & Horwitz, B. A. (2013). PacC and pH-dependent transcriptome of the mycotrophic fungus *Trichoderma virens*. *BMC Genomics*, *14*, 138.

Umar, A., Darwish, D. B. E., & Albalwe, F. M. (2024). Chapter 2 - Fungal secondary metabolites and their role in stress management. In K. A. Abd-Elsalam & H. I. Mohamed (Eds.), *Fungal Secondary Metabolites* (pp. 15-56). Elsevier.

Urquhart, A. S., Hu, J., Chooi, Y.-H., & Idnurm, A. (2019). The fungal gene cluster for biosynthesis of the antibacterial agent viriditoxin. *Fungal Biol. Biotechnol*, *6*, 1-13.

Velkov, T., Horne, J., Scanlon, M. J., Capuano, B., Yuriev, E., & Lawen, A. (2011). Characterization of the N-methyltransferase activities of the multifunctional polypeptide cyclosporin synthetase. *Chem Biol*, *18*(4), 464-475.

Vertuani, G., Boggian, M., Scatturin, A., Ricci, M., Meli Balbocchino, B., Tuttobello, L., & Rossi, C. (1995). Structure activity studies on chemically modified homologues of the antibiotic phytotoxic leucinostatin A. *J Antibiot (Tokyo)*, *48*(3), 254-260.

Vit, A., Misson, L., Blankenfeldt, W., & Seebeck, F. P. (2015). Ergothioneine biosynthetic methyltransferase EgtD reveals the structural basis of aromatic amino acid betaine biosynthesis. *Chembiochem*, *16*(1), 119-125.

Wang, C., & Kuzyakov, Y. (2024). Mechanisms and implications of bacterial-fungal competition for soil resources. *ISME J*, *18*(1).

Wang, G., Li, Y., Yang, B., Li, E., Wu, W., Si, P., & Xing, F. (2022). AwAreA Regulates Morphological Development, Ochratoxin A Production, and Fungal Pathogenicity of Food Spoilage Fungus *Aspergillus westerdijkiae* Revealed by an Efficient Gene Targeting System. *Front Microbiol*, *13*, 857726.

Wang, G., Liu, Z., Lin, R., Li, E., Mao, Z., Ling, J., Yang, Y., Yin, W., & Xie, B. (2016). Biosynthesis of antibiotic leucinostatins in bio-control fungus

Purpureocillium lilacinum and their inhibition on Phytophthora revealed by genome mining. *PLoS Pathog*, *12*(7), e1005685-e1005685.

Wang, X. L., Qiu, S. Y., Zhou, S. Q., Xu, Z. H., & Liu, X. T. (2023). Phosphate-Solubilizing Capacity of *Paecilomyces lilacinus* PSF7 and Optimization Using Response Surface Methodology. *Microorganisms*, *11*(2).

Watanabe, T., Abe, H., & Shibasaki, M. (2021). Catalytic Asymmetric Total Synthesis of Leucinostatin A. *Chem Rec*, *21*(1), 175-187.

Weber, G., Schörgendorfer, K., Schneider-Scherzer, E., & Leitner, E. (1994). The peptide synthetase catalyzing cyclosporine production in Tolypocladium niveum is encoded by a giant 45.8-kilobase open reading frame. *Curr Genet*, *26*(2), 120-125.

Weckwerth, W., Miyamoto, K., Iinuma, K., Krause, M., Glinski, M., Storm, T., Bonse, G., Kleinkauf, H., & Zocher, R. (2000). Biosynthesis of PF1022A and related cyclooctadepsipeptides. *J Biol Chem*, *275*(23), 17909-17915.

Wei, J., Liu, S., Wang, K., Sun, C., Li, S., Liu, X., Yin, X., Bai, S., Liang, G., Crickmore, N., & An, S. (2022). Cyclosporin A acts as a novel insecticide against Cry1Ac-susceptible and -resistant Helicoverpa armigera. *Pestic Biochem Physiol*, *188*, 105283.

Weller, D. M., Landa, B. B., Mavrodi, O. V., Schroeder, K. L., De La Fuente, L., Blouin Bankhead, S., Allende Molar, R., Bonsall, R. F., Mavrodi, D. V., & Thomashow, L. S. (2007). Role of 2,4-diacetylphloroglucinol-producing fluorescent *Pseudomonas* spp. in the defense of plant roots. *Plant Biol*, *9*(1), 4-20.

Wiemann, P., Brown, D. W., Kleigrewe, K., Bok, J. W., Keller, N. P., Humpf, H. U., & Tudzynski, B. (2010). FfVel1 and FfLae1, components of a velvet-like complex in *Fusarium fujikuroi*, affect differentiation, secondary metabolism and virulence. *Mol Microbiol*, *77*(4), 972-994.

Wong, K. H., Hynes, M. J., Todd, R. B., & Davis, M. A. (2009). Deletion and overexpression of the *Aspergillus nidulans* GATA factor AreB reveals unexpected pleiotropy. *Microbiology (Reading)*, *155*(Pt 12), 3868-3880.

Woo, S. L., Hermosa, R., Lorito, M., & Monte, E. (2023). Trichoderma: a multipurpose, plant-beneficial microorganism for eco-sustainable agriculture. *Nat Rev Microbiol*, *21*(5), 312-326.

Xie, L., Zhang, L., Bai, J., Yue, Q., Zhang, M., Li, J., Wang, C., & Xu, Y. (2019). Methylglucosylation of Phenolic Compounds by Fungal Glycosyltransferase-Methyltransferase Functional Modules. *J Agric Food Chem*, *67*(31), 8573-8580.

Xie, L., Zhang, L., Wang, C., Wang, X., Xu, Y. M., Yu, H., Wu, P., Li, S., Han, L., Gunatilaka, A. A. L., Wei, X., Lin, M., Molnár, I., & Xu, Y. (2018).

Methylglucosylation of aromatic amino and phenolic moieties of drug-like biosynthons by combinatorial biosynthesis. *Proc Natl Acad Sci U S A*, *115*(22), E4980-e4989.

Xie, Y., Li, H., Luo, X., Li, H., Gao, Q., Zhang, L., Teng, Y., Zhao, Q., Zuo, Z., & Ren, J. (2022). IBS 2.0: an upgraded illustrator for the visualization of biological sequences. *Mol Microbiol*, *50*(W1), W420-W426.

Xu, F., Butler, R., May, K., Rexhepaj, M., Yu, D., Zi, J., Chen, Y., Liang, Y., Zeng, J., Hevel, J., & Zhan, J. (2019). Modified substrate specificity of a methyltransferase domain by protein insertion into an adenylation domain of the bassianolide synthetase. *J Biol Eng*, *13*, 65.

Xu, L., Wang, J., Zhao, J., Li, P., Shan, T., Wang, J., Li, X., & Zhou, L. (2010). Beauvericin from the endophytic fungus, *Fusarium redolens*, isolated from Dioscorea zingiberensis and its antibacterial activity. *Nat Prod Commun*, *5*(5), 811-814.

Xu, W. F., Yang, J. L., Meng, X. K., Gu, Z. G., Zhang, Q. L., & Lin, L. B. (2021). Understanding the Transcriptional Changes During Infection of Meloidogyne incognita Eggs by the Egg-Parasitic Fungus *Purpureocillium lilacinum*. *Front Microbiol*, *12*, 617710.

Xu, Y., Orozco, R., Kithsiri Wijeratne, E. M., Espinosa-Artiles, P., Leslie Gunatilaka, A. A., Patricia Stock, S., & Molnar, I. (2009). Biosynthesis of the cyclooligomer depsipeptide bassianolide, an insecticidal virulence factor of *Beauveria bassiana*. *Fungal Genet Biol*, *46*(5), 353-364.

Xu, Y., Orozco, R., Wijeratne, E. M., Gunatilaka, A. A., Stock, S. P., & Molnar, I. (2008). Biosynthesis of the cyclooligomer depsipeptide beauvericin, a virulence factor of the entomopathogenic fungus *Beauveria bassiana*. *Chem Biol*, *15*(9), 898-907.

Xu, Y., Zhan, J., Wijeratne, E. M., Burns, A. M., Gunatilaka, A. A., & Molnár, I. (2007). Cytotoxic and Antihaptotactic beauvericin analogues from precursor-directed biosynthesis with the insect pathogen *Beauveria bassiana* ATCC 7159. *J Nat Prod*, *70*(9), 1467-1471.

Yang, J., Mori, T., Wei, X., Matsuda, Y., & Abe, I. (2021). Structural Basis for Isomerization Reactions in Fungal Tetrahydroxanthone Biosynthesis and Diversification. *Angew Chem Int Ed*, *60*(35), 19458-19465.

Yang, X., Feng, P., Yin, Y., Bushley, K., Spatafora, J. W., & Wang, C. (2018). Cyclosporine Biosynthesis in *Tolypocladium inflatum* Benefits Fungal Adaptation to the Environment. *MBio*, *9*(5).

Yao, Y., Yang, E., Pan, Y., Shu, X., & Liu, G. (2023). Mining an O-methyltransferase for de novo biosynthesis of physcion in *Aspergillus nidulans*. *Appl Microbiol Biotechnol*, *107*(4), 1177-1188.

Yeh, H. H., Ahuja, M., Chiang, Y. M., Oakley, C. E., Moore, S., Yoon, O., Hajovsky, H., Bok, J. W., Keller, N. P., Wang, C. C., & Oakley, B. R. (2016). Resistance Gene-Guided Genome Mining: Serial Promoter Exchanges in *Aspergillus nidulans* Reveal the Biosynthetic Pathway for Fellutamide B, a Proteasome Inhibitor. *ACS Chem Biol*, *11*(8), 2275-2284.

Yokota, K., Teraoka, T., Tsujii, Y., Suzuki, H., Murakami, K., Miwa, E., & Higuchi, K. (2010). Effect of high molecular weight carbohydrates on bud cell formation by *Fusarium oxysporum* in potato dextrose broth. *J Gen Plant Pathol*, *76*(3), 219-224.

Yu, W., Pei, R., Zhang, Y., Tu, Y., & He, B. (2023). Light regulation of secondary metabolism in fungi. *J Biol Eng*, *17*(1), 57.

Yu, Z., Zhang, Y. C., Zhang, X., & Wang, Y. (2015). Conversion of food waste into biofertilizer for the biocontrol of root knot nematode by *Paecilomyces lilacinus*. *Environ Technol*, *36*(24), 3148-3158.

Yun, C. S., Motoyama, T., & Osada, H. (2015). Biosynthesis of the mycotoxin tenuazonic acid by a fungal NRPS-PKS hybrid enzyme. *Nat Commun*, *6*, 8758.

Zallot, R., Oberg, N., & Gerlt, J. A. (2019). The EFI Web Resource for Genomic Enzymology Tools: Leveraging Protein, Genome, and Metagenome Databases to Discover Novel Enzymes and Metabolic Pathways. *Biochemistry*, *58*(41), 4169-4182.

Zehetbauer, F., Seidl, A., Berger, H., Sulyok, M., Kastner, F., & Strauss, J. (2022). RimO (SrrB) is required for carbon starvation signaling and production of secondary metabolites in *Aspergillus nidulans*. *Fungal Genet Biol*, *162*, 103726.

Zhang, L., Wang, C., Chen, K., Zhong, W., Xu, Y., & Molnár, I. (2023). Engineering the biosynthesis of fungal nonribosomal peptides. *Nat Prod Rep*, *40*(1), 62-88.

Zhang, W., Watanabe, K., Cai, X., Jung, M. E., Tang, Y., & Zhan, J. (2008). Identifying the minimal enzymes required for anhydrotetracycline biosynthesis. *J Am Chem Soc*, *130*(19), 6068-6069.

Zhang, Y., Yu, W., Lu, Y., Wu, Y., Ouyang, Z., Tu, Y., & He, B. (2024). Epigenetic Regulation of Fungal Secondary Metabolism. *J Fungi (Basel)*, *10*(9).

Zhao, D. X., Beran, M., Kozová, J., & Rehácek, Z. (1991). Formation of cyclosporins by *Tolypocladium inflatum*. *Folia Microbiol*, *36*(6), 549-556.

Zhi, Q.-Q., Wang, Z.-L., Yuan, P.-B., He, L., & He, Z.-M. (2024). The GATA factor AreB regulates nitrogen metabolism, fungal development, and aflatoxin production in *Aspergillus flavus*. *FEMS Microbiol Lett*, *372*.

Zubieta, C., He, X. Z., Dixon, R. A., & Noel, J. P. (2001). Structures of two natural product methyltransferases reveal the basis for substrate specificity in plant O-methyltransferases. *Nat Struct Biol*, *8*(3), 271-279.

Appendices

List of publications

First author

Li Z, Jiao Y, Tang J, Dong X, Thomas R, Xie B, Li Y, Jacques P. The pH-Responsive Regulator PlPacC and GATA Transcription Factor PlAreB are Involved in the Regulation of the Biosynthesis of the Antifungal Lipopeptaibols Leucinostatins in *Purpureocillium lilacinum*. **Microbiol Res (Under review)**

Li Z#, Jiao Y#, Ling J, Zhao J, Yang Y, Mao Z, Zhou K, Wang W, Xie B, Li Y. Characterization of a methyltransferase for iterative *N*-methylation at the leucinostatin termini in *Purpureocillium lilacinum*. **Commun Biol.** 2024 Jun 22;7(1):757.

Zhang H #, **Li Z** #, Zhou S, Li SM, Ran H, Song Z, Yu T, Yin WB. A fungal NRPS-PKS enzyme catalyses the formation of the flavonoid naringenin. **Nat Commun.** 2022 Oct 26;13(1):6361.

Li R#, **Li Z**#, Ma K, Wang G, Li W, Liu HW, Yin WB, Zhang P, Liu XZ. Strategy for efficient cloning of biosynthetic gene clusters from fungi. **Sci China Life Sci.** 2019 Aug;62(8):1087-1095.

Co-author

Jiao Y#, Ling J#, Khan RAA, Luo N, **Li Z**, Li Z, Yang Y, Zhao J, Mao Z, Bills GF, Xie B, Li Y. Genome Mining Reveals Biosynthesis of the Antifungal Lipopeptaibols, Texenomycins, through a Hybrid PKS-NRPS System, in the Fungus *Mariannaea elegans*. **J Agric Food Chem.** 2025 Jan 8;73(1):226-236.

Li W, Yu J, **Li Z**, Yin WB. Rational design for fungal laccase production in the model host *Aspergillus nidulans*. **Sci China Life Sci.** 2019 Jan;62(1):84-94.

Zeng G#, Zhang P#, Zhang Q#, Zhao H, **Li Z**, Zhang X, Wang C, Yin WB, Fang W. Duplication of a Pks gene cluster and subsequent functional diversification facilitate environmental adaptation in *Metarhizium* species. **PLoS Genet.** 2018 Jun 29;14(6):e1007472.